



**HAL**  
open science

## Hierarchically porous materials: synthesis strategies and structure design

Yu Yang, Li-Hua Li, Yu Li, Joanna Claire Rooke, Clément Sanchez, Bao-Lian Su

► **To cite this version:**

Yu Yang, Li-Hua Li, Yu Li, Joanna Claire Rooke, Clément Sanchez, et al.. Hierarchically porous materials: synthesis strategies and structure design. *Chemical Society Reviews*, 2017, 45, pp.481-558  
10.1039/C6CS00829A . hal-01495958

**HAL Id: hal-01495958**

<https://hal.sorbonne-universite.fr/hal-01495958v1>

Submitted on 27 Mar 2017

**HAL** is a multi-disciplinary open access archive for the deposit and dissemination of scientific research documents, whether they are published or not. The documents may come from teaching and research institutions in France or abroad, or from public or private research centers.

L'archive ouverte pluridisciplinaire **HAL**, est destinée au dépôt et à la diffusion de documents scientifiques de niveau recherche, publiés ou non, émanant des établissements d'enseignement et de recherche français ou étrangers, des laboratoires publics ou privés.

# Hierarchically porous materials: synthesis strategies and structure design

Cite this: *Chem. Soc. Rev.*, 2017, 46, 481

Xiao-Yu Yang,<sup>\*a</sup> Li-Hua Chen,<sup>\*a</sup> Yu Li,<sup>\*a</sup> Joanna Claire Rooke,<sup>b</sup> Clément Sanchez<sup>c</sup> and Bao-Lian Su<sup>\*abd</sup>

Owing to their immense potential in energy conversion and storage, catalysis, photocatalysis, adsorption, separation and life science applications, significant interest has been devoted to the design and synthesis of hierarchically porous materials. The hierarchy of materials on porosity, structural, morphological, and component levels is key for high performance in all kinds of applications. Synthesis and applications of hierarchically structured porous materials have become a rapidly evolving field of current interest. A large series of synthesis methods have been developed. This review addresses recent advances made in studies of this topic. After identifying the advantages and problems of natural hierarchically porous materials, synthetic hierarchically porous materials are presented. The synthesis strategies used to prepare hierarchically porous materials are first introduced and the features of synthesis and the resulting structures are presented using a series of examples. These involve templating methods (surfactant templating, nanocasting, macroporous polymer templating, colloidal crystal templating and bioinspired process, *i.e.* biotemplating), conventional techniques (supercritical fluids, emulsion, freeze-drying, breath figures, selective leaching, phase separation, zeolitization process, and replication) and basic methods (sol–gel controlling and post-treatment), as well as self-formation phenomenon of porous hierarchy. A series of detailed examples are given to show methods for the synthesis of hierarchically porous structures with various chemical compositions (dual porosities: micro–micropores, micro–mesopores, micro–macropores, meso–mesopores, meso–macropores, multiple porosities: micro–meso–macropores and meso–meso–macropores). We hope that this review will be helpful for those entering the field and also for those in the field who want quick access to helpful reference information about the synthesis of new hierarchically porous materials and methods to control their structure and morphology.

Received 20th November 2016

DOI: 10.1039/c6cs00829a

## 1. Introduction

Hierarchically porous structures are commonly found in living organisms and are of key importance to achieve optimal properties and performance and to allow adaptation to constant environmental changes through long term evolution. Many biological materials with a remarkable efficiency, such as diatom, butterfly, leaf *etc.*, (Fig. 1), are complex composites with hierarchically porous structures. Their exceptional properties are believed to be due to a functional adaptation of the structure at all levels of hierarchy.

One great interest in science and technology is the implementation of such porous hierarchies in artificial materials from the molecular level to the macroscopic dimensions with the highest possible precision. Over the last decade, significant progress has been made in the design, synthesis and use of hierarchically porous materials in areas ranging from nanoscience to catalysis, separation, energy, life science and other industrial applications. These materials are comprised of a multimodal hierarchically porous structure made of interconnected pores with different lengths ranging from micro (<2 nm), meso (2–50 nm) to macro pores (>50 nm).

### 1.1 The main advantageous features of hierarchically porous materials

Structuring porous hierarchy of materials over different lengths mimicks natural systems and it can lead to a variety of functionalities desirable for a large number of applications. An understanding of the relationships between natural porous architectures and their functionalities is essential to develop new ways for designing advanced hierarchically structured

<sup>a</sup> State Key Laboratory Advanced Technology for Materials Synthesis and Processing, School of Materials Science and Engineering, Wuhan University of Technology, 122, Luoshi Road, Wuhan, 430070, China. E-mail: xyyang@whut.edu.cn, chenlihua@whut.edu.cn, yu.li@whut.edu.cn, baoliansu@whut.edu.cn

<sup>b</sup> Laboratory of Inorganic Materials Chemistry (CMI), University of Namur, 61, rue de Bruxelles, B-5000 Namur, Belgium. E-mail: bao-lian.su@unamur.be

<sup>c</sup> Chimie de la Matière Condensée de Paris, Université Pierre et Marie Curie (Paris VI), Collège de France, 11 Place Marcelin Berthelot, 75231, Paris, France

<sup>d</sup> Clare Hall, University of Cambridge, Cambridge CB2 1EW, UK.

E-mail: bls26@cam.ac.uk

porous materials. Natural assemblies and architectures have possessed remarkably organized and hierarchical three dimensional porous exoskeletons, in spite of having many drawbacks such as low stability and poor resistance to the harsh environments.<sup>1–9</sup> For example, the frustule has been optimized for the photosynthetic process through long-time evolution.

Therefore, using natural systems to construct synthetic hierarchically porous materials could be used to introduce advantageous features in terms of performance and sustainability. A number of important factors are typically considered in selecting methods for fabrication of hierarchically porous materials.

(i) Numerous synthesis approaches. A great number of synthesis strategies have been developed to prepare hierarchically porous materials. These include dual surfactant templating, colloidal crystal templating, polymer templating, bioinspiring process, emulsion templating, SCFs, freeze-drying, BFs, phase

separation, selective leaching, replication, zeolitization, sol–gel controlling, post-treatment and spontaneous formation. Many choices offer possibility of fine control of various structures and morphologies.

(ii) Tunable porous structures. The micro/meso/macro porous structures of hierarchically porous materials can be adjusted by using a combination of various approaches. Desirable structures, ranging from sub-nano to micro meter scales, can be assembled and/or integrated by using nanounits. Although great progress has been made in the design and fabrication of such hierarchical micro/nano structures, precise control of structure is still not an easy task.

(iii) Controllable macroscopic morphologies. The macroscopic morphologies of hierarchically porous materials can be easily controlled by using different methods, such as self-formation to 0D sphere, polymer-templating to 1D fibre, biotemplating to 2D



**Xiao-Yu Yang**

*Xiao-Yu Yang earned his PhD from Jilin University (co-educated at the University of Namur, Belgium). After post-doctoral research at the University of Namur with Prof. Bao-Lian Su, he worked as a “Chargé de Recherches” at the F.N.R.S. (National Foundation of Scientific Research) since 2008. He is currently working as Chutian Professor at Wuhan University of Technology. His research is aimed at novel porous systems, green chemistry, self-assembly techniques and their applications in energy, environment and catalysis.*



**Li-Hua Chen**

*Li-Hua Chen received his BS from Jilin University in 2004, and awarded his PhD degrees, one in inorganic chemistry from Jilin University, China (2009), and another in inorganic materials chemistry from University of Namur, Belgium (2011). In 2011–2012, he held a researcher position at the University of Namur with Professor Bao-Lian Su working on hierarchically porous zeolites. He is currently a full professor working in the State Key Laboratory of Advanced Technology for Materials Synthesis and Processing from the Wuhan University of Technology, China. His research is aimed at new porous materials with designed hierarchically porosity towards catalysis.*



**Yu Li**

*Yu Li received his BS from Xi'an Jiaotong University in 1999 and received his MS from Liaoning Shihua University in 2002. He obtained his PhD from Zhejiang University in 2005. He worked in EMAT at the University of Antwerp with Prof. G. Van Tendeloo in 2005 and then in CMI at the University of Namur with Prof. Bao-Lian Su in 2006. Currently, he is a “Chutian” Professor at Wuhan University of Technology. His research interests include nanomaterials design and synthesis, hierarchically porous materials synthesis, and their applications in the fundamental aspects of energy and environment.*



**Joanna Claire Rooke**

*Joanna Rooke received a MNatSc (Chemistry) degree from the University of Birmingham (2000). She was awarded a PhD, jointly funded by Merck and EPSRC, by the University of Southampton (2004) under the supervision of Prof. M. T. Weller. After a PDRF at the Laboratory of Inorganic Materials Chemistry, University of Namur she moved to LEPMI, INP Grenoble before returning to Namur. Her research interests include synthesis and crystallography of oxynitrides, adsorption of Pt nanoparticles on carbon aerogels and the synthesis of metal oxide catalytic supports.*

film and phase-separation to 3D monolith. Additionally, the use of spontaneous assemblies and/or aggregations of nanounits enables the creation of secondary morphologies on supports. Recently, physiochemical conditions and templating-effects have been utilized widely to assemble desired morphologies.

(iv) Adjustable multiple functions. The high activity and selectivity of hierarchical porosity are ideal goals one seeks in new functioning systems. The introduction of new properties derived from heteroatoms, nanounits and bioentities could endow the hierarchically porous materials with multiple-functions, for example, high effective photon-harvesting, facilitate charge transfer and fast molecular. Hybrids of multiple functions could be designed to create materials with features of atoms, nano-effect and biospecies. As such, the combination could reach “one plus one greater than two” results.

(v) Potential wide utilization. The variety of nanocompositions that can be utilized to construct hierarchically porous materials are at the core of the development of practical applications. The desired porous structures and morphologies could be employed for applications in the energy, environment and living science fields. The hierarchical structures used for this purpose can be designed to protect active sites such as heteroatoms, nanounits and bioentities under different environmental conditions,

operational procedures, as well as to overcome problems with stability during recycling.

## 1.2 The main applications of hierarchically porous materials

A wide range of components are used to synthesize hierarchically structured porous materials thus offering a wide choice in formulating stable materials towards harsh environments such as heat, steam saturated atmospheres as well as harsh chemicals. Mastering these conditions is indeed very important in engineering design. The mechanical and transport properties of these materials can be controlled through manipulation of morphology on the micrometer scale. Hierarchically porous materials with high surface areas, high pore volume ratios, high accessibilities, ready mass transport properties and high storage capacities have been used in various applications where they show their superiority compared to simple porous materials in catalysis,<sup>10–16</sup> adsorption,<sup>17–21</sup> separation,<sup>22,23</sup> sensors,<sup>24–27</sup> energy<sup>28–66</sup> and life sciences.<sup>67–74</sup>

At first, hierarchically porous materials with multiple porosities over lengths in the micro, meso to macro ranges have been intensively used as catalysts and catalyst supports.<sup>10–16</sup> The introduction of micro–mesoporosity into a macroporous solid can provide accurate size and shape selectivities for reactants,



**Clément Sanchez**

*Clément Sanchez is Professor at the Collège de France “Chair Chemistry of Hybrid Materials” and Director of The “Laboratoire de Chimie de la Matière Condensée de Paris” (UMR 757, University of Pierre and Marie Curie-Collège de France-CNRS). He was Director of Research at the French Council Research (CNRS) and Professor at l’Ecole Polytechnique. He received an engineer degree from l’Ecole Nationale Supérieure de Chimie*

*de Paris in 1978 and a “thèse d’état” (PhD) in physical chemistry from the University of Paris VI in 1981. He did a post-doctoral work at the University of California, Berkeley, and is currently performing research at the The Collège de France in Paris. He is specialised in the field of nanochemistry and physical properties of nanostructured porous and non-porous transition metal oxide based gels and porous and non-porous hybrid organic inorganic materials shaped as monolith, microspheres and films. He was the recipient of many national and international awards and is member of several Academies of Sciences (French, European, Spanish).*



**Bao-Lian Su**

*Bao-Lian Su is a member of the Royal Academy of Belgium, a fellow of the Royal Society of Chemistry and a life member of Clare Hall College, University of Cambridge. He holds “Chaire Francqui au titre Belge”. He joined the faculty at the University of Namur and created the Laboratory of Inorganic Materials Chemistry (CMI) in 1995. He is currently a Director of the Laboratory of Inorganic Materials Chemistry (CMI),*

*University of Namur, Belgium. His is an “Expert of the State” in the framework of the Chinese Central Government program of “Thousands Talents” and “Changjiang Professor” appointed by Chinese Ministry of Education. He is “Strategical Scientist” at the Wuhan University of Technology. He has received a series of honours and awards such as the First Prize Invention Award of Sinopec (1992, China), A. Wetrems Prize (2007, Royal Academy of Belgium) and IUPAC Distinguished Award for Novel Materials and their synthesis (2011). His current research fields include the synthesis, the property study and the molecular engineering of organized, hierarchically porous and bio-inspired materials, biomaterials, living materials, leaf-like materials and nano-structures and the immobilisation of living organisms for artificial photosynthesis, nanotechnology, biotechnology, cell therapy and biomedical applications.*

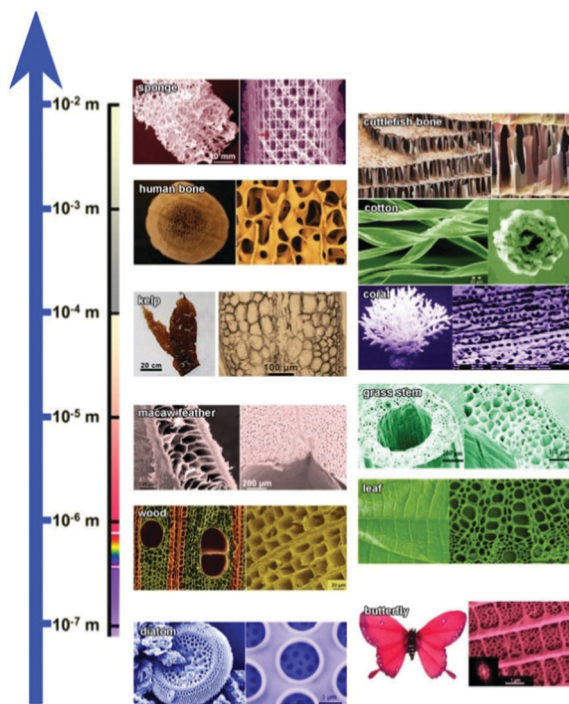


Fig. 1 Overview of hierarchical structured porous natural materials, placed alongside the length scale according to their critical dimensions. The SEM or OM images of original biological hierarchically porous structures are shown from bottom to up: diatom, butterfly, wood, leaf, macaw feather, grass stem, kelp, coral, cotton, human bone, cuttlefish bone, and sponge. Reprinted with permission from ref. 9. Copyright 2011, Wiley-VCH.

intermediates and/or products as well as for catalytic active sites for guest molecules. Catalytic sites are often located in microporous systems while macroporous networks can minimize diffusion barriers and thus enhance mass transport. The presence of micro and mesoporosities can also provide for easy separation of products, reactants and intermediates owing to the shape selectivity character of hierarchically porous materials. The utilization of hierarchically porous materials enables multiple step reactions by constructing structured reactors. Hierarchically porous solids have also been largely used as catalyst supports because they supply the large surface area needed for highly dispersion of active components (metals, metal oxides, enzymes or other species). Currently, many kinds of hierarchically porous materials including metal oxides, carbons, ceramics and polymers, *etc.* are desirable materials as catalysts and catalyst supports largely used in catalytic applications.<sup>10–16,75–83</sup>

Hierarchically porous materials have been studied in the context of the new field of photocatalysis. In addition to the high surface area and low mass transport limitation caused by the presence of meso and macroporosity, access of reactant molecules to photocatalytic active sites is facilitated and, consequently, photocatalytic activities are improved. It is well recognized that hierarchically porous semiconducting materials are very efficient light harvesters that have enhanced light absorption owing to the presence of macrochannels<sup>84–88</sup> that allows deep penetration of the light. In addition, these channels promote light scattering that leads to elongation of the light path.

Photocatalytic activities are greatly enhanced.<sup>84–86</sup> It was also found that a slow photon effect exists in 3D ordered hierarchically meso–macroporous inverse opal semiconducting materials named photonic crystals. Due to the periodic organization of macropores, like the electronic band gap of semiconducting materials, the 3D ordered inverse opal photonic crystals generate a photonic band gap which can prevent the penetration of the light with a frequency corresponding to the photonic band gap into the material. Thus, light of this frequency is reflected. Interestingly, it was revealed theoretically and experimentally that at the red and blue edges of the photonic band gap, the light average velocity of light can be slowed, *i.e.* the average light residence time in materials becomes longer. This is called the slow photon phenomenon.<sup>89–92</sup> Owing to the slow photon effect, the light absorption efficiency of materials can be greatly enhanced and the photocatalytic activity can be highly improved.<sup>89–92</sup> This phenomenon has also been used in solar cells to improve light absorption efficiency.<sup>89–92</sup> The above examples show very clearly the strong impact of hierarchically porous materials have on photocatalysis.

Hierarchical porosity is quite desirable for adsorption and separation processes. The high contact surface area, high storage volume, ready mass transport, shape selectivity and well controlled porosities over different length scales lead to very high adsorption capacities and high separation efficiencies. Currently, hierarchically porous materials based on silica, organosilica, metal oxides have been heavily used in adsorption<sup>17–21</sup> and separation processes.<sup>22,23,93</sup>

Energy conversion and storage is an important field in which hierarchically porous materials have been applied. As described above, owing to the high improvement of light absorption efficiency caused by light harvesting and scattering effects in macrochannels and the slow photon effect, hierarchically porous materials are the prime choices for photosynthetic solar cells, photochemical bioreactors (PBs)<sup>33–35,94</sup> and photovoltaic solar cells such as dye-sensitized solar cells (DSSCs).<sup>36,37</sup>

Life science issues including tissue engineering and drug delivery are other areas for application of hierarchically porous materials. As an example, bone is a kind of natural hierarchically porous material. As a result, its repair needs to employ hierarchically porous materials based systems. Drug delivery has an equal need for hierarchically porous media to promote large storage capacity and controlled delivery in both a spacial and temporal manner.<sup>67–74</sup>

Due to their short solid-state diffusion lengths and large surface areas, a wide range of hierarchically structured porous materials have been utilized to improve the performances of FCs,<sup>38–45,95,96</sup> LIBs<sup>53–57,97–134</sup> and supercapacitor<sup>46–52,135–140</sup> and in other energy storage applications.<sup>58–66</sup> All of these emerging applications are summarized in Table 1.

In order to further applications in the above mentioned fields, the synthesis and design of new advanced hierarchically porous materials have attracted intensive attention. As the hierarchy on porosity, structural, morphological and component levels determines the functionalities and performances of materials, the control of the hierarchy at each level and then at all the levels is crucial. Available processing technologies for the synthesis of hierarchically structured porous materials provide precise control of some variables of hierarchy at different levels

**Table 1** Applications of hierarchical structured porous materials in catalysis, separation, energy and life science

Applications	Types	Features	Ref.
Catalysis	Acid catalyst Oxidation catalyst Photocatalysis	(i) High accessibility of bulky molecules; (ii) high diffusion rate of reactant and product; (iii) usually heteroatoms of zeolites or supported nanometal particles as active sites	10–16, 93 and 141–144
Separation and adsorption	Preconcentration device Bioreactors and DNA purifier Therapeutic apheresis device	(i) High permeability; (ii) homogeneous flow-through pore structure; (iii) controlled pore structures and surface properties; (iv) usually monolithic column used	17–23
Energy	Sunlight conversion (such as DSSCs, PBs) Sensors and fuel cell Lithium-ion battery Supercapacitor	(i) Efficient light-harvesting, especially in biomaterials replica or biocomposites examples; (ii) fast charge separation and high current density; (iii) high gas permeability; (iv) high storage density; (v) fast electron and ion transport; (vi) small resistance	24–66, 95–140 and 145
Life sciences	Life engineering Biomaterial Drug delivery	(i) Biocompatibility and promoting cell adhesion and activity; (ii) good mechanical properties; (iii) controlled shape; (iv) clinical use	67–74, 87, 94 and 146

including porosity variables (bimodal, trimodal or multi modal and pore size at each porous level), structural variables (atomic, molecular, nanostructures and microstructures), component variables (chemical composition, atom distribution, crystalline phase and interfaces at all levels) and morphological variables (shape, grain size and orientation distributions). Even though full control of these variables has not reached the level of naturally porous materials, great progress has been made in the preparation of synthetic hierarchical materials. A summary of the preparation strategies combined with their corresponding morphologies, porous structures and chemical compositions are given in Table 2.

A series of technologies have been applied to the preparation of hierarchically porous materials. These include surfactant templating, emulsion templating, macroporous polymer templating and colloidal crystal templating, bioinspired processes, supercritical fluids (SCF), freeze-drying, breath figures (BFs), selective leaching, phase separation, zeolitization process (including zeolite-related materials) and replication. Sol-gel controlling and post-treatment methods have also been employed. Moreover, an innovative self-formation procedure has been developed and used to synthesize hierarchically porous materials. On the basis of these synthesis strategies, multiple combinations of porous materials such as micro-mesoporous, micro-macroporous, micro-meso-macroporous supports *etc.* have been designed and synthesized.<sup>1–9</sup> Numerous materials, including polymers, oxides, carbons, metals, biocomposites and hybrids have also been transformed into hierarchically porous structures.<sup>14–16,147–151</sup> With the increasing interest in industrial applications, much progress has been made in morphological and structural hierarchization of porous materials, such as creation of spheres, fibers, films and monoliths.

Due to the strong interest that exists in this field, a series of recent reviews have been published.<sup>12–19,137</sup> Each of these reviews addresses mainly one type of hierarchically porous material (zeolite based hierarchically porous materials<sup>14–16</sup> or 3 dimensional ordered hierarchically meso-macroporous materials<sup>137</sup>) and their

applications.<sup>14–16,137</sup> Thus, we felt that a comprehensive review, outlining all the synthesis methods would be informative. In Section 2 of the current review, most of the synthesis strategies used to prepare hierarchically porous materials and the key factors involved are covered. In this section is presented the individual synthesis methods and the combination of different synthesis techniques that have been used to prepare hierarchically porous materials with a defined chemical compositions. A series of hierarchically porous structures and their corresponding compositions are then discussed in detail in Section 3. In this section, we illustrate how to use available synthesis techniques (individual methods or combination of different synthesis strategies) to achieve desired hierarchically porous structures (dual porosities: micro-microporous, micro-mesoporous, micro-macroporous, meso-mesoporous, meso-macroporous, macro-macroporous and finally, multimodal hierarchically porous materials such as micro-meso-macroporous, meso-meso-macroporous) for a specific application. We hope that this review will be helpful to those entering the field and also those working in the field who want quick access to helpful reference information related to the synthesis new hierarchically porous materials and the control of their structures and morphologies needed for a defined application.

## 2. Synthesis strategies of hierarchically porous materials

Over the last decade, a great number of researchers have focused their attention on the development of strategies to prepare hierarchically porous materials. As mentioned in the introduction, many procedures have been devised including dual surfactant templating, colloidal crystal templating, polymer templating, bioinspiring process, emulsion templating, SCFs, freeze-drying, BFs, phase separation, selective leaching, replication, zeolitization, sol-gel controlling and post-treatment.<sup>1–9</sup> These methods can be classified into the following two main approaches:

Table 2 Strategies employed for the synthesis of hierarchical porous materials and corresponding morphologies, pores and compositions

Section 1		Section 2	
Synthesis strategies		Hierarchical structures	
Methods	Morphologies	Porosities	Compositions
Surfactant templating	Powders; spheres <sup>a</sup> films; monoliths	Micro-mesopores; dual mesopores; meso-macropores; dual meso-macropores	Oxides; carbon
Colloidal crystal templating	Powders; films; monoliths	Micro-macropores; meso-macropores; dual meso-macropores; dual macropores	Oxides; polymers; carbon; metals; composites <sup>b</sup>
Macroporous polymer templating	Powders; spheres; fibers; tubes; films; membranes; foams; monoliths	Micro-macropores; meso-macropores	Oxides; carbon; metals; composites
Bioinspiring process	Powders; spheres; fibers; tubes; films; membranes; monoliths	Micro-macropores; meso-macropores	Oxides; carbon; composites
Supercritical fluids	Powders; spheres; fibers; films; monoliths	Meso-macropores; multiple macropores	Oxides; polymers; metals; composites
Emulsion templating	Powders; spheres; films; foams; monoliths	Meso-macropores; multiple macropores	Oxides; polymers; carbon; metals; composites
Freeze-drying	Powders; films; foams; monoliths	Meso-macropores; multiple macropores	Oxides; polymers; carbon; composites
Breath figures	Powders; films	Meso-macropores; dual/multiple macropores	Oxides; polymers; metals; composites
Selective leaching	Powders; monoliths	Meso-macropores; multiple macropores	Oxides; composites
Phase separation	Powders; films; monoliths	Meso-macropores	Oxides; carbon; composites
Zeolitization process	Powders; spheres; fibers; films; foams; monoliths	Micro-macropores; micro-mesopores; micro-meso-macropores	Oxides (usually aluminosilicates and titanosilicates) and MOFs
Replication	Powders; spheres; fibers; tubes; films; membranes; foams; monoliths	Micro-macropores; micro-mesopores; micro-meso-macropores	Oxides; carbon; metals; composites
Sol-gel controlling	Powders; spheres; fibers; films; membranes; foams; monoliths	Micro-macropores; micro-mesopores; micro-meso-macropores; dual mesopores; meso-macropores	Oxides; polymers; carbon; metals; composites
Post-treatment	Powders; spheres; fibers; tubes; films; membranes; foams; monoliths	Micro-macropores; micro-mesopores; micro-meso-macropores; dual mesopores; meso-macropores	Oxides; polymers; carbon; metals; composites
Self-formation	Powders; spheres; monoliths	Meso-macropores; micro-meso-macropores	Oxides; composites

<sup>a</sup> Spheres involve spherical structure, core-shell structure and hollow structure. <sup>b</sup> Composites involve mixed oxides, organic-inorganic hybrids, metal-organic hybrids, polymer-based composites and biomaterials.

2.1 Basic Technology	2.1.1 Surfactant templating	2.1.2 Replication	2.1.3 Sol-gel controlling	2.1.4 Post-treatment
2.2 Chemical Technology	2.2.1 Emulsion templating	2.2.2 Phase separation	2.2.3 Zeolitization process	2.2.4 Self-formation
2.3 Replication-related Chemical Technology	2.3.1 Colloidal templating	2.3.2 Bioinspiring process	2.3.3 Polymer templating	
2.4 Physical-Chemical Technology	2.4.1 Supercritical fluids	2.4.2 Freeze-drying	2.4.3 Breath figures	2.4.4 Selective leaching

Fig. 2 Illustration of various technologies, including 2.1 basic technology (inseparable parts of other techniques involving of surfactant templating, replication, sol-gel controlling and post-treatment), 2.2 chemical technology (typical chemical techniques involving of emulsion templating, phase separation, zeolitization process, and self-formation), 2.3 replication-related chemical technology (replication necessity involving of colloidal crystal templating, bioinspiring process and macroporous polymer templating) and 2.4 physical-chemical technology (basis of some physical techniques involving of SCF, freeze-drying, BFs, and selective leaching) and corresponding sections.

(1) on the basis of introducing macro-porous templates in the reaction media together with small scale templates or (2) by combining chemical and physical supplementary methods. Subsequently, an innovative synthesis strategy based on the self-formation phenomenon has been developed. This method takes advantage of the chemistry of metal alkoxides and metal alkyls to generate a porous hierarchy without the use of external templates.

Notably, the use of a combination of two or more of the abovementioned strategies, which take advantage of different structures and properties at the macroscopic or microscopic scale, has been emphasized for use in the future design of hierarchically porous materials. In particular, the surfactant templating, replication, sol-gel controlling and post-treatment are basic techniques or often serve as inseparable parts of other techniques. It is therefore difficult to separately classify each method. For example, the general concept of replication involves all of the synthesis protocols used for preparation of hierarchically porous materials, because it relies on the formation of the pores from replication of a leaching micro-phase including surfactant templating, colloidal crystal templating, macro-polymer templating, and bio-templating. Similarly, surfactant templating including small organic molecule templating has been the most effective approach employed to introduce ordered micropores and mesopores in synthesizing hierarchical structures. Sol-gel and post-treatment methods are also well-known chemical-physical pathways to create certain types of pores. Moreover, nanotechnology and interdisciplinary methods have been combined and integrated into the above mentioned techniques for the design and synthesis of hierarchically porous materials. For example, CO<sub>2</sub> bubble templating has been combined with emulsion templating and supercritical fluids (SCFs) for the synthesis of the hierarchically porous materials. Meanwhile, the use of surfactants as well as controlling sol-gel conditions have been integrated. Again, macroporous polymers obtained by the SCF technique are the macro- and meso-templating agents used *via* sol-gel process.

In this section, we have divided the methods into four types including (see Fig. 2) (1) basic technologies (inseparable parts of other techniques involving surfactant templating, replication, sol-gel controlling and post-treatment), (2) chemical technologies (typical chemical techniques that include emulsion templating, phase separation, zeolitization and self-formation), (3) replication-related chemical technologies (replication based on colloidal crystal templating, bioinspiring process and macroporous polymer templating) and (4) physical-chemical technologies (based on some physical-chemical techniques including SCF, freeze-drying, BFs, and selective leaching). Our objective is to identify the processes, advantages, features and mechanisms of each synthesis strategy. The detailed porous structures and corresponding compositions of hierarchically porous materials obtained by using these strategies (individual or combined) are described in Section 3.

## 2.1 Basic technologies

**2.1.1 Surfactant templating.** Surfactant self-assembled molecular aggregates or supramolecular assemblies have been employed as the structure-directing agents to build porous architectures. Dual surfactant templating, by careful control of phase separation, can be utilized to synthesize the hierarchical pore structure.

The strategy to create two different sizes of mesopores involves dissolving two different surfactants in an aqueous medium. The interaction of the two types of micelles predetermines whether or not a hierarchical mesostructure can be formed (Fig. 3). Dissolving two different kinds of surfactants in water is the key step to fabricate mesoporous structures with different length scales, where the interaction between the surfactants plays a decisive role.

The formation of various aggregates, generated through micellization of surfactant molecules beyond critical micelle

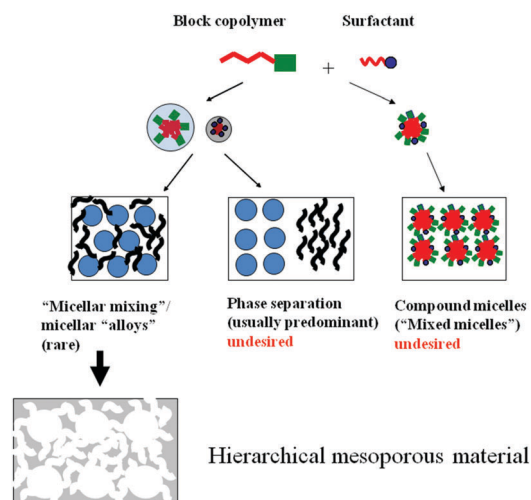


Fig. 3 Illustration of the various ways of co-templating of two surfactants, e.g. using a block copolymer and a low-molecular weight surfactant as templates. Reprinted with permission from ref. 153. Copyright 2011, Wiley-VCH.

concentration (CMC),<sup>152</sup> is driven by the reduction of the free energy of the system, which is caused by reducing contact between the hydrocarbon chain and water in dilute surfactant aqueous solutions (Fig. 3). The water affinities of the surfactant end groups determine the type, sizes and other characteristics of the aggregates formed by the cooperation of many surfactant molecules. The CMC of surfactant aqueous solutions is related to surfactant chemical structure, temperature and/or co-solutes used in the system. In Fig. 3 is illustrated the mechanism of the co-templating of two surfactants used to construct materials with hierarchically porous structures.<sup>153</sup>

Using two surfactants of different molecular dimensions as templates to form hierarchically dual mesoporous materials is a straightforward strategy. Yet, the possibility to form mixed micelles limits the application of this method. There are no reported examples of generating a trimodal mesoporous structure by combining three surfactants.

To overcome the limitation of a three surfactant system, a rigid mold made of macroscopic scale materials or aggregates is used to fabricate hierarchically trimodal porous architectures combined with the dual surfactant templating. This combination is usually called the “true lyotropic liquid crystal approach” (also called nanocasting).<sup>154–158</sup>

In Fig. 4 is shown the typical procedure employed in the true lyotropic liquid crystal approach which results in formation of well-ordered porous materials. The steps involve (i) condensing the precursor with similar polarity around the micelles to replace the solvent and then (ii) removing all the templates, surfactant molecules and macro-temple. A suitable precursor (such as hydrated silicic acid, metal salt or hydrolysable metal species) is always needed in this method to produce materials with perfectly final structures.<sup>159</sup> In general, the polymer colloid is used as a macro-temple to obtain the macropores. The block copolymers (BC) and surfactants (ionic liquid, IL) are used to give robust, very regular superstructured micelles which feature structural motifs on the nanometer scale (lyotropic liquid-crystalline phases),<sup>159</sup> which serve as a template throughout the nanocasting process. The block copolymer self-assembly technique is governed by microphase separation dictated by the mutual incompatibility of the different blocks including in particular water, alcohols or tetrahydrofuran. However, self-assembly of low molecular weight surfactants usually relies on the hydrophobic effect of water.<sup>158–165</sup>

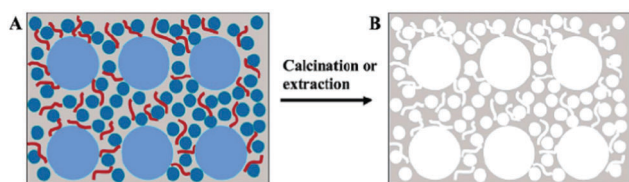


Fig. 4 General templating approach to obtain hierarchically trimodal porous materials with two different surfactant molecules (BC and IL) and polymer colloid. (A) hybrid material (gray, silica; blue, polymer colloid; dark blue, BC micelle; red, IL micelle). (B) Corresponding silica material after calcination or extraction of templates. Reprinted with permission from ref. 165. Copyright 2006, American Chemical Society.

The surfactant templating (sometimes named also nanocasting) approach allows the rational prediction of the pore architecture. Porous silica and metals have been synthesized using this approach.<sup>155</sup> For example, by co-assembly of the polymer colloidal particles, the BCs with a strong hydrophilic/hydrophobic contrast, such as KLE and SE, could result in hierarchical bimodal mesoporous architectures with pores between 6 and 22 nm in the macroporous wall.

**2.1.2 Replication.** The classical method, replication or more precisely called mold or template replication, has received a great deal of attention due to its myriad of applications.<sup>166–168</sup> In particular, carbon replication is the most significant technique. Herein, focus is given mainly to the carbon replication. Indeed, many kinds of rigid and specially designed inorganic templates have been employed to synthesize carbons with uniform pore sizes.

The general template replication procedure for porous carbons involves the following steps: (1) preparation of the carbon precursor/inorganic template composite, (2) carbonization, and (3) removal of the inorganic template. The different approaches taken in this method can be classified into two categories. In the first, inorganic templates such as silica nanoparticles are embedded in the carbon precursor. Carbonization followed by the removal of the template generates porous carbon materials with isolated pores that are initially occupied by the template species. In the second approach, a carbon precursor is introduced into the pores of the template. Carbonization and the subsequent removal of the templates generate porous carbons with interconnected pore structures.

Different from general structural replication, such as opal and inverse opal that have totally opposite structures, the strength of this replication strategy is the injection of a carbon source. This can duplicate the structures of the original template. Because capillary condensation into small pores occurs at low pressure, the carbon precursor is first adsorbed into the small pores (Fig. 5).<sup>169</sup> Obviously, it is important to control the amount of carbon precursor, so that it is selectively incorporated into the framework pores of the silica template. A typical example is the formation of hierarchical mesoporous carbons (meso-nano-C) that are synthesized using hierarchically ordered mesoporous silica (meso-nano-S) materials as templates. Meso-nano-C carbon, obtained as an exact negative replica of the meso-nano-S silica template is composed of 30–50 nm-sized particles with 3D wormhole-like pores.<sup>169</sup>

Because the products have the same structure as the original template, the replication of meso-/macroporous silica enables

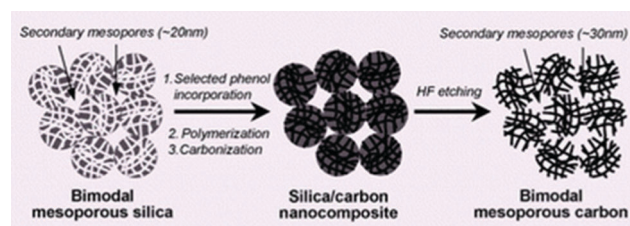


Fig. 5 The schematic of replication for meso-nano-carbon formed by the meso-nano-silica template. Reprinted with permission from ref. 169. Copyright 2003, Royal Society of Chemistry.

the preparation of hierarchical porous carbon with various shapes. The macroscopic shape is controlled by the shape of the silica monolith used as the template, and the macropore diameter can be varied between 0.5–30  $\mu\text{m}$  in a controlled manner.<sup>170–175</sup>

By using the template replication strategy, ordered macroporous carbon with mesoporous walls has also been produced by using aggregates of small silica particles, which are produced by a self-assembled lattice of larger monodisperse polystyrene spheres (PS) (Fig. 6a and b).<sup>176</sup> The size of the large macropores can be manipulated by controlling the diameter of the PS spheres, while the size of the small mesopores is determined by that of the silica nanoparticles. In addition, control of the macroporous morphology of ordered mesoporous carbon has been reported.<sup>177,178</sup> The fabrication of carbon capsules with hollow core/mesoporous shell (HCMS) structures has been obtained using solid cores/mesoporous shell (SCMS) structured silica as a template (Fig. 6c).<sup>12</sup>

By employing this template replication strategy, various mesoporous carbons with hierarchical structures have been prepared, including bimodal mesopores,<sup>169</sup> meso–macroporous monolith,<sup>170–175</sup> photonic crystal structure,<sup>176</sup> core–shell,<sup>12,13</sup>

and even more complex porous structures through the replication of natural template.<sup>179–181</sup> All of the hierarchically porous carbon materials obtained can be used for the preparation of hierarchically porous metals, metal oxides, ceramics and phosphate salts *etc.*

Besides being used for the preparation of hierarchically porous carbon materials, the template replication technology have also been widely employed to synthesize other hierarchically structured porous materials.<sup>173,182–187</sup> For instance, free-standing macroporous nickel films are formed as a replica of the macroporous silicon skeleton<sup>185</sup> The resultant nickel skeleton contains nanopores, making the surface area of the film surface much larger than that of the starting macroporous silicon. Fabrication of hierarchical tube-in-tube carbon nanotubes has also been performed using an anodic aluminium oxide (AAO) film template.<sup>186</sup> An array of mesoporous silica microrods prepared inside macroporous silicon templates with perfluorinated pore walls can easily extracted from the pores.<sup>187</sup> In addition, multi-modal porous  $\text{Co}_3\text{O}_4$ ,  $\text{SnO}_2$ , and  $\text{Mn}_x\text{O}_y$  monoliths can be synthesized by using a template of hierarchically porous silica monoliths.<sup>180,188</sup> The property of the monolith and architecture of the hierarchical pores render these materials interesting for a variety of applications related to the diffusion of gases or liquids, heterogeneous catalysis, gas sensing, and chromatography.

**2.1.3 Sol-gel controlling.** Sol-gel chemistry has evolved into a general approach for preparing porous materials.<sup>189,190</sup> This method typically entails hydrolysis of a solution of a precursor molecule. Generally, a suspension of colloidal particles (the sol) is formed and then a gel composed of aggregated sol particles is obtained. The gel is then thermally treated to yield the desired material and morphologies (such as powder, fiber, film and monolith) (Fig. 7). The chemistry involved in the sol-gel process is based on inorganic polymerization reactions.<sup>191,192</sup> Precursors are usually metallo-organic compounds such as alkoxides  $\text{M}(\text{OR})_n$  ( $\text{M} = \text{Si}, \text{Ti}, \text{Zr}, \text{Al}, \text{etc.}$ ;  $\text{OR} = \text{OC}_n\text{H}_{2n+1}$ ), chelated alkoxides<sup>193,194</sup> or metallic salts such as metal chlorides, sulfates and nitrates. The reaction proceeds through initial hydroxylation of metal alkoxides or metallic salts by hydrolysis of the alkoxy groups or deprotonation of coordinated water molecules.

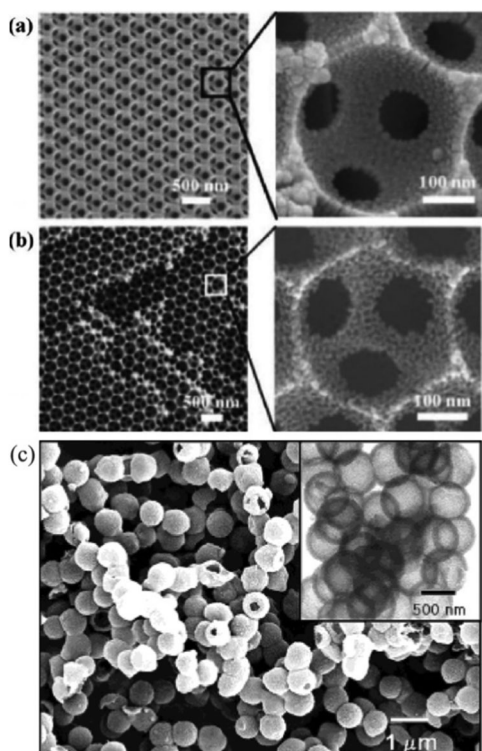


Fig. 6 SEM images at different magnifications of a silica template composed of (a) silica nanoparticles of  $\sim 12$  nm forming the wall of macropores of  $\sim 330$  nm, and (b) the resulting bimodal porous carbon replica composed of macropores of  $\sim 317$  nm connected to small mesopores of  $\sim 10$  nm in. Reprinted with permission from ref. 176. Copy right 2004, Wiley-VCH. (c) SEM image and low-magnification TEM image (inset) of HCMS carbon capsules with core diameters of 500 nm and shell thicknesses of 90 nm obtained from solid cores/mesoporous shell structured silica. Reprinted with permission from ref. 177. Copyright 2002, Wiley-VCH.

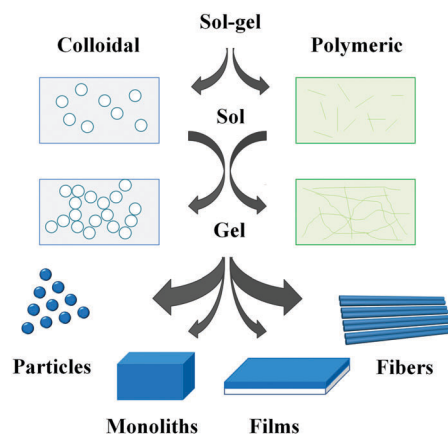


Fig. 7 The schematic of process and products of sol-gel controlling.

Following formation of the reactive hydroxy groups branched oligomers, polymers, nuclei with a metal oxo based skeleton and reactive residual hydroxo and alkoxy groups are generated through polycondensation processes (olation, oxolation).<sup>51,54–56</sup>

These three reactions (hydrolysis, oxolation and ololation) are involved in the transformation of a molecular precursor into a metal oxo-macromolecular network or oxide nanoparticles. Careful control of the sol-gel process directly results in hierarchically porous materials without the need to use additional templates. Sol-gel chemistry can be carried out using the pores of a nanoporous template to obtain tubules and fibrils of a variety of inorganic materials.

The sol-gel control, employed in preparing hierarchically porous materials, can generally be divided into physical assisted methods (such as time) and chemical assisted methods (such as ratio of source). The sol-gel method to hierarchically porous materials is economical and benign to the human health and environment. Some advantageous features of this method are (i) use of nontoxic precursors and solvents (such as silica and aqueous solvents). (ii) Minimization of reaction steps (carefully adjusting ratio of source and time *etc.*). (iii) Room-temperature (or low-temperature) synthesis under ambient conditions and (iv) efficiency for scale-up. The advantageous characteristics of such hierarchically porous materials, especially hybrids, produced using sol-gel control are (i) easy introduction of organic molecules at the nanometer scale inside an inorganic network; (ii) easy creation of entirely new properties (such as optical, electrical, electrochemical, chemical or biochemical);<sup>195,196</sup> and (iii) easy growth of the inorganic extending phase to form nanostructured inorganic or hybrid porous materials.<sup>197–201</sup>

These functionalized hierarchically porous materials often exhibit improved or even unique physical, chemical and other properties. The properties are often achieved through the design and the control of hybrid organic-inorganic interfaces.<sup>202</sup> This approach has proven to be very successful for the controlled design of hierarchical functional 0D, 1D, 2D and 3D materials, such as particles, fibers, films and monoliths. Indeed, using various synthesis strategies it is possible to produce nanostructured materials *via* sol-gel processes with precisely defined and localized functions incorporated into specific positions in order to maximize their properties and interactions with other functions.

**2.1.4 Post-treatment.** The post-treatment approach has been widely investigated to prepare hierarchically porous materials by introduction of secondary porosity. The method is generally divided into three categories. The first involves grafting of additional porous materials on the original porous materials. The second is chemical etching or leaching of the original porous materials to obtain additional pores. The third is assembling or arranging the precursors of porous materials (usually nanosized particles) by chemical or physical assisted method (such as multilayer deposition and ink-jet printing) in order to fabricate new pores. The remarkable advantages of post-treatment are that (i) various functions can be designed to meet different requirements, (ii) multiple structures can be obtained to design organized patterns and morphologies, and (iii) various pore types can be combined to extend desired applications.

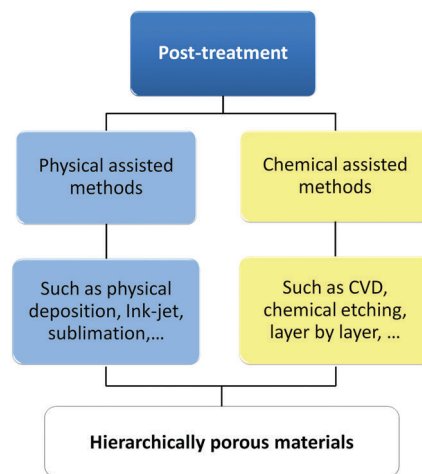


Fig. 8 Classification and corresponding examples of the post-treatment strategy.

Post-treatment can be performed using many methods, such as physical assisted methods and chemical methods (Fig. 8). In this section, we briefly introduce several recent techniques such as ink-jet printing, chemical vapour deposition (CVD) and Layer-by-layer (LBL) of materials, *etc.*

Ink-jet printing to obtain hierarchically porous materials can be achieved by combining silica-surfactant self-assembly to generate mesoporous structures with processing routes. Printing unimodal mesoporous silica on the surface can thus generate a hierarchical structure of mesoporous silica depending on the printing scheme employed. Multilayer printing can create an even more complex hierarchical structure of mesoporous silica.<sup>203</sup> Recently this strategy has been extended to hybrid organosilica with tuneable functionalities.<sup>204</sup> Such hierarchically patterned coatings based on inorganic or hybrid structures could be used to develop hyper-hydrophobic or hyper-hydrophilic coatings and catalytic layers. Moreover, the possibility of using an ink-jet multi-printing head system to graft in “one pot” different organic functionalities from one dot to another is an avenue for fabrication of highly sensitive miniaturized sensors and to applications for heavy metal trapping, artificial noses and molecular recognition applied to the antibody detection for the diagnostic of infections.

Chemical vapor deposition (CVD) is also a technique that can be used to form a solid film. The CVD techniques offer some unique advantages as a deposition process such as excellent uniformity and conformity, high purity, ease of deposition over large substrates, ease of fabricating multi-layered and hetero junction structures, compatibility with manufacturing technology, and many others.<sup>205</sup> By CVD, the additional porous materials can be introduced or grafted on a unimodal or already bimodal porous material to generate new hierarchically porous materials. Many types of precursors are used for this process, including aqueous or ethanolic solutions, molten materials, or gas phase precursors for CVD.<sup>161</sup>

Layer-by-layer (LBL) deposition of charged molecules is a simple and reliable self-assembly technique.<sup>206–214</sup> The key to

deposition of multilayer assemblies is the inversion and subsequent reconstruction of the surface properties. This is achieved by immersing a substrate into a dilute aqueous solution of anionic (or cationic) polyelectrolytes for a period of time to obtain a desired thickness. Next, a substrate covered with adsorbed polyelectrolytes is exposed to a dilute solution of cationic (or anionic) macromolecules, followed by a rinsing step to obtain an irreversibly adsorbed layer. After several dipping cycles, a linear increase of the film thickness is achieved, indicating that the system reaches a steady state regime. The simplicity of the electrostatic self-assembly technique allows fabrication of hierarchically multilayer porous materials from synthetic polyelectrolytes and nanoparticles.<sup>209–211</sup> The multilayer assembly process can be accelerated by utilizing spraying,<sup>214–216</sup> spin-coating,<sup>214,217,218</sup> or printing techniques.<sup>219</sup> These methods have another advantage over the conventional dipping procedure in that only small amount of the solution is needed to cover a large surface area. The layer assembly proceeds through surface overcharging during each deposition step and the film follows a linear growth in both layer thickness and surface coverage with the number of deposition steps. This steady state (linear growth) regime is observed in experiments after deposition of the first few layers. The surface roughness and film porosity depend on the rigidity of the adsorbing species.<sup>220–222</sup>

## 2.2 Chemical technology

The chemical approach to preparing hierarchically porous materials involves only procedures that are based on chemical processes, such as emulsion templating, phase separation, zeolithization and self-formation phenomenon.

**2.2.1 Emulsion templating.** Emulsion templating is one of the most frequently used methods for the preparation of porous materials. Careful adjustment of the oil or water phase of emulsions could lead to the hierarchical structure with pore sizes ranging from nanometers to micrometers. In a typical procedure, the precursor is solidified around the droplets, which is subsequently removed by solvent evaporation to produce the porous materials. In most cases, water is used as one of the solvents. An emulsion can be formed by dispersing water droplets in an oil phase, known as a “water-in-oil (W/O) emulsion”, or dispersing oil droplets in water, known as an “oil-in-water (O/W) emulsion”. Because of the world-wide effort aimed at reducing the use of organic solvents and the sustainable green nature of compressed or supercritical CO<sub>2</sub>, emulsions of CO<sub>2</sub>-in-water (C/W) have been used for preparing porous materials.<sup>223,224</sup>

Emulsion templating is particularly suitable for the synthesis of polymer colloids, porous polymers, or polymer composites. As shown in Fig. 9, when the monomers are dissolved in the continuous phase, monomer polymerization and the subsequent removal of the droplet phase lead to the formation of a porous polymer.<sup>225</sup> To fabricate porous polymers with a hydrophilic surface, W/O emulsions are widely used to tune their porous hydrophobic structures.<sup>226–229</sup> In order to enhance hydrophilicity, a functionalizable co-monomer (such as vinylbenzyl chloride) is added to the non-functionalizable monomer (such as styrene)

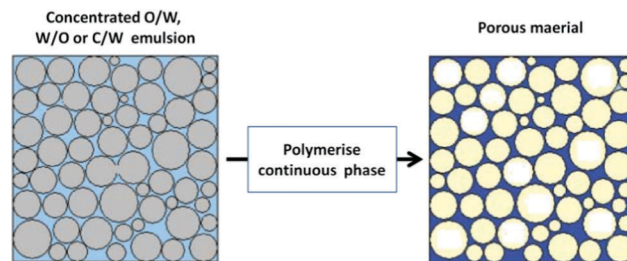


Fig. 9 Schematic representation of polymerization of an emulsion in the continuous phase, for the preparation of, porous materials. Adjusted with permission from ref. 225. Copyright 2005, Royal Society of Chemistry.

in the emulsion. By adjusting the sizes of the droplets, the hierarchically porous materials with the interconnected porosity and a continuous pore size can be obtained.

Microemulsion is a special emulsion templating medium, which utilizes heterogeneous mixtures of one phase in the form of droplets with sizes of 5–50 nm suspended in another immiscible continuous phase. Microemulsion is a thermodynamically stable dispersion stabilized by a surfactant and/or co-surfactants. It is known that there are two types of microemulsions including discrete and bicontinuous microemulsions. Two ways are available to prepare a porous structure by microemulsion. One route uses polymerizable surfactants and the other gelation or freezing of the microemulsion droplets.<sup>230</sup> Because the former can lock the microemulsion structure, it is more useful for the preparation of polymeric colloids or capsules. A few reports have focused on the preparation of porous silica.<sup>231,232</sup> This approach can also be used to create patterned porous and composited structures with dimensions in the range of 10–100 nm.<sup>233–237</sup>

Although it would be interesting to use the microemulsion droplets as templates to build highly porous materials, considerable barriers exist when trying to replicate microemulsions *via* polymerization. A high internal phase emulsion (HIPE) is an emulsion with the volume ratio of the internal droplet phase > 74.05 v/v%. Indeed, HIPEs as templates involve O/W and C/W HIPEs systems, which have been widely used to prepare highly interconnected porous materials.<sup>225–229</sup> In both cases, these micelles are a supramolecular self-assembly of surfactant entities with a concentration above CMC. Because of this, they self-organize within lyotropic mesophases, a hexagonal phase in the present case. To generate macroporous foams, the dispersed phase is washed out in all cases. In an O/W system, emulsions are thermodynamically meta-stable systems. The dispersed and continuous phases will macroscopically phase-segregate with time. To enhance the thermodynamic stability, it is important to use surfactants. As shown in Fig. 10, the surfactant molecules, all with a polar head group and hydrophobic queue, are positioned specifically at the oil/water interface to minimize the interfacial energy. To stabilize these emulsions, the surfactant concentration needs to be always above the CMC. Above this value, the micelles closely pack to generate lyotropic mesophases. Polymerization of the continuous phase and substantial removal of the droplets of the dispersed

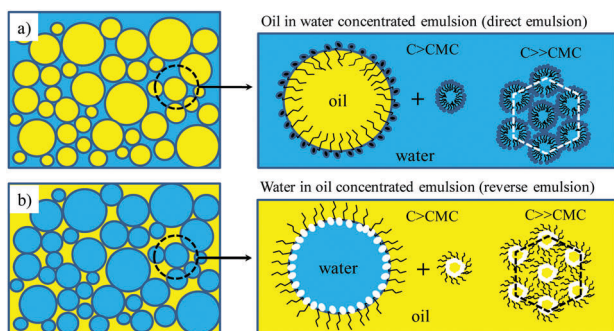


Fig. 10 Schematic representation of: (a) oil in water concentrated emulsion where oil droplets are dispersed within a continuous aqueous phase, (b) water in oil concentrated emulsion where water droplets are dispersed within a continuous oily phase.

phase lead to the formation of solid microcellular foams. These materials are known as polyHIPES. Both organic and inorganic monomers can be used to obtain polyHIPES solid foams. The main goal when developing hybrid materials is to take advantage of the best properties of each component and decreasing or eliminating their drawbacks. This results in the development of new hierarchically porous materials.<sup>238–241</sup>

As a soft templating method, emulsion has been used for the preparation of hierarchically porous materials. The research is highly focused on hierarchically functional porous materials for applications such as tissue scaffolding, drugs/protein delivery, chromatography and supported catalysis.

**2.2.2 Phase separation.** Phase separation is simple method to synthesize porous monoliths *via* the hydrolysis and condensation of inorganic precursors in the aqueous domain of a microphase-separated medium, derived from the self-assembly phase of the template. At first, the phase separation was developed to synthesize macroporous silica through the sol-gel process.<sup>242</sup> This method was extended to siloxane-based organic-inorganic hybrids and metal oxides such as titania, zirconia, and alumina by using a variety of water-soluble polymers, surfactants, or other additives.<sup>243–261</sup> Because most chemically cross-linked rigid (tri- or tetra-functional) networks have controlled inherent porosities, the formation of hierarchically porous materials enables their assembly into a macroporous framework typically on the micrometer scale.

Phase separation in the sol-gel system generates micrometer-range heterogeneity composed of 'gel phase' and 'fluid phase'. After solidification (gelation) of the whole system, the fluid phase can be removed to leave vacant spaces in the micrometer length scale (macropores). The kinetics of the phase separation process in polymer blends and multicomponent glasses can be externally controlled through temperature. The shape and size of the developing phase domains can be blocked by cooling of the system. The process involving structural formation has a spontaneous property similar to that of the chemical sol-gel system. The kinetics of essentially irreversible chemical bond formation governs both the onsets of phase separation and the sol-gel transition. The dissolved starting constituents react homogeneously at a constant temperature in a closed environment

with a predetermined composition in order to avoid evaporation of volatile components.

The dynamics, driven by the interfacial energy, strongly govern the final morphology of the spinodally decomposed phase domains.<sup>262</sup> Sol-gel transition, the key of macropore and mesopore control, is a dynamic freezing process ensured by a cross-linking reaction. The gels with drastically finer phase-separated domains are obtained at higher temperatures due to duplication effects. With an appropriate choice of the reaction parameters, such as starting composition and temperature, the macropore size and volume of the gels can be designed to cover a broad range.<sup>263</sup> The sol-gel phase separation provides monolithic gels that have phase-separated bicontinuous micrometer domains. The rigid inorganic or organic-inorganic hybrid networks are formed during gel-formation. The inherent nanometer length scale vacant spaces filled with solvents in the wet state remain in the continuous gel framework. In order to preserve porosity in the micro- to mesopore regime, the inherent porosity should be augmented by additional treatments, which reorganize the gel network without breaking the existing macroporous framework. Aging in an appropriate solvent can be controlled for converting micropores into larger mesopores in most amorphous gels in the wet state. Typically using tetramethoxysilane (TMOS) as a precursor, phase separation is induced by adding a polar solvent as reported by Kaji *et al.*<sup>264</sup> TEOS is often used and combined with various phase-separation inducers to generate hierarchically porous monolithic materials.<sup>266–268</sup> Moreover, because the domain size is determined by the additive concentration, phase-separation displays an ascending tendency. The volume fraction of the fluid phase can be controlled by the amount of solvent (Fig. 11).<sup>265</sup>

Supramolecular templating is usually used as an attractive assisted method in post gelation aging processes to obtain ordered mesopores in addition to porosity inherent to phase separation. It has been reported that a variety of surfactants induce phase

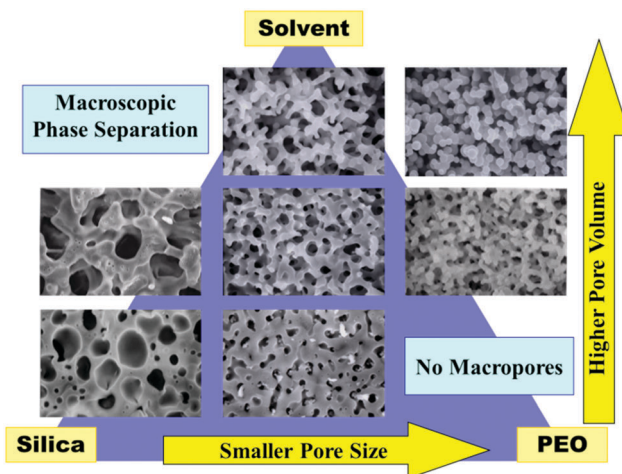


Fig. 11 Relation between coarsening phase-separated domains and structure arrested by the sol-gel transition. The structures observed in resultant gels correspond to those at the bottoms of each row. Earlier sol-gel transition relative to the onset of phase separation results in finer structure. Reprinted with permission from ref. 265. Copyright 2001, American Chemical Society.

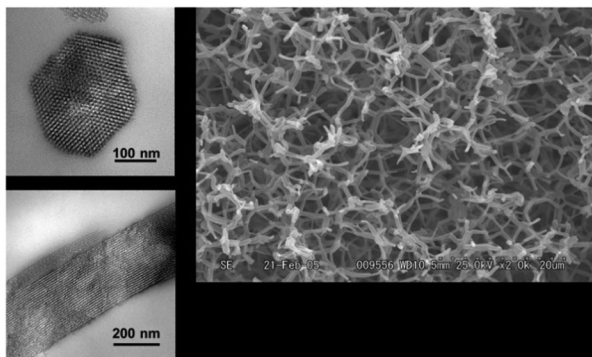


Fig. 12 TEM (right; upper: cross section, lower: longitudinal cross section) and SEM (left) photograph of high-porosity macroporous silica with thin frameworks embedded with fully templated 2D-hexagonal cylindrical pores that are running parallel to the length of the frameworks. Reprinted with permission from ref. 23. Copyright 2008, American Chemical Society.

separation concurrently with sol-gel transition.<sup>119,132,133</sup> The hierarchically porous materials with highly ordered mesopores homogeneously embedded in well-defined macroporous gel skeletons can be obtained through a surfactant templating induced phase separation process (Fig. 12).<sup>23</sup>

In the case of less water-soluble solids such as titania, zirconia, and alkyl-modified silsesquioxanes, aging under severe conditions (such as hydrothermal conditions) is required to tailor the mesopore structure.<sup>108,119,120,134–142</sup>

**2.2.3 Zeolitization.** The zeolitization strategy in combination with other synthesis strategies has been developed to generate hierarchically porous materials. Much attention has been paid in catalysis to the use of this strategy as it provides a zeolite phase in hierarchically porous materials having 2D and 3D microporous structures with large surface area, high adsorption capacity, strong acidity, superior thermal and hydrothermal stabilities, and well-defined pore sizes with excellent shape selectivity in addition to the macroporosities which offer an easy mass transport.<sup>269–282</sup>

The over-growth strategy, based on the control of phase-separation during zeolitization, is used to obtain dually microporous zeolites with hierarchical core/shell structures that can be categorized into three types. The first is the over-growth by isomorphic core (such as ZSM-5/silicalite-1),<sup>283–286</sup> where the core crystals play the structure-directing role. The second is the overgrowth by epitaxial growth, such as zeolite LTA/FAU,<sup>287</sup> MFI/MEL,<sup>288</sup> EMT/FAU,<sup>289</sup> OFF/ERI,<sup>290</sup> MOR/MFI,<sup>291</sup> and CHA/SOD<sup>292</sup> types, involving identical building units with different spatial arrangements. In this route, only some specific crystal faces can be coated, because of the selective overgrowth of zeolite layer. The third is the over-growth on different zeolites, such as FAU/MAZ,<sup>293</sup> BEA/MFI<sup>294</sup> and MFI/AFI<sup>295</sup> types. These are composed entirely of different zeolite structures, resulting in the combination of different chemical and structural properties.

The control of phase-separation during zeolitization can be used to produce hierarchically mesoporous zeolites therefore avoiding the diffusional limitations endured in the small microporous channels. Compared to traditional post-treatment methods

used to synthesize mesoporous zeolites in industrial processes (steaming, leaching with NaOH and HCl solution, and extraction of aluminum species by ammonium hexafluorosilicate (AFS) and  $\text{SiCl}_4$ ),<sup>296–298</sup> the introduction of hard template and soft template during zeolitization provides an important method to fabricate the hierarchical pores in zeolitic materials. It is well known that small molecular templates for zeolites (*e.g.*, tetrapropylammonium and alkali metal ions) tend to form zeolite structures separately, and even presenting other templates such as supramolecular templates. Research has shown that the two different templating systems operate in a competitive rather than a cooperative manner. The method mainly results in the formation of an amorphous mesoporous material, bulk zeolite without mesoporosity, or a physical mixture of two phases.<sup>297,299–301</sup> As a result, restraint and control of phase-separation during zeolitization are the essential problems faced when trying to obtain hierarchical porous zeolite structures (Fig. 13).

It is reported that mesoporous materials with crystalline zeolite frameworks can be synthesized through a crystallization process inside a packed bed of removable hard “solid” nano-templates (*e.g.*, nanoparticles,<sup>302–304</sup> nanotubes,<sup>305</sup> mesoporous carbons,<sup>306</sup> carbon aerogels,<sup>303,307</sup> polymer beads,<sup>308</sup> and other materials<sup>309</sup>). Very recently, a series of solid templates, such as nanosized  $\text{CaCO}_3$ , starch, and bread, have been used for the synthesis of mesoporous zeolites.<sup>118,310</sup> To avoid phase-separation, the synthesis approaches are based on the idea that the small solid template particles are usually pretreated in order to give them surface hydrophilic features, which are easier to assemble to the silica or alumina source during zeolitization.

Compared with hard templates, the use of soft templates for synthesizing mesoporous zeolites using zeolitization is simple if phase-separation can be controlled. This is a big challenge for this synthesis strategy, because soft templates are easy to self-assemble with silica-based species. The hydrophilization of the surface in templating polymers is a good approach to control the existence of phase-separation. Xiao *et al.* have used

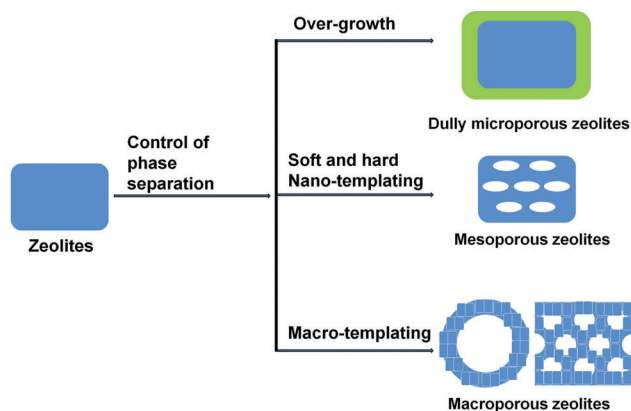


Fig. 13 The zeolitization strategies for synthesizing zeolite with hierarchical structures based on control of phase separation: over-growth to dually microporous zeolites, soft and hard nanotemplating to mesoporous zeolites and macro-templating to macroporous zeolites (left: hollow structure and right: zeolites assemblies with macroporous structure).

hydrophilic cationic polymers such as polydiallyldimethyl ammonium chloride for templating mesoporous zeolites.<sup>311–313</sup> These kinds of mesoscale templates, having a high-density of positive charges, can interact with silica source intensively and easily. The morphology of these templates in aqueous solution is fiberlike, which aid the formation of mesopore channels.<sup>311–313</sup> Pinnavaia *et al.* have synthesized a silylated polyethylenimine polymer as a porogen for the formation of intracrystal mesopores.<sup>314</sup> The presence of  $-\text{SiO}_3$  units on the polymer helps the interaction with the aluminosilicate species in the sol-gel thus avoiding phase-separation.<sup>314</sup> Furthermore, a series of novel strategies have also been developed by Ryoo *et al.* to synthesize mesoporous zeolites using amphiphilic organosilanes as a mesopore-directing agent.<sup>315</sup> The key of this approach is the design of amphiphilic surfactant molecules that contain a hydrolysable methoxysilyl moiety, a zeolite structure-directing group such as quaternary ammonium, and a hydrophobic alkyl chain moiety. [3-(Trimethoxysilyl)propyl]hexadecyldimethylammonium chloride, which contains a surfactant-like long-chain alkylammonium moiety and a hydrolyzable methoxysilyl group, linked together by a Si-C bond. Furthermore, a hexagonally ordered mesoporous zeolite is generated by a surfactant ( $\text{C}_{18}\text{H}_{37}\text{N}^+(\text{CH}_3)_2\text{-C}_6\text{H}_{12}\text{-N}^+(\text{CH}_3)_2\text{-C}_6\text{H}_{12}\text{-N}^+(\text{CH}_3)_2\text{-C}_{18}\text{H}_{37}(\text{Br}^-)_3$ ).<sup>316</sup>

The concept of control of phase-separation during zeolitization has been used with other chemical and physical assisted methods to synthesize hierarchical micro-macroporous zeolite materials, a popular bimodal porous material that includes various hollow zeolite structures and shaped zeolite monoliths. In this method, microsphere is first used as sacrificial template for the formation of the micro/macro porous hollow structure. A secondary hydrothermal treatment can improve the mechanical stability of the LBL-constructed hollow nanozeolite sphere obtained from sphere hard templates.<sup>317–320</sup> Self-supporting micro-macroporous hierarchical materials can be prepared by using a variety of macroporous supports, which have already been employed for robust support,<sup>321</sup> partial zeolitization<sup>322</sup> and complete zeolitization during the formation of micro-macroporous structure.<sup>323,324</sup>

A large number of hierarchically porous zeolites have been produced by using control of phase-separation during zeolitization. These novel materials have not only good acidic and alkaline properties but also the advantages of both large pores (good mass transport) and zeolites (strong acidity). Also, functionalized active sites on the mesopores in zeolite crystals exhibit extraordinary high activities in catalysis.

Metal-organic frameworks (MOFs) are zeolite-related materials with crystalline inorganic-organic hybrid networks. As a result of the combination of metal ions and relatively small organic linkers, the vast majority of MOFs are classified as microporous. Just like hierarchical zeolites, the macropores facilitate mass diffusion, mesopores permit bulk molecules to pass through and micropores offer an abundant number of active sites. Therefore, similar strategies, inspired by traditional zeolites with hierarchical structures, have been developed using meso- and/or macro templating. Co-assembly of structure-directed amphiphilic molecules with metal ion and ligand building blocks results in organic-inorganic

hybrids.<sup>325–332</sup> After template removal by calcination or solvent extraction, ordered or irregular hierarchically porous MOFs can be obtained. The pre-constructed metal oxides can act as hard templates and/or metal sources for the formation of MOF seeds when coordination frameworks, formed by organic ligands with metal ions provided by local dissolution of the metal oxide phase, undergo a secondary growth step in the formation of high quality supported MOFs with hierarchical structure.<sup>333</sup>

It should be noted that MOFs as zeolite-related materials show very special properties for the synthesis approaches to hierarchically porous MOFs, which are largely different from traditional zeolite crystallization (Fig. 14). Ligands, which act as the skeleton in the framework structure of MOFs, can be designed with different sizes, structure and function. So the design of ligands with different sizes on the structures can lead to different lengths of formed chains, which results in unique structures of MOFs with hierarchical micro-mesopores.<sup>334–338</sup> However, it remains a significant challenge to synthesize MOFs with mesoporosity (with pore or channel openings of several nanometres) because of their tendency to reduce or eliminate porosity through interpenetration or other void-filling means. Nanofusion of nanocrystals is another method that is based on the effects of weak interactions of ligands. By using strong stirring, nucleation of large MOF crystals takes place by maximizing the surface between the two mixing phases and permitting multiple coordination between organic ligands and metal cations. This leads to random aggregation of these MOF nanocrystals by nanofusion, and results in appearance of irregular mesopores in the process.<sup>339–341</sup> Recent investigations demonstrated that the kinetic control over the formation and dissolution of nanosized MOFs, or system perturbation, is key to inducing the formation and aggregation of hierarchically porous MOFs.

**2.2.4 Self-formation.** This new self-formation procedure has been thoroughly studied and used to produce hierarchically porous materials.<sup>342–379</sup> These structures are comprised of

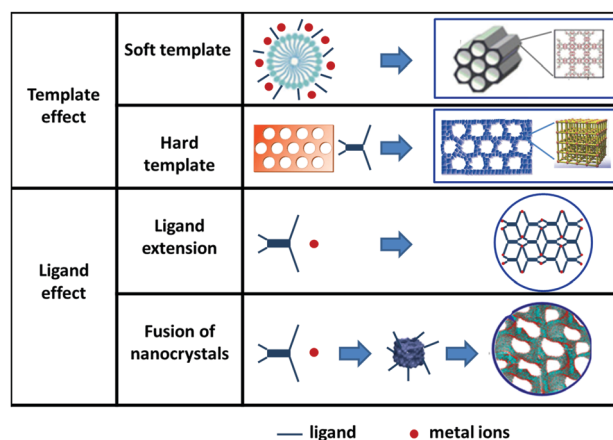


Fig. 14 The strategies for synthesizing MOFs with hierarchical structures based on template effect and ligand effect. Reprinted with permission from ref. 325 for soft template. Copyright 2014, Royal society of chemistry. Ref. 333 for hard template. Copyright 2012, Nature publishing group. Ref. 339 for fusion of nanocrystals. Copyright 2015, American Chemical Society.

parallel macropores with micro/mesoporous walls. A high degree of control over the resulting structural and textural properties of the material is achieved through the use of this synthesis technique. Moreover very pure oxide porous materials can be obtained by starting with just the alkoxide precursors in solutions. Crystalline phases can be easily prepared in the frameworks of macropores.

To explain the formation of these hierarchically porous materials, it is reasoned that adding surfactants contributes to the formation of a double meso–macro-templating interaction that creates a continuous macroporous structure with mesopores aligned perpendicularly to the macropore axis.<sup>255,347,380</sup> However, it is difficult to directly observe the formation of these extended structures of surfactants that result in the formation of macropores. Davis *et al.*<sup>350</sup> have reported the synthesis of ordered macroporous titania by adding dropwise various titanium alkoxides (titanium-ethoxide, -butoxide, -propoxide) to aqueous ammonia in the absence of surfactants. This report indicates that the macroporosity is only dependent on the titanium alkoxides and the solutions used. A microphase-separated domain mechanism was proposed. Su *et al.*, who showed that the spontaneous synthesis of macroporous structures can be conducted at different pH values (neural, acid, and base conditions) in the absence of surfactant. The result indicates that macroporosity is dependent on the characteristics of the metal alkoxide and suggests that the rates of hydrolysis/condensation and/or the nature of the alcohol by-product should be important factors in controlling the preparation pattern.<sup>381,382</sup> On the basis of such a spontaneous phenomenon, a family of hierarchically porous structured materials ( $Y_2O_3$ ,  $ZrO_2$ ,  $Ta_2O_5$ ,  $Al_2O_3$ ,  $Nb_2O_5$ , and aluminosilicates *etc.*) has been developed by Su's group.<sup>345,366,383,384</sup> Meanwhile, a “porogen” concept was proposed. Direct evidences have been provided to confirm the released alcohol and water molecules constitute the so-called “porogen” which leads to the formation of larger water/ethanol macrochannels inside the structure (Fig. 15). As a result, a self-formation mechanism of porous hierarchy has been proposed. The results of an *in situ* study using optical microscopy have proven the self-formation mechanism of porous hierarchically.<sup>345,369–375</sup> This synthesis strategy shows the power of the chemistry of metal alkoxides. Other than metal alkoxides, precursors like alkylmetals can also be used.<sup>345</sup> Funnel-like or straight macrochannels can be formed depending on the reactivity of metal alkoxides because of the sudden release of alcohol and water molecules during rapid hydrolysis and condensation processes. Also, the general synthesis conditions affect the final structures and properties. For example, starting reactant (metal alkoxide), pH values, solvent (water and co-solvent), template (surfactant), synthesis temperature (hydrothermal synthesis) all can be used to vary structures and properties.

Several advantages of this method exist including (1) the direct production of pure oxide materials with hierarchical porosity compared to other synthesis methods, (2) simplicity because this procedure follows a spontaneous route, and (3) facile scale-up to an industrial scale. More importantly, this method can be easily combined with other strategies for the

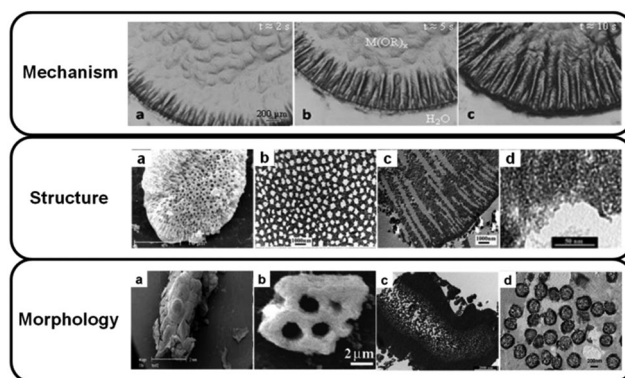


Fig. 15 (mechanism column) Optical microscopy images showing the growth of porosity and formation of a macrochannel pattern. Reprinted with permission from ref. 372. Copyright 2010, American Chemical Society (structure column) (a) SEM image of meso–macroporous  $ZrO_2$ , (b–d) TEM images of meso–macroporous  $ZrO_2$ . Reprinted with permission from ref. 342. Copyright 2003, Wiley-VCH, (morphology column) (a) SEM image of the meso–macroporous products controlled polymerisation of a  $Zr(OC_3H_7)_4$  drop. Reprinted with permission from ref. 366, Copyright 2007, American Chemical Society. (b) Typical SEM image viewed along the direction of the resultant microtubular zirconias, Reprinted with permission from ref. 357, Copyright 2004, Science Direct. (c) Low-magnification TEM image of an ultrathin section of CMI-Ti-80. Reprinted with permission from ref. 346. Copyright 2003, Wiley-VCH. (d) TEM images of as-synthesized bimodal nanoporous aluminosilicates with a hierarchically macroporous core inside an ordered mesoporous shell. Reprinted with permission from ref. 378. Copyright 2009, Wiley-VCH.

fabrication of hierarchically porous materials with specific structures and functions.

It has been demonstrated that the original formation route holds much promise since it is very versatile regarding the chemical composition of the final materials (pure oxides, mixed oxides, carbons) and it also enables fine-tuning of the textural properties of the multiple-sized porosity levels. Further development based on this new and versatile synthesis method is very interesting and necessary. For example, preliminary results have already shown that when combined with templated synthesis, template replicate, or zeolitic crystalline procedure the properties of the final structures and morphologies can be beneficially enhanced (Fig. 15).

### 2.3 Replication-related chemical technology

This technology was developed on the basis of a combination of the basic templating and replication technologies. In this part, colloidal crystal templating, bioinspired process (biotemplating) and polymer templating will be presented.

**2.3.1 Colloidal crystal templating.** In contrast to other approaches, colloidal crystal templating represents a unique route to fabricate materials with well-ordered, periodic pore structures over a large range of size. The porosity resulting from the use of this approach is a direct replica of the periodic array of uniform colloidal particles used as hard template and is easier to be constructed at hierarchical size levels than using other templating methods. When using colloidal crystals templating, additional porosity other than voids of assembled

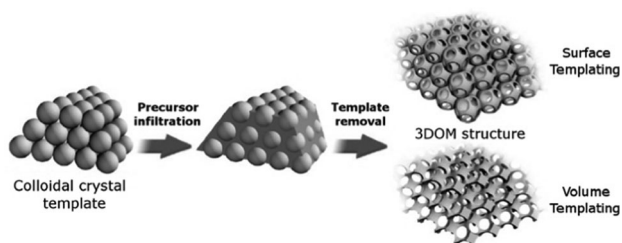


**Fig. 16** Schematic that shows the basic steps in colloidal crystal templating. A surface-templated 3DOM structure is shown at the top right and a volume-templated structure is at the bottom right. Reprinted with permission from ref. 385. Copyright 2007, American Chemical Society.

colloids can be obtained. Therefore, colloidal crystal templating is an exciting path for the preparation of hierarchical materials with innumerable different morphologies and compositions.

The basic steps in colloidal crystal templating are illustrated in Fig. 16, including the formation of a colloidal crystal template, precursor infiltration and template removal. Generally, both surface-templated and volume-templated structures can be produced.<sup>245,246</sup> The three-dimensionally ordered macroporous (3DOM) structures created by surface-templating have an interconnected 'air-sphere' and a strut-like network.<sup>385</sup>

Sol-gel and polymerization are the most widely used reactive solution phase techniques for providing infiltration routes for preparing hierarchical materials. A colloidal suspension can be formed by hydrolysis and condensation of the precursors (the sol), which are then infiltrated into a wholly interconnected network by changing conditions such as pH, temperature or ionic concentration (the gel).<sup>386</sup> Through polymerization, monomers, oligomers and polymers can also be cross-linked into interconnected networks. As an example, metal nitrates and ethylene glycol are infiltrated into the interstitial void space of a colloidal crystal where they react during calcinations to form a glyoxylate.<sup>387</sup>

There are many other reactive solution phase techniques, including nanoparticle suspension, electrochemical deposition, CVD and atomic layer deposition (ALD). The nanoparticle suspension technique is a handy process for infiltration of colloidal crystal templates with nanoparticles by immersion of a colloidal crystal in a suspension of nanoparticles and then evaporation of the supernatant. This technique offers several advantages compared to the former ones including (i) small particles can be freely deposited in the template, (ii) the precursor can avoid the demand in the processes of condensation and crystallization,<sup>249,250</sup> and (iii) problems with rapid condensation and precipitation reactions that obstruct infiltration can be also avoided. For example, 3DOM structures for possible photonics applications have been synthesized by using suspensions of titanium oxide nanoparticles. CVD and ALD techniques are widely used to synthesize and modify 3DOM materials.<sup>245,249</sup> 3DOM carbon displays an excellent performance as a lithium ion battery anode material after being coated with silicon *via* CVD using disilane  $\text{Si}_2\text{H}_6$ ,<sup>388</sup> 3DOM cerium oxide back-filled with titanium oxide by ALD to form core-shell 3DOM networks has been synthesized and shown to

have enhanced photocatalytic activity.<sup>389</sup> By using the electrochemical deposition technique, 3DOM Ni films were made that have good stability and reduced over potential for water splitting<sup>390</sup> and 3DOM/Ge films have high refractive index contrast for photonics applications.<sup>391</sup> By using a similar method, our group prepared a series of 3D hierarchically meso-macroporous inverse opal structures for photocatalysis.<sup>89–91,392,393</sup>

A wide range of techniques have been developed to synthesize hierarchical 3DOM materials with intrinsic secondary porosity. Sol-gel synthesis is a common approach providing 3DOM materials with disordered intrinsic secondary porosity. Generally, ordered intrinsic secondary porosity can be obtained by utilizing surfactant template such as cationic surfactant templates, non-ionic surfactant templates and ionic-liquid surfactant templates. For example, Holland *et al.* synthesized the 3DOM silica xerogel contained mesopores with a wide range of diameters.<sup>308</sup> Velev and co-workers have obtained gold flakes with hierarchical porosity.<sup>394</sup>

Through disassembly and reassembly of three-dimensionally ordered macroporous materials with mesoporous walls (3DOM/m), researchers have created materials with more complex hierarchical porosities. Using the disassembly process, nanoparticles with other compositions (*e.g.* PF resin, carbon, carbon-silica, PMMA and certain transition metal oxide-phosphate glass composites) can be formed.<sup>395–398</sup> Self-reassembly of the particles into ordered arrays can be achieved after disassembly of the 3DOM/m structure.

Combining superior features including high surface areas, effective mass transport, nanoscale structural dimensions, and, in some situations, tunable optical properties, the materials synthesized using the colloidal crystal templating approach have great prospects for a number of applications. These include fuel cells,<sup>176,399</sup> capacitors and battery electrode materials,<sup>400–402</sup> supports for catalysis,<sup>403</sup> sensing materials that produce optical responses to analytes,<sup>404,405</sup> materials that have altered luminescence and lasing properties,<sup>406–408</sup> super hydrophobic materials<sup>409,410</sup> and materials with enhanced electrochemical performance.<sup>411,412</sup>

**2.3.2 Bioinspired processes (bio-templating).** A large number of biological materials with porous structures have perfect properties that result from their functional hierarchical porous structure at different levels.<sup>413</sup> To date, similar synthetic materials have been fabricated through the direct replica of natural materials or biomimetic strategy of spontaneous assembly process. Both of these approaches can be defined as bioinspired processes (Fig. 17). However, the preparation of porous materials using bioinspired approaches still faces multiple challenges.

A rich variety of natural materials with hierarchically porous architectures are utilized as direct biotemplates owing to their low cost and environmentally-friendly properties. Of these materials we cite bacterial threads,<sup>414</sup> echinoid skeletal plates,<sup>415</sup> eggshell membranes,<sup>416</sup> insect wings,<sup>417</sup> pollen grains,<sup>418</sup> plant leaves,<sup>419</sup> wood celluloses,<sup>420,421</sup> protein aggregates,<sup>422</sup> spider silk,<sup>423</sup> diatom,<sup>87,424</sup> and other bio-inspired systems.<sup>146,425</sup> Some studies have used native or chemically treated plant components as templates to fabricate many hierarchically porous materials. In the preparation process, the solutions of inorganic precursors are adsorbed by the plant cell walls through capillary adsorption

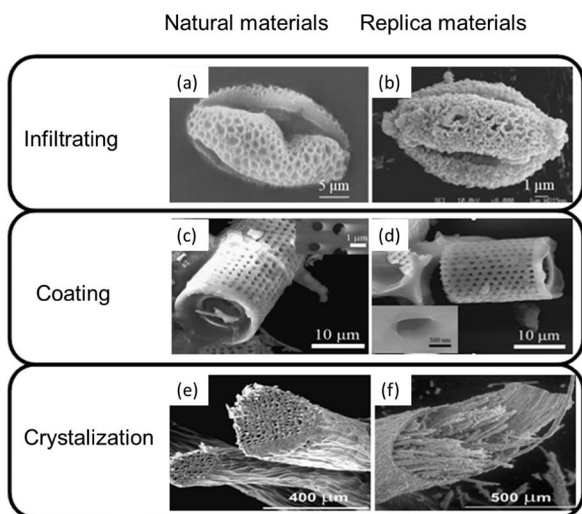


Fig. 17 SEM images of uncoated pollen grain (a) and inorganic replica consisting of silica (b). Reprinted with permission from ref. 418. Copyright 2002, Royal Society of Chemistry. SEM images of initial diatomite (c) and  $\text{TiO}_2$  coated diatomite, TCD5 (d). Reprinted with permission from ref. 427. Copyright 2008, Elsevier B. V. SEM micrograph of the Luffa sponge struts (e) and the silicalite-1 replica of Luffa gourd (particular of the struts) (f). Reprinted with permission from ref. 428. Copyright 2006, Elsevier B. V.

and inorganic materials are deposited on the cell walls.<sup>280,287–291</sup> The inorganic replica maintains the characteristics of porous architecture of the natural templates after the removal of plant components by treatment at high temperatures.<sup>426</sup>

Infiltrating, coating and crystallization are the three main approaches to replicate the biotemplates. Infiltration of nanoparticles or solids is the key step in the synthesis process for fully replication of all hierarchical levels of biological materials.<sup>421,429</sup>

Coating inorganics to the surface of biotemplates followed by calcination at high temperature to remove the template is also a versatile strategy to obtain biomorphic hierarchical porous materials.<sup>179–181</sup> Hierarchical meso-/macroporous  $\text{TiO}_2/\text{SiO}_2$  composite materials fabricated by using LBL coating of  $\text{TiO}_2$  nanoparticles on the surface of diatomite using phytic acid as molecular binder has been demonstrated.<sup>427</sup> The final  $\text{TiO}_2$  nanocrystals are uniformly dispersed on the surface of diatomite and the macroporous structure of the initial diatomite is well preserved in the process.

Crystallization or semi-crystallization of the biotemplate scaffold is an effective approach for replicating the porous structure of biological materials. Hierarchically micro-/macroporous or micro-/meso-/macroporous materials have been fabricated through zeolitization on some biotemplates that have special porous morphologies.<sup>428</sup> The synthesis procedures involve two steps including (1) *in situ* seeding or coating the templates with zeolite nanoparticles and (2) subsequent attachment and a hydrothermal growth of zeolite crystals.<sup>430</sup> Various methods have been applied for the crystallization of biotemplates, such as LBL electrostatic assembly of zeolite nanocrystals on the substrate and transforming the precursors into zeolite by a vapor-phase transport (VPT) method.<sup>431,432</sup>

Furthermore, the concept of bioinspiration has not only been employed to replicate the specific meso/macroporous morphologies of the biotemplates, but also to learn how spontaneous assembly or growth of natural materials takes place to generate remarkable properties and structures. As a result, the biomimetic strategy using common surfactants instead of the employment of biotemplates has also been developed to synthesize hierarchical porous materials.

The formation mechanism of the porous structure of (bio) polymer-silica particles has been investigated.<sup>433</sup> In Fig. 18 is shown a model for silica biomineralization in diatoms, which seems to be mediated by peptides and polyamines.<sup>299,300</sup> Silica from acidified water glass in the presence of structure directing agents directs the main silica formation in diatoms. The course can be adjusted by varying the concentration of dissolved silica and the pH of the medium. This method is a reversible strategy to fabricate other multiple-scaled porous materials.

The preparation of hierarchically meso-/macroporous materials through bio-inspired process can be classified into two different groups distinguished by whether or not surfactant is used. In the latter case, the macropores are generated by microphase separation of water/oil domains and mesocellular foam structure are formed through the generation of titanium phosphonate sols composites.<sup>381,433–435</sup> The oil phase is comprised of surfactant molecules or created by the hydrolysis of titanium tetrabutoxide precursors in the surfactant-free system.

The bioinspired approach is promising due to many advantageous features of the natural templating materials such as

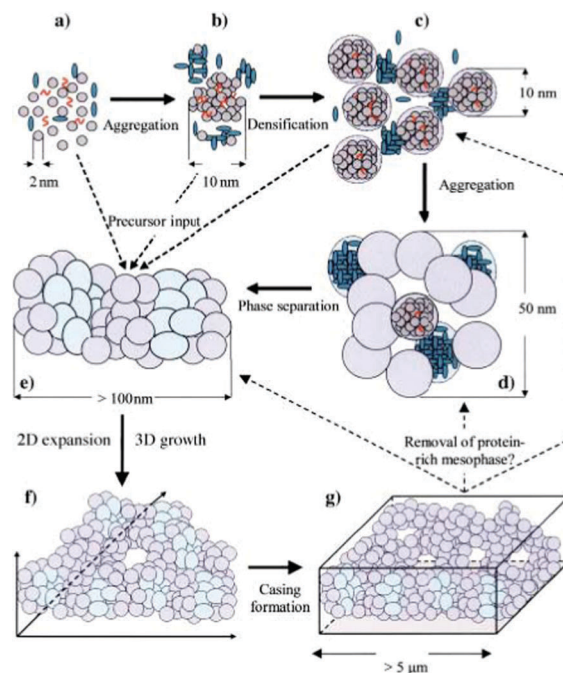


Fig. 18 (a–g) The proposed model of mesophase silica polymerization in diatoms, based on the polymer- and peptide-directed silica syntheses, in which red curved structures, green ellipsoids, and gray spheres denoted for small peptides and/or polyamines, larger organic molecules and small silica sols, respectively. Reprinted with permission from ref. 433. Copyright 2002, Wiley-VCH.

large macroscopic scale, large quantity and reproducibility, low cost and eco-friendliness. The prepared materials with hierarchical porous structures demonstrate good mechanical and thermal stabilities, and some of them even show outstanding optical properties.

However, an important drawback of the biotemplating method is scale up of the production of hierarchically porous materials due to (1) the lack of large quantity of biotemplates, (2) the problem of reproduction, (3) the difficulty to get a homogeneous infiltration in biotemplates in large scale and finally (4) the difficulty of manipulation in large scale.

**2.3.3 Polymer templating.** Polymeric structures that contain macropores can be used as templates for fabrication of hierarchically porous materials. The macroporous polymer plays the role of a scaffold around or within which chemical reactions can take place or nanoparticles can infiltrate, thereby guiding the morphology of the materials. After removal of the polymer, the material retains the structural properties of the original template.

In Fig. 19 is illustrated the routes for the polymer guided preparation of structures. Route 1 involves infiltration with preformed nanoparticles, which pack onto the surface of the polymer structure giving a coating of the polymeric template with interparticulate pores and pores provided by the template (a). Route 2 uses infiltration of a precursor solution that produces porous particles (b) with interparticulate pores along with the macropores of the initial template, nonporous particles (c) with interparticulate pores along with the macropores of the initial template (coating) or nonporous particles (d), with interparticulate pores, formed within the macropores of the initial template, with pores generated as a result of the removal of the polymer strands (casting). Route 3 demonstrates the use of infiltration of a precursor solution containing an additional porogen. This route results in two pore structures, one from the porogen and the other is from the original template whose nature is dependent on whether (e) a coating or (f) a casting process is taking place. It includes the use of monolithic polymer gels prepared by the polymerization of monomers in the presence of surfactant as templates for the fabrication of hierarchical materials, such as  $\text{ZrO}_2$ <sup>436</sup>  $\text{TiO}_2$ <sup>437</sup>  $\text{Al}(\text{or V})/\text{TiO}_2$ ,  $\text{Al}(\text{or V})/\text{ZrO}_2$ <sup>438–440</sup> and  $\text{Au}/\text{TiO}_2$ <sup>441</sup> and  $\text{La}_{0.65}\text{Sr}_{0.3}\text{CoO}_{3-\delta}$ .<sup>442</sup>

When gels prepared from polysaccharides are used as templates to fabricate materials pores across the nanometer to

micrometer scale are generated. Polymer foams produced in this manner have a variety of pore sizes ranging from hundreds of micrometers to a few micrometers to submicrometer.<sup>443–447</sup> The monolithic materials can thus be prepared *via* growth on or replication of the polymer foam. Based on a similar concept, the fabrication of porous films, fibers and beads has been demonstrated with a variety of pore morphologies by using macroporous polymer films as templates.<sup>448–454</sup> The use of macroporous polymer templates has been extended to many oxides (such as  $\text{SiO}_2$ ,  $\text{ZrO}_2$ ,  $\text{TiO}_2$ ,  $\text{Al}_2\text{O}_3$ ,  $\text{Fe}_2\text{O}_3$ ,  $\text{In}_2\text{O}_3$ ,  $\text{SnO}_2$  and  $\text{Ce}_2\text{O}_3$ ), composites, and metals *etc.*

It is clear that the use of multitude of templates have led to production of materials that have diverse structural characteristics, including sphere, fiber, film and monolith structures. The morphology of the macroporous polymer strongly affects the structure of the final material. In addition to the macroporous texture of the final products being determined by the polymer, the mesopores are formed by the aggregation of inorganic species and surfactant templating or a combination of both. In some products, the micropores are introduced by the zeolite. Interestingly, mesopores formed by aggregation of inorganic particles are often characterized by a disordered structure, that can be ordered through use of a surfactant template. Even though controlling the morphology of a material is an art, the change in properties brought about by morphology changes is paramount to the application of these materials.

## 2.4 Physical–chemical technology

The physical–chemical technology includes procedures that use a chemical process first followed by a physical process or the reverse order. For example, the system obtained after a chemical reaction, is subject to a physical step such as treatment with a supercritical fluid (SCF), freeze drying, Breath Figures (BFs) or physical mixing (mechanical or temperature sintering effect) followed by selective chemical leaching.

**2.4.1 Supercritical fluids (SCF).** This technique, which employs just water and  $\text{CO}_2$ , has a wide application because it allows the synthesis of materials with well-defined porous structures without the need to use volatile organic solvents. Removal of the droplet phase is very simple because  $\text{CO}_2$  reverts to the gaseous state upon depressurization. Although the mechanism and method of formation of the hierarchically porous materials using SCF techniques have been thoroughly developed, more experimentation and the development of reliable models of these processes are still required.

Supercritical fluids, which are neither gases nor liquids, can be compressed gradually from low to high density. As a result, they are important and interesting as tunable solvents and reaction media for chemical processes. The SCF technology is a very important method for the synthesis and processing of porous materials with hierarchical structures.<sup>455,456</sup> Several advantageous features of this method are that mass transfer can be improved and surface modification of porous materials can be facilitated because SCF and in particular  $\text{CO}_2$  are extremely versatile wetting agents due to their low surface tension. The reaction conditions, such as temperature, pressure and co-solvents, can be

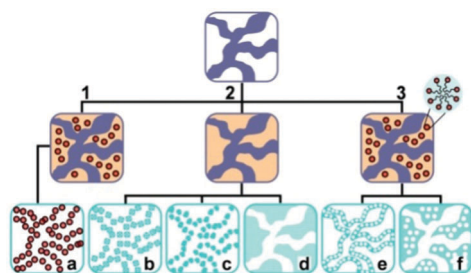


Fig. 19 Templating of a polymer (purple) structure containing macropores (white).

easily tailored for the design of a certain morphology and functionality of porous materials. Most importantly, pore collapse can be avoided because SCF do not give rise to a liquid–vapor interface. The SCF approach utilizes environmentally benign solvents or porogens, such as cheap and non-toxic CO<sub>2</sub>, which can be used alone or combined with small amounts of modifiers. The solvent recovery costs are low, which also leads to energy savings. Removal of the fluid template is easy (for example, CO<sub>2</sub> is a gas under ambient conditions). The use of SCFs allows fast rates to be obtained under mild conditions.

The production of hierarchically structured porous materials using SCF techniques is still at an early stage of development. A large effort has been given to obtaining new materials and demonstrating the potential of processes such as foaming, CO<sub>2</sub> induced phase inversion and supercritical fluid emulsion templating. Polymer foams are formed when a polymer, plasticized by saturation in a supercritical fluid is rapidly depressurized at a constant temperature. As pressure is released, pockets of gas nucleate and grow in the polymer. As the supercritical fluid leaves the polymer, the  $T_g$  (glass transition temperature) increases, generating nuclei due to supersaturation, which grow to form a cellular structure until vitrification occurs. In Fig. 20a is shown a schematic representation of the foaming process. The foam production technology is well established and processes are ready for applications. Membrane production by using a supercritical CO<sub>2</sub> (scCO<sub>2</sub>) induced method is also a very promising application. When a solution of polymer is first immersed as a film into a coagulation, a skin forms at the interface (Fig. 20b). As time proceeds, changes in the concentration occur in the layers further away from the interface, but less rapidly than the interfacial changes. The rate at which the changes occur in the sub-layers has a profound effect on the structure of the derived material. Owing to its variable (with pressure or temperature) solvent density and viscosity, the ‘tunable’ solvent power of the supercritical fluid is a serious advantage when compared with the use of traditional solvents. SCF emulsion templating is also a versatile method to form well-defined hierarchical materials. The basic procedure is summarized in Fig. 20c.

**2.4.2 Freeze drying.** The freeze-drying process described here often mimics the process occurring in natural systems.

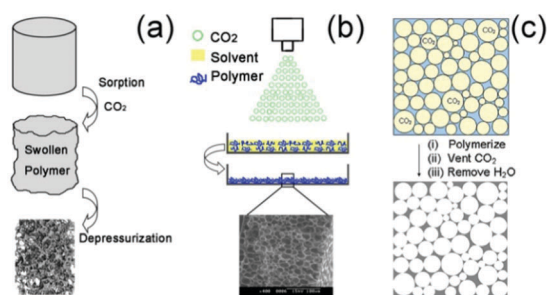


Fig. 20 (a) Schematic representation of the foaming process using scCO<sub>2</sub>, (b) schematic representation of the CO<sub>2</sub> induced phase inversion method, (c) schematic representation of the CO<sub>2</sub>/water emulsion templating process. Reprinted with permission from ref. 457. Copyright 2011, American Chemical Society.

This phenomenon is critical for various applications, such as the cryopreservation of biological cell suspension. Freeze-drying (also known as ice-templating) has been used to fabricate hierarchically porous, complex-shaped polymeric or ceramic supports.<sup>458–460</sup> In the freeze-drying process, a ceramic slurry is poured into a mould and then frozen. The frozen solvent acts as a porogen to generate large pores and also temporarily as a binder to hold the support together for de-moulding. Subsequently, the demoulded part is subjected to freeze-drying under vacuum to sublime the solvent. This avoids drying stresses and shrinkage that lead to cracks and warping often incurred in normal drying. After drying, the compacted material is sintered in order to fabricate a porous material with improved strength, stiffness, and a desired porous microstructure. By controlling the direction of growth of the ice crystals, it is possible to create a preferential orientation of the porosity in the final material.

The freeze drying technique has many advantages. The first is associated with the use of green templates including aqueous solutions, and water ice crystals as templates (or so called ‘porogens’ and ‘pore former’). This is particularly beneficial for biological applications. Second, freeze drying ensures a ready preparation of purified products because the freeze drying process does not bring impurities into the samples. Third, by changing conditions during freezing a wide variety of porous structures can be constructed including numerous pore morphologies and nanostructures (from 2D to 3D structure). Fourth, it is generally applicable to the preparation of various materials including ceramics, polymers, composites and hydrogels.

Macroporous ice-templated polymeric materials were first reported more than 40 years ago.<sup>461,462</sup> Their properties, which differ from those created using polymer gels, soon attracted great attention. Since then, many different polymers (*e.g.* poly(L-lactic acid) and poly(DL lactic-co-glycolic acid)<sup>463,464</sup> gelatin,<sup>465</sup> g-PGA/chitosan,<sup>465–467</sup> collagen and elastin,<sup>468</sup> collagen-glycosaminoglycan,<sup>469</sup> and polyvinylpyrrolidone (PVP) hydrogels,<sup>470</sup> among others) have been constructed using this method. Because of its biocompatible features, this process has been widely used to construct materials employed in biomedicine (*e.g.* for tissue engineering and drug delivery purposes). Since 1980, numerous studies (albeit less than for polymers) have been directed at developing the ice-templating processes for the preparation of different porous ceramic materials with a uniform microstructure.<sup>471–476</sup> In addition to examples of its use to form polymers and ceramics, the process has been applied to composites. This has led to a new class of functional properties including hydroxyapatite (HAP)/collagen<sup>477</sup> (or cerium oxide/poly(vinyl alcohol) (PVA) or PVA/silica).<sup>478</sup> Other hybrid materials, such as silica hydrogels containing proteins or liposomes<sup>344,346</sup> have also been synthesized. The former material, comprised of an esterase protein (pig liver esterase, PLE) dispersed in a poly(vinyl alcohol) (PVA)/silica hybrid hydrogel, is a hierarchical biohybrid material that has a very sophisticated structure with up to six levels of spatial organization. The structure is very similar to that of polymers and ceramics. The addition of micro- or nanoparticles can be justified for several reasons, such as improvement of mechanical properties or activation of catalytic properties.

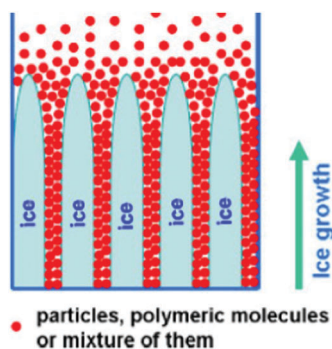


Fig. 21 Schematic representation of the directional freezing process. Ice crystals grow in one direction and the solutes (such as particles, polymeric molecules or mixture of them) are excluded and solidified between the crystals. Reprinted with permission from ref. 479. Copyright 2007, Wiley-VCH.

The freeze-drying process is an excellent and well-defined technique for the fabrication of hierarchically structured porous materials. This method consists of the freezing, retaining the frozen state, and defrosting precursors (or colloid systems), and forming a water solution (or suspension or a hydrogel). Therefore, the solute molecules originally dispersed in the aqueous medium are expelled to the boundaries between adjacent ice crystals (Fig. 21),<sup>479</sup> a phenomenon caused by the formation of crystalline ice (hexagonal ice, typically).<sup>479</sup> While high-vacuum sublimation of ice occurs, freeze-drying gives rise to a macroporous matter. The achievement of monoliths that preserve the size and shape of the container submitted to freezing also takes advantage of the freeze-drying process.

Solvent crystals grow and solute molecules are excluded from the frozen solvent until the sample is completely frozen during the freezing step. Different conditions of freezing, including the temperature, solute concentration, solvent type and direction of freezing, can have a great impact on the resulting pore structure of the materials. The directional freezing<sup>325,345,347</sup> and the growth of solvent (ice) crystal can be controlled. The drying step usually requires the greatest time in the overall process. This time requirement is directly related to the solvent (ice) sublimation rate and is determined by factors such as level of vacuum, shelf temperature, sample volume and exposed surface area, and product resistance.<sup>480</sup>

Tamon and co-workers<sup>481,482</sup> first studied the main process by controlling different variables to tailor the final morphology.<sup>483,484</sup> The structural heterogeneity of the sample in the freezing direction was one of the most interesting observations made (Fig. 22). Three distinct zones can be clearly distinguished in the samples, each characterized by a particular pore shape and dimension. No porosity is observed in zone 1, the closest to the initial coldfinger, and the material in this zone is dense. In zone 2, the material has a cellular morphology. Finally, in zone 3, the ceramic is lamellar with long parallel pores aligned in the direction of movement of the ice front.

Because of the advantages associated with the avoidance of toxic organic solvents and the low experiment temperature during the freeze drying processes, it is believed that applications of this

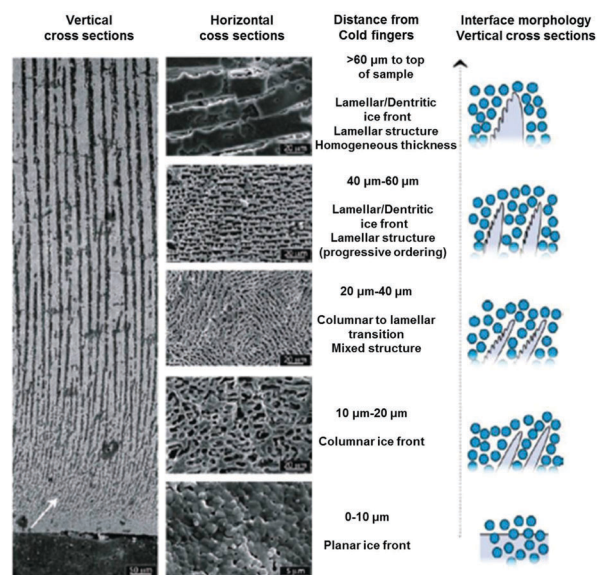


Fig. 22 SEM micrographs of the evolution of the ice-front morphology and final microstructure. Homogeneous layer thickness is attained at about 200–250 mm above the immersion level—the layer thickens progressively with the separation from the immersion level and then becomes constant. Tilting of the lamellae in the first frozen zone can be observed near the immersion level, at the bottom of the vertical-section micrograph (white arrow). The horizontal cross section (parallel to the ice front) micrographs reveal the corresponding evolution of the porous structure and hence the interface morphology (depicted diagrammatically on the right). Reprinted with permission from ref. 484. Copyright 2007, Elsevier B.V.

method will be further investigated. For example, its application to cryopreservation of biological cell suspensions and the purification of pollutants would be interesting. Also, the combination of hierarchy and functionality opens up the possibility of application of these “green” materials to a variety of novel applications in such fields as biotechnology (*e.g.* biosensors and biocatalytic systems for organic synthesis and fuel cell technologies) and biomedicine.<sup>485–487</sup>

**2.4.3 Breath figures.** It has been observed that water molecules in humid air condense on a cold surface and the water droplets pack into ordered hexagonally arranged patterns. This phenomenon is also widely known as Breath Figures (BFs). Only recently, ordered porous (also called honeycomb-structured) films have been prepared by using BFs by using water droplets as templates.<sup>488–505</sup>

BFs have been studied for almost 100 years.<sup>488,506–508</sup> This method, also called “moist-casting”, involves polymer casting from a solution under moist ambient conditions. Cooling the solution surface, caused by solvents evaporation, enables condensation of water droplets followed by their growth and spontaneous ordering on the surface. Subsequent complete evaporation of both the solvent and water results in formation of 2D<sup>488–501</sup> or even 3D<sup>502–505</sup> arrays of often hexagonally ordered air bubbles (droplet imprints), and trapped in the polymer matrix. This technique for film structure formation is extremely attractive as it allows the production of porous materials with pore sizes that are easily tunable by varying the

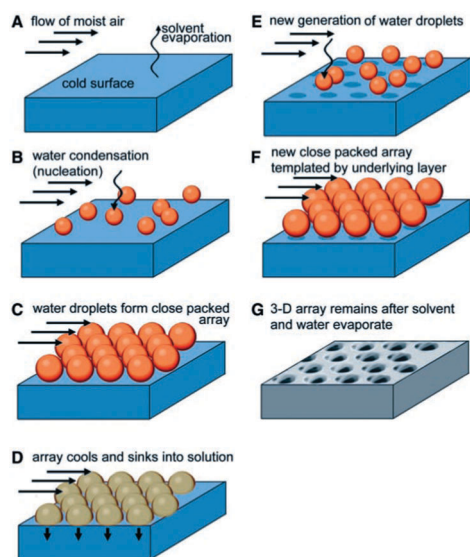


Fig. 23 A scheme showing the formation mechanism of ordered porous films via the BF templating approach. Reprinted with permission from ref. 502. Copyright 2001, American Association for the Advancement of Science.

preparation conditions from 0.2 to 20  $\mu\text{m}$ ,<sup>488–505</sup> such as polymer, biocomposites and composites.

In Fig. 23 is shown the mechanism for formation of the ordered porous films. Evaporative cooling leads to the generation of hexagonally packed water droplets in the polymer solution. When samples are generated from a solvent denser than water, such as carbon disulfide ( $\text{CS}_2$ ), only a single layer is formed. In contrast, when a solvent with a density lower than that of water is used, such as benzene or toluene, the hexagonal array propagates through the film and a 3D structure is formed. The water droplets are stabilized by the polymer in solution and thermocapillary flow arranges them into ordered 3D arrays. The 3D ordered structures are preserved after the organic solvent and water evaporate to solidify the films.

Compared with those on a solid surface, interactions between water droplets and a liquid surface are different because the substrate is locally mobile and curved. Knobler and co-workers suggested that the growth of BFs on liquids evolves through three stages.<sup>509</sup> The first stage involves nucleation and growth of droplets as isolated objects with weak interdroplets interactions. The average diameter  $D$  of droplets increases with time  $t$  following the rule  $D \sim t^a$ ,  $a \approx 1/3$ . At the second stage, maximal surface coverage by water droplets is achieved. The droplets are separated by a liquid film, giving rise to a short ranged hard-sphere-like interaction and leading to uniformity in the size of the droplets. The third stage involves constant surface coverage and coalescence between droplets. The growth rule at this stage follows  $D \sim t^a$ ,  $a \approx 1$ . To form honeycomb structured porous films by BF templating, the hexagonally packed water droplets need to be stabilized by polymer in the organic solutions in order to avoid or reduce the coalescence of the droplets. The dry porous films are formed by precipitation of the polymer around the water droplet during evaporation of the organic solvent and water.<sup>510</sup>

The nature of a solvated polymer greatly influences the formation of porous films.  $\text{CS}_2$  is a good solvent for conjugated polymers, star-/block PS and carboxy-terminated PS while droplet arrays are obtained for PS solution in chloroform, nitrocellulose in amyl acetate and fluorinated polymers in Freon-type solvents. Benzene, toluene and xylene also give good BF arrays<sup>511</sup> with different systems. Honeycomb-structured porous films with pore sizes ranging from 200 nm to 7  $\mu\text{m}$  can be prepared by using BF templating. The formation of porous films of this type *via* BFs with different polymer architectures were reviewed by Stenzel *et al.*<sup>510</sup> BF was described as a dynamic templating method for polymers and nanomaterials.<sup>511</sup>

Utilizing the BF templating approach, some interesting materials such as nanoparticle suspensions without polymer to produce BF-patterned films, have been generated.<sup>512–514</sup> The BF templating method can be used to prepare dodecanethiol-capped macroporous gold (constructed by nanoparticle) with pore diameters from 1.7 to 3.5  $\mu\text{m}$  on an air/water interface. The two-step procedure employed for this purpose begins with formation of a surfactant monolayer on water. Then a gold nanoparticle dispersion in chloroform is drop-casted onto the surfactant monolayer (Fig. 24).<sup>515</sup> Rapid evaporation of the solvent reduces the air/liquid interfacial temperature below its dew point, resulting in the condensation of microscopic water droplets on the surface of the solution. The water droplets self-assemble into ordered arrays under the effects of thermocapillary forces and Marangoni convection.

Control of morphology changes in the fabrication of porous polymer films is realized through the synthesis of star polymers with both the size of the 2,2-bis(methoxy)propionic acid-based dendron end group and the dendron functionality being varied.<sup>516</sup> Xiong *et al.* have also synthesized a monotonous microsphere pattern when the surface tension of the starting polymer solution is higher than that of the condensed liquid.<sup>517</sup>

As one liquid templating methods, BF templating has been used to prepare hierarchically structured porous materials and as a technique for using patterned arrays of condensed water droplets as templates for the preparation of ordered porous thin films.

**2.4.4 Selective leaching.** Selective leaching of one phase of a composite has been used to synthesize a variety of hierarchically porous inorganic materials. Some physical mixing methods such as sintering can be used to form the composite with two immiscible phases. Immersion in an appropriate solution will

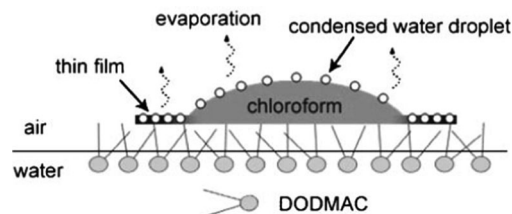


Fig. 24 Illustration of the breath figure film formation at an air/water interface. Reprinted with permission from ref. 515. Copyright 2010, Wiley-VCH.

dissolve the sacrificial phase, leaving a porous monolith of the desired phase. A composite of rock salt NiO and wurtzite ZnO, as an example, has been used to help to understand this process.<sup>518</sup>

Firstly, by employing the uniaxial pressing method, the obtained composite has two immiscible phases (NiO and ZnO phases) that are in intimate contact with one another. After selective leaching, the macroporous NiO can be easily obtained, since ZnO is soluble in alkali solutions while NiO is not.

Selective leaching allows the porosity and pore size to be varied by changing the starting phase ratio, particle diameter and heat treatment. Furthermore, solid-state reactions have been developed to form an intimately mixed two-phase composite, one of which is sacrificial. The porosity and the pore size therefore can be tuned over a wide range. Adjusting the initial volume fraction of the sacrificial phase has a corresponding effect on the porosity. The average pore diameters between 500 nm and 5 mm can be synthesized by using the leaching method. Firstly, nearly identical grain sizes for the two phases are usually preferred. This characteristic is important if a pore structure with open connectivity is desired. A morphology composed of large grains of one phase surrounded by small grains of the other phase can lead to undesired effects on the monolith upon leaching. If the grains of the sacrificial phase are much larger than those of the desired phase, the resulting pores will be large and isolated. Conversely, if the grains of the desired phase are much larger than the sacrificial phase, no connectivity between the grains of the desired phase will exist, and upon leaching, the monolith will turn into a powder. Secondly, leaching must have no effect on the desired phase, and the connectivity of the desired grains is maintained. As the pores are for media leaching, they must be connected and do indeed appear continuous.

Selective leaching has a long history. An example is the depletion gilding by selective leaching of Cu from Au–Cu alloys.<sup>519</sup> It is observed in technologically important alloy systems. Later, this leaching process was also extended to other systems, such as the porous RANEY<sup>®</sup> nickel,<sup>520</sup> macroporous ceramic CaZrO<sub>3</sub><sup>521</sup> and titania.<sup>522</sup> With the development of solid reactions, such as eutectic cooling to crossing phase boundaries, selective leaching can lead to other hierarchically structured materials.<sup>523–527</sup> A general strategy described by Toberer and Seshadri<sup>528</sup> to leach out the sacrificial phase in solution (Fig. 25a) was employed to form a macroporous monolith of the desired phase. Thus far, several procedures for modifying the resulting macroporous material have been described. The first concerns a metal with the macropore structure being retained after reduction of a macroporous oxide (Fig. 25b). The second is production of macropore walls with a conformal coating of a second phase through a process of reactive dip coating (Fig. 25c). The third case is the formation of hierarchically porous monoliths with meso–macroporous structure through the subsequent leaching of a sacrificial element from the macropore walls (Fig. 25d).

The selective leaching processes can be controlled to give rise to unusual hierarchically porous architectures.<sup>386,393,394,397–402</sup> The resulting porous monoliths have served as conformal coatings, porous metals and hierarchically porous structures. Compared to other approaches, the synthesis of materials using leaching shows

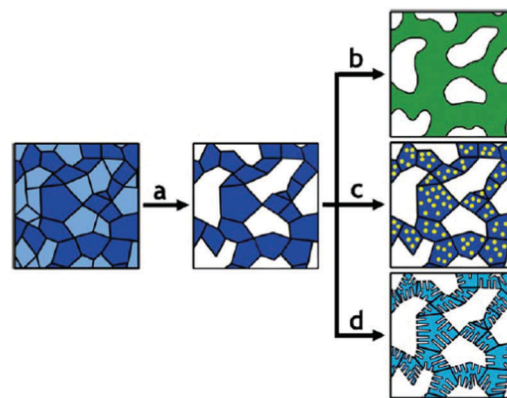


Fig. 25 Scheme showing (a) formation of a macroporous ceramic through selective leaching of a two-phase composite. The resulting material may then be (b) turned into a porous metal, (c) decorated with a conformal coating, or (d) rendered hierarchically porous through vapour-phase leaching. Reprinted with permission from ref. 529. Copyright 2006, Royal Society of Chemistry.

several advantages. As these approaches are quite simple, it is expected that this ease of the leaching process will inspire further investigations into the formation of porous materials through selective leaching methods.

### 3. Design of hierarchically porous structures

Hierarchically structured porous materials often possess remarkable properties. Hierarchies, which are found everywhere from simple unicellular organisms to the more complex human body, are often necessary for the function of living systems. These types of multilevel porous architectures can generally be divided into four categories including (i) hierarchical 0D spheres (such as diatom); (ii) hierarchical 1D fibers (such as tendon); (iii) hierarchical 2D layers (such as abalone shell); and (iv) hierarchical 3D monolithic objects (such as bone). These hierarchical structures are capable of conferring unique properties to materials, which are directly attributed to all levels of structural hierarchy. All of these materials have specific hierarchical composite structures with distinct and highly specific functions, even when they are constructed from very similar elements and macromolecules. Hierarchical structuring of a multi-step assembly enables the construction of materials with highly complex functions.<sup>16,46,69,325,530–635</sup>

Synthetic hierarchically porous materials with multimodal and multiscale porosity are of even higher interest, particularly for catalysis and separation, where optimization of diffusion and confinement regimes is required. Whereas micro- and meso-pores provide size and shape selectivity for guest molecules that enhances host–guest interactions, the presence of macropores can considerably favour diffusion of and the accessibility to the active sites by guest molecules. That is particularly important for the diffusion of large molecules and even small molecules in viscous media.

It is envisaged that by combining macropores, mesopores and micropores the properties of hierarchical pores (including dual micropores (Section 3.1), micro-mesopores (Section 3.2), micro-macropores (Section 3.3), micro-meso-macropores (Section 3.4), dual mesopores (Section 3.5), meso-macropores (Section 3.6), dual/multiple macropores (Section 3.7)) can be exploited simultaneously. Hierarchical materials containing interconnected micro-/macro-/meso-porous structures can have enhanced properties compared to materials with unimodal pore sizes due to increased mass transport through the material as well as high specific surface areas. A multitude of synthetic routes to prepare hierarchically porous materials have recently been developed (see Section 2). Some recent excellent reviews on this topic have been published.<sup>523,529,533,549,550</sup> However, these reviews address only one aspect of porous hierarchy. Here, we review in a more comprehensive way recent progress that has been made in the synthesis of hierarchically porous materials. Specifically, we focus on a group of selected examples to show the formation of a desired hierarchically porous structure can be achieved using the methods presented in Section 2.

### 3.1 Hierarchically dual microporous structures

Zeolites are crystalline materials with open microporous structures. These materials are very hydrothermally and thermally stable, and are of considerable technological importance as shape-selective catalysts, ion-exchange solids and molecular sieves. Introducing mesopores linked to the zeolitic micropores, so as to increase accessibility to the internal surface, has been investigated in an effort to extend the application of zeolites to large molecules.

Hierarchically core-shell zeolite composites possessing a core and a shell of different zeolite structure types have attracted much attention in shape-selective catalysis. These materials are prepared through overgrowth of continuous shells around the core crystals using zeolitization approaches. Many examples are found such as ZSM-5/silicalite-1,<sup>283–286,636</sup> LTA/FAU,<sup>287</sup> MFI/MEL,<sup>288</sup> EMT/FAU,<sup>289</sup> OFF/ERI,<sup>290</sup> MOR/MFI,<sup>291</sup> CHA/SOD,<sup>292</sup> FAU/MAZ,<sup>293</sup> BEA/MFI,<sup>294</sup> BEA-FAU,<sup>637</sup> and MFI/AFI,<sup>295</sup> which combine the chemical or structural properties of two types of microporous materials.

Defect-free single crystal-like composites with no crystal boundaries are expected to be ideal for shape-selective catalysis. A dually microporous composite consisting of a zeolite crystal with an inactive thin shell has been prepared through overgrowth of silicalite-1 shell on proton-exchanged ZSM-5 crystals (Fig. 26).<sup>286</sup> The silicalite-1 shells on ZSM-5 core consist of oriented or randomly oriented polycrystalline material. Their shell thickness ranges from several micrometers to several tens of micrometers. The framework structure of the thin shell is the same as that of the substrate. This hierarchical core-shell zeolite composite has a very thin shell without a crystal boundary.

It is noteworthy that the ultrathin continuous shell may consist of either high silica or all-silica zeolites, which can effectively cover most of the external surface acid sites without compromise of diffusion capacity.<sup>284</sup> As is well known, zeolites with uniform micropores in the range of 0.3–1 nm, have been

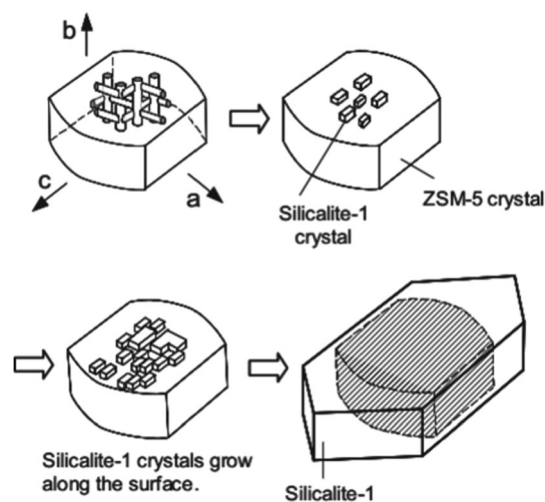
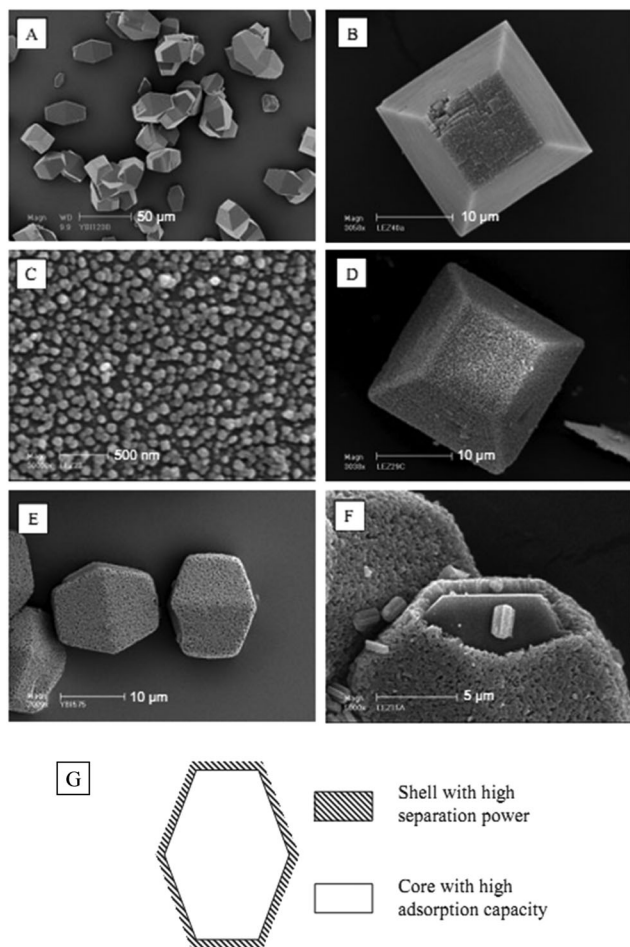


Fig. 26 Graphical illustration of the proposed model for the formation of a silicalite-1 layer on a ZSM-5 crystal. Reprinted with permission from ref. 286. Copyright 2005, Wiley-VCH.

used in chemical-processing industries, namely for catalytic and separation processes. Very often, zeolites that possess a high separation power have a very low adsorption capacity and thus a poor efficiency as storage materials. An example of this is the ten-member-ring (10 MR) high-silica zeolites (ZSM-5, ZSM-11, ZSM-23, and ZSM-35 *etc.*). On the other hand, microporous materials with a low framework density and high adsorption capacity, such as 12 MR BEA-, FAU-type zeolites, are not appropriate for diffusional separation. Thus, dually microporous materials are expected to combine microporous materials with high adsorption capacity and high separation power or with specific catalytic and separation properties. This type of a hierarchical zeolitic composite has been created in the form of a core-shell structure, where the high-adsorption-capacity zeolite is the core and the shell is a zeolite with high separation power. A desired core-shell Beta-zeolites-silicalite-1 composites has been prepared (Fig. 27).<sup>294</sup>

The characteristic feature of the obtained composites is a relatively large single-crystal core and a very thin polycrystalline shell. The incompatibility between the core crystals and the zeolite precursor mixture yielding the shell layer has been circumvented by adsorption of nanoseeds on the core surface, which induces crystallization of the shell. The pretreated core crystals are subsequently subjected to continuous growth in a zeolite precursor mixture. Most of the Beta zeolite crystals are covered with a defect-free silicalite-1 shell. The shell integrity of the calcined composite shows a superior performance in the adsorption of butane, toluene, and 1,3,5-trimethylbenzene.

A systematic study of dually microporous zeolite composites such as SOD-LTA, BEA-LTA, FAU-MFI, MFI-BEA, and MFI-MFI (ZSM-5-silicalite-1) has been carried out by Valchev *et al.*<sup>638</sup> The formation of an intergrown shell structure is induced by preliminary seeding of the core crystals and subsequent secondary growth under hydrothermal conditions (Fig. 28). The utilization of seeds suppressed the influence of framework particularities of the core crystals on the formation of the shell layer. The couples



**Fig. 27** (A) Low- and (B) high-magnification SEM images of  $\beta$ -zeolite crystals used as the core. (C) A pyramidal face of a  $\beta$ -zeolite crystal seeded with silicalite-1 nanocrystals. (D) Close and (E) general views of  $\beta$ -zeolite-silicalite-1 composites. (F) A core-shell composite where the thickness of the shell and the silicalite-1 crystals formed in the synthesis solution can be seen. (G) Schematic representation of a core-shell microcomposite. Reprinted with permission from ref. 294. Copyright 2005, Wiley-VCH.

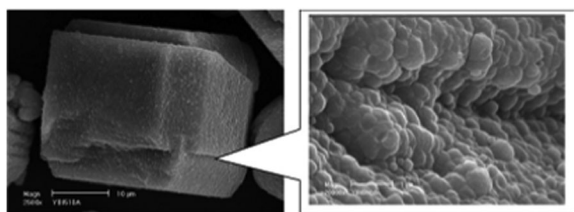


**Fig. 28** SEM micrographs of a ZSM-5-zeolite Beta core-shell composite. The inset represents a close view of the zeolite Beta shell at the interface. Reprinted with permission from ref. 638. Copyright 2006, American Chemical Society.

of zeolitic materials are chosen in a way to reveal the effect of differences between the chemical compositions and crystallization conditions of core and shell zeolites on the formation of the desired composite.

Multiphase microporous materials such as ZSM-5/SAPO-11 and ZSM-5/Cu-ZnO- $\text{Al}_2\text{O}_3$  capsule have been developed. These

hierarchically structured zeolite composites have high selectivities and can be used to efficiently promote a combination of two and more sequential reactions with many synergistic effects.

The combination of two types of microporous materials might be beneficial for some catalytic applications. One can envisage microporous composites with the access to active sites, which are controlled by an inert microporous material with desired separation properties. Further, such materials may serve as microcapsules that can be employed for the encapsulation and slow release of desired compounds. Finally, the core-shell zeolite composites might also be used as chromatographic separation materials.

### 3.2 Hierarchically micro-mesoporous structures

Recently, it has been reported that mesoporous materials with crystalline zeolite frameworks can be synthesized through use of a crystallization process inside a packed bed of removable “solid” nano-templates (*e.g.*, carbon nanoparticles),<sup>302–304</sup> nanotubes,<sup>305</sup> and other materials.<sup>309</sup> ZSM-5 with mesopores of diameter 5–50 nm has been synthesized by growing the zeolite crystals in the pore system of carbon black.<sup>302,303</sup> Pinnavaia and co-workers, on the other hand, prepared ZSM-5 with large mesopores (typical pore size larger than 10 nm) using colloid-imprinted carbons as the template.<sup>304</sup> Jacobsen and co-workers have synthesized mesoporous silicalite-1 with secondary mesopores using carbon nanotubes as the template.<sup>305</sup> The synthesis approaches are based on the idea that the small solid particle templates can be removed to introduce additional porous structures within zeolites.

As the first example, nanocarbon particles (about 12 nm) as mesoscale templates are added into the starting aluminosilicate gels.<sup>302</sup> After crystallization, these nanocarbon particles are embedded in ZSM-5 crystals. Removal of the carbon matrix by calcination results in the creation of mesoporosity in ZSM-5 zeolite (Fig. 29). Usually, these nanocarbon particles are pre-treated with acid or alkaline solutions so that they easily disperse into aqueous solution used for synthesizing various mesoporous zeolites (such as MTW, MEL, and TS-1).<sup>639–641</sup> On the other hand, sphere-like nanocarbon particles after calcination often result in cave-like mesopores, which are not open to the external surface of zeolite crystals. Thus, carbon nanotubes or carbon nanofibers are considered as nano-templates<sup>305,642,643</sup> for the synthesis of mesoporous zeolites, where the mesopores can pass through zeolite crystals.

When the walls of mesoporous zeolites are thick enough to stabilize zeolite nanocrystals, the ordered cubic mesoporous (20–40 nm) silicalite-1 zeolite is templated from an ordered cubic mesoporous (20–40 nm) carbon.<sup>644</sup> Carbon aerogels (CAs) are also good templates for creation of mesoporosity in zeolite crystals.<sup>303,307,645</sup> CAs are usually in a monolithic form and their structures and properties depend on the agglomerate structures of uniform spherical carbon particles.<sup>646</sup>

Very recently, other nanosized particles such as  $\text{CaCO}_3$ , starch and bread have been used to synthesize the mesoporous zeolites.<sup>118,310,647</sup> Compared with nanostructured carbons, these solid templates are cheap and readily available.

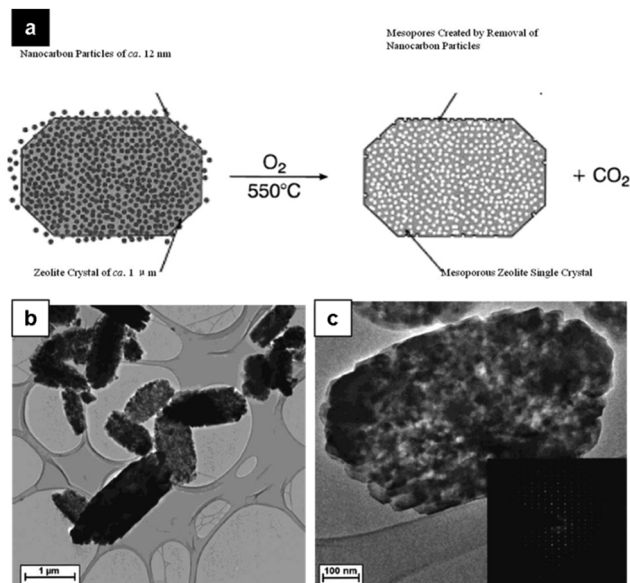


Fig. 29 (a) Growth of zeolite crystals around carbon particles. The zeolite is nucleated between the carbon particles; the pores are sufficiently large, and the gel is sufficiently concentrated to allow growth to continue within the pore system; (b) TEM overview of mesoporous ZSM-5 single crystals obtained by controlled combustion of carbon particles. It is seen that the crystals are 1  $\mu\text{m}$  and porous due to the removed carbon particles; (c) TEM of an isolated single ZSM-5 crystal and the diffraction pattern obtained from the same crystal. The size of the selected area aperture for electron diffraction was 1  $\mu\text{m}$  and covered the entire crystal shown. Reprinted with permission from ref. 302. Copyright 2000, American Chemical Society.

Post-treatments, after zeolitization, are usually used in industrial processes to obtain mesoporous zeolites. These methods include steaming, leaching with NaOH and HCl and extraction of aluminum species by ammonium hexafluorosilicate (AFS) and  $\text{SiCl}_4$ .<sup>296,297</sup>

Treatment of zeolites with steam at temperatures higher than 500  $^\circ\text{C}$  leads to hydrolysis of Al–O–Si in the framework of zeolites. Upon continuous hydrolysis, the zeolitic framework is partially removed leaving mesopores in the crystals.<sup>648</sup> Then, the amorphous aluminosilicate fragments in the mesopores are dissolved by using HCl solution. For example, Lohse *et al.* showed that a 10 nm mesopore system is formed upon steaming of zeolite Y. After extraction of extra framework material with acid, the pore diameter increases to 20 nm.<sup>298</sup> Compared with acid treatment, which preferentially removes framework Al atoms, alkali treatment selectively extracts framework Si atoms, forming mesoporous ZSM-5 zeolite (Fig. 30).<sup>649–653</sup> As a result, alkaline-treated ZSM-5 zeolites exhibit good catalytic properties.

The advantage of using extraction of aluminum species by AFS and  $\text{SiCl}_4$  is that the reagent that removes the aluminum from the framework also supplies the needed silicon to fill the vacancies.<sup>531,532</sup> Therefore, silicon-rich zeolites can be obtained. However, this kind of zeolites contains smaller mesopores than those obtained by steaming-treatment of zeolites due to silicon filling in the vacancies of zeolitic framework.

It is difficult to obtain crystalline zeolite that contains both micro- and mesoporous structures in a single phase even when

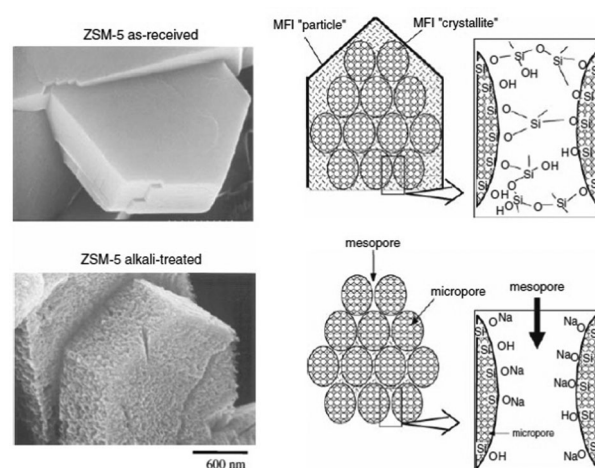


Fig. 30 Schematic diagram of dissolution of ZSM-5 by NaOH aqueous solution. Reproduced from ref. 653. Copyright 2010, Springer.

the aluminosilicate gel is directly crystallized in the presence of an ordinary organic surfactants and molecular templates for zeolites. From the analysis of the phase-separation phenomenon, we know that it is difficult for the surfactants to modulate the zeolite crystal growth into a mesoporous structure, if the surfactants are expelled from the aluminosilicate domain during the zeolite crystallization process.

Tremendous progress has been made in by controlling the sol-gel process by using the one-step hydrothermal synthesis of hierarchical mesoporous zeolites, templated from a mixture of small organic ammonium salts and mesoscale cationic polymers by Xiao *et al.*<sup>654</sup> Hierarchically mesoporous  $\beta$ -zeolite (Fig. 31) is crystallized in the presence of TEOAH and the mesoscale cationic polymer, polydiallyldimethylammonium chloride (PDADMAC). The presence of hierarchical mesoporosity in the mesoporous  $\beta$ -zeolite sample is attributed to the use of the molecular and aggregated cationic polymer PDADMAC. The cationic polymers can effectively interact with negatively charged inorganic silica species in alkaline media, resulting in the hierarchical mesoporosity. Because the composition, molecular weight, architecture and zeolite structure of cationic polymers are altered by various small organic ammonium ions, a series of hierarchical mesoporous zeolites such as ZSM-5 and FAU used widely in

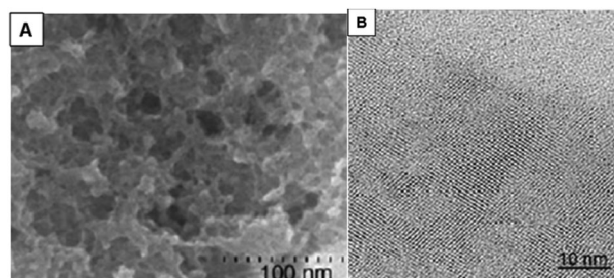


Fig. 31 SEM and TEM images of calcined Beta-H: (A) SEM images high magnification (each marker represents 100 nm); (B) TEM images at high magnification. Reprinted with permission from ref. 654. Copyright 2010, Wiley-VCH.

industry have been synthesized.<sup>311–313</sup> Pinnavaia *et al.* have also synthesized intra crystal mesopores by a silylated polyethyleneimine polymer.<sup>314</sup> The presence of  $-\text{SiO}_3$  units on the polymer strongly interact with aluminosilicate species in a sol-gel. After growth of zeolite crystals and calcination for removing the polymer porogen, uniform intra crystal mesopores in MFI zeolites are formed.<sup>314</sup>

Xie *et al.* used polyvinyl butyral (PVB) as a template for creation of mesoporosity in zeolite crystals of Beta and ZSM-11. Mesoporous Beta clearly presents both ordered micropores and disordered mesopores in a single crystal.

The increasing interest in microporous materials with ordered mesoporous structures has led to progress in constructing hierarchical ordered mesoporous zeolites using surfactant templating such as cationic surfactants.

Conventional surfactants such as CTAB have been used to template mesoporosity in zeolite crystals.<sup>655–658</sup> This approach is partially successful, but the relative weak interaction existing between the surfactant and silica-based species results in the formation of aggregated zeolite nanocrystals with a disordered mesoporosity.

A direct route has also been developed by Ryoo *et al.*<sup>659</sup> to synthesize mesoporous zeolites using amphiphilic organosilanes as a mesopore-directing agent. The mesopore diameters of the product are the range of 2–20 nm. Both the molecular structure of the mesopore-directing silanes and the hydrothermal synthesis conditions can influence the pore size of the material, which is very desirable and important for applications as shape-selective catalysts, ion-exchange solids, and molecular sieves. The key feature of this method is the design of amphiphilic surfactant molecules that contain a hydrolyzable methoxysilyl moiety, a zeolite structure-directing group such as quaternary ammonium and a hydrophobic alkyl chain. [3-(Trimethoxysilyl)propyl]hexadecyldimethylammonium chloride ( $[(\text{CH}_3\text{O})_3\text{SiC}_3\text{H}_6\text{N}(\text{CH}_3)_2\text{C}_{16}\text{H}_{33}]\text{Cl}$ , TPHAC), which contains a surfactant-like long-chain alkylammonium moiety and a hydrolyzable methoxysilyl group, linked together by a Si-C bond, was used in this case. Organic molecules that are capable of strongly interacting with the growing crystal surface can effectively modulate the crystallization process of inorganic materials. In this strategy, globular MFI zeolite particles have a highly mesoporous structure, as indicated by high-resolution SEM and TEM images (Fig. 32).

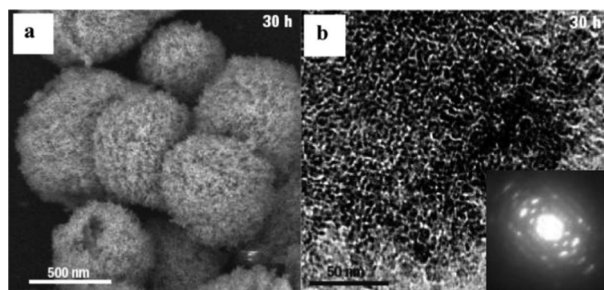


Fig. 32 SEM (a) and TEM (b) images of mesoporous MFI zeolite synthesized using the amphiphilic organosilanes. Reprinted with permission from ref. 659. Copyright 2006, Nature publishing group.

In addition to original micropores and the formation of new voids between the nanosheet, zeolite nanosheets can be categorized into hierarchically structured mesoporous zeolites.<sup>660,661</sup> This is an important breakthrough in mesoporous zeolite synthesis. Ryoo *et al.* developed ultrathin MFI zeolite nanosheets, which correspond to only a single unit-cell thickness (2.0 nm along *b*-axis). The zeolite nanosheets are hydrothermally synthesized using an organic surfactant functionalized with a diquaternary ammonium, *i.e.*,  $\text{C}_{22}\text{H}_{45}-\text{N}^+(\text{CH}_3)_2-\text{C}_6\text{H}_{12}-\text{N}^+(\text{CH}_3)_2-\text{C}_6\text{H}_{13}$  as the head group. The headgroup serves as a zeolite-structure directing agent (SDA), while the hydrophobic interaction between the  $\text{C}_{22}$ -alkyl tails leads to supramolecular organization of the surfactant molecules into a lamellar structure. The zeolite nanosheets are conceptually similar to ITQ-2, obtained by swelling the Al-MWW (P) with CTAB and delaminating the MWW precursor.<sup>662–664</sup> Depending on the synthesis conditions, the zeolite nanosheets are self-organized into an ordered multilamellar stack or a disordered unilamellar assembly (Fig. 33).<sup>660</sup> The latter retains a high mesoporosity upon removal of the surfactant through calcination.

A series of ordered mesoporous zeolites (Fig. 34) that possess crystalline microporous walls and have mesopores in the range from 2 to 50 nm have been synthesized.<sup>316</sup> Hexagonal ordered mesostructures are generated by aggregation of the surfactant molecules, whereas the crystallization of microporous frameworks is directed by quaternary ammonium groups within the mesopore walls. One notable member of this dual-porogenic surfactant family has a molecular formula of  $\text{C}_{18}\text{H}_{37}-\text{N}^+(\text{CH}_3)_2-\text{C}_6\text{H}_{12}-\text{N}^+(\text{CH}_3)_2-\text{C}_6\text{H}_{12}-\text{N}^+(\text{CH}_3)_2-\text{C}_{18}\text{H}_{37}(\text{Br}^-)_3$  (abbreviated as 18-N<sub>3</sub>-18). This surfactant has a zeolite-directing head group composed of three quaternary ammonium ions connected with  $-\text{C}_6\text{H}_{12}-$  alkylspacers and two hydrophobic  $-\text{C}_{18}\text{H}_{37}$  alkyl tails. The wall thicknesses, framework topologies and mesopore sizes can be controlled with different surfactants.

Recently, research has focused on active carbons with hierarchical structures. These materials have high surface areas (up to  $1000 \text{ m}^2 \text{ g}^{-1}$ ), which lead to enhancements of matter diffusion. A micro-meso hierarchical porous carbon (HPC) was prepared by using a combination of surfactant templating and post activation, and explored as a counter electrode in Dye Sensitized Solar Cells (DSSCs).<sup>665</sup> The mesoporous carbon (MC)

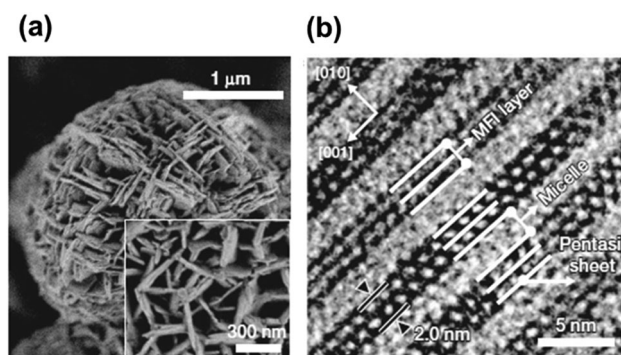


Fig. 33 (a) SEM image and (b) HRTEM images of the plate of MFI zeolite nanosheets. Reproduced by permission of ref. 660. Copyright (2009) Nature publishing group.

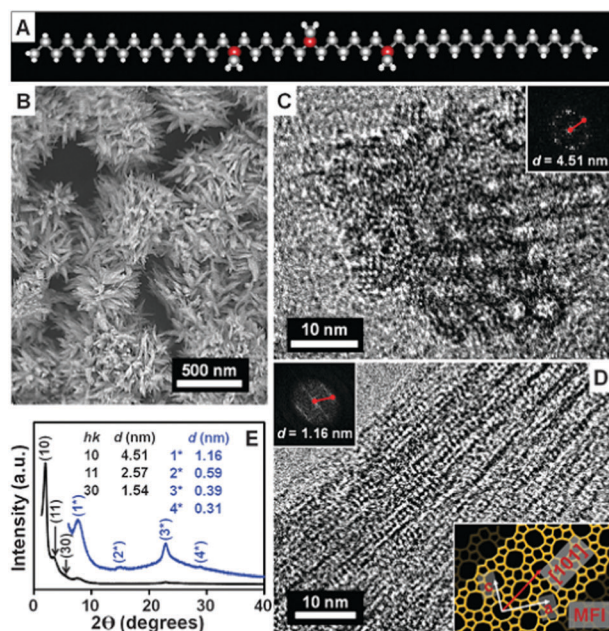


Fig. 34 (A) 18-N<sub>3</sub>-18 surfactant (white spheres, hydrogen; gray spheres, carbon; red spheres, nitrogen). (B) SEM, (C and D) TEM, [(C) and (D), insets] Fourier diffractogram, and (E) XRD pattern of hexagonally ordered crystalline MMS after surfactant removal. Reprinted with permission from ref. 316. Copyright 2011, American Association for the Advancement of Science.

was firstly prepared by using surfactant templating. The micropores were directly generated within the mesopore wall of MC and preserved during KOH activation. This HPC electrode exhibited high electrocatalytic activity due to its low crystallinity and unique structural characteristics such as high surface area and hierarchical pore structure containing abundant both micropores and mesopores.

Using a template to generate a mesoporous structure has been used extensively for the formation of the microporous MOF (Fig. 35a).<sup>325</sup> Cross-linking *via* metal–ligand bonding occurs to form an extended microporous coordination network punctuated by ideally ordered mesopores. Such a co-assembly of metal ion and ligand building blocks for MOFs formation with the surfactants requires that the synthetic conditions be precisely controlled. For example, the pH value, as an extremely important parameter for hierarchical micro–meso MOFs, plays a defining role in the type and strength of interactions between the precursors and template. Yuan *et al.*<sup>327</sup> described mesoporous MOFs, prepared by using a rational templating method, that display hexagonal mesoporosity that is related to the surfactant F127-induced co-assembly process. The mesopore walls were fully composed of crystalline metal disulfonates (Fig. 35b).

By extending the ligands, the pores in MOF materials can be expanded to mesopore range.<sup>666</sup> Lin *et al.*<sup>336,337</sup> constructed a series of mesoporous chiral metal–organic frameworks, with the framework formula [LCu<sub>2</sub>(solvent)<sub>2</sub>] (where L is a chiral tetracarboxylate ligand derived from 1,1'-bi-2-naphthol) by the design of suitable long-chain ligands. As a result of the different lengths of the ligands, the MOFs are highly porous with tunable void spaces and show tunable channel openings of 1.3 × 1.1 nm

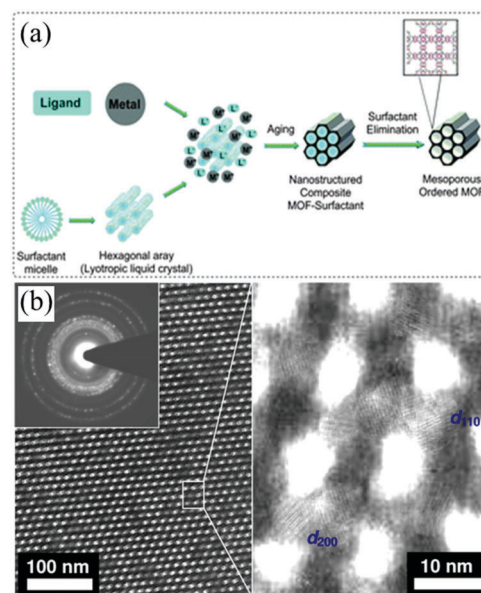


Fig. 35 (a) Synthesis strategy mesoporous MOFs by supramolecular templating. (b) TEM images and electron diffraction pattern of MOF-1. Reprinted with permission from ref. 325 for (a). Copyright 2014, Royal Society of Chemistry and ref. 327 for (b). Copyright 2012, American Chemical Society.

to 3.2 × 2.4 nm along the *a/b* axis and from 0.8 × 0.8 nm to 2.1 × 2.1 nm along the *c* axis (Fig. 36).

Recently, a general template-free method for synthesis of hierarchically micro–mesoporous MOFs, so-called nanofusion, has been reported.<sup>339</sup> This method yields hierarchical MOF materials with intriguing porosity on a gram scale. In contrast to their corresponding microporous frameworks, the hierarchical MOF materials prepared in this way exhibit exceptional properties when tested for the adsorption of large organic dyes. This is due to the enhanced pore accessibility and electrolyte diffusion within the mesopores. Following addition of the organic ligand to the metal ion precursor solution, the mixture was stirred vigorously. The discrete nanosized MOF crystals were quickly embedded in an amorphous matrix, and mesopores formed spontaneously (Fig. 37a). For example, Hierarchical ZnMOF-74 could be prepared within as short as 15 min by stirring at room temperature, by Yue *et al.*<sup>340</sup> This material has thick pore walls and large mesopores formed between particle aggregates (Fig. 37b). The fact that high a micropore volume of 0.22 cm<sup>3</sup> g<sup>-1</sup> is obtained after a short reaction times provides evidence for the existence of large quantities of crystalline particles that form the pore walls. When the synthesis time is extended to 10 days, the resulting Zn-MOF-74 material exists as almost discrete interconnected particles (Fig. 37e). They are less crystalline and consequently exhibit ~10% of the micropore volume of Zn-MOF-74/0.25 along with the largest mesopore width and mesopore volume (0.48 cm<sup>3</sup> g<sup>-1</sup>).

### 3.3 Hierarchically micro–macroporous structures

Hollow zeolitic structures are typical hierarchically micro/macro bimodal porous materials. The PS microsphere was the first to be used as a sacrificial template for the formation

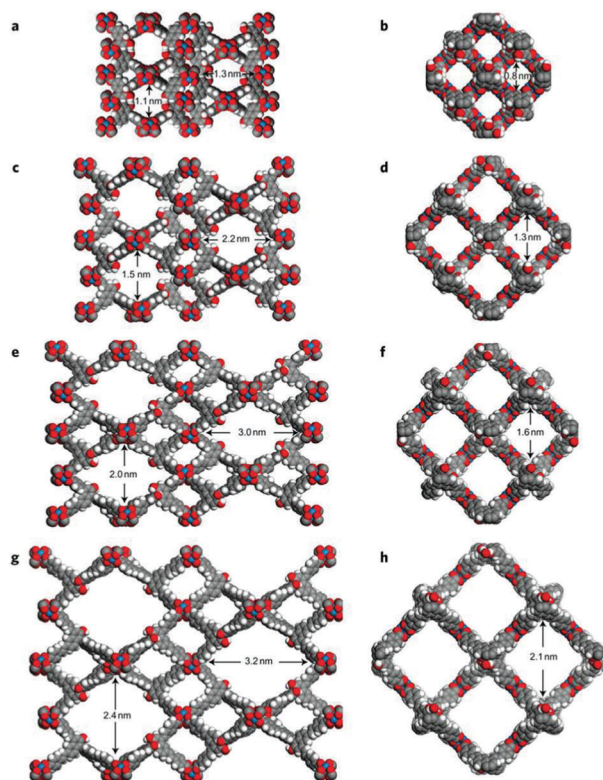


Fig. 36 From top to down, show the packing diagrams of CMOF-1b to -4b, respectively. Left side structures (a, c, e and g) were viewed down the *a/b* axis and right side structures (b, d, f and h) were viewed down the *c* axis. Reprinted with permission from ref. 336 and 337. Copyright 2010, Nature publishing group.

of the micro/macro porous hollow structure through the LBL technique.<sup>667</sup> The nanozeolite particles and oppositely charged polyelectrolytes are then alternately deposited onto the charged PS templates to form nanozeolite/polydiallyldimethylammonium (PDDA) shells (Fig. 38). The size of the hollow is based on the size of PS spheres. A series of hollow nanozeolite microspheres can be obtained<sup>317,318</sup> by changing the type of nanozeolites and thickness of deposited layers. Valtchev *et al.*<sup>319,320</sup> have further shown that secondary hydrothermal treatment can improve the mechanical stability of the LBL-constructed hollow nanozeolite sphere using PS hard templates.

Carbon black microspheres can also be used as the template to synthesize hollow hierarchical structures. Chu and co-workers<sup>668</sup> synthesized nest-like hollow hierarchical MCM-22 microspheres (MCM-22-HS) (Fig. 39). The MCM-22/C composite microspheres are obtained when carbon black microspheres with a diameter of 4–8  $\mu\text{m}$  are added to a conventional MCM-22 synthetic solution under rotating crystallization conditions. The carbon black microspheres are then removed by calcination. The shell of MCM-22-HS is hierarchically constructed of intergrown flaky MCM-22 crystals.

Mesoporous silica (MS) spheres were first used as a template by Dong *et al.*<sup>669</sup> to prepare hollow nanozeolite spheres. In this process, MS spheres act not only as structure templates but also as silica nutrients for the growth of zeolitic shells (Fig. 40). In addition, because of the adjustable morphologies of MS, hollow

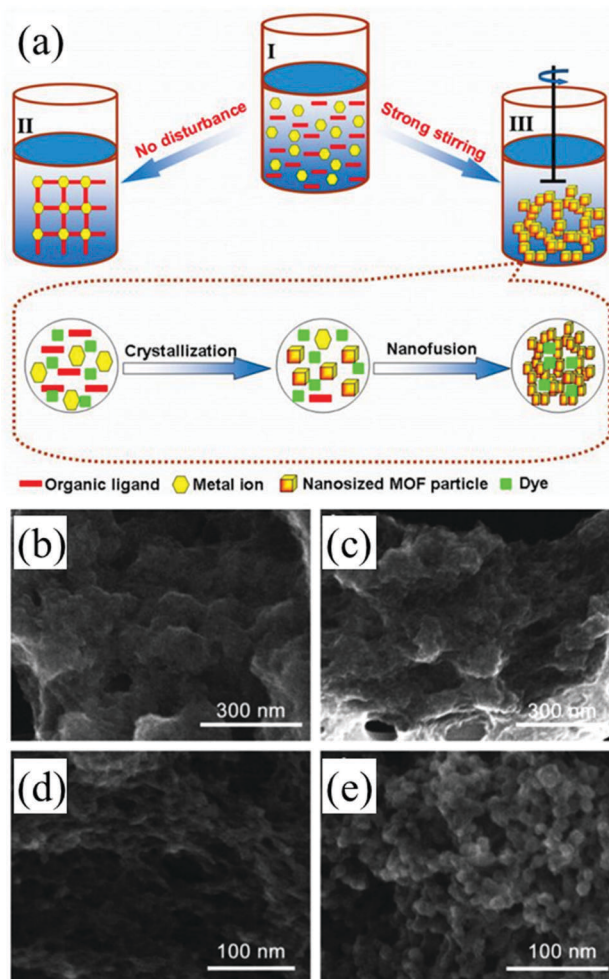


Fig. 37 (a) Schematic diagram of the formation of hierarchical superstructure of MOFs; SEM images of bimodal Zn-MOF-74 series synthesized with different reaction time (b) 0.25 h, (c) 1 h, (d) 24 h, and (e) 240 h. Reprinted with permission from ref. 341 for (a). Copyright 2015, American Chemical Society and ref. 340 for (b–d). Copyright 2013, American Chemical Society.

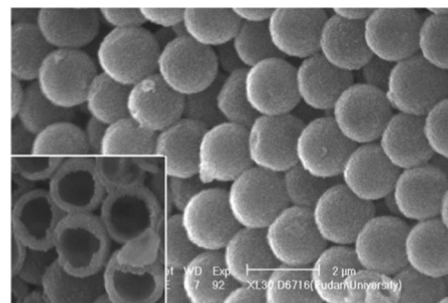


Fig. 38 Hollow nanozeolite BEA spheres by using PS spheres with a diameter of 1.47  $\mu\text{m}$  as templates via a LBL technique. Reprinted with permission from ref. 667. Copyright 2000, Royal Society of Chemistry.

zeolite microcapsules with various non-spherical shapes are also obtained using this approach.<sup>670</sup> To further develop of this strategy, seed-induced hydrothermal crystallization in alkaline

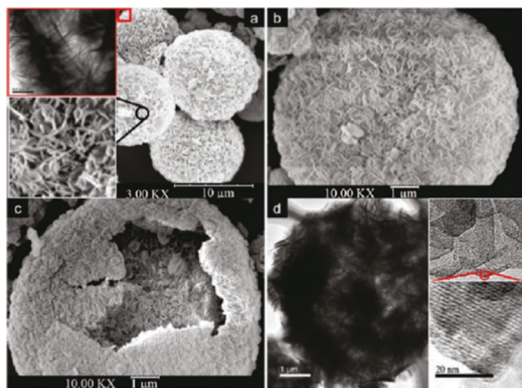


Fig. 39 Schematic representation of the growth process of the MCM-22-HS. SEM and TEM images of the product MCM-22-HS. Reprinted with permission from ref. 668. Copyright 2010, American Chemical Society.

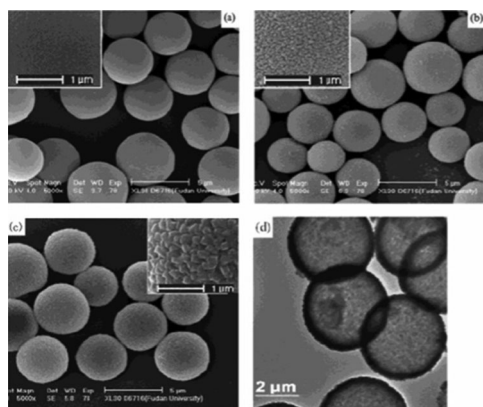


Fig. 40 SEM images of (a) the original MS spheres, (b) monolayer seeds coated MS spheres, and (c) hollow zeolite capsules, (d) TEM image of the same sample shown in (c). Reprinted with permission from ref. 669. Copyright 2002, Royal Society of Chemistry.

aqueous solution was employed to improve the mechanical stability and intactness of the hollow structure.<sup>671,672</sup>

It is worth mentioning that due to their inherent mesoporosity MS templates make guest encapsulation much easier compared to that using a nonporous PS template. So the guest species, such as  $\text{Fe}_2\text{O}_3$ ,<sup>669,670</sup> Ag,<sup>670,673</sup> Pt,<sup>674</sup> and PdO,<sup>673</sup> nanoparticles as well as micrometer-sized carbon and polymer,<sup>673</sup> which have been pre-incorporated into the mesopores of the MS templates, can be entrapped inside the generated hollow capsules along with digestion of the MS cores.

Furthermore, fly ash cenosphere (FAC, an aluminosilicate-rich waste from power plants) is used as a hollow spherical template and nutrients to prepare hollow zeolitic microspheres with cancrinite zeolite shell through *in situ* transformation of FAC in vapor phase.<sup>675–677</sup> Xiong *et al.*<sup>678</sup> employed spherical mesoporous DAM-1 or SBA-15 as a silicon source and substrate to prepare hollow ZSM-5 spheres by using a combination of pulsed laser deposition (PLD) and VPT processes. The size of ZSM-5 crystals in the shell can be easily adjusted by changing the crystallization time or PLD coating thickness.

In addition to these unique spheres, other zeolitic hollow structures are obtained by using other templates (such as  $\text{CaCO}_3$  and  $\text{Fe}_3(\text{SO}_4)_2(\text{OH})_5 \cdot 2\text{H}_2\text{O}$ ) along with various morphologies.<sup>679</sup> Using the same method, HZSM-5 zeolite microboxes with a regular hollow core are generated by using mild alkaline treatment of ZSM-5 single-crystals with  $\text{Na}_2\text{CO}_3$  solution.<sup>680</sup> Recently, a dissolution/recrystallization process<sup>681,682</sup> was developed for the formation of hollow TS-1 crystals<sup>559</sup> and ZSM-5 nanoboxes with a size smaller than 200 nm.

Following the precedent of using digestible templates,<sup>7</sup> mesoporous silica fibre<sup>683</sup> as a template and a silica source have been used to synthesize the hexagonal hollow ZSM-5 tube. Other easily removed templates, such as carbon fibers, are used to create hollow structures. For example, hollow nanozeolite fibres are obtained by depositing nanozeolite particles on micron-sized carbon fibre templates *via* seed-induced hydrothermal growth<sup>684</sup> and LBL method.<sup>685,686</sup> The electrophoretic assembly of nanozeolites on the surface of carbon fibers also has been used to prepare zeolite hollow fibers (Fig. 41).<sup>687</sup>

The zeolitization process can be combined with colloidal crystal templating to form hierarchical macro-/microporous structures. Stein and co-workers were the first to employ a precursor in the synthesis of a 3DOM material that contains both a silica source and Structure Directing Agent (SDA) to generate the ordered micropore network.<sup>308</sup> A colloidal crystal is made by centrifuging PS spheres and then infiltrated with a solution containing TEOS and the TPAOH. Hydrothermal treatment is conducted to convert the amorphous silica to a silicalite-1 (MFI) structure. Some researchers have discussed various routes to making 3DOM zeolites, such as the vacuum-assisted method using nanocrystals of silicalite-1 and ZSM-5 as a precursor.<sup>688,689</sup> Zhou and Antonietti<sup>690</sup> constructed a novel 3D bimodal porous silica framework with well-defined macroporous and super-microporous lamellar nanostructures by simultaneously using three-dimensional order PS pattern and an amphiphilic ionic liquid as a template. Dong *et al.*<sup>184,551</sup> reported the preparation of a robust 3D zeolite monolith with

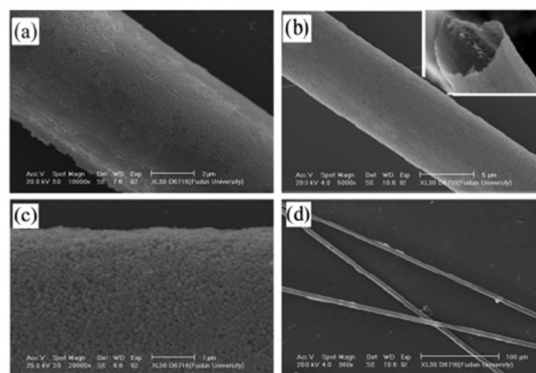


Fig. 41 SEM images of zeolite coated fibers (a) and hollow zeolite fibers (b–d) prepared at pH 2.5 and step voltage 1 V, 2 V, 2 3 10 min; (c) and (d) are high and low magnification micrographs of (b), respectively. Reprinted with permission from ref. 687. Copyright 2001, Royal Society of Chemistry.

an ordered closed macropore by using hydrothermal treatment of the array of nanozeolite pre-coated MS spheres. This method was expanded to produce macroporous zeolites containing encapsulated Ag nanocrystals, PdO nanocrystals, or hollow carbon spheres.<sup>691</sup> Moreover, 3D ordered macroporous ZrO<sub>2</sub>/zeolite nanocomposites are also obtained by using hydrothermal treatment of the polyelectrolyte-coated 3D ordered macroporous activated sulfated zirconia in a synthetic solution of zeolite NaY.<sup>692</sup>

Zeolitization on some bio-templates with special macroscopic morphologies can result in zeolite-related hierarchically micro-/macroporous materials. Mann *et al.*<sup>693</sup> constructed a hierarchical zeolite fibre by filtrating nanozeolite suspension into bacterial super cellular thread. Silicalite-1 nanocrystals are aggregated specifically within the organized micro-architecture. Starch gels have also been used by Mann *et al.*<sup>694</sup> to prepare microporous silicalite monoliths and thin films with hierarchical meso- and macroporous structures. Dong *et al.*<sup>414</sup> developed a process involving replication of cell walls (HL2) by zeolites, and Shin *et al.*<sup>695</sup> utilized surfactant-assisted sol-gel nanocasting of wood-cell walls to obtain silica negative replicas. Besides these templates, Liu *et al.*<sup>696</sup> used cotton threads as templates to prepare silicalite-1 hollow structures by *in situ* hydrothermal synthesis without a surface pretreatment.

The hierarchical porous system generated from diatomite can also be used to produce microporous zeolite species. One approach to transform diatomaceous earth to zeolites involves coating the diatoms with zeolite nanoparticles.<sup>430</sup> Anderson and coworkers<sup>697</sup> transformed diatomite to a zeolite through hydrothermal treatment of ultrasonic seeded or un-seeded diatomite in synthesis solutions containing adsorbed silicon or aluminium sources. Wang *et al.*<sup>432</sup> have partly transformed diatomaceous silica into a zeolite by using the vapor phase transport (VPT) method.

Preparation of hollow zeolite structures without using macrotemplate has been reported.<sup>698,699</sup> Han *et al.*<sup>698</sup> synthesized hollow sodalite spheres and NaA crystals by introducing cross-linked polyacrylamide (C-PAM) hydrogels into zeolite synthesis gels. The three-dimensional C-PAM networks with adjustable pore sizes provide unique scaffolds for zeolite nucleation and growth, which produces hollow zeolite structures due to the operation of a surface-to-core zeolite crystallization process (Fig. 42). Naik *et al.*<sup>699</sup> found that silicalite-1 hollow spheres with a diameter of 100–300 nm can be produced by using self-assembly of silicalite-1 nanocrystals under sonication in ammonia-ethanol solution, when the size of zeolite nanocrystals are smaller than 30 nm.

Hierarchical all-zeolite monoliths are also directly generated from nanozeolite colloid or zeolite powders by using physical methods or a self-assembly strategy. Wang *et al.*<sup>700</sup> prepared hierarchical zeolite structures with designed shapes by gel-casting of colloidal nanocrystal suspensions. Macroporous NaP zeolite monoliths (M-ZPMs) with designed shapes such as cylinder, rectangular-prism, and donut shapes are synthesized by gel-casting of the aged zeolite gel with colloidal silica as a binder and subsequent VPT synthesis.<sup>701</sup> Sebastián *et al.*<sup>702,703</sup> have directly prepared micro/macroporous hierarchical titanasilicate

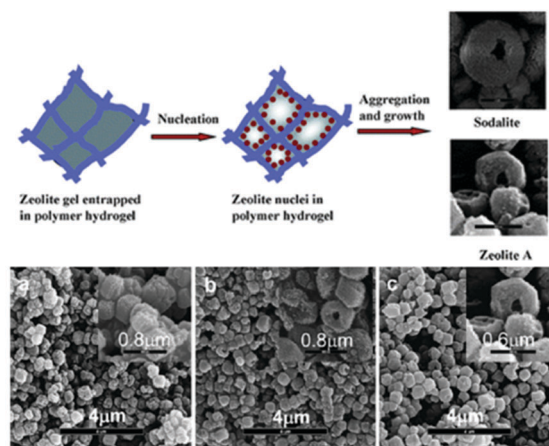


Fig. 42 Schematic representation of the fabrication of hollow structures including sodalite spheres and hollow zeolite NaA crystals by crystallization in cross linked polyacrylamide hydrogels. SEM images of samples prepared with different amount of AM by heating at 90 °C for 5 h. Reprinted with permission from ref. 698. Copyright 2008, American Chemical Society.

microspheres with an umbite structure by using a direct liquid-phase hydrothermal synthesis method under a range of conditions. Hua *et al.*<sup>704</sup> proposed a one-step method to prepare MFI zeolite microspheres without the need of pre-synthesizing zeolite nanocrystals in the presence of Pluronic triblock copolymer F127. The formation of micrometer-sized sphere is attributed to the use of F127 in the synthesis. Vasiliev *et al.*<sup>705</sup> used a Pulsed Current Processing (PCP) technique to directly prepare binderless hierarchically porous monoliths from zeolite powders.

Polymer foams can be described as polymeric solid materials consisting of cellular-like pores. Lee *et al.*<sup>706</sup> investigated the use of (an ether-based) polyurethane (PU) as a support to produce self-standing micro-macroporous zeolite monoliths. The resulting zeolite monoliths have highly ramified networks of interconnecting macropores with tailorable sizes and shapes (Fig. 43).

Further studies were conducted in order to assess the role of the PU foam in directing the growth of zeolite materials.<sup>447</sup> Ether-based and ester-based PU foam templates were employed for the fabrication of silicalite-1 monoliths. As a result of a thin coating of the inorganic material on the PU support, monoliths are comprised of thin ( $\sim 1 \mu\text{m}$ ) and smooth walls of zeolite material with hollow struts prepared from an ether-based PU template. Likewise, the orientation of the crystal growth is affected. In the same study, the authors also showed that the macroporosity of the final material (ranging between 800–2500  $\mu\text{m}$ ) can be tailored by using foams with varying pore sizes. All materials have relatively high surface areas ( $\sim 420 \text{ m}^2 \text{ g}^{-1}$ ) primarily due to the presence of the silicalite-1 pores in the system.

The above technique has also been adapted to the preparation of TS-1 monolithic materials. Lee *et al.*<sup>707</sup> demonstrated the importance of using macroporous monolithic zeolite (ZSM-5) over a non-porous pelletized zeolitic material for catalytic reactions. The final monoliths have a macropore size of 100–300  $\mu\text{m}$  with packed zeolite nanocrystals ( $\sim 5 \mu\text{m}$ ) forming the skeleton of the monolith.

Hierarchically porous carbon materials are in general prepared by using replication approaches or templating replication/activation

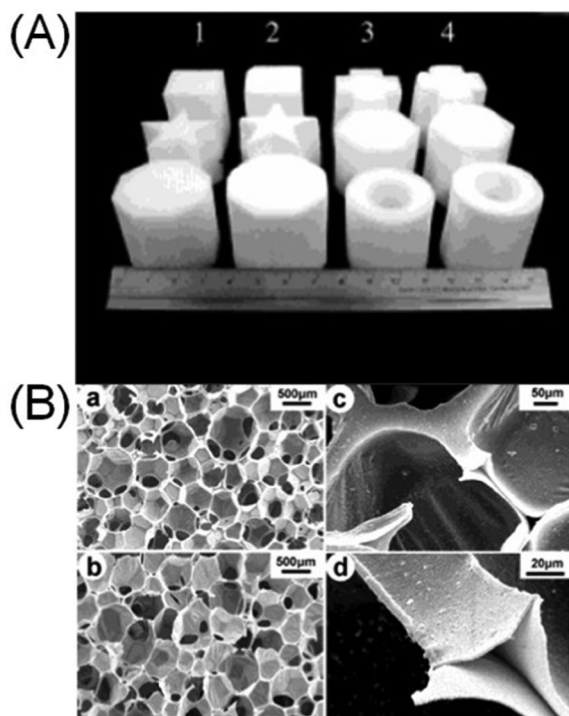


Fig. 43 (A) Photographic images of PUF templates in various shapes (column 1 and 3) and the corresponding monoliths of SLF (column 2 and 4). (B) SEM images showing the morphologies and connectivity of the macroporous cells of PUF (a), the resulting SLF (b), and the typical SLF strut at two different magnifications (c) and (d). Reprinted with permission from ref. 706. Copyright 2001, Wiley-VCH.

combination methods,<sup>708–711</sup> where porous silica or non-silica oxides are impregnated with a carbon precursor, followed by carbonization under nonoxidizing conditions and removal of the template. The replication of hierarchical porous silica enables the preparation of hierarchical porous carbon. The carbon materials are a positive replica of the silica on the micrometer scale, but a negative replica on the nanometre scale. For example, Fang and co-workers<sup>712</sup> fabricated hierarchical nanostructured hollow core/mesoporous shell carbons using solid core/mesoporous shell silica as a template. The hierarchical nanostructure has macropores (macroscopic hollow core) in combination with micropores in the mesoporous shell. The core sizes of 180–340 nm and shell thicknesses of 40–70 nm can be obtained by simply varying the amount of TEOS or adjusting the molar ratio of octadecyltrimethoxysilane (C18-TMS) to TEOS. Cheng and co-workers<sup>713</sup> prepared a 3D periodic hierarchical porous graphitic carbon by using Ni(OH)<sub>2</sub>/NiO as a hard template and phenolic resin as a carbon precursor. The obtained hierarchical micro-macroporous carbon has macroporous core diameters of about 1 mm, a BET surface area of 970 m<sup>2</sup> g<sup>-1</sup>, a total pore volume of 0.69 cm<sup>3</sup> g<sup>-1</sup> with a micropore volume of 0.3 cm<sup>3</sup> g<sup>-1</sup>. When used as electrodes for electrochemical capacitors, the macropores facilitate the formation of ion-buffering reservoirs that minimize the diffusion distances to the interior surfaces and the micropores strengthen the electric-double-layer capacitance. Both the energy and the power densities at high

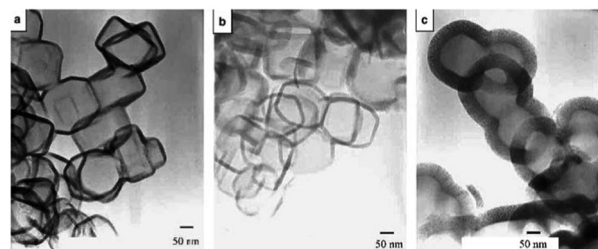


Fig. 44 TEM images of carbon materials prepared *via* CVD using silicalite-I as the template at various CVD temperatures: (a) 900 °C, (b) 950 °C and (c) 1000 °C. Reprinted with permission from ref. 715. Copyright 2005, Elsevier B. V.

rate are greatly improved compared to using activated carbon (AC) or ordered mesoporous carbons (OMC) as electrode materials.

The use of zeolites as templates has been extensively explored to synthesise microporous carbon materials.<sup>714</sup> Using zeolite Beta or silicalite-I as templates and acetonitrile as the carbon source (*via* CVD), hollow shells of porous nitrogen-doped carbon materials with high surface areas can be produced.<sup>715</sup> The carbon materials generally retain the particle morphology of the zeolite templates. However, when CVD is performed at temperatures  $\geq 900$  °C, hollow carbon shells that are hexagonal, cubic, or rectangular shapes are the predominant morphology (Fig. 44). Carbon materials prepared below 950 °C with zeolite Beta as a template have a high surface area of up to 2270 m<sup>2</sup> g<sup>-1</sup> and contain significant amounts of non-graphitic (*i.e.* amorphous) carbon that exhibits structural pore channel regularity replicated from the zeolite. Thus, by choice of zeolite template and CVD conditions it is possible to nanocast nanoporous carbon materials that exhibit a hollow-core particle morphology, high surface area and zeolite-type pore channel ordering or hollow shells with significant levels of graphitization.<sup>715</sup>

The templating procedure is tedious due to the need to fabricate some templates that have special nanostructures or molecular structures and to remove hard-templates and/or for a post activation treatment. The development of other template-free preparation methods which are much simpler and more cost effective has been explored. Wang and co-workers<sup>716</sup> prepared honeycomb-like hierarchical micro-macroporous carbons from the microwave popping of maize followed by thermal carbonization. The popcorn (Fig. 45A) shows a honeycomb-like macrostructure with pore sizes of 30–40  $\mu$ m. After 900 °C carbonization, the macrostructure was transformed from popcorn to popcarbon. Sample popcarbon-900 retains the honeycomb-like macrostructure

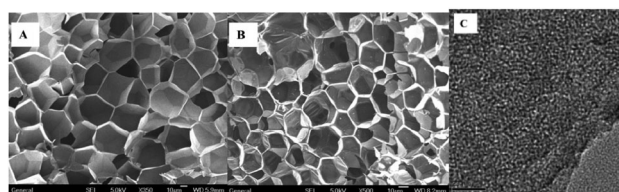


Fig. 45 SEM images of (A) popcorn, (B) popcarbon-900 and (C) TEM image of popcarbon-900. Reprinted with permission from ref. 716. Copyright 2007, American Chemical Society.

with smaller pore sizes of 20–30  $\mu\text{m}$  (Fig. 45B). Inspection of a TEM image (Fig. 45C) shows the existence of disordered micropores in popcarbon-900. The obtained hierarchical micro–macroporous popcarbon materials have adjustable pore volumes and surface areas as well as honeycomb-like macrostructures by changing the moisture content.

Zou *et al.*<sup>717</sup> fabricated hierarchical porous carbons (HPCs) by constructing carbonyl (–CO–) crosslinking bridges between polystyrene chains. The formation mechanism is shown in Fig. 46A. The –CO– bridge simultaneously provide both a high crosslinking density and a large amount of oxygen atoms to the hierarchical porous polystyrene materials. Thus, the carbonizability of crosslinking polystyrene framework and the inheritability of hierarchical nanoporous structure is achieved. The micropores derive from the network inside crosslinking polystyrene-based carbon nanoparticles and macropores (50–400 nm) derive from the aggregation of these network nanoparticles. The TEM images in Fig. 46B and C reveal that numerous micropores exist among the crosslinking polystyrene chains inside the network nanoparticles. Nitrogen sorption analysis (Fig. 46D) shows that the adsorption increases very sharply at low relative pressure ( $p/p_0$ ), indicating the existence of micropores. That the adsorption amount gradually increases to a non-plateau near the  $p/p_0$  of 1.0 demonstrates the presence of mesopores and macropores. The BET surface area, micropore surface area and total pore volume of HPC are  $679\text{ m}^2\text{ g}^{-1}$ ,  $390\text{ m}^2\text{ g}^{-1}$  and  $0.66\text{ cm}^3\text{ g}^{-1}$ , respectively.

Hierarchically micro–macroporous MOF materials can be produced by using various strategies. By using electrospinning, Smarsly *et al.*<sup>718</sup> synthesized composite MOF–polymer nanofibers, a novel class of hierarchical nanostructures that combine the advantages of both types of materials. The diameter (roughly 150–300 nm) of the nanofibers could be adjusted by changing the polymer concentration. The nanoparticle loading could be as high as 1 : 1 by weight ratio of ZIF-8 to PVP. Zeng and Eddaoudi<sup>330</sup>

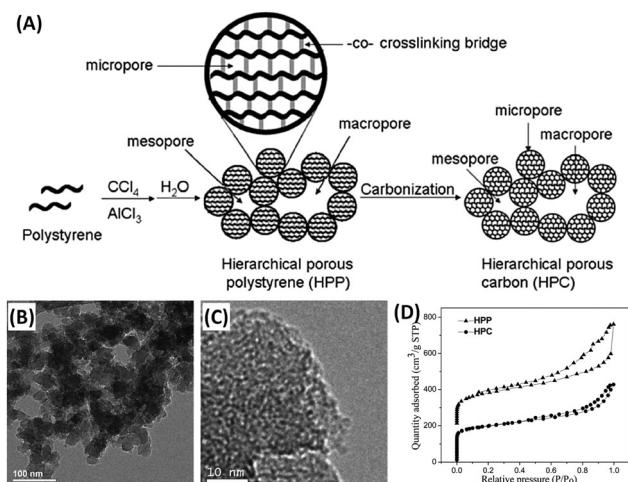


Fig. 46 (A) A scheme of preparation mechanism of hierarchical porous polystyrene (HPP) and carbon (HPC) materials, (B and C) TEM images of HPP and (D) nitrogen adsorption–desorption isotherms of HPP and HPC. Reprinted with permission from ref. 717. Copyright 2010, Royal Society of Chemistry.

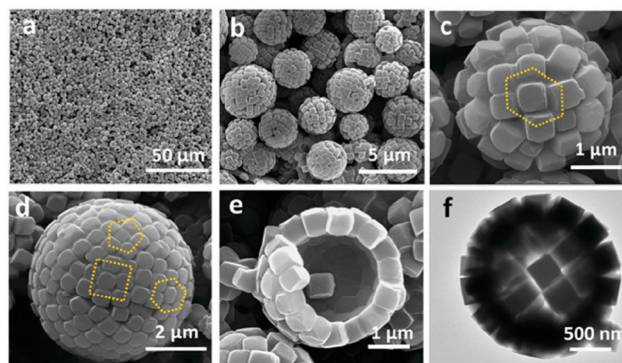


Fig. 47 SEM images (a–e) and TEM image (f) of small Fe-soc-MOF hollow colloidosomes. Reprinted with permission from ref. 330. Copyright 2013, American Chemical Society.

also described a one-step emulsion-based technique that permits the assembly of metal–organic framework (MOF) faceted polyhedral building blocks into 3D hollow superstructures. The shell of each hollow MOF colloidosome is composed of a monolayer of cubic blocks, whose dimensions can be precisely controlled by varying the amount of emulsifier used in the synthesis (Fig. 47).

### 3.4 Hierarchically micro–meso–macroporous structures

Hierarchical structures including micro–meso–macro porosity serve as good catalysts, which can be used to promote various kinds of reactions. In general, micropores, mainly microporous zeolites, oxides and carbon, are often as block units to fabricate mesopores and macropores. The materials with hierarchically micro–meso–macroporosity with defined pore size at each level attract much attention due to their outstanding properties for use in catalysis, separation, energy conversion, storage and biomedical for tissue engineering and drug delivery. A tremendous studies have been carried out on these materials. For the sake of clarity, we divide these studies into those that probe three categories of chemical compositions including zeolite-based, oxide-based and carbon-based micro–meso–macro materials.

**3.4.1 Zeolite-based hierarchically micro–meso–macroporous materials.** Zeolite nanocrystal aggregates with interconnected hierarchically micro–meso–macroporous systems have been prepared *via* a quasi-solid state crystallization process. These hierarchically porous materials, constructed from zeolite nanocrystals, exhibit strong catalytic activity. A meso–macroporous aluminosilicate precursor formed by the self-formation procedure (Section 2.2.4)<sup>9,75–86,317,320,321,323,324,326–353,356,358</sup> is mixed with a structure directing agent (SDA) such as tetrapropylammonium (TPA). A supplementary silica source is added which facilitates transformation of the amorphous phase of the meso–macroporous aluminosilicate to a crystalline micro–meso–macroporous aluminosilicate with zeolite ZSM-5 architecture.<sup>719</sup>

During the transformation, mesoporosity and macroporosity are transmitted to the final materials. The key to the success of this method is to find a suitable crystallization process that not only transforms the amorphous phase into zeolite crystals but also protects the meso–macroporous structure. The structure of the meso–macroporous aluminosilicate is easily destroyed

during conventional hydrothermal reactions owing to its amorphous framework. Therefore, minimizing the damage caused by hydrothermal synthesis to the mesoporous and macroporous structure remains a great challenge to the synthesis of micro-meso-macroporous zeolitic aluminosilicates. The quasi-solid state crystallization (QSSC) process is used to crystallize the walls of the mesopores within the amorphous meso-macroporous aluminosilicate yielding a hierarchically porous material with a well-organized zeolite architecture (Fig. 48). The crystallization process is performed under QSSC using glycerol, as opposed to

fully hydrothermal conditions with water. This means that the structure directing agent can still strongly interact with growing crystal domains, through the formation of covalent bonds with added additional  $\text{SiO}_2$  and  $\text{Al}_2\text{O}_3$  sources by fine tuning the synthetic system, *i.e.* the synthetic gel, medium, temperature *etc.* The glycerol plays an important role in this transformation. As the glycerol becomes more fluid-like it acts as a flux which improves Brownian motion aiding the diffusion of solid particles which is the rate determining step in solid state chemistry. The mesoporous and macroporous structures are then preserved.

It is worthy to note that the synthesis of micro-meso-macroporous materials with zeolitic architecture by using the QSSC process in glycerol is not limited to only ZSM-5 zeolite. This principle has been extended to the synthesis of micro-meso-macroporous Beta (MMM-Beta)<sup>720</sup> (Fig. 49A–E) and zeolites TS-1 (MMM-TS-1) (Fig. 49F).<sup>719,721</sup>

SEM and XRD studies reveal that MMM-Beta and MMM-TS-1 architectures with meso-macroporous structure can be successfully synthesized using the glycerol system, in a manner that is similar to the case of hierarchically micro-meso-macroporous aluminosilicate with zeolite ZSM-5 architecture. MMM-Beta shows a type-I isotherm (Fig. 49C) with a hysteresis at higher  $P/P_0$  due to the presence of the microporosity and inter particle mesoporosity. The narrow distributions show MMM-Beta contains micropores (around 0.5 nm), mesopores (around 3.8 nm) and macropores (around 100–200 nm). The  $^{27}\text{Al}$  MAS NMR spectrum of MMM-Beta (Fig. 49D) contains a very strong peak around 55 ppm, corresponding to tetrahedral Al sites in crystalline zeolite. It is believed that this strategy provides a unique, effective, low cost and potentially general approach for the synthesis of hierarchically micro-meso-macroporous materials with zeolitic architecture.

Most importantly, even after calcination at 550 °C for 5 h, the TS-1 nanocrystals in the macroporous walls do not aggregate

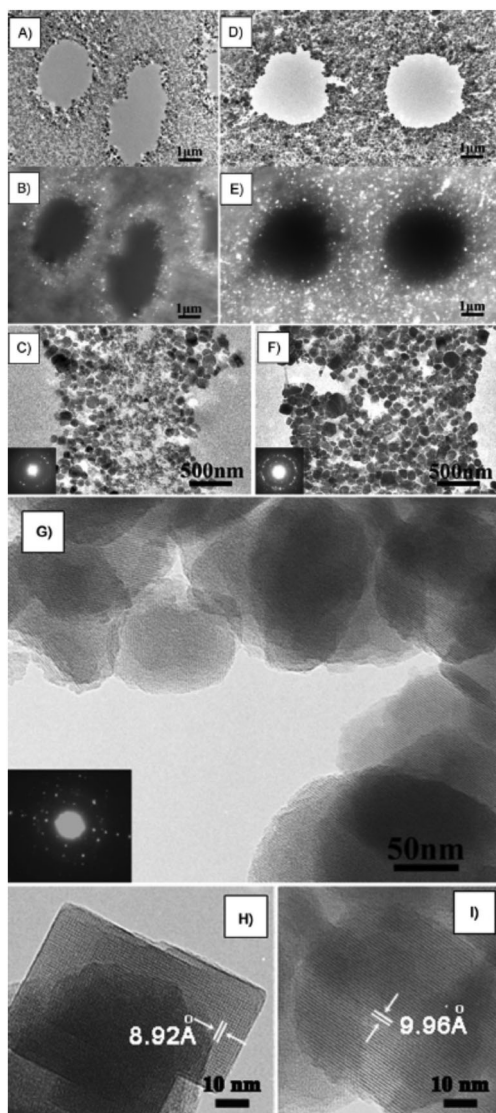


Fig. 48 TEM investigation of the formation of micro-meso-macroporous aluminosilicate. (A–C) Correspond to MMM(1) with (A) bright-field and (B) dark-field images taken on the same area and (C) a higher-magnification view of (A). (D–F) Correspond to MMM(2) with (D) bright-field and (E) dark-field images taken on the same area and (F) a higher-magnification image of (D). (G–I) HRTEM images of MMM(2). The insets in (C, F, and G) are the corresponding selected-area electron diffraction patterns taken from numerous particles. Scale bars: (A, B, D and E) 1  $\mu\text{m}$ , (C and F) 500 nm, (G) 50 nm, (H and I) 10 nm. Reprinted with permission from ref. 719. Copyright 2011, Wiley-VCH.

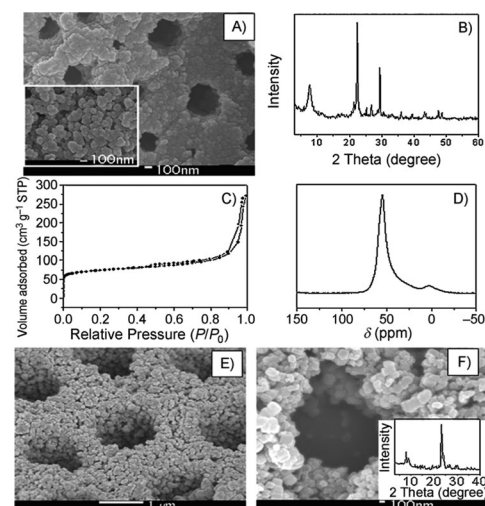


Fig. 49 (A) SEM image (inset: high magnification image), (B) wide-angle XRD pattern, (C)  $\text{N}_2$  isotherm, and (D)  $^{27}\text{Al}$  MAS NMR spectrum of MMM-Beta. (E and F) SEM images and wide-angle XRD patterns (inset of F) of MMM-TS-1. Scale bars: (A) 100 nm, inset: 100 nm, (E) 1  $\mu\text{m}$ , (F) 100 nm. Reprinted with permission from ref. 719. Copyright 2011, Wiley-VCH.

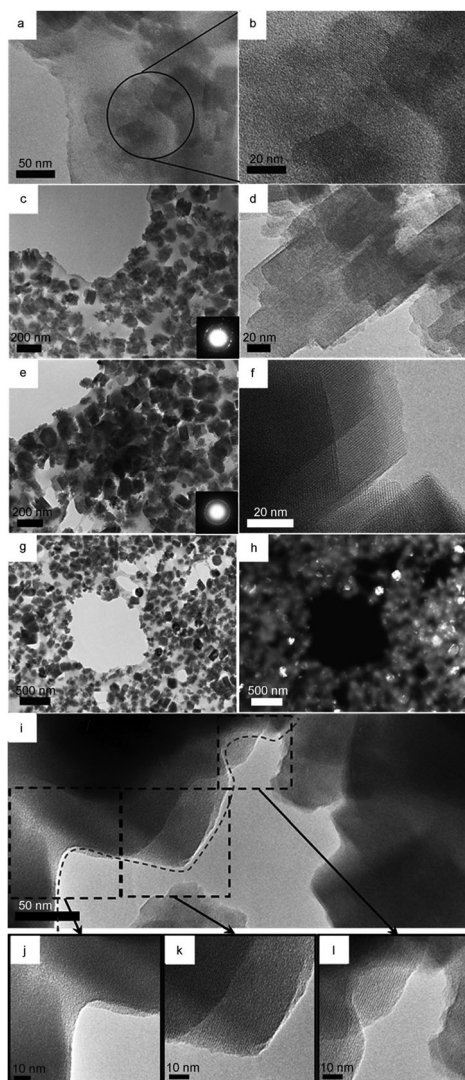


Fig. 50 TEM images of products obtained after various crystallization periods. (a and b) MMM-TS-1 (1 day); (c and d) MMM-TS-1 (2 days); (e–l) MMM-TS-1 (3 days). Reprinted with permission from ref. 722. Copyright 2011, Wiley-VCH.

and, as a result, mesoporosity remains intact as can be seen by viewing the high resolution TEM image displayed in Fig. 50.<sup>722</sup>

The TEM study demonstrates that each zeolite nanocrystal has a highly microporous crystalline zeolite MFI structure (Fig. 50k and l, magnified images corresponding to the regions highlighted in Fig. 50i) and, also, that the large particle aggregates are comprised of zeolite nanocrystals bonded together through interconnecting amorphous regions (Fig. 50j). This is a unique structural characteristic, which results in a great improvement in the stability of the hierarchically porous structure, and which also is a critical factor in avoiding the collapse of the macropore walls in the final product.<sup>722</sup>

Furthermore, inspection of TEM images (Fig. 51)<sup>723</sup> confirms that MMM-Beta is completely composed of randomly orientated highly crystalline zeolite Beta nanocrystals. This means that amorphous domains of the initial precursors are completely transformed into highly crystalline zeolitic phases

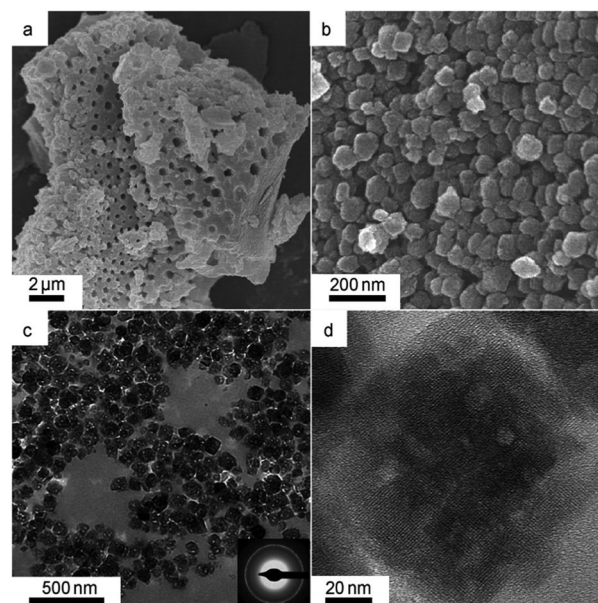


Fig. 51 (a and b) SEM and (c and d) TEM investigations of MMM-Beta. The inset in (c) is the corresponding selected area electron diffraction (SAED) pattern taken from many particles. Reprinted with permission from ref. 723. Copyright 2011, Wiley-VCH.

in the final MMM-Beta after quasi-solid-state transformation process for 8 d at 150 °C. These mesopores and micropores are located in the same matrix as part of a pore system with a new hierarchical architecture. As estimated using TEM, the mesopore size is ~2.5 nm. Hence it can be said that there are dual modal mesoporous systems in the final MMM-Beta, including the larger interconnected mesopores formed by the aggregation of zeolite Beta nanocrystals and micropores distributed in each zeolite Beta nanocrystal. The small mesopores distributed in each zeolite Beta nanocrystal further improve the accessibility and catalytic selectivity of the final product, which is important for the practical applications in reactions.

Fan and co-workers have carried out in depth work on the fabrication of hierarchical structured materials for photocatalysis by using bio-inspired leaf structure,<sup>94,419,724–730</sup> diatom structure,<sup>87,424</sup> wood structure<sup>425,731,732</sup> and butterfly wing structure<sup>724,733–740</sup> designs. These designs not only mimic or copy the hierarchical structure of the natural material, but also perfectly mimic the natural process. This is very close to the Holy Grail of natural mimicking. For example, 3D hierarchical structures of leaves are designed as a promising prototype for efficient mass flow including gas exchange, water transportation (Fig. 52) and light harvesting.<sup>419</sup> N-doped TiO<sub>2</sub> replicas could be obtained *via* a two-step infiltration process with hierarchically porous natural leaves as bio-templates. The replicas show a hierarchy at the macro-, micro- and nanoscales, where the macropores are caused by convexly shaped epidermal leaf cells (Fig. 52a), mesopores are caused by tubelike parallel bundle sheath extensions (Fig. 52b), and intercross meso-macropores are caused by the differentiation of columnar palisade mesophyll cells and irregularly arranged spongy cells (Fig. 52c). There is no clear collapse shown by the porous framework (Fig. 52d). Very interestingly, the

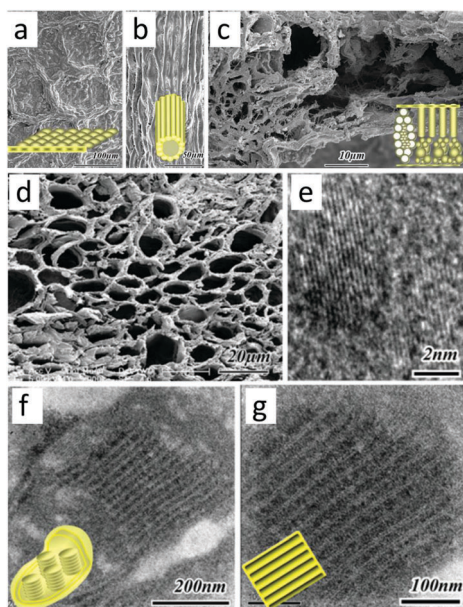


Fig. 52 FESEM images (a–d) and TEM images (e–g) of N-TiO<sub>2</sub>. Reprinted with permission from ref. 419. Copyright 2010, Wiley-VCH.

results of a TEM study show the existence of nanolayered lamellar structures of granums in chloroplast, which might be key to photocatalysis (Fig. 52e–g). After deposited with Pt nanoparticles, the obtained N-TiO<sub>2</sub>-Pt composites show highly effective light-harvesting, photoconversion and catalytic modules, suggesting that such a hierarchical system is possible to realize artificial photosynthesis.

Another example is the fabrication of bio-inspired butterfly wings with diverse brilliant colors caused by hierarchical architectures.<sup>724,733–740</sup> Most recently, a hierarchically porous structured system has been constructed by controlled assembly of light-harvesting plasmonic nanoantennas onto a typical photocatalytic unit with butterfly wings' hiererarchical architectures.<sup>88</sup> Fan *et al.* demonstrated that different hierarchical structures of butterfly wings' can act as macro-templating to fabricate the hierarchically porous BiVO<sub>4</sub>/Au nanocomposite (Fig. 53a and b). Pure monoclinic bismuth vanadate (BVO) wings synthesized *via* a sol-gel using butterflies' wings have a quasi honeycomb architecture (Fig. 53a and b). Au nanorods (Au NRs) were dispersed into the pore structure of BVO to form light harvesting nanoantennas. Most importantly, the structural effects on the obvious far red-to-NIR photocatalysis enhancement was directly attributed to the unique hierarchically porous structure. For example, the color of the region close to Au NRs in Fig. 53c(1) is brighter than Fig. 53c(2 and 3), indicating the electric field intensity near Au NRs in the holes of BVO wing is higher than that on the surface of outside of pores and slab of BVO.

*Luffa* sponge, a typical example of a plant template, possesses a net-like fibrous vascular system and a microcellular architecture with continuous hollow microchannels (macropores with diameter of 10–20 μm) which form vascular bundles and yield a multimodal hierarchical pore system.<sup>414</sup> Biomorphic, self-supporting, MFI-type zeolite, frameworks with hierarchical

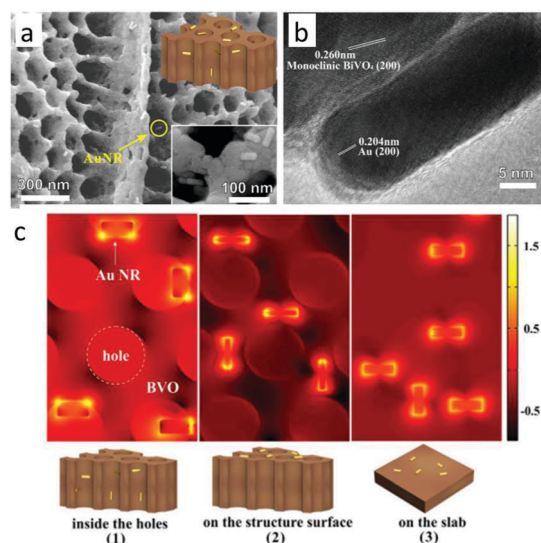


Fig. 53 FESEM image (a) and HRTEM image (b) of Au NRs-loaded BVO wing. A part of log(RE) distribution of simulative Au NRs-loaded BVO at 750 nm (c). Reprinted with permission from ref. 88. Copyright 2016, Nature publishing group.

porosity and complex architecture were prepared using *Luffa* sponge as a macroscale sacrificial structure builder.<sup>414</sup> The XRD pattern of the silicalite-1 replica is characteristic of pure MFI structure. The N<sub>2</sub> sorption isotherms of calcined samples are type I, typical of microporous materials. The occurrence of an additional step and a corresponding hysteresis loop at  $p/p_0 = 0.2–0.4$  indicates the presence of mesopores. SEM images of the calcined free-standing zeolitic replicas reveal that the inorganic framework mimics intricately the original *Luffa* sponge micro-/macroarchitecture, and an external scaffold of well intergrown zeolite crystals supports the entire framework. Furthermore, a continuous bundle of zeolitic microchannels/rods is formed inside the struts of the zeolite scaffold, yielding a bio-inspired catalytic string microreactor (ZSM-5 replica). Despite their size, the low density and complexity of the biomorphic zeolitic macrostructures, zeolite replicas of *Luffa* sponge exhibit reasonable mechanical stability.

Sponges<sup>741</sup> and starch gels<sup>669</sup> have also been used as templates to produce macroporous sponge-like monoliths or meso-macroporous thin films. In comparison with other templates, starch is readily available, inexpensive and easy to process, and methods using this substance is facile, low-cost, environmentally benign and amenable to scale-up. Two methods using starch gels or starch sponges as templates have been investigated. First, macroporous monoliths with continuous mesoporous walls consisting of aggregated microporous silicalite nanoparticles were fabricated by preparing silicalite–starch gel composites and subsequent air-drying and calcination. A range of macroporous monoliths with different macropore sizes (0.5–50 μm) was prepared by varying the amount of starch and the starch/silicalite weight ratio. Hierarchical micro-mesoporous films without macroporous frameworks were prepared by using gels containing low concentrations (2 wt%) of starch as

the template. The final films remain intact in water, ethanol or acetone due to their densities and microstructures. Second, macroporous starch sponges prepared by freezing and thawing of starch gels are used as templates to be infiltrated with colloidal suspensions of silicalite nanoparticles, followed by air-drying and calcination to produce micro-/macroporous silicalite. These two routes can be respectively termed *in situ* preparation of silicalite-starch gel composites and the utilization of preformed starch sponges. In both cases, the resulting materials possess at least two levels of hierarchical pores, namely, micropores in the silicalite walls and macropores in the open-framework monoliths. Incomplete coalescence of the silicalite nanoparticles can also produce a third level of mesoporosity in the hierarchical porous materials.<sup>694</sup>

Reboul and Furukawa reported the synthesis of porous aluminium coordination polymer  $[Al(OH)(ndc)]_n$  fabricated by using replication.<sup>333</sup> They developed a coordination replication method by applying the replacement process to introduce organic elements into a pre-shaped dense metal oxide phase. This process leads to simultaneous formation of coordination complexes on the molecular scale and to construction of a mesoscopic MOF architecture by replicating the parent metal oxide phase. A two-dimensional honeycomb pattern and a three-dimensional inverse opal structure were first constructed as model parent architectures to demonstrate the potential of their strategy in terms of the construction of a mesoscopic MOF architecture (Fig. 54). After coordination replication, selection of both 1,4-naphthalenedicarboxylic acid ( $H_2ndc$ ) as an organic ligand and a randomly structured alumina aerogel as the parent architecture led to formation of a hierarchical, porous system constructed from highly hydrophobic MOF crystals with efficient mass transport properties for water/ethanol vapor-phase separation.

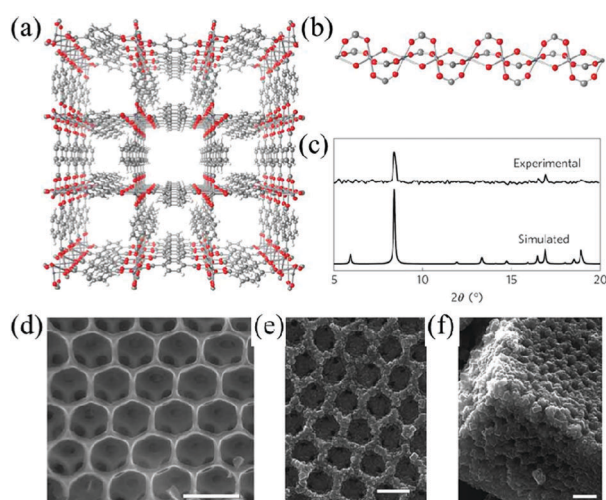


Fig. 54 (a and b) The crystal structure of the aluminium naphthalenedicarboxylate framework. (c) Synchrotron X-ray diffraction pattern of the replica and the simulated pattern of  $[Al(OH)(ndc)]_n$ . (d) SEM image of the three-dimensional alumina inverse opal crystal before transformation. (e and f) Images of the MOF replica after transformation. All scale bars, 1  $\mu$ m. Reprinted with permission from ref. 333. Copyright 2012, Nature publishing group.

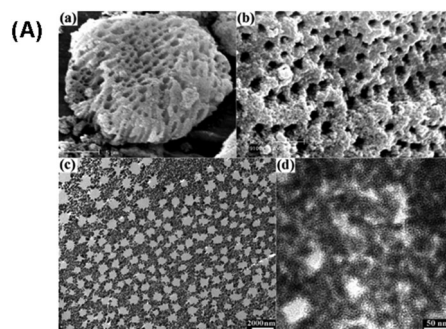


Fig. 55 (A) SEM images of the synthesised zirconia particles showing uniform macroporosity; (c) low-magnification TEM image of a cross-section of the synthesised zirconia showing the uniform macropore structure with mesovoids in the walls; (d) high-magnification TEM image of a region of the macropore walls, showing the assembly of zirconia nanoparticles into wormhole-like super micropores with irregular mesovoids. Reprinted with permission from ref. 355. Copyright 2004, Royal Society of Chemistry.

**3.4.2 The oxides-based hierarchically micro-meso-macroporous materials.** Three length-scaled porous  $ZrO_2$  with an aligned microtubular structure and extremely high surface area of  $>900 \text{ m}^2 \text{ g}^{-1}$  and pore volume of  $3.0 \text{ cm}^3 \text{ g}^{-1}$  were prepared by mixing zirconium propoxide with water-chloroform co-solvent to form an emulsion system. The final macroporous (300–500 nm) material consists of an irregular mesoporous (20–60 nm) framework of super microporous (1.5 nm) nanoparticles of  $\sim 25 \text{ nm}$  size, (Fig. 55).<sup>355</sup> A significant advantage of the hierarchically three-length-scaled pore system that arises from the exceptionally high surface area is facile mass transport from and to the reaction sites, especially required for applications in fields of catalysis, separation and adsorption.

Mixed macroporous metal oxides that contain both textural mesoporosity and microporosity<sup>742–744</sup> have also been fabricated. Recently, Lomoschitz *et al.* have synthesized PS colloidal crystal films using a vertical dip-casting technique.<sup>744</sup> Dip-casting is also used to infiltrate the crystals with a solution containing chelated sol-gel precursors and the non-ionic surfactant, Brij 56 ( $C_{16}H_{34}(OCH_2CH_2)_{10}$ ). Films containing additional organic functionalities in the network were synthesized starting with a trialkoxysilane precursor containing phenyl or methyl groups. These films are composed of either zirconium silicate or titanium silicate. It was found that rather than acting as a soft template for producing mesopores, Brij 56 aids formation and stabilization of the nanoparticles that comprise the walls of the framework. Mesopores are formed between the aggregated clusters of nanoparticles that comprise the wall. Significant microporosity is also present and attributed to the aggregation of individual  $\sim 2 \text{ nm}$  nanoparticle grains.

Fujishima *et al.* used PS colloidal crystals for infiltration with hydroxyapatite nanoparticles.<sup>745</sup> Calcination at  $330 \text{ }^\circ\text{C}$  produces well-ordered 3DOM structures that contain micro-/mesoporosity. However, calcination at  $700 \text{ }^\circ\text{C}$  destroys the ordered macroporous structure.

**3.4.3 The carbon-based hierarchically micro-meso-macroporous materials.** Wood processing is an effective, low cost and

potentially general approach for the synthesis of hierarchically porous carbon foams comprised of activated carbon. High heating rates and high pressures have been used to fabricate carbon particles with hierarchical porous structures by controlling microtexture of materials through the formation of plastic phases.<sup>746,747</sup> Kurosaki *et al.* reported that a three-dimensional hierarchical porous microtexture without wood cell structure can be formed through application of flash heating instead of charring by slow heating.<sup>748</sup> Flash heating followed by subsequent low-temperature heat treatment (380 °C) can also be used in synthesising hierarchical micro-meso-macroporous carbon materials with high BET surface areas (670 m<sup>2</sup> g<sup>-1</sup>).<sup>749</sup> In fact, heat treatment leads to the formation of surface mesopores and micropores of the cross-linked carbon beams in the final material with macropores between the beams. The appearance of such mesopores shows that this synthesis strategy is able to form shape-controlled multiporous carbon with hierarchical micro-meso-macropores.

Many 3DOM carbon materials initially synthesized using colloidal crystal templating contain micropores as a result of the carbonization of the precursors. Carbonized phenolic resins, sucrose-derived carbons and carbonized poly(furfuryl alcohol) are some examples of the “hard” carbons.<sup>750</sup> These materials contain sheets of graphene assembled in a disordered fashion, in contrast to the ordered layered structure of hexagonal graphite.<sup>750</sup> Pores exist between these mismatched sheets, which however are easily lost after pyrolysis at high temperatures (>900 °C).<sup>750</sup> Pyrolysis of polymeric carbon precursors can also generate micro-/mesoporosity as the result of removal of organic groups in the wall framework.<sup>751</sup> The literature contains multiple descriptions of 3DOM non-graphitizing carbon materials with hierarchical porosity. Lei *et al.* used a Stöber silica colloidal crystal assembled *via* vertical deposition and infiltration with a solution containing sucrose and sulfuric acid.<sup>752</sup> Heat treatment and pyrolysis produced 3DOM carbon with a high BET surface area (~400 m<sup>2</sup> g<sup>-1</sup>), mainly from the presence of micro-/mesopores. Stein and co-workers have published multiple reports of the preparation of micropore-containing 3DOM carbon materials by infiltrating PMMA colloidal crystals with base-catalyzed resole solutions of resorcinol and formaldehyde.<sup>753–755</sup> Treatment of the 3DOM carbon using suitable oxidizing agents, such as fuming nitric acid, can further increase the microporosity of the material.<sup>756</sup> Such treatment can equally increase the capacitance of 3DOM carbon by adding oxygen-containing functional groups to the surface.<sup>755</sup> Furfuryl alcohol has also been used as a precursor for these types of hierarchical structures.<sup>757</sup> A silica colloidal crystal is infiltrated with furfuryl alcohol that is polymerized by an oxalic acid catalyst. Carbonization and template removal generates a hard microporous carbon 3DOM structure.

Kanamori *et al.* applied the principle of polymerization-induced phase separation to preparation of a rigidly cross-linked organic systems. The method utilizes living radical polymerization of divinylbenzene in the presence of polymeric component to induce the phase separation.<sup>758</sup> The volume and size of continuous macropores are controlled independently, in a manner similar to the inorganic counterparts described above. The micrometer-sized gel frameworks, however, are mostly

microporous and mesoporous, and their drastic tailoring is not easily performed.

Similar methods have been developed using other types of monomers and catalysts. For example, atom transfer radical polymerization (ATRP) of 1,3-glycerol dimethacrylate (GDMA) in the co-presence of PEO gives similar macroporous polymer monoliths.<sup>759</sup> The use of an organotellurium catalyst also enables extensive structure control of macroporous polymer monolith derived from polydivinylbenzene (PDVB) at lower temperatures (~80 °C).<sup>760</sup> Further, *N,N*-methylenebis(acrylamide) is polymerized in the presence of PEO to give macroporous polymer monoliths. Partly due to the polar surface, the poly(arylamide) monoliths have a relatively high BET specific surface area. Finally, a large volume of micro- and mesopores can be obtained by supercritical drying using CO<sub>2</sub>.<sup>761</sup>

The porous PDVB monolith contains a large number of phenyl groups in the network and is expected to be a good source of carbon materials. Macroporous PDVB monoliths, prepared by living radical polymerization, are directly carbonized and activated in inert and slightly oxidative atmospheres, respectively, to produce carbon monoliths with retained macropores and developed micropores.<sup>122,623</sup> In Fig. 56a and b are compared the macropore structures of dried PDVB and the corresponding carbonized monolith with macroporous morphology. Macropore size become smaller due to the shrinkage during carbonization, which is mainly attributed to the partial pyrolysis of the aliphatic portions preexisting in the PDVB networks. While the macropores are retained in the carbonized sample, the fine structure inside the skeletons of macropores is different from that of PDVB. The PDVB networks possess various sizes of pores in the skeleton of the PDVB gel, while virtually no pores are found in the carbonized skeletons. Depending on the carbonization temperature, the specific surface area reaches 1500 m<sup>2</sup> g<sup>-1</sup> due to the developed micropores.

The features of fine pores in the skeletons and development of micropores are improved by sulfonation of the PDVB networks before carbonization. Efficient sulfonation makes the pyrolyzing networks more rigid and stable, and the fine pores in the skeletons tend to remain after carbonization. The carbon monoliths can be further activated using a slightly oxidative atmosphere to obtain activated carbon monoliths with specific surface area of >2300 m<sup>2</sup> g<sup>-1</sup>. The activated carbon monoliths

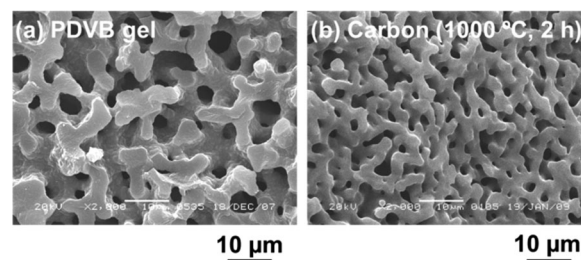


Fig. 56 Comparison of macroporous structures in (a) dried PDVB and (b) carbonized samples. Although macropore size becomes smaller due to the shrinkage during carbonization, co-continuous structure is retained. Reprinted with permission from ref. 631. Copyright 2012, Wiley-VCH.

with trimodal pores (macro/meso/micropores) are found to act as monolithic polarizable electrode materials for electric double-layer capacitors with good electrochemical performances.<sup>261</sup>

### 3.5 Hierarchically dual mesoporous structures

Dually mesoporous structured materials can be efficiently synthesized using the surfactant templating approach. Because of the delicate phase behaviour of surfactant mixtures in an aqueous environment, mixing templates has to be carefully controlled to ensure successful formation of dually mesoporous structured materials. For instance, using CTAC and F127 as surfactants, Imai and co-workers fabricated silica nanoparticles that possess a bimodal mesostructure (2.3 and 20 nm), where larger pores originate from the phase-separation of F127.<sup>762</sup> Further studies by this group showed that mesopore sizes can be adjusted through mixing of chemically compatible block-copolymers.<sup>763</sup> Ivanova and co-workers demonstrated that it is difficult to prepare hierarchical mesoporous structures by self-assembly of standard BCs and surfactants, such as Pluronics and CTAB. Therefore, the surfactant templating method can be used as a path for fabricating dually mesoporous structured materials only if the choice of surfactants is well suitable. For example, C16mimCl is a promising surfactant exploited in dually mesoporous structured materials owing to its highly polarizable head group that can induce a weak attraction between themselves and BC micelles to form the desired structure.

In fact, fluoro-/hydrocarbon mixtures are known to form separated micelles,<sup>764–766</sup> as long as both surfactants have correct sizes. The mixture of these micelles can be employed for concurrent templating of silica by two independent, self-organized templates. The special feature of the fluoro-/hydrocarbon template is that it forms two individual micellar species under all conditions as is evidenced by a mutual structural cross-influence (Fig. 57).<sup>767</sup> The combination of a special small fluorosurfactant with 'KLE' [ $\text{H}(\text{CH}_2\text{CH}_2\text{CH}_2(\text{CH})\text{CH}_2\text{CH}_3)_x-(\text{OCH}_2\text{CH}_2)_y\text{OH}$ ] and 'SE' [poly(styrene)-poly(ethylene oxide)] copolymers in a certain range of concentrations generates small mesopores between the larger spherical mesopores.<sup>767</sup> Careful analysis of pore architecture by using nitrogen sorption measurements and transmission electron microscopy (TEM) aids in establishing

the parts of the phase diagrams independently from the relative template concentration. For the KLE and OTN [ $\text{CF}_3(\text{CF}_2)_{6-16}\text{C}_2\text{H}_4\text{EO}_{4-5}$ ] mixture, miscibility over the whole range of compositions has been observed. For high KLE content, a mixed micellar phase is formed where the two different micelles are packed in a type of organized array. For other compositions, the mutual presence of surfactants lowers the order and mixed micellar phases with liquid structures are observed. At ratios approaching 1 : 1, the liquid mixture undergoes "crystallization" and the coexistence of two highly organized liquid-crystal phases is clearly identified by using TEM. Similar results were obtained by Grosso and Linden, in studies of a method based on the use of a mixture of two surfactants as structure-directing agents: the non-ionic triblock-*co*-polymer F127 and the cationic fluorocarbon surfactant IC-11 [ $\text{C}_8\text{F}_{17}\text{CH}_2\text{OHCH}_2\text{NH}(\text{C}_2\text{H}_5)_2\text{Cl}$ ].<sup>768</sup>

Coppens and co-workers reported the fabrication of bimodal mesoporous silica in a two step process. In the first step, a primary mesoporous MCL-41 ( $\approx 2$  nm) material is prepared hydrothermally using CTAB with a comparatively small molecular structure as a template. Then a pore system (16–50 nm, dependent on solvent) is introduced *via* hydrothermal treatment of the synthesized MCM-41 materials in the presence of P123.<sup>769</sup> A hysteresis loop is seen in the isotherms around  $P/P_0 = 0.8$ – $0.98$  a flat hysteresis loop is located at  $0.4$ – $0.55$ .

The larger mesopores are about 20 nm and their distribution is quite broad. However, in all cases, structural control is difficult and most of the bimodal mesoporous materials lack well-defined pore structures on at least one length scale.

Nonionic template [Si]-MSU-X mesoporous silica with a bimodal pore systems in the pore size range of 3.0–9.0 nm has been obtained by adding different dilute electrolytes (NaCl,  $\text{NH}_4\text{Cl}$  or HF) to the gel mixture.<sup>770</sup> The existence of two different mesophases (lamellar and hexagonal) derives from two pore size distributions (Fig. 58). Cations exert structure-directing effects on a proposed flexible PEO/water/silicate ternary complex, leading to modified micelle packing and subsequently modified pore symmetries of materials are formed. On the other hand, anions change the rate and extent of TEOS hydrolysis and condensation *via* the formation of 5-coordinate intermediates of varying strengths. Studies of this special anion effect show that

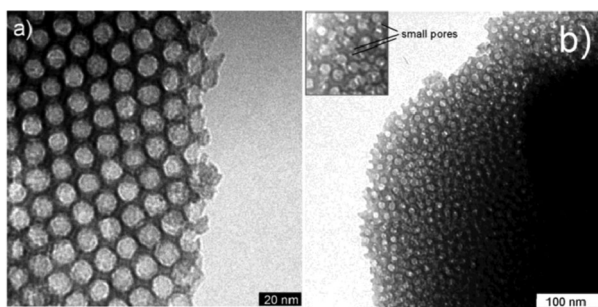


Fig. 57 TEM pictures of samples KLE-1 (a) and KLE-2 (b). As the OTN content increases, the ordering of the sample decreases (b). For the sample KLE-2, the small pores generated by the OTN oligomer can be visualized between the KLE pores (see the inset). Reprinted with permission from ref. 767. Copyright 2004, American Chemical Society.

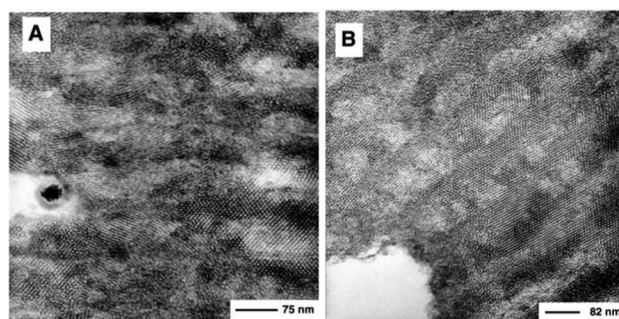


Fig. 58 TEM images of hydrothermally treated and calcined Si-MSU-X mesoporous silicas prepared from dilute electrolyte solutions: (A) NaCl solution, (B)  $\text{NH}_4\text{Cl}$  solution, (C) HF solution. Reprinted with permission from ref. 770. Copyright 2001, Royal Society of Chemistry.

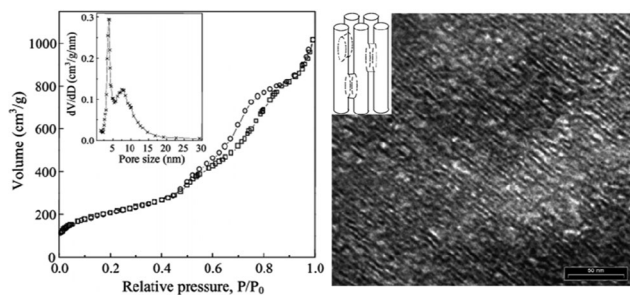


Fig. 59 (left) Typical TEM image of hydrotreated samples showing the existence of double-mesopores. A model of pore systems is schematically shown in the inset. (right) Nitrogen adsorption–desorption isotherms of the hydrotreated and calcined sample and its pore size distribution plot (inset). Reprinted with permission from ref. 771. Copyright 2002, Royal Society of Chemistry.

not only does fluoride greatly increase TEOS condensation and decrease particle sizes of spherical morphology, it can also increase pore diameters. Therefore, the sol–gel processes can be modified and controlled to achieve the synthesis of bimodal porous silicas by adding dilute solutions of electrolytes.

Hierarchically porous structures can be effectively fabricated by employing chemical etching.<sup>771</sup> For instance, when mesoporous silica is treated in a solution of  $\text{NH}_4\text{OH}$ , bimodal mesoporous materials are formed (Fig. 59). Treatment temperature and time can affect the pore structure features. Ammonia molecules, playing a crucial role in the pore expansion process, can penetrate inside the nanochannels more easily than does water. As a result, the channels undergo pore size expansion from 2.3 to *ca.* 4 nm. Due to the low thermal stability of surfactant CPCL (melting point of 86 °C), part of the surfactant species in the meso-channels start to decompose upon hydrothermal treatment. In addition, the silica walls tend to collapse inward due to leaching out of surfactant molecules during hydrothermal treatment. The porosities of the two types of mesopores can be controlled by changing the treatment time and concentration of ammonia.

### 3.6 Hierarchically meso–macroporous structures

Hierarchically bimodal mesoporous–macroporous materials can be prepared by using a self-assembled surfactant or amphiphilic block copolymer in conjunction with macrotemplates such as colloidal crystals, bio-templates, macro-polymers, emulsions, or by phase separations and sol–gel control. Developments made in selective leaching and self-formation have led to the design and synthesis of the meso–macroporous structures. A large number of studies have been carried out in this area. For the sake of clarity, this part will be organized using a synthetic methods based format rather than be chemical compositions of the materials as was employed in discussing material in Section 3.4. The synthetic methods discussed below include nanocasting, colloidal crystal templating, bio-inspired, macroporous polymer templating, emulsion templating, selective leaching, phase separation and self-formation strategy. By using selected examples, we would like to show how to achieve the synthesis of hierarchically meso–macroporous materials, which have desired

mesopore and macropore sizes, shapes and ratios by utilizing these synthesis routes.

**3.6.1 Surfactant templating combined with dispersed colloidal particles templating.** A silicate with a bimodal meso–macropore size distribution can be prepared by using a nanocasting technique.<sup>772</sup> The gel used for the synthesis of the mesophase is generated by self-assembly of a surfactant and silica precursor while the micropores are obtained utilizing colloidal particles. An eggshell-type macrostructured material with an MCM-48-type cubic mesophase was fabricated by adding latex spheres to a mixed solution of CTAC/hydroxide and TEOS (Fig. 60).<sup>773</sup> Skeletal-structured bimodal porous silicates with both an MCM-41 mesophase and a well-ordered skeletal macropore can be prepared by using this method<sup>774</sup> and by carefully controlling the steps involving impregnating the latex spheres and removal of the polymer and surfactant by calcination. The mesoporous phase of this macrostructured material contains a superior 3D ordered macroporous structure with a size ranging from several to hundreds of micrometers located between the walls of the macropores with a MCM-41 structure. The BET surface area of the material is larger than  $1200 \text{ m}^2 \text{ g}^{-1}$ , with a pore volume of  $\sim 1.27 \text{ cm}^3 \text{ g}^{-1}$ .

This method has the advantage that functionalized organic molecules can be directly incorporated into the framework of meso–macroporous materials. For example, dye (2,4-dinitrophenylamine) functionalized mesostructured silica was fabricated with control of the hierarchical pore architecture.<sup>775</sup> Confining the

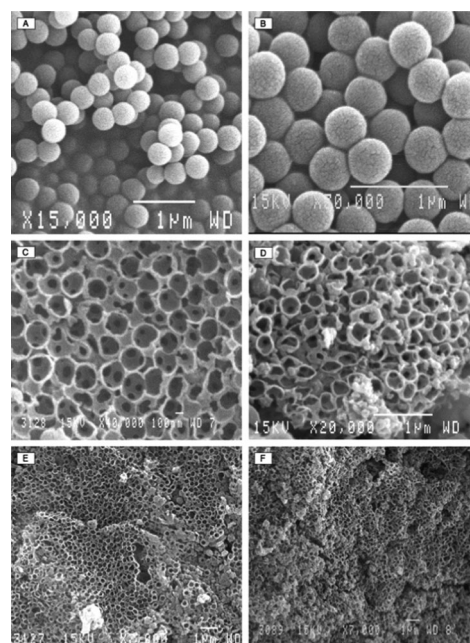


Fig. 60 (A) SEM of latex beads before impregnation, (B) SEM of latex beads impregnated by silica, (C) SEM of sample showing different types of macroporous voids, (D) SEM of sample showing a dispersion of macropores (not representative of the whole sample), (E) SEM of sample showing a better dispersion of macropores (compared to sample F), and (F) SEM of sample showing a poor dispersion of macropores (compared to sample E). Reprinted with permission from ref. 773. Copyright 2009, Elsevier B. V.

evaporation-induced precipitation of reactants within the regular voids of a colloidal crystal (140 nm PS spheres) leads to spatial patterning on the macroscale. A hierarchically ordered organic functionalized silica meso-macrophase can be obtained after the removal of the latex and surfactant templates through extraction. That intact and covalent linked chromophore groups exist in the mesostructured silica network of the hierarchical structure was proven by using Fourier transform-infrared (FT-IR) and diffuse reflectance UV-Vis. This fabrication method can also be extended to the preparation of many other organosilane based materials tailored to specific applications, including ferrocene-based devices in electrochemical sensors, dye-based pH sensors, selective chromatographic supports for combinatorial chemistry, and rhodium/ruthenium-based organometallic complexes for catalysis.<sup>384</sup> During this direct process, the hybrid structures of 3D ordered macroporous silicas with mesoporous walls incorporate in highly dispersed polyoxometalate clusters. The obtained functionalized materials exhibit interesting catalytic performances in the epoxidation of cyclooctene with an anhydrous  $\text{H}_2\text{O}_2/t\text{-BuOH}$  solution at room temperature.<sup>776</sup>

Several reports have detailed the use of the sedimentation-aggregation based colloidal templating techniques to prepare hierarchically meso-macroporous silica materials. Sedimentation-aggregation is a process in which a colloidal dispersion of monodispersed spheres is allowed to sediment in a solution containing a precursor.<sup>777</sup> Kaliaguine and his group used the sedimentation-aggregation technique to produce a hierarchical silica structure with disordered macropores.<sup>778</sup> In this method, PS spheres are added to a solution containing CTAC and CTAOH either before or after the addition of TEOS to the solution. After calcination, the structure contains disordered macropores that are surface-templated with the “air-sphere” morphology. An enhanced order is obtained by adding PS spheres before the addition of the silica source. The authors attribute this result to formation of more evenly-dispersed PS spheres in the less viscous TEOS-free solution.<sup>778</sup>

**3.6.2 Colloidal crystal templating combined or not with SCFs and surfactant templating, respectively.** Ihm and co-workers have developed a sedimentation-aggregation approach using ordered colloidal packing templating to create an interesting 3DOM/m silica structure.<sup>779</sup> SEM images reveal that the 3DOM structure in the calcined product consists of interconnected donut-like rings around the contact points of PS spheres. Hexagonally arranged mesopores are present in the walls. They have also reported how the PS sphere size affects the morphology.<sup>780</sup> Small spheres with 800 nm sizes create either a strut-like 3DOM network or individual ‘donuts’. Nanoparticles with a toroidal shape are formed from condensation of the silica around two touching spheres. Subsequently, the colloidal crystal templating is expanded to hierarchically 3DOM structures composed of different components and composites through combinations with various methods, such as sol-gel control, surfactant templating, replication *etc.*

Hierarchically 3DOM sol-gel based materials have been synthesized.<sup>643,644</sup> Condensation and drying of a sol-gel precursor provides the intrinsic secondary porosity from an interconnected

network of covalently bound polymeric chains or aggregated colloidal particles.

TEOS has been widely used as a sol-gel precursor to fabricate the 3DOM silica.<sup>11,781,782</sup> For instance, a hierarchical silica film was prepared from a monolayer of a PS colloidal crystal *via* infiltration of a solution of TEOS in water/ethanol containing HCl.<sup>781</sup> After removal of the PS colloidal templates, a highly ordered hierarchically porous silica film possessing a BET surface area value of about  $470 \text{ m}^2 \text{ g}^{-1}$  is obtained. Siloxanes, another sol-gel precursor, can also be employed to introduce additional porosity in a 3DOM material. Kuroda *et al.* described the preparation of stable mesostructured films by using self-assembly of different organoalkoxysilanes.<sup>783</sup> The siloxane precursor,  $\text{C}_n\text{H}_{2n+1}\text{Si}(\text{OSi}(\text{OME})_3)_3$ ,<sup>784</sup> ( $n$ : 10 or 16), is hydrolyzed in an acidified water/ethanol mixture and then infiltrated into a colloidal crystal film through dip-coating. Mesostructure in the 3DOM silica frameworks can be adjusted by varying the alkyl chains in the condensing silica network. 2D hexagonal structures are formed by using C10 alkyl chains and lamellar structures are formed by using C16 alkyl chains.

Alkoxide sol-gel precursors, such as zirconium and titanium alkoxides, have been used to prepare 3DOM oxides.<sup>785-788</sup> Typically, an acidified titanium alkoxide sol is first infiltrated in the space between the substrate and PS spheres. Heat treatment then condenses the titania sol to form rings of titania gel. After annealing the gel to remove the PS spheres, the produced anatase titania rings have significant mesoporosity ( $\sim 3.5 \text{ nm}$ ) in the spaces between the growing crystal grains.<sup>788</sup>

Other 3DOM oxides, such as nickel oxides and iron oxides, have been synthesized by using the oxalate precipitation method. The walls of the 3DOM structure contain aggregated crystallites with mesoporosity.<sup>234,653</sup> Vertical deposition is employed to synthesize hierarchical  $\text{SnO}_2$  and Pt-doped  $\text{SnO}_2$  3DOM films.<sup>789</sup> This method has been extended to the synthesis of 3DOM tungsten carbide with textural mesoporosity.<sup>790</sup> Electrochemical deposition has also been employed to generate  $\text{Co}_3\text{O}_4$  films *via* coating a PS monolayer on an indium tin oxide (ITO) substrate.<sup>791</sup> Clusters of  $\text{Co}_3\text{O}_4$  are nanocrystalline and contain mesopores (2–10 nm). A different drying procedure, in which low surface tension cyclohexane solvent is used to exchange with the initial solvent, was used to synthesize a 3DOM vanadium oxide gel with hierarchical porosity.<sup>123</sup>

Nanocomposites,<sup>792</sup> are employed in another method for synthesizing hierarchical carbon structures from materials templated by colloidal particles. The silica precursors in conjunction with polymeric carbon precursors, as mixed sol-gel precursors, can be used to form 3DOM C/SiO<sub>2</sub> nanocomposites by colloidal crystal templating.<sup>377,793</sup>

3DOM metals, such as Au and Ag, have also been prepared by deposition of nanoparticles in a polymeric colloidal crystal followed by extraction of the polymer spheres.<sup>394,410,794</sup> Another example was reported by Zhang *et al.* using hydrothermally synthesized luminescent rare-earth fluoride nanocrystals to prepare hierarchical 3DOM structures.<sup>408</sup> Typically, a suspension of  $\text{NaYF}_4$  nanocrystals, co-doped with Yb and Er, is injected into confined PS fcc colloidal crystals (Fig. 61). After removal of the PS template, a hierarchical 3DOM metal material is obtained, in

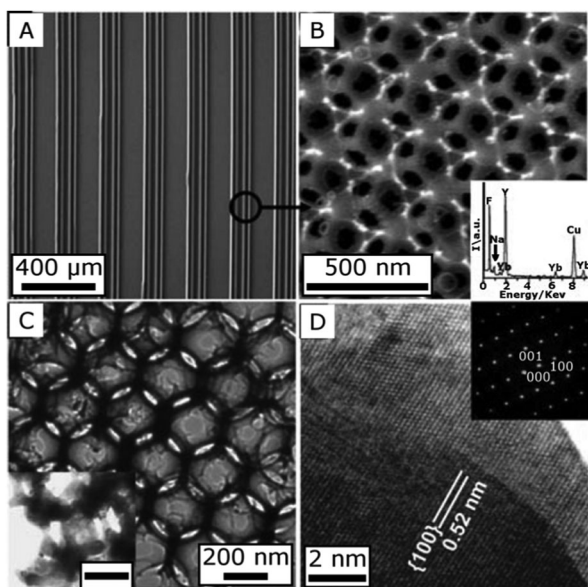


Fig. 61 A set of SEM (A and B) and TEM (C and D) micrographs of luminescent hexagonal  $\text{NaYF}_4$  doped with Yb and Er. The image in (A) shows the structure formed from the PDMS stamp and (B) gives a magnified view showing the 3DOM structure. The HRTEM image in (D) shows the lattice fringes of a single crystal. The inset in (B) is the energy dispersive X-ray spectrum for the sample. The inset in (C) shows a magnified region of the wall structure (scale bar = 50 nm). The inset in (D) is the selected area electron diffraction pattern, which is consistent with the hexagonal  $\text{NaYF}_4$  crystal structure. Reprinted with permission from ref. 408. Copyright 1999, Royal Society of Chemistry.

which luminescence peaks are suppressed by the presence of photonic stop bands.

A different type of hierarchical structure is created by using a bimodal colloidal crystal and vertical lifting deposition with 660 nm PS spheres and 10 nm silica nanoparticles.<sup>795</sup> Calcination of the binary colloidal crystal produces a 3DOM silica network. Furthermore, the electroless plating of gold is used to form hierarchical gold colloidal crystals with textural porosity. Nandiyanto *et al.* reported the preparation of trimodal colloidal crystals from PS spheres with different diameters and silica nanoparticles with a mean diameter of 5 nm.<sup>796</sup> Experiments were conducted to determine the ideal diameter ratios of the colloidal spheres for obtaining ordered porous networks. The results show that a mass ratio of the large to the small PS spheres between 45 and 55 provides the best ordered arrangement of the small pores.

In the SCFs approach for synthesizing hierarchical 3DOM structures with intrinsic porosity, avoidance of capillary pressures exerted on the gel during liquid evaporation is accomplished by replacing it with a low surface tension fluid. To produce a hierarchical 3DOM silica aerogel, Cabañas *et al.* conducted a synthesis in a pressurized reactor containing pre-formed polymeric colloidal crystals, TEOS, water and supercritical  $\text{CO}_2$ .<sup>797</sup> Condensation is restricted to the interstitial spaces of the templates, because benzenesulfonic acid as an acid catalyst is adsorbed on the spheres during a pre-treatment step. Calcination of the templates yields mesoporous 3DOM

aerogels that have a high BET surface area of  $\sim 500 \text{ m}^2 \text{ g}^{-1}$  and that, exhibit less shrinkage than material synthesized by using xerogel 3DOM silica. Later studies showed that the concentration of the acid catalyst influences the morphology of the 3DOM silica, which varies from incompletely infiltrated networks at lower concentrations and completely filled networks at higher concentrations.<sup>798</sup>

Surfactant templating has allowed researchers to produce many mesoporous materials that contain different types of mesostructures, pore sizes and compositions. Stein and co-workers reported that using the cationic surfactant CTAOH in the preparation of 3DOM/m (3DOM with ordered mesoporous framework) silica dramatically increases the BET surface area ( $1337 \text{ m}^2 \text{ g}^{-1}$ ) compared to 3DOM silica produced without a soft template (less than  $230 \text{ m}^2 \text{ g}^{-1}$ ).<sup>799</sup> The related surfactant CTAB was applied in the synthesis of hierarchically 3DOM/m structured dye-modified silica by infiltration of a gravity sedimented PS colloidal crystal.<sup>775</sup> After chemical extraction of the template, a hierarchical structure with worm-like mesopores is obtained. Cationic surfactants have also been used for the synthesis of 3DOM/m silica films through several other routes, including infiltration accomplished by spin-coating<sup>379,800,801</sup> and an electrochemical deposition technique.<sup>801</sup>

Nonionic surfactants have been extensively used as amphiphiles in a variety of 3DOM silica syntheses. Generally, under acidic conditions P123 surfactant is used as a soft template to produce a 2D hexagonal arrangement of mesopores, while the use of F127 surfactant has a tendency to lead to formation of cubic mesostructures. Moreover, a Brij-type surfactant can be used to generate both cubic and 2D hexagonal mesophases.

Luo *et al.* infiltrated PS colloidal crystals with a precursor containing acid-hydrolyzed TEOS and P123.<sup>802</sup> After drying and calcination of the infiltrated templates, a 3DOM/m silica material was produced that has ordered mesopores and a BET surface area of  $915 \text{ m}^2 \text{ g}^{-1}$ . Additionally, mesoporous SBA-15 structure templated by P123 were also introduced into the framework of 3DOM/m silica.<sup>670,671</sup>

Similarly, infiltration with TEOS and F127 has been used in the synthesis of 3DOM/m silica.<sup>803,804</sup> For example, Villaescusa *et al.* used an ethanolic solution containing dilute aqueous HCl, TEOS, and F127 to form the meso-macroporous structure *via* spin-coating to infiltrate the colloidal crystal templates.<sup>804</sup> Also, samples have been coated with a thin shell of silica on the PS spheres using a CVD process with  $\text{SiCl}_4$  and  $\text{H}_2\text{O}$ . CVD deposition of silica further strengthens the film (Fig. 62).

In synthesis of 3DOM/m silica using F127 and P123, alcohols have been employed as co-solvents to alter and/or change the size of mesopores. Short chain alcohols are weak amphiphiles that act as co-solvents to alter the properties of micellar surfactant aggregates.<sup>372,805–807</sup> For example, Sen *et al.* used *n*-pentanol and *n*-butanol to obtain disordered, columnar, spherical or cubic mesopores in the calcined 3DOM/m silica materials.<sup>805,806</sup>

Brij 56 surfactant ( $\text{C}_{16}\text{H}_{34}(\text{OCH}_2\text{CH}_2)_{10}$ ) has been used to create hierarchical 3DOM/m silica.<sup>257,678–680</sup> This surfactant is capable of forming a true lyotropic liquid crystal phase when placed in a sol-gel silica precursor.<sup>808</sup> Cubic and 2D hexagonal

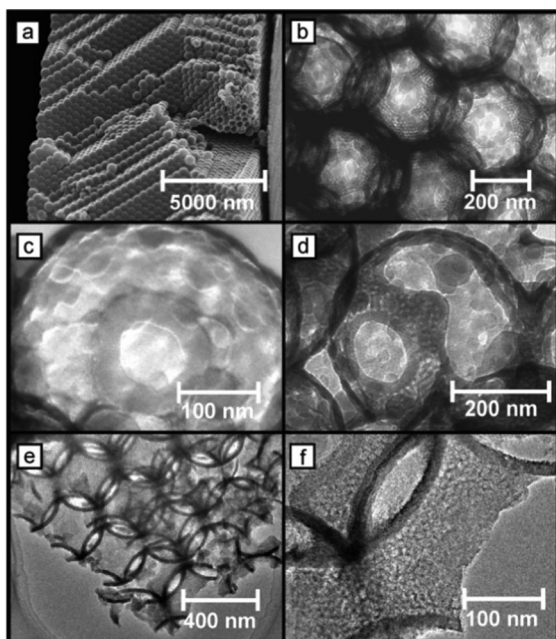


Fig. 62 (a) SEM image of a cross section of a macroporous cavity film made from a silica-stabilized polystyrene sphere crystal. (b–d) Are HRTEM images of a thin piece of the same film. (b) Picture showing, simultaneously, the order at the macropore and the mesopore level. (c) An example of the stabilizing dense silica shell on top of which the mesoporous network is built up by infiltration. For the sake of clarity, the polystyrene sphere used as a template has been dissolved to show only the shell. (d) Mesoporous network on top of dense silica spherical shells. The circular windows interconnecting the macropores can be clearly seen. Images shown in panels (e) and (f) correspond to a disordered mesoporous network built in a macroporous lattice of dense silica shells. The different density of both kinds of silica can be clearly appreciated. Reprinted with permission from ref. 804. Copyright 2005, American Chemical Society.

mesophases are also formed by varying the amount of Brij 56 used and by adding the swelling agent dodecane to the precursor. It is important to note that the effects of confinement are crucial in governing the mesopore architecture for purely mesoporous samples.<sup>257,679,680</sup>

The combination of colloidal crystal templating and surfactant templating opens a new pathway to construct other 3DOM/m oxides. A hierarchical titania film with a poly(dimethyl siloxane)-*block*-methyl methacrylate poly(ethylene oxide) surfactant has been prepared by using atom-transfer radical polymerization.<sup>809</sup> This surfactant in combination with THF, isopropyl alcohol, HCl, and titanium tetraisopropoxide is added to a dispersion of PMMA spheres with PDMS grafted on the surface. The resulting films contain a disordered network of pores from PMMA spheres at around 1  $\mu\text{m}$ .

Multiple routes have been investigated for the synthesis of alumina. These routes utilize a combination of colloidal crystal templating and surfactant templating in order to ensure that hierarchically structured alumina materials are created. The synthesis of amorphous alumina with hierarchical porosity has been reported.<sup>810–812</sup> Highly ordered mesopores (4–6 nm) are observed to be present in the walls of 3DOM structure. Furthermore, several methods have been developed for preparation of

3DOM/m  $\gamma$ -alumina.<sup>813–815</sup> For example, Dai and co-workers showed that a 3DOM/m  $\gamma$ -alumina structure can be made from precursors containing both ordered macropores and 4–8 nm ordered mesopores by using F127 surfactant and aluminum nitrate in a 95 : 5 wt% ethanol : water solution.<sup>814</sup> In addition, 3DOM/m MgO and  $\text{Ce}_x\text{Zr}_{1-x}\text{O}_2$  have been synthesized by using phase segregation.<sup>814</sup> Further, 3DOM/m MgO is prepared by dissolving magnesium nitrate, citric acid, and F127 into an ethanol/water solution. After adding PS colloidal templates, the mixture is dried and calcined to yield the hierarchical ordered meso-macroporous MgO. 3DOM/m  $\text{Ce}_x\text{Zr}_{1-x}\text{O}_2$  is made in a similar fashion with cerium nitrate and zirconium oxynitrate as precursors. Both samples contain disordered mesopores.<sup>814</sup> Other coating and/or doping methods have been developed to fabricate the 3DOM compounds, such as  $\text{MoVTeNbO}_x$ <sup>816</sup> and cerium oxide.<sup>256</sup> Composites containing silica and another oxide with a 3DOM/m structure have been generated.<sup>347,817</sup>

A non-ionic surfactant has also been used to create 3DOM/m metal structures.<sup>818</sup> Yamauchi and Kuroda used the non-ionic surfactant  $\text{C}_{16}\text{EO}_8$ , to prepare 3DOM/m Pt films.<sup>818</sup> Pt is first electrodeposited in the interstitial spaces of the colloidal crystal. After removal of the template, the 3DOM/m Pt film with ordered macropores is formed without having any large-scale defects or cracks. X-ray diffraction data confirm the presence of Pt metal and the identity of the disordered mesostructure.

3DOM/m silica has proven to be an effective mold for nanocasting 3DOM/m carbon.<sup>99</sup> In a typical procedure, a vapor-phase polymerization of phenol and paraformaldehyde is conducted on the surface of 3DOM/m silica. Carbonization of the polymer followed by removal of the silica by HF produces the 3DOM/m carbon. In this material, the 3DOM structure of the template is directly maintained, while the mesoporous walls are inverse replicas of the original walls of 3DOM/m silica. Furthermore, graphitic carbon can be added to the mesopores of the 3DOM/m carbon by CVD using acetonitrile vapor.<sup>99</sup> The same nanocasting method employed synthesis for 3DOM/m carbon is also applicable to the preparation of a 3DOM carbon-silicon composite.<sup>402</sup>

A precursor containing the block copolymer surfactant F127 has been employed in the synthesis of 3DOM/m carbon, having highly ordered macropores and spherical mesopores of  $\sim 10$  nm in diameter arranged in a cubic structure.<sup>820</sup> An extra thermal treatment step<sup>819</sup> is conducted at 140  $^\circ\text{C}$  to further strengthen the polymer network. SAXS patterns and TEM images confirm that by changing the amount of F127, both cubic (Fig. 63A–C) and 2D hexagonal (Fig. 63D–F) mesopore morphologies can be generated. These morphologies are different from that of non-hierarchical, bulk mesoporous carbon due to the effect of confinement in the colloidal crystal template. Mesopore sizes are small for the 3DOM/m carbon samples ( $\sim 3$  nm) and nitrogen sorption isotherms evidence that significant microporosity exists.

Resols and block copolymer surfactants have also been used for the synthesis of 3DOM/m silica-carbon composites. Wang and Stein devised an inorganic-organic co-assembly process for synthesizing 3DOM/m C/SiO<sub>2</sub> composites.<sup>821</sup> These workers built upon an existing methods for creation of mesoporous

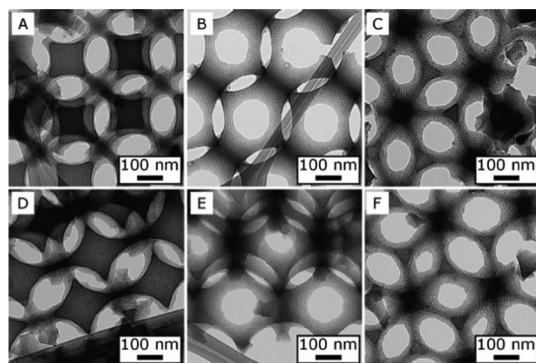


**Fig. 63** Two different 3DOM/m carbon samples, one with a cubic mesostructure (A–C) and one with a hexagonal mesostructure (D–F), are shown in these TEM micrographs. To aid in the comparison, images (A and D) are taken along the [100] axis, images (B and E) are taken along the [110] axis and images (C and F) are taken along the [111] axis. Reprinted with permission from ref. 819. Copyright 2005, Royal Society of Chemistry.

nanocomposites by using a precursor containing a polymerizable organic phase, a polymerizable inorganic phase and a surfactant.<sup>822</sup> This co-assembly method proved to be effective in generating organic–inorganic meso–macroporous composites.<sup>823,824</sup> A monolithic (mm-sized) 3DOM/m composite<sup>821</sup> containing wormhole-like mesopores  $\sim 7$  nm in diameter is obtained. Calcination of the 3DOM/m C/SiO<sub>2</sub> composite produces a 3DOM/m silica monolith, while treatment of the composite with HF generates a 3DOM/m carbon monolith with a high BET surface area of 1900 m<sup>2</sup> g<sup>-1</sup>.

A simple vapor phase deposition technique was employed to prepare a 3DOM/m carbon based composite.<sup>401</sup> In this process, liquid SnCl<sub>4</sub> is gasified in an evacuated vessel containing 3DOM/m carbon to produce SnO<sub>2</sub> nanoparticles into the framework. Shi *et al.* argued that a relatively low-temperature process might serve as an effective way to synthesize a wide range of hierarchically structured carbides.<sup>825</sup> Utilization of these conditions results in a pseudomorphic transformation with the original 3DOM/m structure (Fig. 64). A 3DOM/m carbon–titanium oxide composite was prepared by using a triconstituent precursor containing a titanium alkoxide as the inorganic phase. The carbon–TiO<sub>2</sub> is then converted to titanium carbide *via* the magnesiothermic reduction.

**3.6.3 Bio-inspired.** Bio-templating, using either small-sized natural materials (such as cell, bacteria, diatom and pollen) or large-sized natural ones (such as eggshell, sponge, saccharide, and wood), provides unique opportunities for generating well-organized hierarchical meso–macropore structures.

Cells are the basic organizational units of all known living organisms. Cells have fixed morphologies and high availabilities, making their application to the synthesis of porous materials with tunable macroporous architecture feasible. Sun *et al.*<sup>826</sup> synthesized hierarchical meso-/macroporous titania with tunable macroporous morphology and enhanced photocatalytic performances by using assemblies of differently shaped cells as macrotemplates.<sup>827</sup> Three kinds of cell-assemblies used include spherical *Saccharomyces cerevisiae* cells, baculiform *Stenotrophomonas acidaminiphila* cells, and filamentous *Grifola frondosa* cells (Fig. 65).<sup>667,702</sup> Removal of

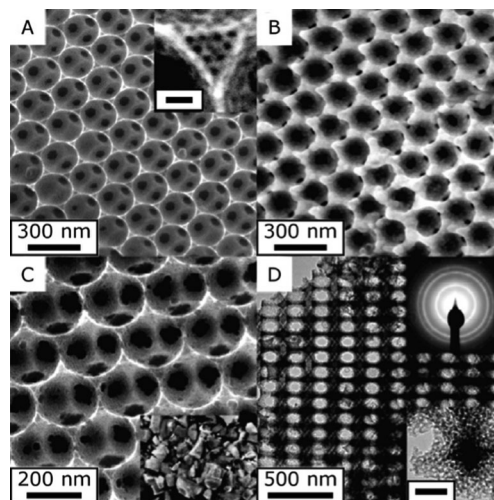


**Fig. 64** SEM and TEM micrographs that show the morphology of a 3DOM/m carbon–silica composite (A) and 3DOM/m silicon carbide (B–D) prepared from the composite. The inset in (A) is an HR-SEM image of the pore network in the composite (scale bar = 20 nm). In (B), an MgO by-product is present, which is removed during processing. The inset in (C) is a photograph of the monolithic pieces of the SiC. The top inset in (D) is the SAED pattern for the polycrystalline SiC and the bottom inset a higher magnification TEM image (scale bar = 50 nm). Reprinted with permission from ref. 825. Copyright 2010, American Chemical Society.

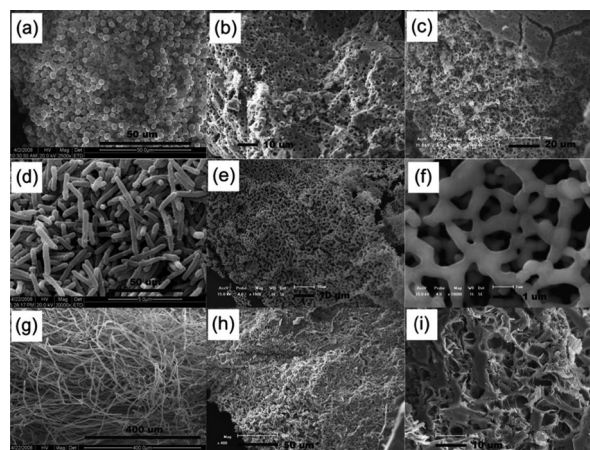


**Fig. 65** SEM images of the fixed and freeze-dried cell-assemblies (a, d and g) and the titania materials using cells assembled as macrotemplates (b and c for sample A; e and f for sample B; and h and i) for sample C). Reprinted with permission from ref. 667, 702. Copyright 2009, Royal Society of Chemistry.

the surfactant and cell macrotemplates gave rise to corresponding titania materials that are hierarchically porous and exhibit relatively homogeneous and uniform macropores with wormhole-like mesopores, respectively. The macroporous structure morphology can be easily controlled by choosing the morphology of the cells. Wormhole-like mesopores are usually formed by the agglomeration of titania nanoparticles possessing large surface areas.

Bacteria are unicellular microorganisms widespread on earth. They have a wide range of shapes, ranging from spheres to rods and spirals, and are also good candidates of macro-templating

for the creation of the hierarchical structures. A bacterial superstructure consisting of a thread of coaligned multicellular filaments of *Bacillus subtilis*<sup>828</sup> has been used to extend the length scale pattern of inorganic materials.<sup>414,828</sup> By using the replication process this bacteria could be employed to fabricate well-ordered porous channels in the silica-based materials.<sup>829</sup> The bacterial superstructure is employed as the hard template to form ordered macroporous fibers of either ordered mesoporous silica (MCM-41) or amorphous silica by the process of replication. Rigid white fibres with a striated surface texture running parallel to the fibre axis are produced following drying of threads dipped into a silica sol. After infiltration with MCM-41 sol, the resulting intact fibre with hierarchical meso/macroporous structure consisting of a porous framework of coaligned 0.5  $\mu\text{m}$ -wide channels enclosed in walls of mesoporous silica is produced. The formation of ordered meso- and macropores in MCM-41 replica demonstrates how supramolecular and supercellular templates might be employed to produce hierarchically structured inorganic materials.<sup>414</sup>

Diatoms are diploid unicells with silica cell walls (frustules), which have 3D amorphous silica shells with cylindrical structure and regular arrays of submicron internal pores.<sup>292,705–707</sup> Because of this they can be utilized as hard templates for many hierarchically porous materials, including metal oxides, carbon, and so on. Inverse carbon replicas of the silica templates with porosity related to the inter-cavities generated among the packed carbon rods have been synthesized.<sup>179,180</sup> The resulting material is more or less comprised of an interconnected system of hollow carbon tubes when the pore system is only coated rather than being completely filled and the additional pore systems are formed because of the voids among the hollow tubes in these carbons.<sup>181</sup> The additional porosity is formed within the well-organized carbon macrotubes as a result of the vacant spaces between adjacent tubes. The surface area is significantly improved from the silica diatom ( $13 \text{ m}^2 \text{ g}^{-1}$ ) to the carbon replica ( $169 \text{ m}^2 \text{ g}^{-1}$ ) and the macroporosity illustrates a novel hierarchical porous structure. The replication of hexagonal arranged pore structure of diatomite can be considered as a micrometric model to demonstrate the nano-scaled carbon replication of MCM-41 silica materials.

Other small biological species can be utilized as hard templates for the preparation of hierarchically porous materials. Meso-macroporous micron-sized particles of silica, calcium carbonate or calcium phosphate materials have been prepared by replicating the complex surface morphology of pollen grains from flowers and trees.<sup>418</sup> Using this approach, a well-defined meso-macroporous texture is obtained. For example, the silica replicas can reach a very high surface area greater than  $800 \text{ m}^2 \text{ g}^{-1}$ . A biomorphic hierarchically meso-macroporous mixed ZnO/Al<sub>2</sub>O<sub>3</sub> framework with specific tubular trichome on the surface has been fabricated by using a legume as the biotemplate and a polycrystal Zn–Al mixed metal oxide framework is gained after calcination.<sup>830</sup> The high dispersion of nanocrystals in this hierarchical structure results in the wide pore size distribution (3–30 nm) and high specific surface area ( $55.44 \text{ m}^2 \text{ g}^{-1}$ ) of the biomorphic Zn–Al mixed meso-macroporous metal oxide framework.<sup>830</sup>

Eggshell membranes are stable in aqueous and alcoholic media and undergo pyrolysis on heating.<sup>831</sup> They are also utilized in the synthesis of hierarchical meso-macroporous materials. Hierarchical meso-macroporous fibrous networks of ZnO have been produced using a solution soaking approach followed by thermal treatment.<sup>832</sup> Mesoporous ZnO with the average pore size 20–30 nm constitutes the wall of the macroporous fibers. Interwoven meshwork composed of hierarchical meso-macroporous structured TiO<sub>2</sub> is fabricated through an aqueous soaking technique followed by calcination process.<sup>833</sup> The resulting TiO<sub>2</sub> meshwork composed of intersecting fibers assembled from nanocrystallites in three dimensions has a hierarchical porous structure with pore size values ranging from 2 to 4  $\mu\text{m}$ . It is worthy to note that the glycoprotein of eggshell mantle macromolecules has been used as the soluble species at various hierarchy levels to form templated mineral hybrids, which are predefined by the subtle structures of the hybrids. Mesoscopically ordered inorganic/biotemplate complexes are fabricated by cross-linking and polymerizing the inorganic species driven by self-assembly of the hydrophilic groups of glycoprotein.<sup>834,835</sup> A simple bio-inspired bottom-up strategy have been developed to prepare hierarchical meso-macroporous metal oxides (such as ZnO, Co<sub>3</sub>O<sub>4</sub> and PdO) by the assembly of nanocrystallites.<sup>836</sup> Interestingly, the hierarchical macroporous fibers, obtained by eggshell membrane templating, can be transformed into tubular structures by using the soaking technique combined with calcination treatment. SnO<sub>2</sub> nanoparticles are reported to assemble into tubular fibers,<sup>837</sup> and then further arrange to form arrays of macroporous meshworks to preserve the morphology of the template. TiO<sub>2</sub> tubes contain anatase nanocrystals with well-ordered hierarchical macroporous networks have been produced using a template of the intact organic membranes isolated from eggshells.<sup>838</sup> Such macroporous microstructure thin films with  $\sim 25 \mu\text{m}$  in thickness consist of interwoven TiO<sub>2</sub> tubes with less than 1.4  $\mu\text{m}$  in diameter, while the tube walls consist of anatase nanocrystals about 10 nm in diameter. The specific surface area of the resulting TiO<sub>2</sub> network is  $62 \text{ m}^2 \text{ g}^{-1}$ .

Some saccharides are excellent candidates for large-sized natural templates in the synthesis of porous materials, because they form complex aggregates with various scales and morphologies in the solution. For example, the cationic polyelectrolyte chitosan, which is a source of different structures in solution,<sup>839</sup> has been successfully used to prepare a monolithic siliceous meso-macroporous materials.<sup>840</sup> Aggregation of the hydrated chitosan helices in the form of bundles of parallel fibers with different sizes can be gelled to produce the same structures. The macroscopic fibers are formed by a sponge-like siliceous network with macropore width of 0.57  $\mu\text{m}$ . The siliceous walls are comprised of microporous-mesoporous networks with multitude pore size distribution at 0.84, 1.0, 1.2, 1.5 nm and a broad band between 3 and 10 nm.

Starch sponge with interconnected macroporous structure has been also used to produce hierarchical architectures in the form of macroporous monoliths or thin films with meso-macroporosity.<sup>694</sup> This process is facile, cost efficient, environmentally

friendly and industrially scalable because starch is abundant, inexpensive, and easy to process.<sup>841</sup> TiO<sub>2</sub> materials with hierarchically meso-macroporous structures have been synthesized using starch gel as a templating agent.<sup>841</sup> The TiO<sub>2</sub> nanoparticles are deposited as coherent layers on the thin walls of the starch frameworks with continuous macropores in the range of 10–100 μm. The final TiO<sub>2</sub> monolith is composed of loosely packed TiO<sub>2</sub> nanoparticles of ~10 nm in diameter.<sup>841</sup>

Wood is an excellent candidate for use as a large-sized structural template for the synthesis of many hierarchically porous materials. This is mainly due to its diversity in terms of species and porous structures, abundance, renewability and low cost.<sup>842,843</sup> Studies using native or chemically treated wood tissues as templates have been reported. For example, silica negative replicas have been prepared by Shin *et al.* via surfactant-assisted sol-gel nanocasting of wood-cell walls.<sup>844</sup> Liu *et al.* prepared hierarchical porous wood-templated ZnO material through a simple hydrothermal bioinspired approach.<sup>426</sup> Zinc ions are introduced through capillary adsorption and are homogeneously deposited on the cell walls of wood during the process. ZnO ceramics with macropore diameters of 15–20 μm and mesopore diameters of ~30 nm that mimic the porous characteristics of the wood template have been produced after calcination. Deshpande *et al.* reported the synthesis of highly crystalline porous oxide replicas by using nanoparticle impregnation.<sup>845</sup> Mechanically stable samples of pure Ce<sub>0.5</sub>Zr<sub>0.5</sub>O<sub>2</sub> are formed by impregnating Ce<sub>0.5</sub>Zr<sub>0.5</sub>O<sub>2</sub> nanoparticle sols into wood tissue followed by careful drying and calcination at 500 °C.<sup>846</sup> The resulting materials have a hierarchical meso-macroporous texture with an average mesopore diameter of 3–4 nm and surface area of ~30 m<sup>2</sup> g<sup>-1</sup>.<sup>845</sup>

**3.6.4 Macroporous polymer templating.** Polymers containing macrostructured or hierarchically structured pores have been used as structural templates to fabricate hierarchically porous materials. Their morphological variability, structural stability and easy removal make them applicable to these synthesis procedures.

Hierarchically porous metal oxides and metallic spheres are widely prepared using polymer spheres. Meyer *et al.*<sup>847</sup> have investigated titania and silica spheres with “golf-ball-like” morphologies that were prepared using polystyrene/divinyl benzene (PS-DVB) spheres. The final inorganic beads are macroporous in nature (~50 nm). The mesopores are interparticulate voids as a result of spaces between the nanoparticles. PS-DVB spheres have been also used for the preparation of a wider range of metal oxides (ZrO<sub>2</sub>, Fe<sub>2</sub>O<sub>3</sub>, In<sub>2</sub>O<sub>3</sub>, Ce<sub>2</sub>O<sub>3</sub>, TiO<sub>2</sub>, Al<sub>2</sub>O<sub>3</sub> and SnO<sub>2</sub>) using preformed nanoparticle solutions or from metal salt solutions for the infiltration of the template spheres.<sup>452</sup> Successful replication was obtained for TiO<sub>2</sub>, ZrO<sub>2</sub>, SnO<sub>2</sub> and CeO<sub>2</sub> whereas impregnation with indium oxide colloidal solution resulted in hollow spheres. Cracked spheres are obtained when using aluminum or iron oxide sols. All the inorganic spheres are crystalline with crystal phases consisting of the lowest stable form of the oxide, whereas the TiO<sub>2</sub> spheres have both anatase and rutile phases. Mesopores also originate from voids between the nanoparticles. By mixing two sols, binary metal oxide replication, such as TiO<sub>2</sub>/Al<sub>2</sub>O<sub>3</sub>, TiO<sub>2</sub>/Fe<sub>2</sub>O<sub>3</sub>

and TiO<sub>2</sub>/In<sub>2</sub>O<sub>3</sub>, can be achieved.<sup>848</sup> Non-functionalized PS-DVB (~15 μm) macroporous (50–500 nm) template spheres have also been used to fabricate the hierarchically porous binary metal oxides spheres (the second metal oxide (Al<sub>2</sub>O<sub>3</sub>, In<sub>2</sub>O<sub>3</sub> and Ga<sub>2</sub>O<sub>3</sub>) is 5, 10 and 15 wt% relative to TiO<sub>2</sub>) by impregnation of mixed metal alkoxide precursor solutions. The average crystal size of TiO<sub>2</sub> is consequently higher (~16 nm) than the mixed metal oxides (6–10 nm), consistent (inversely proportional) with the surface area observations. The mixed metal oxides show interparticulate mesopores, and the macropores (a few hundred nanometers) originate from the template.

The use of PS-DVB beads has also been extended to the preparation of porous metallic (gold) spheres.<sup>454</sup> The polymeric template is soaked in a preformed gold sol containing gold nanoparticle (6–7 nm).<sup>724,725</sup> The meso-macroporosity in the final materials is due to the low degree of fusion of the nanoparticles at the low calcination temperature used. An increase in calcination temperature results in the loss of surface area and destruction of the hierarchical porous structure.

An acidic cation exchange resin sphere comprised of polystyrene cross-linked with divinyl benzene sulfonic acid functionality, having diameter of ~450 μm and pore sizes in the range of 10–600 nm, has been used to synthesize the hierarchical porous Fe<sub>2</sub>O<sub>3</sub>, Al<sub>2</sub>O<sub>3</sub> and TiO<sub>2</sub> beads using a repeated infiltration/precipitation/drying method.<sup>849</sup> On precipitation of the metal hydroxide, the sulfonate groups are then free to interact with various metal ions in subsequent cycling steps. Numerous coatings are required in higher valence metal ions as the exchange capacity of resin decreases with the increase of the metal ions valence. The final Fe<sub>2</sub>O<sub>3</sub>, Al<sub>2</sub>O<sub>3</sub> and TiO<sub>2</sub> beads are around 410, 270, 430 μm in diameter, respectively, with macropores of 0.5–2 μm and 50–100 nm, 50–100 nm, 1–3 μm, and mesopores of 3.5, 5.2 and 8.5 nm. Mesopores in these cases result from interparticle voids.

Other macroporous polymer spheres, such as polyacrylonitrile (PAN) beads to mixed Ti/Zr beads,<sup>381</sup> polyacrylamide (PAM) beads to zirconia, titania, alumina mixed SiO<sub>2</sub>/TiO<sub>2</sub> or SiO<sub>2</sub>/Al<sub>2</sub>O<sub>3</sub> beads,<sup>239,361,850,851</sup> and macroporous alginate beads to magnetic silica beads,<sup>729,730</sup> have been used as macrotemplates for the production of materials with pore hierarchy. For example, Sizgek and co-workers<sup>852</sup> used preformed polyacrylonitrile (PANI) beads as a solid macroporous template and F127 as the structure directing agent for generating mesostructures (Fig. 66). Mixed Ti/Zr beads are prepared by infiltrating the preformed PANI template beads with the mixed metal oxide precursor solution. Amorphous mixed oxide spheres (0.7–1 μm) with bimodal mesoporosity 4.5 nm and 45 nm are produced when calcined at 500 °C. Variation in the mesopore size is achieved by changing the calcination temperature (500–700 °C, 5.1–11.6 nm). However, use of the high calcination temperature of 700 °C results in individual titania and zirconia crystals, in agreement with the thermal stability of the mesophase, which start to deteriorate at around 650 °C.

Polymeric fibers, including cellulosic fibers in paper, cloth and cotton, have been applied as templates to produce hierarchically meso-macroporous films over a range of length scales.<sup>853–855</sup>

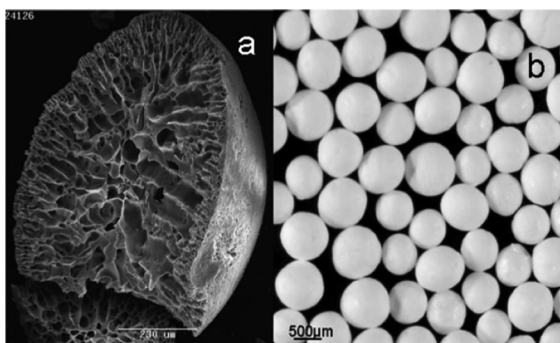


Fig. 66 (a) SEM image of a cross-section of the zirconium titanate bead after removal of PAN and surfactant templates and (b) photo of zirconium titanate mixed oxide beads (calcined at 500 °C). Reprinted with permission from ref. 852. Copyright 2009, American Chemical Society.

These templates are composed of bundles of nanofibers. After infiltration, precipitation, drying and calcination, the paper, cloth and cotton adsorbed in the organic precursor give rise to an oxide structures containing a carbon-like char with an overall morphology mimicking that of the fibril structure of cellulose. The products have mesopores as well as large micrometer sized pores between the fibers. Notably, the hollow fibers of oxides such as titania composed of anatase particles ( $\sim 10$  nm) are obtained (Fig. 67).<sup>854</sup> Interfiber large mesopores or small macropores are present in addition to the tube pores of 10–80 nm and interparticulate mesoporosity.<sup>855</sup> A range of fibrous templates are the collagen-based matrix obtained from natural materials such as above mentioned avian eggshells.<sup>711,716,735,736</sup>

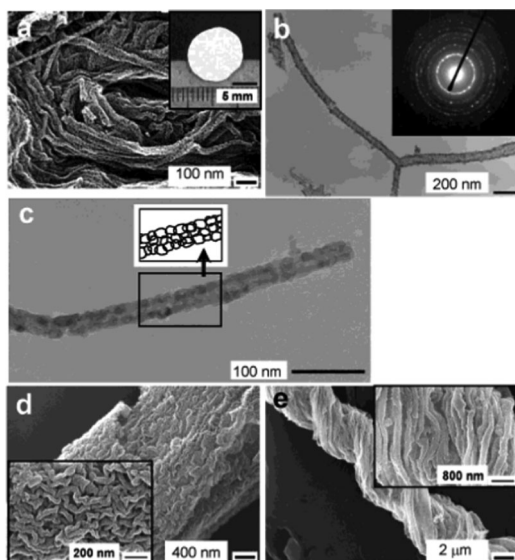


Fig. 67 Titania replicas of natural cellulosic substances. Deposition of titania thin films is repeated 20 times for each sample. (a) SEM image of "titania paper", showing titania nanotube assemblies. The inset shows the photograph of a sheet of "titania paper". (b) and (c) TEM of individual titania nanotubes isolated from the assembly. Inset of (b), SAED pattern from the nanotube assembly. Inset of (c), schematic illustration of the boxed area, showing titania nanotube wall is composed of fine anatase particles. (d) SEM image of "titania cloth". (e) SEM image of "titania cotton". Reprinted with permission from ref. 854. Copyright 2003, American Chemical Society.

Electrospun fibrous polymer mats can be applied as templates to prepare a range of materials (organic, inorganic or composites) with pore sizes on multiple length scales. For example, electrospun poly(L-lactide) (PLA) fibers with a diameter between 0.3–3.5  $\mu\text{m}$  have pores on the surface with an average size of 100 nm in width and 250 nm in length. PLA fibrous mat producing films of  $\sim 50$  nm to several micrometers thick can then be used as scaffolds for producing secondary materials.<sup>315,316</sup>

Meso-macroporous poly(*p*-xylylene) (PPX) mats have been synthesized *via* CVD of PPX onto electrospun PLA fibers. Macroscopic mats of PPX tubes are formed with large pores as a result of intertubular voids. The tubes have inner diameters in the range of 0.05–3.5  $\mu\text{m}$  and a wall thickness of 0.1–1  $\mu\text{m}$ , (lengths of  $> 100$   $\mu\text{m}$ ). Moreover, the polyimide (PI) mats can be prepared by dip coating of the fibrous PLA mat into polyamic acid followed by low temperature annealing to degrade the PLA template and convert the polyamic acid to PI. Such PI tubes have an inner diameter of 1–2  $\mu\text{m}$  and large intertubular pores. Polymeric-metallic hybrid fibrous mats have also been synthesized by using physical vapor deposition to coat PLA with aluminum or gold before CVD of PPX followed by thermal decomposition of PLA giving tubes containing metal on the inner surfaces (inner diameter of 0.5–1.5  $\mu\text{m}$ ) and a PPX outer coating. The composite tubes with smaller internal diameters (a few nanometers to tens of nanometers) have been prepared by altering the size of the initial fiber templates. This can also be accomplished by including palladium(II) diacetate or pyridine in the polymeric solution (PLA/dichloromethane or poly(tetramethylene adipamide) (PA)/formic acid, respectively).<sup>450</sup>

Oxides tubular mats<sup>856</sup> have been successfully prepared using electrospun PLA and chemical-assisted post-treatment (such as coating techniques). Careful manipulation of the post-synthesis procedure is necessary in order to mimic the original structure in the final material. For instance, impregnation of titanium(IV) isopropoxide, results in  $\text{TiO}_2$  present interwoven hollow fibers having a diameter of  $\sim 0.8$ –1.2  $\mu\text{m}$  and a relatively smooth outer surface. The tubes are made up of anatase  $\text{TiO}_2$  particles with mesoporous interparticulate voids (Fig. 68). The macropores are a result of intertubular voids and inner tube diameters. The atomic layer deposition (ALD) process has also been used to deposit  $\text{TiO}_2$  coatings onto electrospun poly(vinyl

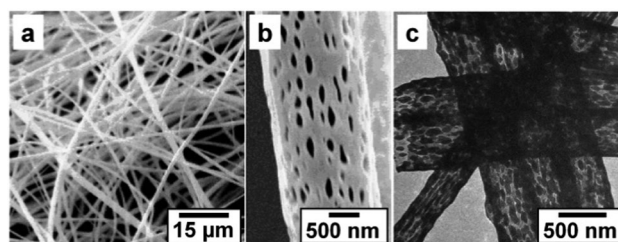


Fig. 68 SEM images of the poly(L-lactide) electrospun fibers. (a) Overview of the fibrous mat produced using the electrospinning technique, (b) surface structure of the polymer fiber observed at higher magnification, (c) TEM image of the titanium dioxide tubes that shows the mimicking nature of the sol-gel coating technique. Reprinted with permission from ref. 856. Copyright 2001, Wiley-VCH.

pyrrolidone) (PVP) fibers.<sup>857</sup> The polymeric fibers had an average diameter of  $\sim 500$  nm with mats consisting of interfiber pores of a few micrometers in size. Layers of amorphous titania films are sequentially deposited at  $70$  °C using titanium(IV) isopropoxide and water. Removal of the PVP core *via* calcination at  $500$  °C for 4 h results in anatase polycrystalline  $\text{TiO}_2$  tubes made up of small platelet grains (10–250 nm) with mesoporous voids as evidenced from TEM analysis. The uniform  $\text{TiO}_2$  coating can also be clearly observed using TEM revealing a wall thickness of  $\sim 60$  nm.

Metallic (Au, Cu or Ni) tubular mats can be generated by using polymeric fibrous mats.<sup>451</sup> Wet chemical processes are used to coat metal salts into/onto the polymeric fibers, followed by reduction of the metal salts. Electrospun polycarbonate (PC) fibers ( $\sim 163$  nm) are used as templates for producing Cu and Ni hollow fibers, whereas electrospun PLA ( $\sim 250$  nm) fibers are used for producing Au hollow fibers. Both templates are activated with an acidic solution of  $\text{SnCl}_2$  and  $\text{PdCl}_2$  prior to impregnation with the metal salt solutions in order to promote binding of the metal colloids to the polymeric template. The morphologies of PC and PLA fibers are successfully replicated after polymer removal. The diameters of the Cu, Au and Ni hollow fibers are  $\sim 475$ ,  $\sim 450$  and  $700$  nm, respectively, with corresponding wall thicknesses in the ranges of 150, 100 and 200 nm. The tube walls are made up of crystalline metallic particles of 5–25 nm in size with interparticulate voids.

Commercial ultrafiltration membranes, such as cellulose acetate membranes with thickness of  $120$   $\mu\text{m}$  and pore sizes of  $\sim 500$  nm to  $1$   $\mu\text{m}$ , have also been used as templates to produce hierarchically porous materials.<sup>858</sup> For example, an  $80$   $\mu\text{m}$  thick titanium dioxide film is obtained with pore diameter of  $100$  nm to  $<1$   $\mu\text{m}$ , depending on the initial membrane pore size used. The packing of the nanoparticulate titania (45–150 nm in diameter) in the structure results in interparticulate mesopores. This led to studies where additional porogens are added during casting of the membranes to produce hierarchical silica films<sup>859</sup> and metal oxide films ( $\text{TiO}_2$  and  $\text{ZrO}_2$ ) *via* a homogeneous coating inside the thickness of the membrane.<sup>860</sup> In all cases, the nanoparticulate nature of titania making up the structure gives mesoporosity to the materials.

With the repetition of coatings it is possible to change the chemical composition, allowing the preparation of more complex structured materials.<sup>860</sup> The combination of coating and casting results in a mesoporous silica (pores of 2.5 nm) containing interconnected macropores of less than  $1$   $\mu\text{m}$  coated with titania (Fig. 69). Alternatively, a porous structure of titania/zirconia was prepared by applying two coatings of titania followed by two coatings of zirconia. This gives individual layers of anatase titania and tetragonal zirconia crystals. In comparison, the use of a mixed precursor solution,<sup>861</sup> as detailed below, results in a primarily amorphous mixed Ti/Zr oxide with pore morphologies (calcination at  $550$  °C) that are dependent on (i) the original membrane pore structure (generally  $\sim 1$   $\mu\text{m}$ ), (ii) Removal of the membrane scaffold on which the inorganic material is coated (pores centered around  $\sim 80$  nm, again depending on the membrane), and (iii) interparticulate voids ( $<8$  nm).

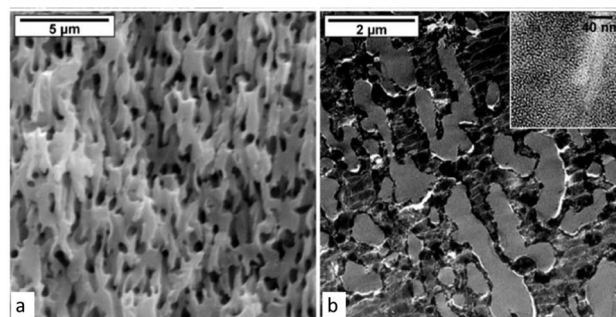


Fig. 69 The sequential coating approach was used to obtain complex materials: (a) SEM image of the  $\text{TiO}_2/\text{SiO}_2$  material (2 layers  $\text{TiO}_2$  followed by cast with silica in the presence of C16E10); (b) TEM image of an ultramicrotome of the  $\text{TiO}_2/\text{SiO}_2$ . Inset shows the mesoporous character of the silica as observed by TEM. Reprinted with permission from ref. 860. Copyright 2006, Royal Society of Chemistry.

Preformed nanoparticles of titania, zirconia, tin oxide, cerium oxide, iron oxide, indium oxide and alumina can also form hierarchically meso–macroporous structures, templated by cellulose acetate and polyamide membranes immersed in these individual sols.<sup>862</sup> The metal oxide films contain macropore sizes of  $0.1$ – $2$   $\mu\text{m}$  along with interparticulate voids. Solutions containing mixtures of the oxide particles with similar weight ratios can be applied to the membrane.  $\text{TiO}_2/\text{In}_2\text{O}_3$ ,  $\text{TiO}_2/\text{ZrO}_2$  and  $\text{TiO}_2/\text{SnO}_2$  materials, which have similar structures to those obtained using the individual oxide, have been prepared using this approach. The notable difference is the surface area, which is much higher in the mixed systems due to the increased separation of the phase domains during the heating step.

Other compounds possessing hierarchically meso–macroporous structures can be prepared using a spin-coated cellulose acetate thin film (thickness  $\sim 5$   $\mu\text{m}$ ).<sup>863</sup> A precursor solution of lithium acetate, cobalt acetate and citric acid in ethylene glycol is used for infiltration. By heating the products to  $450$  °C, nanocrystals of  $\text{LiCoO}_2$  ( $\sim 12.5$  nm) form. Pores less than  $1$   $\mu\text{m}$  in diameter are found in the final structure along with interparticulate pores (mesoporosity). The same approach has been used for the preparation of a  $\text{LiNi}_{1-x}\text{Co}_x\text{O}_2$  film.<sup>864</sup> These materials with hierarchically meso–macroporous structures are quite desirable as cathode materials for Li ions batteries.

Polymer foams with 3D cellular-like porous structure can be employed to produce hierarchically porous materials. Meso–macroporous silica monoliths have been synthesized using preformed silica particles by Huerta *et al.*<sup>865,866</sup> The monoliths have a macrocellular porous network ( $\sim 100$ – $1000$   $\mu\text{m}$ ), interparticulate voids (larger mesopores) and BET surface areas of  $1000$   $\text{m}^2$   $\text{g}^{-1}$  with two distinct mesopore sizes centered at 3 and 25 nm. These are comprised of intra-particle pores that result from surfactant templating/assembly and inter-particle pores that are voids generated between particles. There exists trimodal porous silica monoliths, consisting of macropores templated by PU and a bimodal mesoporous system.<sup>866</sup> The dual mesoporosity in the final monolith can be adjusted and the macropore size can be varied by either using starting materials with different pore sizes or by adjusting the number of coating

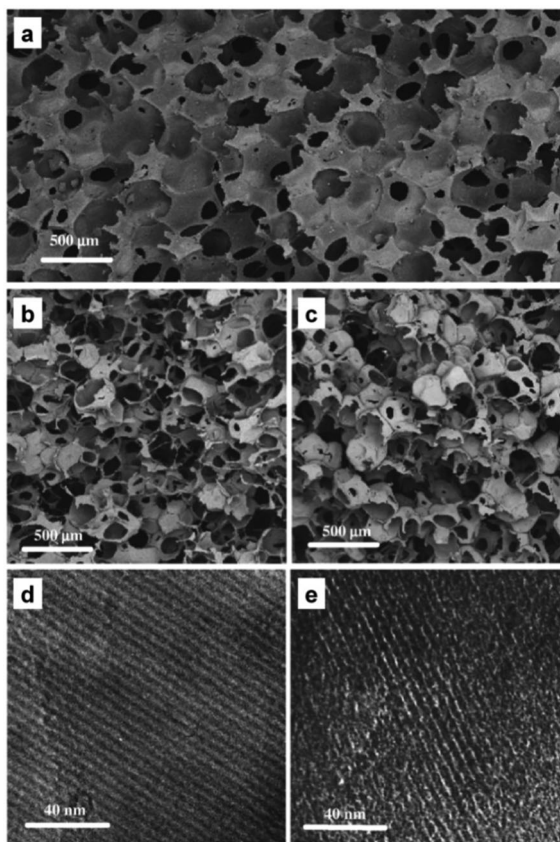


Fig. 70 (a–c) SEM images of the apolyurethane foam, (b) silica, (c) carbon monoliths, and TEM images of the porous structure of (d) silica and (e) carbon. Reprinted with permission from ref. 172. Copyright 2007, Elsevier B. V.

cycles, which influences the thickness of the walls hence affecting the macropore size.

A similar technique has been employed by Alvarez and co-workers<sup>172</sup> to produce meso–macroporous silica and carbon monoliths using commercial PU foam. Both silica and carbon monoliths have macropores of  $\sim 200 \mu\text{m}$ , which derive from the macroporous polyurethane template ( $50\text{--}200 \mu\text{m}$ ), and interconnected thin walls. These materials contain ordered cubic mesopores ( $\sim 7.2 \text{ nm}$  for silica and  $3.4 \text{ nm}$  for carbon, Fig. 70). Xue *et al.*<sup>867</sup> have demonstrated that a PU foam (3D support) along with an evaporation-induced coating and self-assembly process (EISA) can be used for production of ordered mesoporous carbon–silica composites possessing a macroporous framework. The macroporous architecture of the PU template is replicated in the composite material ( $200\text{--}500 \mu\text{m}$ ).

This approach was also extended to produce pure silica monoliths with variable morphologies.<sup>868</sup> By adjusting the volume ratio of the silica sol (P123 as mesostructured template) to the PU scaffold, the silica monoliths can be assembled into stacked polyhedrons with macrocellular cavities ( $100\text{--}500 \mu\text{m}$ ) connected *via* silica cell membranes as a result of the coating of the cell walls. The size of the polyhedrons is similar to the original macropores of the templates. The silica monoliths exhibit an ordered mesoporous structure. Ordered mesostructured

carbonaceous materials with a macroporous morphology have also been reported by Zhao *et al.*<sup>869</sup> In their work, F127 was used as a structuring agent allowing for the formation of an ordered mesoporous structure (from a 3D body-centered cubic to a 2D hexagonal). The resulting carbon monoliths are amorphous in nature even at  $900 \text{ }^\circ\text{C}$ .

Other macroporous polymeric foams have been employed as scaffolds for the fabrication of hierarchically porous materials. Macroporous PS foams,<sup>446</sup> consisting of an open cellular network with pores ranging between  $0.3$  and  $5 \mu\text{m}$  with adjacent windows ranging between  $0.1\text{--}1 \mu\text{m}$ , have been used as templates to prepare hierarchically porous inorganic materials. In the process, the monoliths are dried and then calcinated a various temperatures  $\text{SiO}_2$  at  $500 \text{ }^\circ\text{C}$  for  $6 \text{ h}$ ,  $\text{TiO}_2$  at  $350 \text{ }^\circ\text{C}$  for  $24 \text{ h}$  and  $\text{ZrO}_2$  at  $400 \text{ }^\circ\text{C}$  for  $24 \text{ h}$  to remove the PS template and surfactant yielding a meso–macroporous network. Silica monoliths have a mesopore size of  $\sim 5 \text{ nm}$  with an ordered hexagonal-type mesostructure and macropores in the range of  $150\text{--}500 \text{ nm}$ . They also exhibit high surface areas  $250\text{--}750 \text{ m}^2 \text{ g}^{-1}$ , which increase with increasing silica content. Both zirconia and titania monoliths exhibit lower surface areas ( $83 \text{ m}^2 \text{ g}^{-1}$  and  $155\text{--}220 \text{ m}^2 \text{ g}^{-1}$ , respectively) compared to silica and display less long range order in their mesostructures ( $5 \text{ nm}$  and  $7 \text{ nm}$  pores, respectively).

Polyacrylamide (PAM) foam, with large open cellular pores ( $1\text{--}3 \mu\text{m}$ ) and thinner walls, or smaller pores ( $1.5 \mu\text{m}$ ) with thicker walls, has also been used for the production of hierarchically meso–macroporous materials.<sup>445</sup> After replication, the resulting structure of the final titania monoliths consists of macroporous voids between titania particles. Smaller pore-sized templates result in smaller titania particles ( $\sim 1 \mu\text{m}$  as opposed to  $\sim 2 \mu\text{m}$ ). The pore size of the resulting macroporous structure decreases with an increase in the titania precursor. The mesoporous voids are comprised of aggregates of nano-sized particles.

Macroporous PVA templates<sup>444</sup> have also been used to create zirconia monoliths with macrocellular pores and mesopores ( $\sim 10 \text{ nm}$ ) owing to interparticulate voids. Urea formaldehyde (UF) resin templates can also be used to fabricate hierarchically porous metal oxide monoliths (silica, zirconia and titania monoliths).<sup>870</sup> The use of varying PEG concentrations, which results in silica monoliths displays a bimodal macropore size distribution. P123, is helpful to produce an ordered mesostructured network.

**3.6.5 Emulsion templating.** Dispersing scandium alkoxide, tungsten powder or gold nanoparticles in the aqueous phase of an emulsion has been used to create hierarchically porous structures. Electrodeposition has been used to lead coat a polyHIPE which was previously introduced in the aqueous phase of the native HIPE.<sup>871</sup> The obtained macroporous hybrids were used as scaffolds for osteoblast growth and bone formation.<sup>753,754</sup> Metal particles can be generated on a preformed organic polyHIPE monolith by immobilization or impregnation of the metallic precursor onto the previously formed material. The incorporation of nickel into polyHIPE both by chemical reduction of nickel ions and electrodeposition have been studied.<sup>872,873</sup> A hybrid Pd/polymer porous material with hierarchical porous structure has been formed using

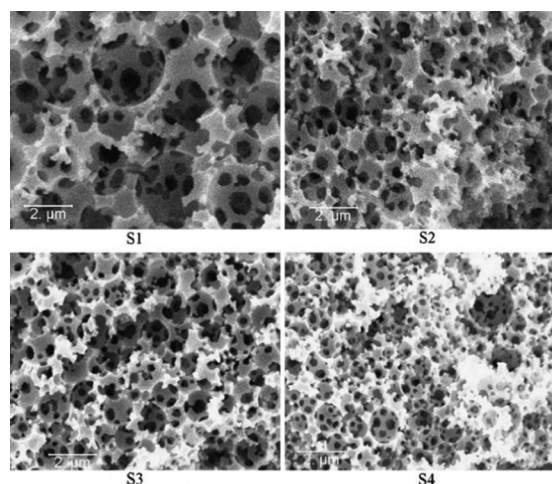


Fig. 71  $\times 10\,000$  SEM micrographs of PS polyHIPEs obtained from emulsions elaborated with increasing shear frequencies. Reprinted with permission from ref. 767. Copyright 2008, Springer.

the generation of palladium nanoparticles on the inner surface of S/DVB polyHIPE by using an impregnation–reduction methods (Fig. 71).<sup>757,758</sup> The hybrid material contains typical macroporous void spaces, and Pd nanoparticles are distributed inside the polymer matrix. In addition, the introduction of clay into the HIPE formulation does not have an effect on its stability and the obtained materials have effective porosity and an interconnection porous structure.<sup>759,760</sup> A similar attempt was made to prepare a hierarchical structure using other materials, such as titania nanoparticles, carbon nanotubes and hybrid materials.<sup>446,874–879</sup>

Hierarchically structured organic–inorganic hybrids have been generated using a procedure that is based on an elastomeric organic polymer. Firstly, a styrene, divinylbenzene and methacryloxy propyltrimethoxy silane (MPS) – a trialkoxy silane bearing a vinyl group – are radical copolymerized to form an organic network, which is removed by calcination of the silica macroporous foam replica.<sup>880</sup> Similar developments have been discussed by others.<sup>346–348,881–883</sup> Bismarck *et al.*,<sup>350</sup> have dispersed carbon black in a S/DVB organic phase using graft polymerization before emulsification in order to stabilize the carbon black dispersion. In this way, a chemically-bonded organic–inorganic hybrid was formed. These hierarchically porous monoliths have good mechanical and thermal stabilities. Copolymerization of organic comonomers with an organometallic monomer generates materials that contain metal atoms linked a covalent bond.<sup>381,801</sup> A novel method has been developed for producing hierarchically meso–macroporous materials with a more regular structure using high internal phase emulsion (polyHIPE methodology).<sup>353,884</sup> PolyHIPE-supported organotin chloride monoliths have expected fully interconnected porous structure, with every void (5–20  $\mu\text{m}$  in diameter) being connected to all of its neighbours by numerous interconnecting pores (2–5  $\mu\text{m}$  in diameter).<sup>884</sup> The same approach was followed using Ti-doped, Au-doped and Ru-doped polyHIPE foams.<sup>213,214</sup>

Bi-liquid foams when combined with lyotropic mesophases are used to directly generate hierarchical porosity.<sup>885</sup> It is well known that the viscosity of concentrated oil-in-water emulsions

increases dramatically when the oil volume fraction reaches values above 0.64.<sup>217,220</sup> This enhanced viscosity for the starting emulsions increases the shear applied to the oily droplets, thus inducing smaller macrocellular voids within the solid-state replica. The size of the largest interconnecting pores decreases from 1.4 to 0.5 and 0.25  $\mu\text{m}$  respectively whereas the average smallest interconnecting pore sizes remain constant at 50 nm. All of the porous materials possess a secondary micro–mesoporosity as evidenced by specific surface areas of (BET)  $\sim 800\text{ m}^2\text{ g}^{-1}$ . This porosity is promoted by using tetradecyl trimethyl ammonium bromide (TTAB) as concomitant mesoscopic texturing agent.<sup>364</sup>

Based on knowledge gained from studies with silica foams, various functional foams have been developed. These include  $\text{Eu}^{3+}$ @organo–Si(HIPE) macro–mesocellular hybrid foams used in light emitting devices<sup>365</sup> and Pd@organo–Si(HIPE) hybrid monoliths used as cycling Heck catalysts,<sup>383,800,886</sup> enzyme@organo–Si(HIPE) hybrid monoliths used as highly efficient bio-catalysts<sup>638,720,887</sup> and carbonaceous foams used as energy materials.<sup>260,261,758–761,769,888–890</sup>

In addition to surfactants, the internal dispersed phase of emulsions can also be stabilized by colloidal particles adsorbed at the liquid interface. These particles-stabilized emulsions are known as Pickering emulsions and are termed either with O/W or W/O emulsions.<sup>891,892</sup> W/O Pickering emulsions using latex nanoparticles as stabilizing agents can be used to generate cellular monoliths.<sup>893–897</sup> O/W Pickering emulsions have been used to a much lesser extent. Several ceramic foams (alumina, silica, iron oxide) and macrocellular foams have been generated by using O/W Pickering emulsion.<sup>783,784</sup> The macroporous solid state foams have average cavity sizes that are in the same range as those of oil droplets in the starting emulsions, proving thereby that evaporation is associated with a weak shrinking of the foam skeleton. In addition, the high magnification image (Fig. 72) shows that the walls and surface of the resulting membranes are fully covered with densely packed PS-*co*-PNIPAM core-shell nanoparticles.<sup>898</sup>

**3.6.6 Selective leaching *via* oxido-reduction.** In the selective leaching technique, a significant volume loss usually occurs upon reduction of the metal, which expresses itself as smaller pores penetrating into the pore walls, although the mesopores are rather transient.<sup>899</sup>

Seshadri *et al.* have developed a novel strategy for forming hierarchically porous materials by using this volume loss. This

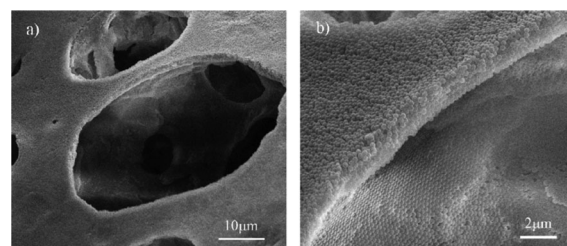
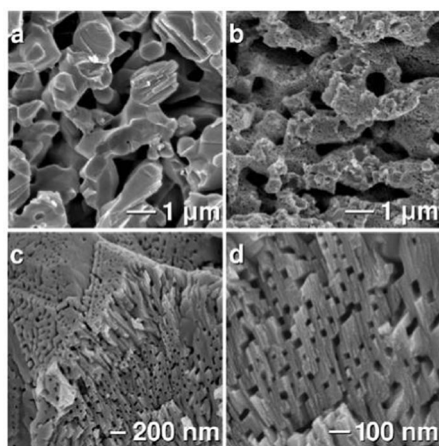


Fig. 72 Microstructure of macroporous materials prepared from a hexane-in-water emulsion containing 80 internal phase volume of oil and 5 wt% PS-*co*-PNIPAM particles in the initial aqueous dispersion. Reprinted with permission from ref. 898. Copyright 2010, American Chemical Society.



**Fig. 73** (a) SEM micrograph of macroporous  $\text{Mn}_3\text{O}_4$ . (b) Upon reduction in a 5%  $\text{H}_2/\text{N}_2$  atmosphere to  $\text{MnO}$ , the macropores are maintained and an additional level of porosity has been induced. The mesoporous fracture surface on the right side of image (c) is shown at higher magnification in micrograph (d). Reprinted with permission from ref. 900. Copyright 2006, American Chemical Society.

process requires temperature control. Significant volume loss occurs during reduction of  $\text{Mn}_3\text{O}_4$  to  $\text{MnO}$  at low temperatures in a flowing 5%  $\text{H}_2/\text{N}_2$  atmosphere. Pressing and firing can form the minimal densification of pellets of macroporous  $\text{Mn}_3\text{O}_4$  with some grain connectivity (Fig. 73a).<sup>900</sup> The macropore network and grain connectivity are retained in the reduction of  $\text{Mn}_3\text{O}_4$  pellets to  $\text{MnO}$  (Fig. 73b) and the macropore walls are penetrated with mesopores as volume loss inherent in the phase change (Fig. 73c). The formed macropores are 1 mm in diameter and the mesopores are 50 nm. The rectangular pores aligned across a grain suggest that the pore orientation is dominated by crystallographic relations (Fig. 73d).

It is interesting to note that the mesopores close without changing the macropore network during the reoxidation of hierarchically porous  $\text{MnO}$  to  $\text{Mn}_2\text{O}_3$ . The reduction of  $\text{Mn}_2\text{O}_3$  to  $\text{MnO}$  re-enables the formation of mesopores in the macropore walls. As the pore forming process relies solely on strain due to a phase change with corresponding oxygen loss, the process may be cycled. By several redox cycles, the  $\text{MnO}$  sample can have pores with two different length scales. Some broadening of the mesopore size distribution is observed. This is a very good example of morphological regeneration of a porous material.<sup>900</sup> The morphology of the initial pores (50 nm in diameter) is similar to that of the regenerated pores obtained by the reduction of  $\text{Mn}_3\text{O}_4$ . Such mesopore regeneration may prove to be useful in high temperature applications.

It is crucial to know that hierarchically porous structures consist of macropore walls, which are composed of mesoporous single crystals. A hierarchically porous pellet of  $\text{MnO}$  is back filled with epoxy and polished, and a lamella is formed using a focused ion beam (Fig. 74).<sup>901</sup> The pore walls are composed of [100] crystal faces, which possess the lowest energy of the rock salt lattice. These porous crystals are reminiscent of those found in sea urchin spines and in their synthetic replicas. Porous single crystals are extremely unusual

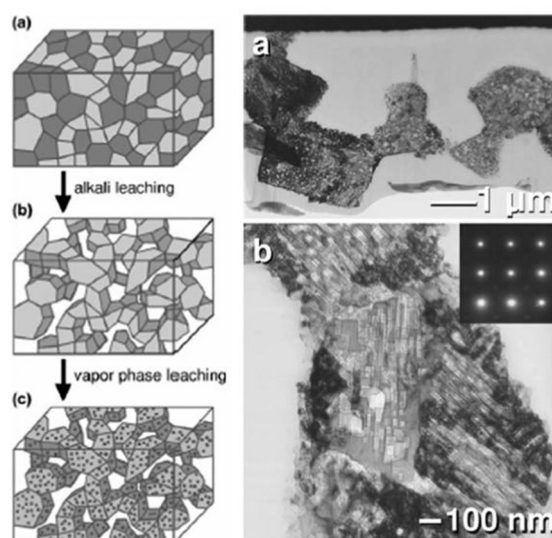


**Fig. 74** (left) Scheme showing formation of hierarchically porous monoliths. Starting from a dense two-phase composite (a) of  $\text{ZnO}$  and  $\text{ZnMn}_2\text{O}_4$ , alkali leaching removes the  $\text{ZnO}$  phase, leaving macroporous  $\text{ZnMn}_2\text{O}_4$  (b). Vapor phase leaching of  $\text{Zn}$  in flowing hydrogen forms mesopores in the macropore walls of part b giving a hierarchically porous material (c). (right) (a) TEM micrograph of  $\text{MnO}/\text{epoxy}$  lamella formed with a focused ion beam. When seen at higher magnification, (b) the lamella has density variations due to the presence of pores. The region on the left has been tilted into the [100] zone axis (inset). Reprinted with permission from ref. 901. Copyright 2006, American Chemical Society.

and show potential for improved performance over their polycrystalline analogues due to the absence of grain boundaries. For high temperature applications, porous single crystals are significantly more stable due to their lowered surface energies and the elimination of grain boundaries as the primary means of mass transport. Electrical transport is improved due to the absence of grain boundary scattering. In nature, sea urchins form spines of porous calcite single crystals.<sup>902</sup> Earlier efforts to produce porous single crystals have either relied on controlled nucleation within a porous template<sup>903,904</sup> or etching of a bulk single crystal.<sup>905</sup> In contrast, pores can be induced in crystalline grains through controlled phase changes that result in volume loss.

**3.6.7 Phase separation.** Supramolecular templating is an attractive alternative to the post-gelation aging processes to generate tailored mesopores with higher degrees of order in pore size, shape and spatial arrangement. Several kinds of surfactants can be used to induce phase separation concurrently with the sol-gel transition.<sup>246,785,787</sup> The triblock copolymer, Pluronic P123, and the additive, 1,3,5-trimethylbenzene (TMB), can be introduced to enhance long-range ordering of mesophases in a TMOS-derived system.<sup>247</sup> With an appropriate post-gelation time for aging that enables reorganization of the micropore structure within the frameworks comprised of 2D hexagonal mesopores, large monolithic pieces of hierarchically porous silica can be fabricated. The porosity of the macropores reaches 90% by volume, whereas 50% of silica frameworks remain porous mainly with sharply template mesopores.

Pure silica formation has been exploited to produce various possible morphologies, shapes and chemical doping compositions. Tetramethoxysilane (TMOS) has been widely used as a precursor often combined with a variety of phase-separation inducers.<sup>244,245,906,907</sup> Water glass (alkaline silicate solution) as well as colloidal dispersion of silica can also be used as precursors owing to their low cost.<sup>781,908</sup> The strong attractive interaction between silica and additive molecules makes it possible to template mesoscale structures on the structural unit of the gels by surfactants. The size of mesopores can be controlled independently of those of the macropores unless local dissolution of the gel skeletons causes significant deformation of the whole macroporous framework during the solvent exchange. Conventional methods of tailoring mesoporous structures by aging wet silica gels under basic and/or hydrothermal conditions can be applied to generate monolithic macroporous silica gels without essentially disturbing the pre-formed macroporous structure.<sup>782</sup> For example, it is possible to obtain hierarchically porous monolith with a sharp distribution of macropores  $\sim 1.5 \mu\text{m}$  and mesopores  $\sim 10 \text{ nm}$ .<sup>9</sup> While mesopores can be enlarged up to  $100 \text{ nm}$  in diameter, the approximate range of macropores homogeneously formed throughout the specimen is between  $100 \text{ nm}$  and  $50 \mu\text{m}$  in diameter.

A similar process has been used to prepare hierarchical meso-macroporous siloxane-based organic-inorganic hybrids such as networks from precursors containing trialkoxysilyl group,<sup>252</sup> and bridged alkoxyxilanes.<sup>253,254,264,266,786,788</sup> For example, the preparation of such hierarchically porous gels from bis(trimethoxysilyl)ethane (BTME) in the presence of Pluronic P123 mimic those derived from pure silica.<sup>254</sup> Alkyl bridges ranging from methylene to propylene behave similarly in templating and phase separation, and the tendency for phase separation decreases with an increase in the number of carbons in the bridge.<sup>252,788</sup> The micrometer-range gel frameworks of these materials are embedded with templated pores (typically 2D hexagonal cylindrical) with inter-pore walls being essentially microporous silsesquioxane networks. Porous monoliths derived from phenylene/biphenylene bridged polysilsesquioxane can be converted to SiC ceramics or SiC/C composites by heat treatment under a reducing atmosphere while preserving the macroporous features designed in the precursory hybrid gels (Fig. 75).<sup>126,127</sup> In the case of carbonizing monolithic macroporous gels, *in situ* carbonization compared with bulk gas-phase activation reactions under oxidative atmosphere is favored in order to obtain better homogeneity.<sup>267</sup>

Slowing gelation of titanium alkoxides and zirconium alkoxides, is required in order to obtain hierarchically porous monolithic gels, as they possess higher reactivity rates than those of silicon towards hydrolysis/polycondensation.<sup>23,255–257,262,268,347,816,817,883,909–913</sup> The hydrolysis/polycondensation reaction of titanium alkoxides can be controlled, and an appropriate amount of PEO can be incorporated to adjust phase separation dynamics to obtain a better defined macroporous structures.<sup>257</sup> By controlling the grain growth of the anatase crystallites during aging and heat-treatment, gaps between crystallites form sharply distributed mesopores in the size range of  $5\text{--}10 \text{ nm}$ . Hasegawa *et al.* have



Fig. 75 Appearance and microstructure of macroporous SiC/C composite prepared from bis(trimethoxysilyl)biphenylene. Reprinted with permission from ref. 226. Copyright 2009, Royal Society of Chemistry.

recently reported that inclusion of various inorganic salts into the titania sol-gel system offers the benefit of obtaining crack-free macroporous monoliths by the control over an extended range of gelation time.<sup>118,689</sup> Furthermore, monolithic pure zirconia with controlled macropores can also be prepared. Zirconia tends to form gels with amorphous structural units and changes from monoclinic to tetragonal as the heat-treatment temperature increases.<sup>23</sup>

Similar to the case of titanium and zirconium, the high reactivity of aluminum alkoxides toward hydrolysis can be controlled to obtain mechanically stable monolithic alumina. Polymerization-induced phase separation has been successfully combined with the gel-forming reaction, assisted by epoxide ring-opening to adjust pH in a desired timescale.<sup>882</sup> The added PEO is mainly distributed in the fluid-phase and it has a minor effect on the mesopore formation. Macroporous morphologies of  $\gamma$ -alumina ceramics are very stable. Upon heat-treatment, the monolithic gels transformed from amorphous  $\gamma$ -alumina ( $\sim 800 \text{ }^\circ\text{C}$ ) to  $\alpha$ -alumina ( $\sim 1100 \text{ }^\circ\text{C}$ ) crystalline form, accompanied by some pore shrinking, yet without damaging the macroporous framework. Further, Yttrium-aluminum garnet (YAG) can be produced using the method of co-hydrolysis of the corresponding metal salts.<sup>881</sup> The monolithic macroporous single phase YAG specimen is easily produced by simple heat-treatment of the resultant gel. Other alumina-based complex oxides such as magnesium-aluminum spinel can also be prepared in this manner.

Another application of epoxide-mediated gel-formation accompanied by phase separation is to ionic crystalline phases containing oxoacids as anions. Among others, calcium phosphates represented by hydroxyapatite are an important group of bioactive compounds already utilized as artificial bone, bone cement and other kind of hard tissue replacements. Carefully selected additives are added to a solution containing calcium salt and phosphoric acid in order to inhibit preferential growth of large crystalline particles but to enable formation of macroscopically homogeneous monolithic gels (Fig. 76).<sup>914</sup> The resultant macroporous monolith retains inherent mesoporosity arising from

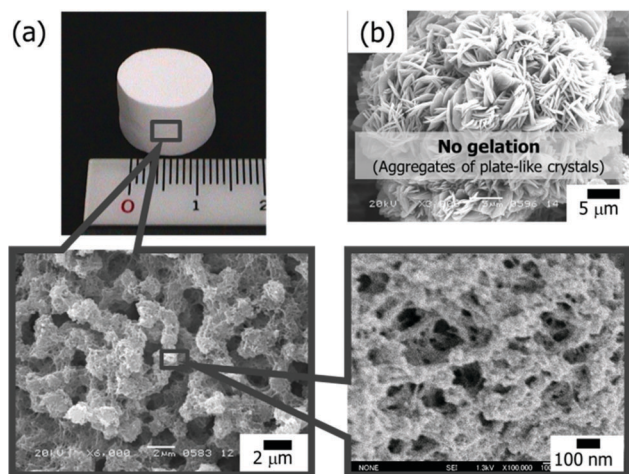


Fig. 76 SEM images of dried samples of monolithic macro/mesoporous  $\text{CaHPO}_4$  gels prepared (a) with and (b) without HPAAs. Reprinted with permission from ref. 914. Copyright 2011, Springer.

tenuous aggregation of nano-sized crystallites of mainly monetite,  $\text{CaHPO}_4$ , and their size distributions are more or less broad compared with those observed in amorphous or templated systems.

**3.6.8 Bubbling process: gas leaching.** Easy leaching templating methods such as air bubbles, self-generation gas and solvable salts have been developed to create macropores during the formation of the mesoporous phase, which provide a green way to fabricate hierarchical porous structures.

Macroskeletal mesoporous silicate foams with open-cell randomly shaped macro-voids on the (sub) millimetre scale have been prepared from metastable PEO-surfactant air-liquid foams, generated by strong stirring under neutral aqueous conditions.<sup>915</sup> It is claimed that the macroscale morphologies can be adjusted by changing the turbulence of the reaction media, a parameter that is difficult to control. Since this observation, a bubbling process has been developed to produce air-liquid foams,<sup>916–918</sup> which may allow complete control over the shapes of the bubbles, cell sizes and a more easily maintained liquid fraction of the foam.

Mann *et al.* have reported a gas-templating route that provides a new class of bioactive silica gels with hierarchical pores.<sup>919</sup> This gas-template is totally different from the above-mentioned bubbling process, which produces air-liquid foams.<sup>916–918</sup> The gas ( $\text{CO}_2$  bubbles) is generated by *in situ* decomposition of a mixture of sodium bicarbonate and sodium hydrogen pyrophosphate, leading to the formation of large macropores while the reaction proceeds within the silica bioglass during gelation (Fig. 77). Finely divided calcium carbonate is also included in the reaction mixture as a space filler, and it is removed after gelation by acid washing to produce additional pores with dimensions usually less than a micrometre. A closed approach has also been reported for the preparation of osseous calcium phosphate cements.<sup>920</sup> The process involves adding  $\text{NaHCO}_3$  into the initial cement powder (Biocement D) and employing two different liquids. One liquid is a basic solution

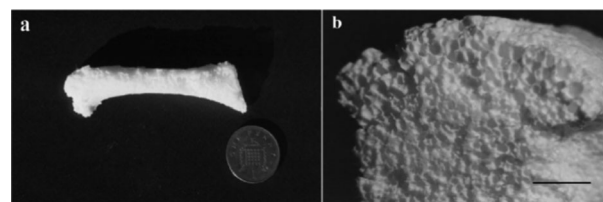


Fig. 77 Optical photographs showing highly porous silica monoliths: (a) low magnification image of shaped bioglass; (b) higher magnification image showing macroporous texture. Scale bar in (b) is 0.5 cm. Reprinted with permission from ref. 919. Copyright 2003, Royal Society of Chemistry.

that allows the formation of the paste whereas the other is an acidic solution that helps generate  $\text{CO}_2$  bubbles. This last step ensures that macropores are formed in calcium phosphate cements. This strategy can be extended to both colloidal and sol-gel methods for the formation of silica gel (or organo-functionalized silica gels) with high porosity. The porous silica gels can be strengthened by organic polymerization, which induces nucleation of calcium phosphate from simulated body fluid, and acts as a slow-release vector for the anti-inflammatory drug ibuprofen.

Using a multiphase procedure, and acid-catalyzed silica sol-gel chemistry with inorganic salts and self-assembling block copolymers, hierarchically meso-macroporous materials have been fabricated (Fig. 78).<sup>921</sup> Inorganic salts are crucial for

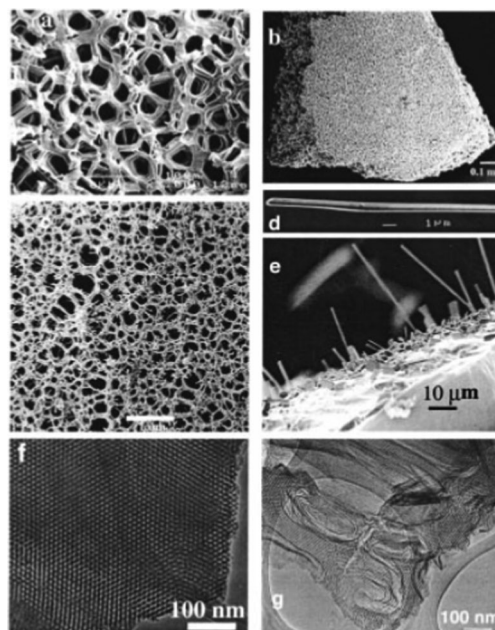


Fig. 78 (a and b) Scanning electron micrographs (SEM) at different magnifications of as-synthesized meso-macrostructured silica membranes prepared by using P123 (EO20PO70EO20) block copolymer species in NaCl solution after washing with deionized water; (c) an SEM image showing smaller macropores (compared to a), in a silica membrane prepared with a small amount of ethylene glycol under otherwise identical conditions; (d and e) SEM images of (d) an acicular NaCl single-crystal and (e) inorganic salt NaCl crystals co-grown with the silica membrane. Reprinted with permission from ref. 921. Copyright 1999, American Chemical Society.

the production of meso-macroporous silica structures, which grow at the interface of the inorganic salt solution droplets. The electrolyte strength of the inorganic salts and amphiphilic block copolymer structure directing agents can alter the network of meso-macrostructured silica. The sizes of the salt solution droplets (e.g. NaCl, LiCl, KCl, NH<sub>4</sub>Cl, or NiSO<sub>4</sub>) can determine the macropore dimensions and they can be regulated by varying the evaporation rate of the solvent. In the presence of silica, amphiphilic block copolymer species assemble to form well-ordered composite meso-phases at the interstices separating the electrolyte droplets. Although inorganic salt crystals are inevitably co-grown with the silica membrane, altering the inorganic salt concentration can be used to regulate the morphology of the silica membrane.

**3.6.9 Coating combined with chemical etching and replication.** Various types of hierarchically porous nanostructures have been prepared using a combination of coating along with chemical etching and replication.<sup>547,800–822</sup> Here we present a classical example to describe this method (Fig. 79).<sup>922</sup>

Through co-hydrolysis and subsequent sol-gel condensation of TEOS and organic template micelles, microporous particles (zeolites) with a mesoporous shell layer are coated on each core particle to form the bimodal porous silicate with a zeolite core/mesoporous shell (ZCMS) structure. In this situation, the 3D interconnected randomly distributed mesopore arrangement shells gives precise control of this novel structure. Interestingly, the hierarchical structures carbon and silica nanocases can be synthesized using the ZCMS silicate as a template.

Furthermore, nanosized particles with porous structures can be assembled to prepare hierarchically porous materials by using a post-synthesis process. Chemical bonds with the mesoporous supports can be formed while the wall of mesoporous silicates are coated or doped with zeolite nanocrystals. This imparts microporosity and results in the formation of a meso-structured zeolite phase.<sup>923–932</sup> A series of steam stable meso-structured aluminosilicates can be obtained by assembly from zeolite-type seeds.<sup>923–928</sup> A mesoporous material with semi-crystalline zeolitic walls can be fabricated by using a novel synthetic approach, called zeolite-coating, which involves templated

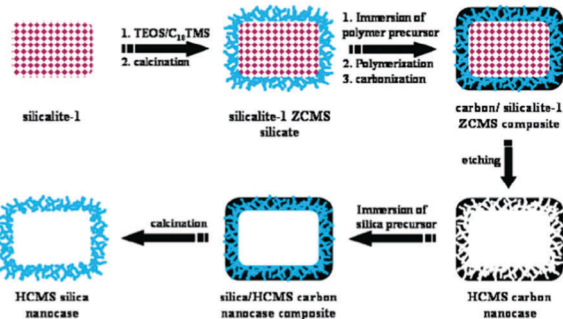


Fig. 79 Schematic illustration for synthesis of silicalite-1 zeolite core/mesoporous shell (ZCMS) particles and corresponding pseudo-hexagonal prismatic hollow core/mesoporous shell (HCMS) carbon and silica nanocases. Reprinted with permission from ref. 922. Copyright 2005, American Chemical Society.

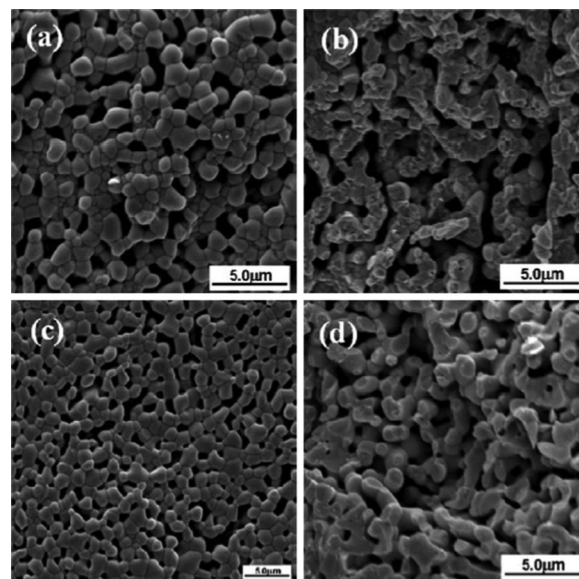


Fig. 80 SEM images of pellet prepared with 40 vol% SnO<sub>2</sub>-60 vol% CeO<sub>2</sub> nano-powders made by combustion CVD from single precursor solution. (a) Surface and (b) cross-sectional views of pellet sintered at 1450 °C × 5 h. (c) Surface and (d) cross-sectional views of pellet after reduction at 727 °C × 2 h. Reprinted with permission from ref. 933. Copyright 2003, Wiley-VCH.

solid-state secondary crystallization of zeolites, starting from the amorphous mesoporous materials with the corresponding elemental composition.<sup>829,830</sup>

Sublimation is a very simple process to use for preparation of materials, and it also can be used as post-treatment method to produce hierarchical materials. As an example, a sublimation method to prepare hierarchically meso-macroporous CeO<sub>2</sub> has been reported (Fig. 80).<sup>933</sup> This process uses combustion CVD to prepare the intimately distributed 40 vol% SnO<sub>2</sub>-60 vol% CeO<sub>2</sub> composite. The SnO<sub>2</sub> phase is removed *via* sublimation during the firing process, because the melting point of SnO<sub>2</sub> (1630 °C) is near that of typical firing temperatures of CeO<sub>2</sub> (usually 1350–1500 °C). Removal of the SnO<sub>2</sub> phase generates the macroporosity and the inherent mesoporosity in the macroporous wall which remains intact during firing treatment. Distortion or collapse of the host material can be prevented at the high sublimation temperature. Sublimation presents however a potential problem when using low temperature ‘pore formers’. Although the sintering temperature is very high, this approach offers the advantage that additional porosity can be directly introduced into ceramic production without needing additional procedure.

**3.6.10 Self-formation.** Based on the power of the chemistry of metal alkoxides and alkylmetals, a large number of hierarchically structured meso-macroporous materials with well-ordered tubular or very versatile macrochannels have been prepared by using a ‘one-pot’ self-formation process.<sup>346–348,350,353–355,358,361,364,365,381,800,801,885</sup>

Zirconium oxides with hierarchically porous structures have been synthesized *via* hydrolysis of the corresponding metal alkoxides in the presence or absence of a single surfactant (either cationic or non-ionic). This process leads to formation of a parallel-arrayed funnel-like macroporous structure (Fig. 81).<sup>348,383</sup>

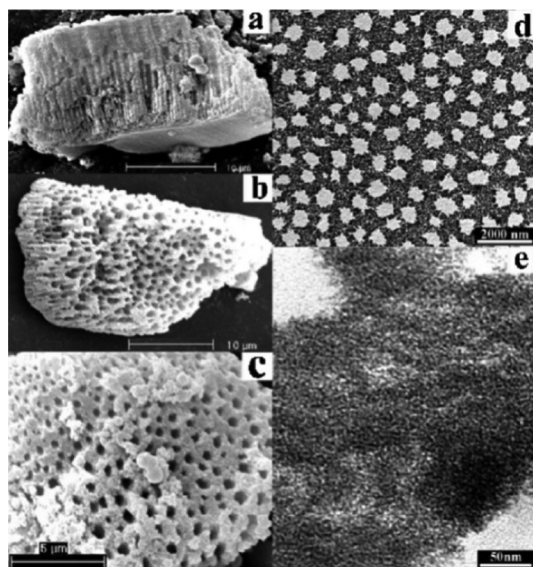


**Fig. 81** (a–c) SEM images of the synthesised meso-macroporous zirconia particles; (d) low-magnification TEM image of a cross-section of meso-macroporous zirconia along the macrochannel direction; (e) high-magnification TEM image of the macroporous structure, showing that the macrostructure framework is composed of wormhole-like mesopores. Reprinted with permission from ref. 348. Copyright 2003, Royal Society of Chemistry.

Based on the self-formation phenomenon, zirconium oxide particles are arranged in a regular array of parallel or funnel-like shape of 300–800 nm in diameter. The macropores are separated by walls that contain mesochannels in a wormhole-like array. The self-formation phenomenon also provides materials with high surface areas (up to  $900 \text{ m}^2 \text{ g}^{-1}$ ) and pure crystalline phases. The presence of a surfactant is advantageous as it can modify the textural properties without affecting the self-formation of meso-macroporous hierarchy. Generally, the surface area of the materials synthesized in the presence of surfactants is higher than that generated without using surfactants. The final phase of the crystallinity is affected by the synthesis temperature. An increase of the hydrothermal treatment temperature to  $130 \text{ }^\circ\text{C}$  (generally reported  $60\text{--}80 \text{ }^\circ\text{C}$ ) leads to formation of thermally stable meso-macroporous zirconia with a nanocrystallized framework.<sup>379</sup>

Similar to the use of  $\text{Zr}(\text{OR})_4$ , other metal alkoxides including  $\text{Ti}(\text{OR})_4$ ,  $\text{Al}(\text{OR})_3$ ,  $\text{Y}(\text{OR})_3$ ,  $\text{Nb}(\text{OR})_5$ ,<sup>348,355,365,381,800,801</sup> have been used to prepare hierarchically bimodal and even trimodal porous structures. In these cases, the macropore diameters, meso- and micropore sizes, surface areas and porous volumes are influenced by the type of inorganic precursor and the presence or not of surfactant molecules. The spontaneous formation of meso-macroporous structure has proven to be a facile method to prepare these materials.

Multi-component oxides play a vital role as catalysts and supports for catalytically active species destined for use in chemical and petrochemical processes.<sup>886</sup> Again, the self-formation synthesis method is simple for the fabrication of a series of hierarchical meso-macroporous binary mixed metal

oxides. Bimodal binary oxides including titania-zirconia (TZ), titania-alumina (TA), alumina-zirconia (AZ) and zirconia-silica (ZS), have been prepared in the presence of mixed alkoxide solutions. These structures have advantages, such as large pore volumes and high surface areas. Similarly, the fabricated hierarchically meso-macroporous binary mixed oxides have a one-dimension tubular macroporous framework delimited by interconnected wormhole-like mesopores. The addition of a secondary oxide results in a crystalline modification.<sup>353</sup> Moreover, the mesopore and macropore sizes can be controlled by adjusting the amounts of the components and the high thermal stabilities of these materials have been demonstrated. The presence of the second component in sufficient amounts inhibits crystallization and the consequent structural growth results in a higher surface area as well as controlled pore sizes in the case of TZ, ZS, TA, and AZ. Even after calcination at  $500 \text{ }^\circ\text{C}$ , these binary oxides have low crystallinities or even are amorphous.<sup>353</sup>

Metal phosphates are active solid acid-base catalysts, redox catalysts and photocatalysts. Thermally stable hierarchically meso-macroporous  $\text{ZrPO}$  materials, prepared by using the self-formation strategy, possess a uniform macroporous structure with small mesoporous walls, which should be significant from a technological point of view. Although the surface areas and pore volumes decrease with an increase of the calcination temperature, a high surface area of  $132 \text{ m}^2 \text{ g}^{-1}$  with a pore volume of  $0.23 \text{ cm}^3 \text{ g}^{-1}$  and a narrow pore size distribution centered at around 2 nm can still be produced after calcination at  $800 \text{ }^\circ\text{C}$ , suggesting the formed materials have a very high thermal stability. It is important to note that both as-prepared and calcined meso-macroporous  $\text{ZrPO}$  display a small amount of microporosity. The hierarchically structured titanium phosphate materials with multiscaled and tunable porosity have been prepared either using a neutral surfactant or without surfactant. In both cases, the self-formation phenomenon operates (Fig. 82).<sup>365</sup> The macroporosity can even be tuned by addition of the surfactant, which leads to the formation of a uniform 3D co-continuous macroporous structure. The walls between the macropores of these  $\text{TiPO}$  materials are comprised of mesopores in a wormhole-like array. A hierarchical structure of meso-macroporous phosphated aluminum (oxyhydr)oxide (PAL) materials was prepared *via* this self-formation process with the use of precursor aluminum *sec*-butoxide in a mixed solution of  $\text{H}_3\text{PO}_4$  and  $\text{Na}_2\text{HPO}_4$ . Direct phosphation results in the incorporation of phosphorus into the inorganic framework of aluminum (oxyhydrate) oxides by the Al–O–P bonds. The macroporous structures are uniform, with sizes of 500–1800 nm, and the macropore walls are composed of accessible mesopores of a scaffold-like nanoparticle assembly.<sup>364</sup> These hierarchical PAL structures exhibit high thermal stability (at least  $800 \text{ }^\circ\text{C}$ ) and they possess surface hydroxyl groups and acidic sites.

In comparison to the funnel-like channels of meso-macroporous zirconias, titanias and aluminas, the macropores of aluminosilicates are comprised of more or less straight tubes with openings ranging from 0.5 to  $2 \text{ } \mu\text{m}$ , which are parallel to

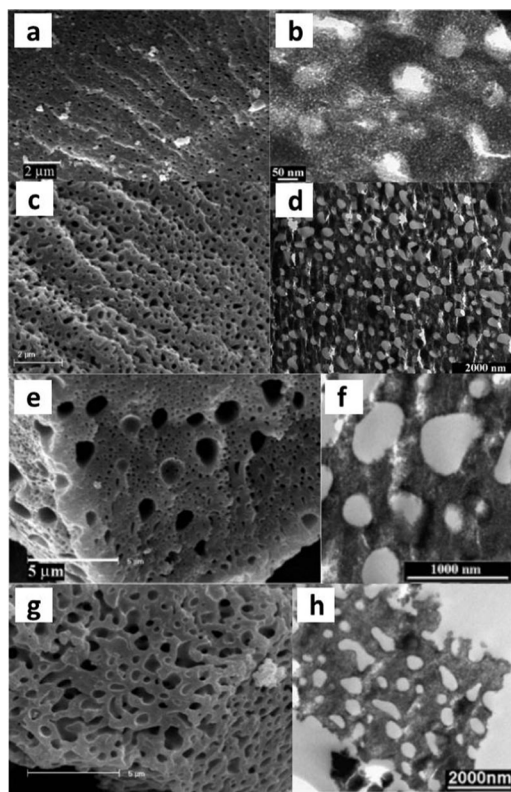


Fig. 82 SEM and TEM images of the meso-macroporous titanium phosphates synthesized (a and b) in the absence of surfactant, and in the presence of (c and d) 5%, (e and f) 10%, and (g and h) 15% surfactant Brij 56. Reprinted with permission from ref. 365. Copyright 2006, American Chemical Society.

each other. The walls consist of wormhole-like disordered mesopores of 4 nm in diameter with specific surface areas reaching  $600 \text{ m}^2 \text{ g}^{-1}$ . Further, the use of an aluminosilicate ester containing an Al–O–Si linkage on the molecular scale enables precise control of the structure and active sites in the generated mesoporous materials. The Al species can be incorporated in the tetrahedral network with the formation of Al–O–Si bonds in these aluminosilicates.<sup>372–374,934</sup>

### 3.7 Hierarchically dual macroporous and multiple macroporous structures

Through the use of colloidal crystal templates that contain particles with a multimodal distribution of sizes, it is possible to create hierarchical structures with multi-modal macropores with different sizes.

Multimodal colloidal crystals have been used as templates in the formation of ordered trimodal colloidal crystal films with thicknesses up to  $6 \mu\text{m}$ .<sup>935</sup> Two types of polymer spheres, PS spheres (465 nm) and PMMA spheres (84 nm) are co-deposited with silica nanoparticles that have a diameter of 6 nm. The large PS spheres self-assemble into fcc arrays. The PMMA spheres pack into the tetrahedral and octahedral interstices in the PS lattice. The silica nanoparticles fill the voids in the PS and PMMA spheres. Calcination of the trimodal colloidal crystal removes the polymer spheres and sinters the silica particles together to form the hierarchically porous 3DOM framework.

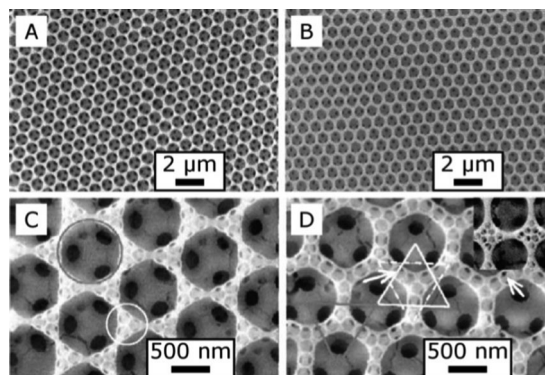


Fig. 83 SEM images showing the morphology of a hierarchical structure templated from binary colloidal crystals. (A and C) Are from a sample with a concentration ratio of large to small spheres of 0.12. (B and D) Are from a sample with a concentration ratio of large to small spheres of 0.14. The white arrows in (D) show the extra pores generated by increasing the volume fraction of 200 nm spheres. Reprinted with permission from ref. 936. Copyright 2008, American Chemical Society.

The large spheres form an interconnected fcc array of 456 nm-sized pores and the walls contain 80 nm-sized pores that are connected by 25 nm-sized pore windows.

Increasing the deposition speed of multimodal colloidal crystals, by boosting the solvent evaporation rate, can after template removal by calcination generate a hierarchical structure consisting of a trimodal distribution of pore sizes 1000 nm and 180 nm (by PS spheres) and 7 nm (silica nanoparticles).<sup>936</sup> It was found that additional pores can be added to the wall framework by increasing the ratio of the concentration of the small to large colloidal spheres (Fig. 83). Wang *et al.* described a process involving horizontal deposition to increase both the deposition speed and the sizes of the binary colloidal crystals.<sup>937</sup> In this case, the suspension of small (154 nm) and large PS spheres (789 or 1000 nm) is prepared then spread on a glass slide. The binary colloidal spheres self-assemble during the evaporation-driven process. Infiltration is conducted by spin-coating a TEOS-containing solution. Toluene is then used to dissolve the PS spheres. The resulting hierarchical structure has the characteristic interconnected fcc network of large pores with smaller macropores present in the walls.

A variety of different multimodal colloidal crystals can be produced by changing the relative sizes of the colloidal spheres. Wang *et al.* conducted theoretical calculations to elucidate the range of binary colloidal crystals created by co-deposition of large and small spheres.<sup>795,938</sup> Binary colloidal crystals were assembled to confirm the predictions. Depending on the concentrations of the small and large particles, defects and additional patterns can be produced. This process ultimately forms the binary colloidal crystal.

Ohshima and co-workers used ice templating with a well-dispersed aqueous suspension containing poly[styrene-(*co*-2-hydroxyethyl methacrylate)] spheres and colloidal silica particles.<sup>939</sup> Immersion in liquid nitrogen, freeze drying and final calcination produces the final structure consisting of honeycomb-like aligned pores from the ice. A silica 3DOM structure is contained in the walls

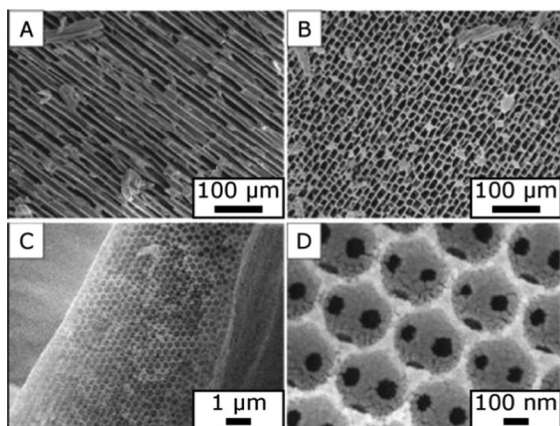


**Fig. 84** SEM micrographs of the hierarchical ice-templated sample that illustrate its porosity. Image (A) shows a view of the material parallel to the axis of the temperature gradient (freezing direction), while (B) is perpendicular to the axis of the temperature gradient. Image (C) is a more magnified view of the image in (A), and (D) shows the 3DOM structure with the additional porosity from spaces between colloidal particles. Reprinted with permission from ref. 377. Copyright 2006, American Chemical Society.

with additional mesopores in the regions where the silica particles construct the framework (Fig. 84).<sup>939</sup>

A method to generate colloidal crystals with multiple sphere diameters and then to form their hierarchical inverse structure involves the use of heterostructured colloidal crystal films. These films are comprised of multiple layers of colloidal spheres, each layer containing monodispersed spheres with a different diameter than those in the adjoining layers. Vertical deposition techniques can be used to produce infiltrated colloidal crystal films that serve as substrates for a second deposition step using spheres of a different diameter.<sup>940,941</sup> Another LBL technique has also been used to generate the heterostructure for synthesizing such a structure.<sup>942</sup> A monolayer of PS spheres is first spin-coated onto a substrate, and then the monolayer is peeled off and placed in a solution containing a metal salt precursor. The infiltrated film is collected, redeposited onto a substrate and then heat treated. Another monolayer of smaller spheres is then placed in the precursor solution where it deposits onto the initial monolayer. After calcination of the bilayer, a porous film with bimodal porosity is obtained. Tin oxide, iron oxide, and indium oxide films have been produced using this method with different sizes of both large and small spheres.<sup>942,943</sup> Excellent response time and sensitivity to ammonia gas can be achieved when using  $\text{In}_2\text{O}_3$  films formed in this manner as gas sensing membranes.<sup>943</sup>

Colloidal lithography can also be used to form hierarchically heterostructured films.<sup>944</sup> Different morphologies of hierarchical gold can be synthesized by altering the sequence of depositing the PS monolayers and electrodepositing gold. One hierarchical structure is generated by first infiltrating a PS monolayer with a sol-gel alumina precursor and then removing the template.<sup>944</sup> The alumina pore array is filled with small PS spheres, which are then infiltrated with gold by electrodeposition. By removing the alumina and the PS spheres, a hierarchical film of macroporous gold nanoclusters arranged in a non-close packed hexagonal array is formed.

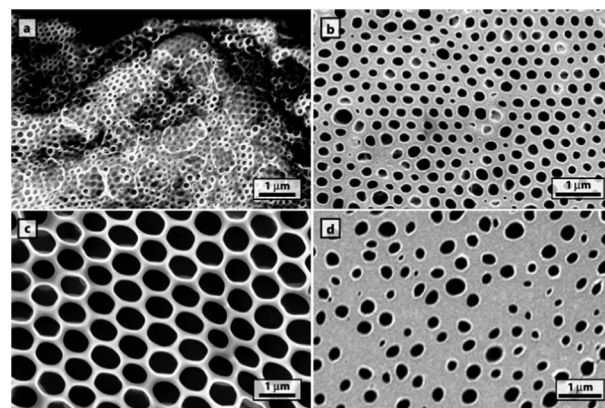


**Fig. 85** SEM images of PEO-*b*-PFOMA films cast from 0.1 wt% Freon dispersions under high humidity. The PEO block molecular weight was 2 kDa and the PFOMA block molecular weight is (a) 10, (b) 25, (c) 70, (d) 140 kDa. Reproduced from ref. 945 by permission of American Physical Society.

Recently, a wide range of ordered porous polymer films has been prepared using the Breath Figures (BF) technique through the design and synthesis of polymer molecules, along with selected use of a stabilizer and solvent.<sup>488–505</sup> Conjugated rod-like polymers have been used to prepare films with hexagonally ordered bubble arrays.<sup>501</sup> Similarly, porous poly(ethylene oxide)-*b*-polyfluorooctylmethacrylate (PEO-*b*-PFOMA) diblock copolymer films are drop cast onto substrates from Freon (1,1,2-trichlorotrifluoroethane) in a humid atmosphere. Water droplet nucleation influences the final pore size and packing order in the polymer films (Fig. 85).<sup>945</sup> Furthermore, a spreading technique without additives over various substrates was developed to synthesize  $\alpha$ -carboxylic polystyrene (PS-COOH), a polymer with end of chain ionic group.<sup>946</sup> With similar process, the honeycomb structure biohybrids film was prepared.<sup>947</sup>

Functional nanoparticles can be incorporated into the polymer solutions to make hierarchically structured functional arrays by using BF templating. This process involves self-assembly of condensed water droplets and nanoparticles. For example, after the evaporation cooling process and complete removal of water and chloroform, a uniform layer of CdSe/PS is formed on the surface ordered BF-templated pores.<sup>500</sup> Addition of a suspension of silica nanoparticles in ethanol to a PS-chloroform solution has also been used to BF-patterned PS/silica films.<sup>948</sup>

Magnetic nanoparticles and conducting polymers have potential applications in areas related to batteries, electro displays, molecular electronics, and nonlinear optical materials.  $\text{Fe}_3\text{O}_4$  nanoparticles are prepared by thermal decomposition of  $\text{Fe}(\text{acac})_3$  in phenyl ether and then blended with a 4-dodecylbenzenesulfonic acid-doped polyaniline chloroform solution. The magnetic properties of the honeycomb-structured composite films were investigated using a vibrating sample magnetometer.<sup>949</sup> Furthermore, purified multiwalled carbon nanotubes (CNT) are dispersed in a solution of amine-terminated PS in benzene and ordered macroporous nanocomposite films are fabricated by using the BF-templating method. Highly stable CNT scaffold films with diverse morphologies, formed after pyrolysis of the nanocomposites (Fig. 86),<sup>950</sup> have high electrical conductivity and field-emission properties.

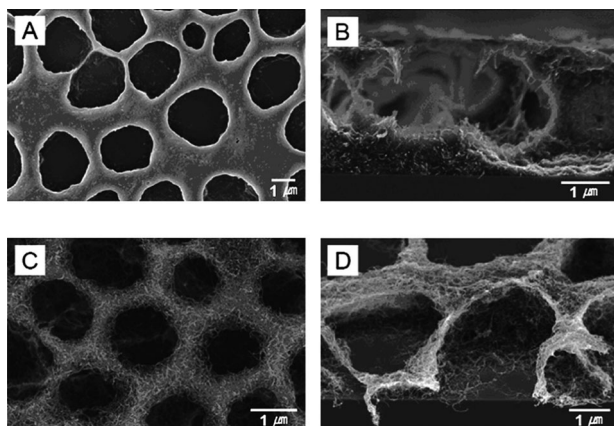


**Fig. 86** SEM images of monolayered cellular scaffolds before and after pyrolysis. (A) Plane-view of the porous PS/CNT nanocomposite film. (B) Cross-sectional image of the PS/CNT nanocomposite film. (C) Plane-view of the highly entangled CNT scaffold after pyrolysis of the polymer matrix. (D) 60° tilted SEM image of the fractured CNT scaffold. Reproduced from ref. 950 by permission of Royal Society of Chemistry.

Various polymeric foams have been produced using SCFs, such as polyetherimide, polyethersulfone, PMMA and polystyrene. The influence of process parameters including saturation pressure, temperature and processing time have been studied.<sup>951,952</sup> Reverchon and Cardea<sup>953</sup> synthesized cellulose acetate membranes with a control of the morphology and pore size (cell diameters 2–50 μm) by phase inversion assisted by scCO<sub>2</sub> (Fig. 87). A section of the membrane, formed by multiple regularly open cells (size ranging from 5 μm to 20 μm, mean diameter of ~10 μm) is shown.

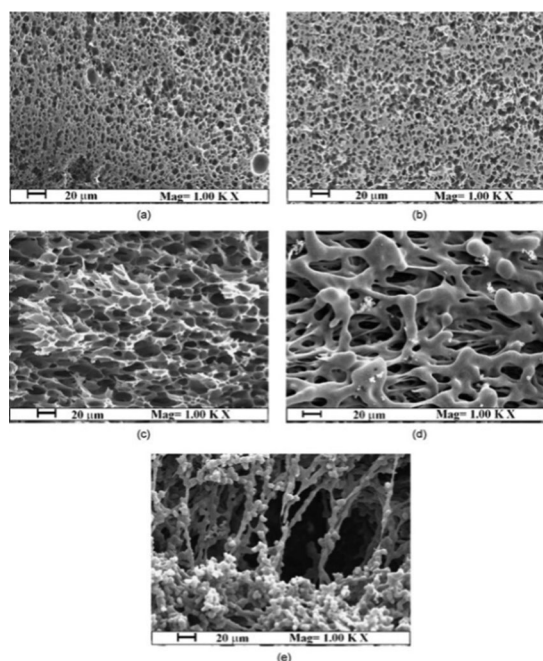


**Fig. 87** Effect of the polymer concentration on the membrane section at  $P = 200$  bar,  $T = 45$  °C: (a) 40% (w/w); (b) 30% (w/w); (c) 20% (w/w); (d) 15% (w/w); (e) 10% (w/w). Reprinted with permission from ref. 953. Copyright 2004, Elsevier B. V.

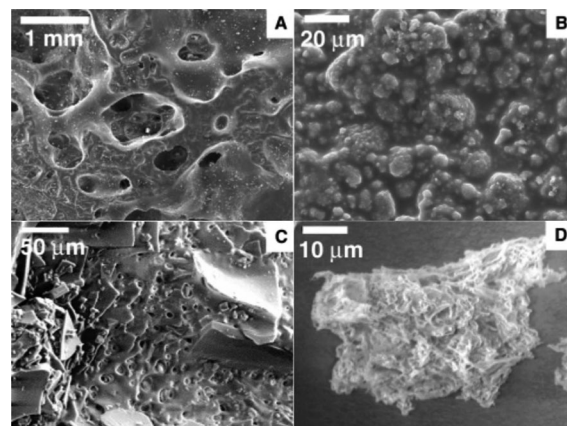


**Fig. 88** SEMs of the composites. (A and B) Images of internal fracture surface of composite of HA (40 wt%) and PLGA (60 wt%). At low magnification the distribution of HA and the porosity is evident, at higher magnification the intimate mixing of HA and PLGA is observed. (C) Catalase (50 wt%) incorporated into a PLGA matrix (50%). Micron-scale pores in the polymer and the distinctive protein particle morphology are evident. (D) High-surface area microparticle composite [fluorescein (sodium salt) (8 wt%) and PCL (92 wt%)] produced by direct atomisation. Reprinted with permission from ref. 456. Copyright 2001, Royal Society of Chemistry.

Macroporous TRIM polymer beads can also be prepared by combining O/W suspension polymerization and scCO<sub>2</sub> (as the porogenes and solvent),<sup>954</sup> The pore size varies from a hundred nanometers to a few micrometers and can be tuned by varying the supercritical fluid solvent density and other synthesis parameters.

Biocomposite materials with macroporous structures can also be synthesized by using SCFs technology. For example, CO<sub>2</sub>-induced plasticization has been exploited to lower the viscosity of biodegradable polymers, such as poly(D,L-lactide) (PLA), (polylactide-co-polyglycolide) (PLGA), and polycaprolactone, to such an extent that bioactive guests can be mixed into the polymer at room temperature (Fig. 88).<sup>456</sup> These porous structured biocomposites contain pore sizes ranging from 50 nm to 5 μm. Biocomposites are formed and the encapsulated enzymes (*e.g.*, ribonuclease A, catalase, *p*-D-galactosidase) retain their activities.

Materials with multiple macroporous structures can also be synthesized by using the freeze drying technology (or ice templating). Many polymers<sup>463–469</sup> with multiple macroporous structure have been synthesized using this approach. Dilute aqueous polymer solutions are frozen in liquid nitrogen and then freeze dried to produce polymeric nanofibres with diameters in the range of 200–600 nm.<sup>955</sup>

Macroporous ceramic materials (in particular, bundles of aligned silica fibers) have also been synthesized using the ice-template method.<sup>471</sup> The different porous ceramic materials have uniform microstructures with macroporosity.<sup>472–476,956</sup> Composites including hydroxyapatite (HAP)/collagen<sup>477</sup> (or cerium oxide/poly(vinyl alcohol) (PVA) or PVA/silica),<sup>478</sup> which have structures that are similar to those of polymers and ceramics, have also been synthesized. Monte *et al.* recently prepared hierarchically organized structures by applying the ice-templating process to a silica hydrogel containing proteins

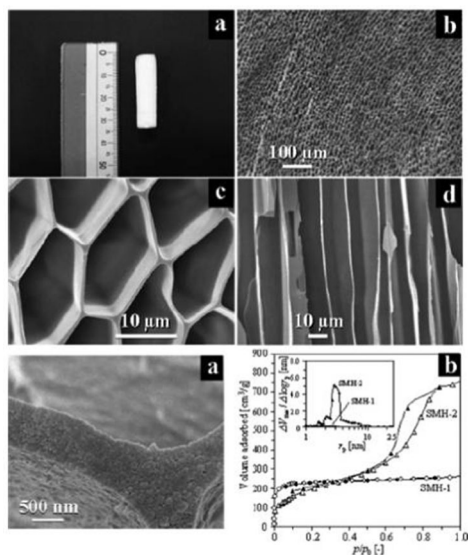


Fig. 89 Morphology and structure of silica monoliths exhibiting a micro honeycomb structure. Upper: (a) an overall image, (b) cross section, (c) microchannel structure, and (d) longitudinal section. Lower (e) detail of a cross section. Nitrogen isotherms (f) are also represented. The inset shows the mesopore size distribution in the desorption branches. Reprinted with permission from ref. 481. Copyright 2004, Royal Society of Chemistry.

or liposomes.<sup>344,346</sup> The former, comprised of an esterase protein (pig liver esterase, PLE) dispersed in poly(vinyl alcohol) (PVA)/silica hybrid hydrogel, is a hierarchical biohybrid material exhibiting a very sophisticated structure with up to six levels of space organization.

Hydrogels (silica gel)<sup>958</sup> with multiple macroporous structures, synthesized by using the ice template method (Fig. 89),<sup>481</sup> have straight macropores with a polygonal cross section that are alligned parallel to the freezing direction. Besides possessing ordered macroporosity, micro- and mesopores develop inside the honeycomb walls by freeze-drying *tert*-butyl alcohol solutions. Using a similar approach, a 3D macroporous structured composite of multiwall carbon nanotubes (MWCNT) and

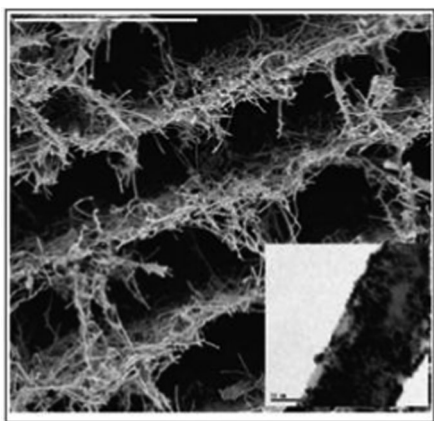


Fig. 90 SEM micrograph of a cross-sectioned monolithic Pt/MWCNT 3D architecture (the bar is 20 μm in length). The inset shows a TEM micrograph of the MWCNT surface decorated with Pt nanoparticles (here the bar is 50 nm). Reprinted with permission from ref. 957. American Chemical Society.

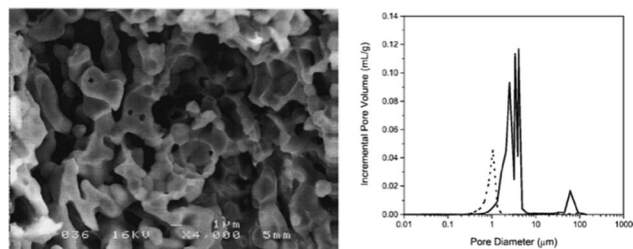


Fig. 91 SEM micrographs of 50 : 50 NiO/YSZ composite after acid leaching. Plots of pore size distribution of 100% YSZ and NiO/YSZ cermet with ratio of 1 : 1 after reduction by H<sub>2</sub> and leaching in nitric acid. (---) is 100% YSZ cermet, and (—) is NiO/YSZ cermet with ratio of 1 : 1. Reprinted with permission from ref. 523. Copyright 2002, Wiley-VCH.

chitosan (CHI) (Fig. 90) was also generated<sup>957</sup> by employing a MWCNT dispersion and ensuring the homogeneity of the suspension.<sup>959</sup>

Porous Y<sub>2</sub>O<sub>3</sub>-stabilized ZrO<sub>2</sub> (YSZ) has been synthesized by leaching nickel out of a NiO/YSZ composites using 2.2 M HNO<sub>3</sub> at 353 K.<sup>523</sup> Porosities >75% can be achieved without structural collapse of the YSZ phase. The pore range of macroporous sheets of YSZ is around 1–5 mm in diameter (Fig. 91). Porous zirconia is obtained after removal of the magnesia phase from a composite of magnesia and zirconia.<sup>524</sup> Similarly, porous Vycor glass has been produced through acid leaching of the borosilicate rich phase.<sup>525</sup>

Metathesis is amenable to selective leaching, as a soluble salt obtained as a second phase is soluble in water. PbZrO<sub>3</sub><sup>960</sup> composites with multiple macroporous structures were obtained by metathetic reactions in the solid state. A variant of solid-state metathesis has been used to prepare the macroporous oxides PbTiO<sub>3</sub> and La<sub>1-x</sub>Sr<sub>x</sub>MnO<sub>3</sub> (x = 0.0 and 0.3) at reduced temperatures.<sup>222</sup> By combining metathesis with self-propagation, the method can be employed to form powders of ZrN and GaN to MoS<sub>2</sub>.<sup>526,527</sup> The use of metathetic routes to produce a soluble salt as a second phase have been widely developed for synthesis of multiple macroporous oxides (such as LaMnO<sub>3</sub>).<sup>398,399</sup>

A variety of liquid and gas-phase reactions have been utilized to synthesise hierarchical porous monoliths. Reactive dip

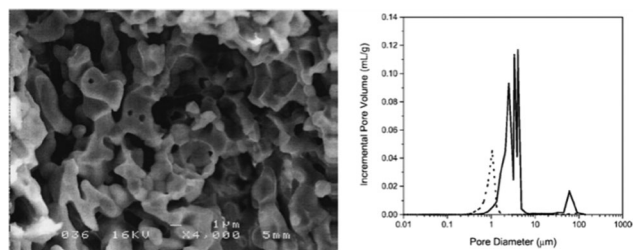


Fig. 92 (A) Scheme describing preparation of macroporous monoliths. A single-phase metal–organic precursor is formed in solution (a). The precipitated precursor is decomposed in air and the resulting powder is pressed into a pellet and sintered in air (b). The resulting oxide composite is leached in base to form a macroporous oxide (c). The oxide can be reduced in hydrogen to form a porous metal (d), or may be subjected to reactive dip coating (e); (B) SEM image of conformal coating of La<sub>4</sub>Ni<sub>3</sub>O<sub>10</sub> submicronparticles on inner surface of porous Ni<sub>0.7</sub>Zn<sub>0.3</sub>O. Reproduced from ref. 518 by permission of Springer.

coating can be used to form conformal coatings of a second phase along the inner pore walls of NiO (Fig. 92).<sup>518</sup> Gas-phase reactions can also be used to alter the chemical characteristics of the porous material. A flowing 5% H<sub>2</sub>/N<sub>2</sub> atmosphere has been used to reduce porous monoliths of NiO and ZnFe<sub>2</sub>O<sub>4</sub> to form their metallic states.<sup>518</sup> The pore structure is maintained and the faceted nature of the original NiO structure is smoothed. Multiple macroporous oxides appear to fracture at grain boundaries.<sup>961</sup>

## 4. Summary

One general purpose of the review of “hierarchical natural porous materials” is to inspire scientists to develop synthesis strategies that can be used to produce target hierarchical structures and multimodal porosities in one solid body. Some natural materials, regarded as perfect hierarchically structured materials, possess growth mechanisms that are based only on weak interactions. Unlike their natural counterparts, engineered systems require the use of a wider selection of chemical and biological substances, some of which may be sacrificial, and many different chemical or physical processes some of which require high temperatures.

A vast array of methods involving the use of surfactant templating, nanocasting, macroporous polymer templating and colloidal crystal templating have been developed in this area. In addition to macrotemplating methods, a series of technologies has been applied to the construction of hierarchically porous materials. These include bioinspired processes, SCFs, emulsion templating, freeze-drying, BFs, selective leaching, phase separation, zeolitization process, replication, sol-gel controlling, post-treatment and self-formation process. The majority of these man-made synthesis strategies enable easy and independent control over the macroporosity, mesoporosity and microporosity.

Furthermore, materials having a combination of multi-scaled porosities integrated into one moldable body should be useful in improving reaction yields of catalytic reactions and for various other practical applications. Adsorption/separation qualities and/or structural properties of the materials can be enhanced. Synthetic routes have been devised to prepare various porous combinations such as dual micropores, micro-mesopores, micro-macropores, micro-meso-macropores, dual mesopores, meso-macropores, dual/multiple macropore.

## 5. Outlook

Using the large selection of synthesis strategies and controlled pores combination summarized in this review, it is now possible to design hierarchically porous architectures with good control over pore size, connectivity and geometry. It is also possible to fine-tune the porous architectures to suit particular applications. Yet, challenges still remain. These challenges are related to better synthesis control, product stability, understanding of structural effects on mass or charge transport, application development and system integration, in particular, the last but

not the least the development of scalable synthesis process. It is crucial to establish a predictive science of synthesis for a predictive property.

An important development in designing new synthesis methods involves the use of a combination of two or more strategies including surfactant templating, nanocasting, sol-gel controlling and post-treatment. These approaches have many advantages because they are able to introduce different integrated structures and properties at the macroscopic or microscopic scale. Difficulties still exist with combining different techniques to form the targeted structures. For better synthetic control, a deeper understanding of the interactions between multiple templates (or techniques) is crucial. For example, although a single surfactant can be used to form a corresponding porous structure, in two surfactants templating it is difficult to gain a one-to-one correspondence between the templates and pores. Use of a combination of multimodal templates or techniques faces further challenges including the need for establishing better order in the multimodal templates and developing techniques to create hierarchically porous materials with different structures and functionalities.

Great opportunities exist now for modeling mass transport through hierarchically porous structures with different pore geometries and perhaps charge transport through conductive walls. Such knowledge can also provide guidance to achieve local/regional control of mass transport through an extended porous structure, possibly by exploiting tricontinuous systems or through selective functionalization of specific pore regimes. It is therefore critical that new methods become available to produce multiple well-defined porous structures. In addition, approaches are needed for determining the most appropriate methods among those that are known that can be used for this purpose.

Different hierarchical structuring of a multi-step assembly enables the construction of highly complex functions. However, the development of new morphologies control techniques is desirable. It is important to point out that many of the morphologies of hierarchically structured materials are difficult to control at all levels (from 0D, 1D, 2D to 3D architectures). However, in different applications, different morphologies and desired mechanical stabilities or perhaps flexibilities are preferred yet they are not easily achieved in nanostructured inorganic materials systems. At this point, spheres, fibers, films, and monoliths have been formed with polymer-based hybrids systems using orientated growth techniques, but this list will likely be expanded in the future.

Concerning the development of applications, the creation of multiple-functionalities in multiple-level pores still presents a major challenge, an area where progress has just begun to be made. With the increase in complexity of these systems and prospects for selective mass transport, it should become possible to develop hierarchical functions that combine several effects, such as optical effects with interfacial chemistry, or selective uptake with high surface area electrodes, catalysts and sorbents. The next step will be to integrate these functions into small systems (*e.g.*, laboratories on chips) and larger systems

(e.g., graded bioengineering structures that permit cell growth and need to include larger pores than those discussed here). If progress in this field continues at its current rate, these types of applications should be developed in the near future. Here is a concrete example on how to tailor synthesis strategy for the application of hierarchically porous materials. Recently, the hierarchical catalysis concept was proposed. In traditional industrial catalysis procedures, several catalysis and separation processes are used to reach the final desired product through multi-step pathways. Improvements in efficiency demand the reduction of reaction and separation steps. Ideally, multiple step reaction would be carried out in a cascade manner in one reactor using one catalyst and without the need for separation processes. We call this new concept “hierarchical catalysis”. Industrial production requires the use of processes that are green and occur with the production of less or even no waste, with improved efficiencies, low cost and optimal selectivities of products. The introduction of hierarchically porous materials and the hierarchical catalysis concept can potentially revolutionize industrial chemistry. However, the big challenge in this area will be to design hierarchically porous materials that have desired functionalities with right porosities at right places in pores with right geometries. The development of structured reaction for catalysis, adsorption, separation, enzymatic reaction also benefits from the contribution from hierarchically porous materials. The most recently published review paper<sup>962</sup> concerning the applications of hierarchically porous materials illustrates clearly the superiority of hierarchically porous materials in energy conversion and storage, catalysis, photocatalysis, adsorption, separation, sensing and biomedical. These are good examples showing how to design and synthesize new and advanced hierarchically porous materials that have enhanced performances. It is recognized that one porous level more in materials can generate more functionalities.<sup>962</sup>

Successful development of hierarchically porous materials in many applications requires joint efforts of workers in different disciplines including biology, chemistry, materials science and engineering science. Furthermore, innovative technologies associated with hierarchically porous materials should beneficially impact energy production, energy conversion, energy storage, and will even open new doors in the medical sciences, clinical research and healthcare management. In view of the recent advances in hierarchically porous materials and their applications assures that the future in this research area is bright.

## Acknowledgements

Authors acknowledge the financial supports from Changjiang Scholar Innovative Team granted by Chinese Ministry of Education (IRT\_15R52), from Natural Science Foundation of China (NFSC-51472190, NFSC-21301133), from International Collaboration program granted by Chinese Ministry of Science and technology (ISTC-2015DFE52870), from the Scientific Research Starting Foundation for Returned Overseas Chinese Scholars program, Ministry of Education, China (Grant No. [2015] 311),

and Hubei Provincial Natural Science Foundation (2016CFA033, 2014CFB160, 2015CFB428). B. L. Su acknowledges the Chinese Central Government for an “Expert of the State” position in the Program of the “Thousand Talents”, the Chinese Ministry of Education for a “Changjiang Chaire Professor” position and a Clare Hall Life Membership at the Clare Hall and the financial support of the Department of Chemistry, University of Cambridge. L. H. Chen, Y. Li and X. Y. Yang acknowledge Hubei Provincial Department of Education for the “Chutian Scholar” program. We also thank Prof. Zhong-Yong Yuan in Nankai University, Dr Nan Jiang, Zhi-Yi Hu, Jie Ying, Yi Lu, Dr Shao-Zhuan Huang, Dr Jun Jin, Wei Geng, Li Wang, Dr Jing Liu, Ming-Hui Sun, Chao Wang, Min Yan, Jie Hu, Yu-Xuan Xiao, Hao Wei, Wang Yong in Wuhan University of Technology, and Prof. Patrick Mariano in University of New Mexico for editing, error-checking, revision and discussion.

## Notes and references

- 1 J. Aizenberg and P. Fratzl, *Adv. Mater.*, 2009, **21**, 387–388.
- 2 P. Fratzl, *J. R. Soc., Interface*, 2007, **4**, 637–642.
- 3 P. Fratzl and R. Weinkamer, *Prog. Mater. Sci.*, 2007, **52**, 1263–1334.
- 4 R. Lakes, *Nature*, 1993, **361**, 511–515.
- 5 S. Mann, *Biomineralization: principles and concepts in bioinorganic materials chemistry*, Oxford University Press, USA, 2001.
- 6 P. B. Messersmith, *Science*, 2008, **319**, 1767.
- 7 E. Munch, M. E. Launey, D. H. Alsem, E. Saiz, A. P. Tomsia and R. O. Ritchie, *Science*, 2008, **322**, 1516.
- 8 C. Sanchez, H. Arribart and M. M. G. Guille, *Nat. Mater.*, 2005, **4**, 277–288.
- 9 B. L. Su, C. Sanchez and X. Y. Yang, *Hierarchically Structured Porous Materials*, Wiley-VCH Verlag & Co. KGaA, Germany, Weinheim, 2012.
- 10 W. Zhong, H. Liu, C. Bai, S. Liao and Y. Li, *ACS Catal.*, 2015, **5**, 1850–1856.
- 11 Q. Sun, N. Wang, D. Xi, M. Yang and J. Yu, *Chem. Commun.*, 2014, **50**, 6502–6505.
- 12 J. Liu, G. Jiang, Y. Liu, J. Di, Y. Wang, Z. Zhao, Q. Sun, C. Xu, J. Gao and A. Duan, *Sci. Rep.*, 2014, **4**, 7276.
- 13 G. Collins, M. Bloemker, M. Osiak, J. D. Holmes, M. Bredol and C. O'Dwyer, *Chem. Mater.*, 2013, **25**, 4312–4320.
- 14 Q. Sun, Z. Dai, X. Meng and F.-S. Xiao, *Chem. Soc. Rev.*, 2015, **44**, 6018–6034.
- 15 C. M. A. Parlett, K. Wilson and A. F. Lee, *Chem. Soc. Rev.*, 2013, **42**, 3876–3893.
- 16 Y. Wei, T. E. Parmentier, K. P. de Jong and J. Zecevic, *Chem. Soc. Rev.*, 2015, **44**, 7234–7261.
- 17 L. Meng, X. Zhang, Y. Tang, K. Su and J. Kong, *Sci. Rep.*, 2015, **5**, 7910.
- 18 S. Chakraborty, Y. J. Colon, R. Q. Snurr and S. T. Nguyen, *Chem. Sci.*, 2015, **6**, 384–389.
- 19 G. Srinivas, V. Krungleviciute, Z.-X. Guo and T. Yildirim, *Energy Environ. Sci.*, 2014, **7**, 335–342.
- 20 J. Wei, D. Zhou, Z. Sun, Y. Deng, Y. Xia and D. Zhao, *Adv. Funct. Mater.*, 2013, **23**, 2322–2328.

- 21 V. Scott, S. Gilfillan, N. Markussen, H. Chalmers and R. S. Haszeldine, *Nat. Clim. Change*, 2013, **3**, 105–111.
- 22 T.-Y. Ma, H. Li, A.-N. Tang and Z.-Y. Yuan, *Small*, 2011, **7**, 1827–1837.
- 23 J. Konishi, K. Fujita, S. Oiwa, K. Nakanishi and K. Hirao, *Chem. Mater.*, 2008, 2165–2173.
- 24 L. Shi, Z. Chu, Y. Liu, W. Jin and N. Xu, *Adv. Funct. Mater.*, 2014, **24**, 7032–7041.
- 25 S. Bai, K. Zhang, L. Wang, J. Sun, R. Luo, D. Li and A. Chen, *J. Mater. Chem. A*, 2014, **2**, 7927–7934.
- 26 Q. Zhao, M. Yin, A. P. Zhang, S. Prescher, M. Antonietti and J. Yuan, *J. Am. Chem. Soc.*, 2013, **135**, 5549–5552.
- 27 J. Kuang, L. Liu, Y. Gao, D. Zhou, Z. Chen, B. Han and Z. Zhang, *Nanoscale*, 2013, **5**, 12171–12177.
- 28 Y. Xiao, L. Zheng and M. Cao, *Nano Energy*, 2015, **12**, 152–160.
- 29 S.-X. Wang, S. Chen, Q. Wei, X. Zhang, S. Y. Wong, S. Sun and X. Li, *Chem. Mater.*, 2015, **27**, 336–342.
- 30 J. Jin, S.-Z. Huang, J. Shu, H.-E. Wang, Y. Li, Y. Yu, L.-H. Chen, B.-J. Wang and B.-L. Su, *Nano Energy*, 2015, **16**, 339–349.
- 31 G. Hasegawa, K. Kanamori, T. Kiyomura, H. Kurata, K. Nakanishi and T. Abe, *Adv. Energy Mater.*, 2015, **5**, 1400730.
- 32 J. H. Pikul, H. G. Zhang, J. Cho, P. V. Braun and W. P. King, *Nat. Commun.*, 2013, **4**, 1732.
- 33 N. Jiang, X. Y. Yang, Z. Deng, L. Wang, Z. Y. Hu, G. Tian, G. L. Ying, L. Shen, M. X. Zhang and B. L. Su, *Small*, 2015, **11**, 2003–2010.
- 34 N. Jiang, X.-Y. Yang, G.-L. Ying, L. Shen, J. Liu, W. Geng, L.-J. Dai, S.-Y. Liu, J. Cao and G. Tian, *Chem. Sci.*, 2015, **6**, 486–491.
- 35 N. Jiang, G.-L. Ying, S.-Y. Liu, L. Shen, J. Hu, L.-J. Dai, X.-Y. Yang, G. Tian and B.-L. Su, *Chem. Commun.*, 2014, **50**, 15407–15410.
- 36 Y.-Z. Zheng, J.-X. Zhao, S.-Q. Bi, X. Tao, M. Huang and J.-F. Chen, *Electrochim. Acta*, 2015, **157**, 258–265.
- 37 Z. Zhao, G. Liu, B. Li, L. Guo, C. Fei, Y. Wang, L. Lv, X. Liu, J. Tian and G. Cao, *J. Mater. Chem. A*, 2015, **3**, 11320–11329.
- 38 S. Wang, Z. Cui and M. Cao, *Chem. – Eur. J.*, 2015, **21**, 2165–2172.
- 39 J. Wang, R. Ma, Z. Zhou, G. Liu and Q. Liu, *Sci. Rep.*, 2015, **5**, 9304.
- 40 J. Liang, R. F. Zhou, X. M. Chen, Y. H. Tang and S. Z. Qiao, *Adv. Mater.*, 2014, **26**, 6074–6079.
- 41 H.-W. Liang, X. Zhuang, S. Bruller, X. Feng and K. Mullen, *Nat. Commun.*, 2014, **5**, 4973.
- 42 W. He, C. Jiang, J. Wang and L. Lu, *Angew. Chem., Int. Ed.*, 2014, **53**, 9503–9507.
- 43 Y. Chen, Y. Zhang, Y. Lin, Z. Yang, D. Su, M. Han and F. Chen, *Nano Energy*, 2014, **10**, 1–9.
- 44 J. Ying, X.-Y. Yang, G. Tian, C. Janiak and B.-L. Su, *Nanoscale*, 2014, **6**, 13370–13382.
- 45 J. Ying, X.-Y. Yang, Z.-Y. Hu, S.-C. Mu, C. Janiak, W. Geng, M. Pan, X. Ke, G. Van Tendeloo and B.-L. Su, *Nano Energy*, 2014, **8**, 214–222.
- 46 S. J. Yang, M. Antonietti and N. Fechner, *J. Am. Chem. Soc.*, 2015, **137**, 8269–8273.
- 47 C. Long, X. Chen, L. Jiang, L. Zhi and Z. Fan, *Nano Energy*, 2015, **12**, 141–151.
- 48 R. Liu, L. Wan, S. Liu, L. Pan, D. Wu and D. Zhao, *Adv. Funct. Mater.*, 2015, **25**, 526–533.
- 49 J. Ding, H. Wang, Z. Li, K. Cui, D. Karpuzov, X. Tan, A. Kohandehghan and D. Mitlin, *Energy Environ. Sci.*, 2015, **8**, 941–955.
- 50 A. J. Amali, J.-K. Sun and Q. Xu, *Chem. Commun.*, 2014, **50**, 1519–1522.
- 51 A. Achour, J. B. Ducros, R. L. Porto, M. Boujtita, E. Gautron, L. Le Brizoual, M. A. Djouadi and T. Brousse, *Nano Energy*, 2014, **7**, 104–113.
- 52 D.-C. Guo, J. Mi, G.-P. Hao, W. Dong, G. Xiong, W.-C. Li and A.-H. Lu, *Energy Environ. Sci.*, 2013, **6**, 652–659.
- 53 X. Huang, H. Yu, J. Chen, Z. Lu, R. Yazami and H. H. Hng, *Adv. Mater.*, 2014, **26**, 1296–1303.
- 54 Y. Yu, C. Yan, L. Gu, X. Lang, K. Tang, L. Zhang, Y. Hou, Z. Wang, M. W. Chen, O. G. Schmidt and J. Maier, *Adv. Energy Mater.*, 2013, **3**, 281–285.
- 55 Y. Yu, C. Yan, L. Gu, X. Lang, K. Tang, L. Zhang, Y. Hou, Z. Wang, M. W. Chen and O. G. Schmidt, *Adv. Energy Mater.*, 2013, **3**, 281–285.
- 56 G. Tong, J. Guan and Q. Zhang, *Adv. Funct. Mater.*, 2013, **23**, 2406–2414.
- 57 Y. Ma, C. Fang, B. Ding, G. Ji and J. Y. Lee, *Adv. Mater.*, 2013, **25**, 4646–4652.
- 58 B. Zhao, Q. Wang, S. Zhang and C. Deng, *J. Mater. Chem. A*, 2015, **3**, 12089–12096.
- 59 B. Zhang, M. Xiao, S. Wang, D. Han, S. Song, G. Chen and Y. Meng, *ACS Appl. Mater. Interfaces*, 2014, **6**, 13174–13182.
- 60 Y. Yan, Y. X. Yin, Y. G. Guo and L. J. Wan, *Adv. Energy Mater.*, 2014, **4**, 1301584.
- 61 J. Liu, K. Tang, K. Song, P. A. van Aken, Y. Yu and J. Maier, *Nanoscale*, 2014, **6**, 5081–5086.
- 62 M. Klose, K. Pinkert, M. Zier, M. Uhlemann, F. Wolke, T. Jaumann, P. Jehnichen, D. Wadewitz, S. Oswald, J. Eckert and L. Giebeler, *Carbon*, 2014, **79**, 302–309.
- 63 H. D. Yoo, I. Shterenberg, Y. Gofer, G. Gershinsky, N. Pour and D. Aurbach, *Energy Environ. Sci.*, 2013, **6**, 2265–2279.
- 64 W. Xia, B. Qiu, D. Xia and R. Zou, *Sci. Rep.*, 2013, **3**, 1935.
- 65 M. D. Slater, D. Kim, E. Lee and C. S. Johnson, *Adv. Funct. Mater.*, 2013, **23**, 947–958.
- 66 J. Ding, H. Wang, Z. Li, A. Kohandehghan, K. Cui, Z. Xu, B. Zahiri, X. Tan, E. M. Lotfabad and B. C. Olsen, *ACS Nano*, 2013, **7**, 11004–11015.
- 67 Y. Yang, H. Wang, F.-Y. Yan, Y. Qi, Y.-K. Lai, D.-M. Zeng, G. Chen and K.-Q. Zhang, *ACS Appl. Mater. Interfaces*, 2015, **7**, 5634–5642.
- 68 M. Xu, H. Li, D. Zhai, J. Chang, S. Chen and C. Wu, *J. Mater. Chem. B*, 2015, **3**, 3799–3809.
- 69 S. Tsujimura, K. Murata and W. Akatsuka, *J. Am. Chem. Soc.*, 2014, **136**, 14432–14437.
- 70 R.-L. Liu, W.-J. Ji, T. He, Z.-Q. Zhang, J. Zhang and F.-Q. Dang, *Carbon*, 2014, **76**, 84–95.

- 71 W. He, D. Min, X. Zhang, Y. Zhang, Z. Bi and Y. Yue, *Adv. Funct. Mater.*, 2014, **24**, 2206–2215.
- 72 J. Shi, C. Yang, S. Zhang, X. Wang, Z. Jiang, W. Zhang, X. Song, Q. Ai and C. Tian, *ACS Appl. Mater. Interfaces*, 2013, **5**, 9991–9997.
- 73 C. Qi, Y.-J. Zhu, B.-Q. Lu, X.-Y. Zhao, J. Zhao, F. Chen and J. Wu, *Chem. – Eur. J.*, 2013, **19**, 5332–5341.
- 74 S. C. Davis, V. C. Sheppard, G. Begum, Y. Cai, Y. Fang, J. D. Berrigan, N. Kroeger and K. H. Sandhage, *Adv. Funct. Mater.*, 2013, **23**, 4611–4620.
- 75 M. F. Finol, J. Rooke, S. Siffert, R. Cousin, P. Carniti, A. Gervasini, J.-M. Giraudon, B.-L. Su and J.-F. Lamonier, *New J. Chem.*, 2014, **38**, 1988–1995.
- 76 T. Barakat, J. Rooke, R. Cousin, J.-F. Lamonier, J.-M. Giraudon, B.-L. Su and S. Siffert, *New J. Chem.*, 2014, **38**, 2066–2074.
- 77 J. C. Rooke, T. Barakat, J. Brunet, Y. Li, M. F. Finol, J.-F. Lamonier, J.-M. Giraudon, R. Cousin, S. Siffert and B. L. Su, *Appl. Catal., B*, 2015, **162**, 300–309.
- 78 T. Barakat, J. C. Rooke, M. Franco, R. Cousin, J. F. Lamonier, J. M. Giraudon, B. L. Su and S. Siffert, *Eur. J. Inorg. Chem.*, 2012, 2812–2818.
- 79 J. Rooke, T. Barakat, M. F. Finol, P. Billemont, G. De Weireld, Y. Li, R. Cousin, J.-M. Giraudon, S. Siffert and J.-F. Lamonier, *Appl. Catal., B*, 2013, **142**, 149–160.
- 80 L. Xiaoyun, S. Minghui, J. C. Rooke, C. Lihua and S. Bao-Lian, *Chin. J. Catal.*, 2013, **34**, 22–47.
- 81 T. Barakat, J. C. Rooke, E. Genty, R. Cousin, S. Siffert and B.-L. Su, *Energy Environ. Sci.*, 2013, **6**, 371–391.
- 82 T. Barakat, J. C. Rooke, H. L. Tidahy, M. Hosseini, R. Cousin, J. F. Lamonier, J. M. Giraudon, G. De Weireld, B. L. Su and S. Siffert, *ChemSusChem*, 2011, **4**, 1420–1430.
- 83 M. F. Finol, J. Rooke, B.-L. Su, M. Trentesaux, J.-M. Giraudon and J.-F. Lamonier, *Catal. Today*, 2012, **192**, 154–159.
- 84 Y. Li, Z. Y. Fu and B. L. Su, *Adv. Funct. Mater.*, 2012, **22**, 4634–4667.
- 85 L.-H. Chen, X.-Y. Li, Z. Deng, Z.-Y. Hu, J. C. Rooke, A. Krief, X.-Y. Yang and B.-L. Su, *Catal. Today*, 2013, **212**, 89–97.
- 86 X.-Y. Li, L.-H. Chen, Y. Li, J. C. Rooke, C. Wang, Y. Lu, A. Krief, X.-Y. Yang and B.-L. Su, *J. Colloid Interface Sci.*, 2012, **368**, 128–138.
- 87 X. Chen, C. Wang, E. Baker and C. Sun, *Sci. Rep.*, 2015, **5**, 11977.
- 88 R. Yan, M. Chen, H. Zhou, T. Liu, X. Tang, K. Zhang, H. Zhu, J. Ye, D. Zhang and T. Fan, *Sci. Rep.*, 2016, **6**, 20001.
- 89 M. Wu, J. Liu, J. Jin, C. Wang, S. Huang, Z. Deng, Y. Li and B.-L. Su, *Appl. Catal., B*, 2014, **150**, 411–420.
- 90 M. Wu, J. Jin, J. Liu, Z. Deng, Y. Li, O. Deparis and B.-L. Su, *J. Mater. Chem. A*, 2013, **1**, 15491–15500.
- 91 M. Wu, A. Zheng, F. Deng and B.-L. Su, *Appl. Catal., B*, 2013, **138**, 219–228.
- 92 H. Zhao, M. Wu, J. Liu, Z. Deng, Y. Li and B.-L. Su, *Appl. Catal., B*, 2016, **184**, 182–190.
- 93 S. Mitchell, N.-L. Michels, K. Kunze and J. Pérez-Ramírez, *Nat. Chem.*, 2012, **4**, 825–831.
- 94 H. Zhou, J. Guo, P. Li, T. Fan, D. Zhang and J. Ye, *Sci. Rep.*, 2013, **3**, 1667.
- 95 J. H. Bang, K. Han, S. E. Skrabalak, H. Kim and K. S. Suslick, *J. Phys. Chem. C*, 2007, **111**, 10959–10964.
- 96 S. Somacescu, J. M. C. Moreno, P. Osiceanu, B.-L. Su and V. Parvulescu, *J. Phys. Chem. C*, 2010, **114**, 19365–19372.
- 97 H. Zhou, S. Zhu, M. Hibino, I. Honma and M. Ichihara, *Adv. Mater.*, 2003, **15**, 2107–2111.
- 98 K. T. Lee, J. C. Lytle, N. S. Ergang, S. M. Oh and A. Stein, *Adv. Funct. Mater.*, 2005, **15**, 547–556.
- 99 Z. Wang, F. Li, N. S. Ergang and A. Stein, *Chem. Mater.*, 2006, **18**, 5543–5553.
- 100 Y. S. Hu, P. Adelmhelm, B. M. Smarsly, S. Hore, M. Antonietti and J. Maier, *Adv. Funct. Mater.*, 2007, **17**, 1873–1878.
- 101 L. Wei, Q. Chen and X. Kong, *J. Am. Ceram. Soc.*, 2011, 3078–3083.
- 102 G. P. Hao, W. C. Li, S. Wang, G. H. Wang, L. Qi and A. H. Lu, *Carbon*, 2011, 3762–3772.
- 103 A. Padhi, K. Nanjundaswamy and J. B. Goodenough, *J. Electrochem. Soc.*, 1997, **144**, 1188.
- 104 A. Padhi, K. Nanjundaswamy, C. Masquelier, S. Okada and J. Goodenough, *J. Electrochem. Soc.*, 1997, **144**, 1609.
- 105 J. B. Goodenough, *J. Power Sources*, 2007, **174**, 996–1000.
- 106 M. Takahashi, S. Tobishima, K. Takei and Y. Sakurai, *J. Power Sources*, 2001, **97**, 508–511.
- 107 X.-Y. Yang, Z.-Q. Li, B. Liu, A. Klein-Hofmann, G. Tian, Y.-F. Feng, Y. Ding, D. S. Su and F.-S. Xiao, *Adv. Mater.*, 2006, **18**, 410–414.
- 108 C. M. Doherty, R. A. Caruso, B. M. Smarsly and C. J. Drummond, *Chem. Mater.*, 2009, **21**, 2895–2903.
- 109 C. M. Doherty, R. A. Caruso, B. M. Smarsly, P. Adelmhelm and C. J. Drummond, *Chem. Mater.*, 2009, **21**, 5300–5306.
- 110 N. N. Sinha, C. Shivakumara and N. Munichandraiah, *ACS Appl. Mater. Interfaces*, 2010, 2031–2038.
- 111 J. Liu, T. E. Conry, X. Song, M. M. Doeff and T. J. Richardson, *Energy Environ. Sci.*, 2011, 885–888.
- 112 F. Jiao, J. Bao, A. H. Hill and P. G. Bruce, *Angew. Chem.*, 2008, **120**, 9857–9862.
- 113 J. Luo, Y. Wang, H. Xiong and Y. Xia, *Chem. Mater.*, 2007, **19**, 4791–4795.
- 114 D. Tonti, M. J. Torralvo, E. Enciso, I. Sobrados and J. Sanz, *Chem. Mater.*, 2008, **20**, 4783–4790.
- 115 T. Sri Devi Kumari and T. Prem Kumar, *Ionics*, 2010, **16**, 61–66.
- 116 F. Jiao and P. G. Bruce, *Adv. Mater.*, 2007, **19**, 657–660.
- 117 J. Y. Baek, H. W. Ha, I. Y. Kim and S. J. Hwang, *J. Phys. Chem. C*, 2009, **113**, 17392–17398.
- 118 L. Wang, C. Yin, Z. Shan, S. Liu, Y. Du and F. S. Xiao, *Colloids Surf., A*, 2009, **340**, 126–130.
- 119 J. C. Lytle, H. Yan, N. S. Ergang, W. H. Smyrl and A. Stein, *J. Mater. Chem.*, 2004, **14**, 1616–1622.
- 120 Z. Wen, Q. Wang, Q. Zhang and J. Li, *Adv. Funct. Mater.*, 2007, **17**, 2772–2778.
- 121 Q. Wang, Z. Wen and J. Li, *J. Power Sources*, 2008, **182**, 334–339.
- 122 P. Liu, S. H. Lee, C. E. Tracy, Y. Yan and J. A. Turner, *Adv. Mater.*, 2002, **14**, 27.

- 123 J. S. Sakamoto and B. Dunn, *J. Mater. Chem.*, 2002, **12**, 2859–2861.
- 124 S. Li, Y. Sun, X. Feng and C. Chen, *Energy Environ. Sci.*, 2011, 2854–2857.
- 125 X. Xia, J. Tu, J. Xiang, X. Huang, X. Wang and X. Zhao, *J. Power Sources*, 2010, **195**, 2014–2022.
- 126 X. Huang, J. Tu, Z. Zeng, J. Xiang and X. Zhao, *J. Electrochem. Soc.*, 2008, **155**, A438.
- 127 X. Huang, J. Tu, X. Xia, X. Wang, J. Xiang, L. Zhang and Y. Zhou, *J. Power Sources*, 2009, **188**, 588–591.
- 128 Y. Yuan, X. Xia, J. Wu, J. Yang, Y. Chen and S. Guo, *Electrochem. Commun.*, 2010, **12**, 890–893.
- 129 H. G. Jung, S. W. Oh, J. Ce, N. Jayaprakash and Y. K. Sun, *Electrochem. Commun.*, 2009, **11**, 756–759.
- 130 I. Moriguchi, Y. Shono, H. Yamada and T. Kudo, *J. Phys. Chem. B*, 2008, **112**, 14560–14565.
- 131 Y. G. Guo, Y. S. Hu and J. Maier, *Chem. Commun.*, 2006, 2783–2785.
- 132 H. Yan, S. Sokolov, J. C. Lytle, A. Stein, F. Zhang and W. H. Smyrl, *J. Electrochem. Soc.*, 2003, **150**, A1102.
- 133 N. S. Ergang, J. C. Lytle, H. Yan and A. Stein, *J. Electrochem. Soc.*, 2005, **152**, A1989.
- 134 F. Jiao, K. M. Shaju and P. G. Bruce, *Angew. Chem., Int. Ed.*, 2005, **44**, 6550–6553.
- 135 X.-h. Xia, J.-p. Tu, X.-l. Wang, C.-d. Gu and X.-b. Zhao, *J. Mater. Chem.*, 2011, **21**, 671–679.
- 136 A. Rudge, J. Davey, I. Raistrick, S. Gottesfeld and J. P. Ferraris, *J. Power Sources*, 1994, **47**, 89–107.
- 137 K. Naoi, S. Suematsu and A. Manago, *J. Electrochem. Soc.*, 2000, **147**, 420.
- 138 A. Laforgue, P. Simon and J.-F. Fauvarque, *Synth. Met.*, 2001, **123**, 311–319.
- 139 X. Yang, D. Wu, X. Chen and R. Fu, *J. Phys. Chem. C*, 2010, **114**, 8581–8586.
- 140 Y. Li, X. Zhao, Q. Xu, Q. Zhang and D. Chen, *Langmuir*, 2011, **27**, 6458–6463.
- 141 D. L. Yang, B. Du, Y. X. Yan, H. Q. Li, D. Zhang and T. X. Fan, *ACS Appl. Mater. Interfaces*, 2014, **6**, 2377–2385.
- 142 H. Zhou, L. Ding, T. X. Fan, J. Ding, D. Zhang and Q. X. Guo, *Appl. Catal., B*, 2014, **147**, 221–228.
- 143 H. Zhou, J. J. Guo, P. Li, T. X. Fan, D. Zhang and J. H. Ye, *Sci. Rep.*, 2013, **3**, 9.
- 144 H. Zhou, J. Y. Pan, L. Ding, Y. W. Tang, J. Ding, Q. X. Guo, T. X. Fan and D. Zhang, *Int. J. Hydrogen Energy*, 2014, **39**, 16293–16301.
- 145 Z. T. Liu, T. X. Fan and D. Zhang, *J. Am. Ceram. Soc.*, 2006, **89**, 662–665.
- 146 R. Yan, M. Chen, H. Zhou, T. Liu, X. Tang, K. Zhang, H. Zhu, J. Ye, D. Zhang and T. Fan, *Sci. Rep.*, 2016, **6**, 20001.
- 147 N. D. Petkovich and A. Stein, *Chem. Soc. Rev.*, 2013, **42**, 3721–3739.
- 148 B. Fang, J. H. Kim, M.-S. Kim and J.-S. Yu, *Acc. Chem. Res.*, 2013, **46**, 1397–1406.
- 149 A. Inayat, B. Reinhardt, H. Uhlig, W.-D. Einicke and D. Enke, *Chem. Soc. Rev.*, 2013, **42**, 3753–3764.
- 150 S. Dutta, A. Bhaumik and K. C. W. Wu, *Energy Environ. Sci.*, 2014, **7**, 3574–3592.
- 151 S. Mitchell, A. B. Pinar, J. Kenvin, P. Crivelli, J. Kaerger and J. Perez-Ramirez, *Nat. Commun.*, 2015, **6**, 8633.
- 152 R. Nagarajan, *Langmuir*, 1985, **1**, 331–341.
- 153 Ö. Sel and B. M. Smarsly, *Hierarchically Struct. Porous Mater.*, 2012, 41–53.
- 154 G. S. Attard, J. C. Glyde and C. G. Göltner, *Nature*, 1995, **378**, 366–368.
- 155 G. S. Attard, J. M. Corker, C. G. Göltner, S. Henke and R. H. Templer, *Angew. Chem.*, 1997, **109**, 1372–1374.
- 156 C. G. Göltner, S. Henke, M. C. Weissenberger and M. Antonietti, *Angew. Chem.*, 1998, **110**, 633–636.
- 157 C. Göltner and M. Weissenberger, *Acta Polym.*, 1998, **49**, 704–709.
- 158 F. Schüth, *Angew. Chem., Int. Ed.*, 2003, **42**, 3604–3622.
- 159 B. Smarsly and M. Antonietti, *Eur. J. Inorg. Chem.*, 2006, 1111–1119.
- 160 N. T. Southall, K. A. Dill and A. Haymet, *J. Phys. Chem. B*, 2002, **106**, 521–533.
- 161 A. H. Lu and F. Schüth, *Adv. Mater.*, 2006, **18**, 1793–1805.
- 162 S. Polarz and M. Antonietti, *Chem. Commun.*, 2002, 2593–2604.
- 163 M. Antonietti, *Colloid chemistry*, Springer, Berlin Heidelberg, 2003.
- 164 B. Smarsly, S. Polarz and M. Antonietti, *J. Phys. Chem. B*, 2001, **105**, 10473–10483.
- 165 O. Sel, D. Kuang, M. Thommes and B. Smarsly, *Langmuir*, 2006, **22**, 2311–2322.
- 166 F. Rodríguez-Reinoso, H. Marsh and E. Heintz, *Introduction to carbon technologies*, 1997.
- 167 S. Subramoney, *Adv. Mater.*, 1998, **10**, 1157–1171.
- 168 J. H. Knox, B. Kaur and G. Millward, *J. Chromatogr. A*, 1986, **352**, 3–25.
- 169 J. Lee, J. Kim and T. Hyeon, *Chem. Commun.*, 2003, 1138–1139.
- 170 A. Taguchi, J. H. Smätt and M. Lindén, *Adv. Mater.*, 2003, **15**, 1209–1211.
- 171 A. H. Lu, J. H. Smätt, S. Backlund and M. Lindén, *Micro-porous Mesoporous Mater.*, 2004, **72**, 59–65.
- 172 S. Alvarez and A. B. Fuertes, *Mater. Lett.*, 2007, **61**, 2378–2381.
- 173 J. H. Smätt, S. Schunk and M. Lindén, *Chem. Mater.*, 2003, **15**, 2354–2361.
- 174 C. M. Yang, J. H. Smätt, B. Zibrowius and M. Lindén, *New J. Chem.*, 2004, **28**, 1520–1525.
- 175 A. H. Lu, J. H. Smätt and M. Lindén, *Adv. Funct. Mater.*, 2005, **15**, 865–871.
- 176 G. S. Chai, I. S. Shin and J. S. Yu, *Adv. Mater.*, 2004, **16**, 2057–2061.
- 177 S. B. Yoon, K. Sohn, J. Y. Kim, C. H. Shin, J. S. Yu and T. Hyeon, *Adv. Mater.*, 2002, **14**, 19.
- 178 M. Kim, K. Sohn, H. B. Na and T. Hyeon, *Nano Lett.*, 2002, **2**, 1383–1387.
- 179 S. Holmes, B. Graniel-Garcia, P. Foran, P. Hill, E. Roberts, B. Sakakini and J. Newton, *Chem. Commun.*, 2006, 2662–2663.

- 180 X. Cai, G. Zhu, W. Zhang, H. Zhao, C. Wang, S. Qiu and Y. Wei, *Eur. J. Inorg. Chem.*, 2006, 3641–3645.
- 181 M. Pérez-Cabero, V. Puchol, D. Beltrán and P. Amorós, *Carbon*, 2008, **46**, 297–304.
- 182 A.-H. Lu, W. Schmidt, A. Taguchi, B. Spliethoff, B. Tesche and F. Schüth, *Angew. Chem., Int. Ed.*, 2002, **41**, 3489–3492.
- 183 M. Kang, S. H. Yi, H. I. Lee, J. E. Yie and J. M. Kim, *Chem. Commun.*, 2002, 1944–1945.
- 184 J. Roggenbuck and M. Tiemann, *J. Am. Chem. Soc.*, 2005, **127**, 1096–1097.
- 185 X. Zhang, K. N. Tu, Y. H. Xie, C. H. Tung and S. Xu, *Adv. Mater.*, 2006, **18**, 1905–1909.
- 186 G. Che, B. B. Lakshmi, E. R. Fisher and C. R. Martin, *Nature*, 1998, **393**, 346–349.
- 187 X. Chen, M. Steinhart, C. Hess and U. Gösele, *Adv. Mater.*, 2006, **18**, 2153–2156.
- 188 J. H. Smatt, C. Weidenthaler, J. B. Rosenholm and M. Linden, *Chem. Mater.*, 2006, **18**, 1443–1450.
- 189 B. O'Regan, J. Moser, M. Anderson and M. Graetzel, *J. Phys. Chem.*, 1990, **94**, 8720–8726.
- 190 B. O'regan and M. Gratzel, *Nature*, 1991, **353**, 737–740.
- 191 C. J. Brinker and G. W. Scherer, *Sol-gel science: the physics and chemistry of sol-gel processing*, Academic Press, 1990.
- 192 J. Livage, M. Henry and C. Sanchez, *Prog. Solid State Chem.*, 1988, **18**, 259–341.
- 193 C. Sanchez, J. Livage, M. Henry and F. Babonneau, *J. Non-Cryst. Solids*, 1988, **100**, 65–76.
- 194 F. Ribot, P. Toledano and C. Sanchez, *Chem. Mater.*, 1991, **3**, 759–764.
- 195 C. Sanchez, B. Julián, P. Belleville and M. Popall, *J. Mater. Chem.*, 2005, **15**, 3559–3592.
- 196 C. Sanchez, B. Lebeau, F. Chaput and J. P. Boilot, *Adv. Mater.*, 2003, **15**, 1969–1994.
- 197 S. Mann, S. L. Burkett, S. A. Davis, C. E. Fowler, N. H. Mendelson, S. D. Sims, D. Walsh and N. T. Whilton, *Chem. Mater.*, 1997, **9**, 2300–2310.
- 198 J. S. Beck, J. C. Vartuli, W. J. Roth, M. E. Leonowicz, C. T. Kresge, K. D. Schmitt, C. T. W. Chu, D. H. Olson and E. W. Sheppard, *J. Am. Chem. Soc.*, 1992, **114**, 10834–10843.
- 199 A. Monnier, F. Schüth, Q. Huo, D. Kumar, D. Margolese, R. Maxwell, G. Stucky, M. Krishnamurty, P. Petroff and A. Firouzi, *Science*, 1993, **261**, 1299.
- 200 C. G. Goltner and M. Antonietti, *Adv. Mater.*, 1997, **9**, 431–436.
- 201 J. Y. Ying, C. P. Mehnert and M. S. Wong, *Angew. Chem., Int. Ed.*, 1999, **38**, 56–77.
- 202 C. Sanchez, G. J. A. A. Soler-Illia, F. Ribot and D. Grosso, *C. R. Chim.*, 2003, **6**, 1131–1151.
- 203 C. Sanchez, C. Boissière, D. Grosso, C. Laberty and L. Nicole, *Chem. Mater.*, 2008, **20**, 682–737.
- 204 B. Fousseret, M. Mougnot, F. Rossignol, J.-F. O. Baumard, B. Soulestin, C. D. Boissière, F. O. Ribot, D. Jalabert, C. Carrion, C. M. Sanchez and M. Lejeune, *Chem. Mater.*, 2010, **22**, 3875–3883.
- 205 R. Vedula, S. Kaza and S. B. Desu, *Chem. Vap. Deposition*, 2001, 243–285.
- 206 G. Decher, *Science*, 1997, **277**, 1232–1237.
- 207 H. Kerdjoudj, N. Berthelemy, F. Boulmedais, J.-F. Stoltz, P. Menu and J. C. Voegel, *Soft Matter*, 2010, **6**, 3722–3734.
- 208 J. L. Lutkenhaus and P. T. Hammond, *Soft Matter*, 2007, **3**, 804–816.
- 209 S. Monika, *Curr. Opin. Colloid Interface Sci.*, 2003, **8**, 86–95.
- 210 S. Srivastava and N. A. Kotov, *Acc. Chem. Res.*, 2008, **41**, 1831–1841.
- 211 S. Sukhishvili and A. Svetlana, *Curr. Opin. Colloid Interface Sci.*, 2005, **10**, 37–44.
- 212 S. A. Sukhishvili, E. Kharlampieva and V. Izumrudov, *Macromolecules*, 2006, **39**, 8873–8881.
- 213 G. Sukhorukov, A. Fery and H. Möhwald, *Prog. Polym. Sci.*, 2005, **30**, 885–897.
- 214 K. Ariga, J. P. Hill and Q. Ji, *Phys. Chem. Chem. Phys.*, 2007, **9**, 2319–2340.
- 215 A. Izquierdo, S. S. Ono, J. C. Voegel, P. Schaaf and G. Decher, *Langmuir*, 2005, **21**, 7558–7567.
- 216 K. C. Krogman, J. L. Lowery, N. S. Zacharia, G. C. Rutledge and P. T. Hammond, *Nat. Mater.*, 2009, **8**, 512–518.
- 217 C. J. Lefaux, J. A. Zimmerman, A. V. Dobrynin and P. T. Mather, *J. Polym. Sci., Part B: Polym. Phys.*, 2004, **42**, 3654–3666.
- 218 P. A. Patel, A. V. Dobrynin and P. T. Mather, *Langmuir*, 2007, **23**, 12589–12597.
- 219 C. M. Andres and N. A. Kotov, *J. Am. Chem. Soc.*, 2010, **132**, 14496–14502.
- 220 J. Jeon, V. Panchagnula, J. Pan and A. V. Dobrynin, *Langmuir*, 2006, **22**, 4629–4637.
- 221 P. A. Patel, J. Jeon, P. T. Mather and A. V. Dobrynin, *Langmuir*, 2006, **22**, 9994–10002.
- 222 J. J. Cerda, B. Qiao and C. Holm, *Soft Matter*, 2009, **5**, 4412–4425.
- 223 C. T. Lee Jr, P. A. Psathas, K. P. Johnston, J. D. Grazia and T. W. Randolph, *Langmuir*, 1999, **15**, 6781–6791.
- 224 R. Butler, C. M. Davies and A. I. Cooper, *Adv. Mater.*, 2001, **13**, 1459–1463.
- 225 H. Zhang and A. I. Cooper, *Soft Matter*, 2005, **1**, 107–113.
- 226 N. Cameron and D. Sherrington, *Biopolymers Liquid Crystalline Polymers Phase Emulsion*, 1996, pp. 163–214.
- 227 E. Ruckenstein, *Polymer Synthesis/Polymer Catalysis*, 1997, pp. 1–58.
- 228 M. S. Silverstein, H. Tai, A. Sergienko, Y. Lumelsky and S. Pavlovsky, *Polymer*, 2005, **46**, 6682–6694.
- 229 N. R. Cameron, *Polymer*, 2005, **46**, 1439–1449.
- 230 C. Stubenrauch, R. Tessorf, R. Strey, I. Lynch and K. A. Dawson, *Langmuir*, 2007, **23**, 7730–7737.
- 231 P. Schmidt-Winkel, W. W. Lukens Jr, P. Yang, D. I. Margolese, J. S. Lettow, J. Y. Ying and G. D. Stucky, *Chem. Mater.*, 2000, **12**, 686–696.
- 232 P. Schmidt-Winkel, C. J. Glinka and G. D. Stucky, *Langmuir*, 2000, **16**, 356–361.
- 233 D. Zhao, P. Yang, N. Melosh, J. Feng, B. F. Chmelka and G. D. Stucky, *Adv. Mater.*, 1998, **10**, 1380–1385.
- 234 D. Zhao, J. Feng, Q. Huo, N. Melosh, G. H. Fredrickson, B. F. Chmelka and G. D. Stucky, *Science*, 1998, **279**, 548–552.

- 235 P. Yang, D. Zhao, B. F. Chmelka and G. D. Stucky, *Chem. Mater.*, 1998, **10**, 2033–2036.
- 236 P. Feng, X. Bu, G. D. Stucky and D. J. Pine, *J. Am. Chem. Soc.*, 1999, **122**, 994–995.
- 237 X. Zhang, F. Zhang and K. Y. Chan, *Scr. Mater.*, 2004, **51**, 343–347.
- 238 A. Imhof and D. J. Pine, *Adv. Mater.*, 1998, **10**, 697–700.
- 239 H. Zhang and A. Cooper, *Chem. Mater.*, 2002, **14**, 4017–4020.
- 240 P. Krajnc, D. Štefanec and I. Pulko, *Macromol. Rapid Commun.*, 2005, **26**, 1289–1293.
- 241 O. Kulygin and M. S. Silverstein, *Soft Matter*, 2007, **3**, 1525–1529.
- 242 K. Nakanishi and N. Soga, *J. Am. Ceram. Soc.*, 1991, **74**, 2518–2530.
- 243 K. Nakanishi, *Bull. Chem. Soc. Jpn.*, 2006, **79**, 673–691.
- 244 S. Kuwatani, R. Maehana, K. Kajihara and K. Kanamura, *Chem. Lett.*, 2010, 712–713.
- 245 K. Kajihara, S. Kuwatani, R. Maehana and K. Kanamura, *Bull. Chem. Soc. Jpn.*, 2009, **82**, 1470–1476.
- 246 K. Nakanishi, T. Nagakane and N. Soga, *J. Porous Mater.*, 1998, **5**, 103–110.
- 247 T. Amatani, K. Nakanishi, K. Hirao and T. Kodaira, *Chem. Mater.*, 2005, **17**, 2114–2119.
- 248 K. K. Unger, N. Tanaka and E. Machtejevas, *Monolithic silicas in separation science: concepts, syntheses, characterization, modeling and applications*, Wiley-VCH, 2010.
- 249 M. Iwasaki, S. Miwa, T. Ikegami, M. Tomita, N. Tanaka and Y. Ishihama, *Anal. Chem.*, 2010, **82**, 2616–2620.
- 250 K. Miyamoto, T. Hara, H. Kobayashi, H. Morisaka, D. Tokuda, K. Horie, K. Koduki, S. Makino, O. Núñez and C. Yang, *Anal. Chem.*, 2008, **80**, 8741–8750.
- 251 H. Eghbali, K. Sandra, F. Detobel, F. Lynen, K. Nakanishi, P. Sandra and G. Desmet, *J. Chromatogr. A*, 2011, **1218**, 3360–3366.
- 252 K. Nakanishi and K. Kanamori, *J. Mater. Chem.*, 2005, **15**, 3776–3786.
- 253 S. Inagaki, S. Guan, Y. Fukushima, T. Ohsuna and O. Terasaki, *J. Am. Chem. Soc.*, 1999, **121**, 9611–9614.
- 254 K. Nakanishi, Y. Kobayashi, T. Amatani, K. Hirao and T. Kodaira, *Chem. Mater.*, 2004, **16**, 3652–3658.
- 255 J. Konishi, K. Fujita, K. Nakanishi, K. Hirao, K. Morisato, S. Miyazaki and M. Ohira, *J. Chromatogr. A*, 2009, **1216**, 7375–7383.
- 256 G. Hasegawa, K. Kanamori, K. Nakanishi and T. Hanada, *J. Am. Ceram. Soc.*, 2010, **93**, 3110–3115.
- 257 J. Konishi, K. Fujita, K. Nakanishi and K. Hirao, *Chem. Mater.*, 2006, **18**, 6069–6074.
- 258 Y. Tokudome, K. Nakanishi and T. Hanada, *J. Ceram. Soc. Jpn.*, 2009, **117**, 351–355.
- 259 Y. Tokudome, K. Nakanishi, S. Kosaka, A. Kariya, H. Kaji and T. Hanada, *Microporous Mesoporous Mater.*, 2010, **132**, 538–542.
- 260 J. Hasegawa, K. Kanamori, K. Nakanishi and T. Hanada, *C. R. Chim.*, 2010, **13**, 207–211.
- 261 G. Hasegawa, M. Aoki, K. Kanamori, K. Nakanishi, T. Hanada and K. Tadanaga, *J. Mater. Chem.*, 2011, 2060–2063.
- 262 S. Murai, K. Fujita, T. Hirao, K. Nakanishi and K. Hirao, *Opt. Mater.*, 2007, **29**, 949–954.
- 263 P. J. Flory, *Principles of polymer chemistry*, Cornell Univ Press, 1953.
- 264 G. Hasegawa, K. Kanamori, K. Nakanishi and T. Hanada, *J. Mater. Chem.*, 2009, **19**, 7716–7720.
- 265 N. Tanaka, H. Kobayashi, K. Nakanishi, H. Minakuchi and N. Ishizuka, *Anal. Chem.*, 2001, **73**, 420–429.
- 266 G. Hasegawa, K. Kanamori, K. Nakanishi and T. Hanada, *Chem. Mater.*, 2010, **22**, 2541–2547.
- 267 G. Hasegawa, K. Kanamori, K. Nakanishi and T. Hanada, *Chem. Commun.*, 2010, **46**, 8037–8039.
- 268 X. Meng, K. Fujita, S. Murai, J. Konishi, M. Mano and K. Tanaka, *Opt. Express*, 2010, **18**, 12153–12160.
- 269 D. W. Breck, *Zeolite molecular sieves: structure, chemistry, and use*, Wiley-Interscience, New York, 1974.
- 270 R. M. Barrer, *Hydrothermal chemistry of zeolites*, Academic Press, London, 1982.
- 271 H. v. Békum, *Introduction to zeolite science and practice*, Elsevier Science, 2001.
- 272 R. Xu, *Chemistry of zeolites and related porous materials: synthesis and structure*, Wiley-Interscience, 2007.
- 273 A. Corma, *Chem. Rev.*, 1995, **95**, 559–614.
- 274 M. E. Davis, C. Saldarriaga, C. Montes, J. Garces and C. Crowder, *Nature*, 1988, **331**, 698–699.
- 275 Q. Huo, R. Xu, S. Li, Z. Ma, J. M. Thomas, R. H. Jones and A. M. Chippindale, *J. Chem. Soc., Chem. Commun.*, 1992, 875–876.
- 276 X. Zou, T. Conradsson, M. Klingstedt, M. S. Dadachov and M. O’Keeffe, *Nature*, 2005, **437**, 716–719.
- 277 C. C. Freyhardt, M. Tsapatsis, R. F. Lobo, K. J. Balkus and M. E. Davis, *Nature*, 1996, **381**, 295–298.
- 278 P. Wagner, M. Yoshikawa, K. Tsuji, M. E. Davis, M. Lovallo and M. Tsapatsis, *Chem. Commun.*, 1997, 2179–2180.
- 279 A. Burton, S. Elomari, C. Y. Chen, R. C. Medrud, I. Y. Chan, L. M. Bull, C. Kibby, T. V. Harris, S. I. Zones and E. S. Vittoratos, *Chem. – Eur. J.*, 2003, **9**, 5737–5748.
- 280 K. G. Strohmaier and D. E. W. Vaughan, *J. Am. Chem. Soc.*, 2003, **125**, 16035–16039.
- 281 A. Corma, M. J. Díaz-Cabañas, J. Martínez-Triguero, F. Rey and J. Rius, *Nature*, 2002, **418**, 514–517.
- 282 J. L. Paillaud, B. Harbuzaru, J. Patarin and N. Bats, *Science*, 2004, **304**, 990.
- 283 M. Niwa, N. Katada and T. Murakami, *J. Phys. Chem.*, 1990, **94**, 441.
- 284 D. Van, Vu, M. Miyamoto, N. Nishiyama, Y. Egashira and K. Ueyama, *J. Catal.*, 2006, **243**, 389–394.
- 285 C. S. Lee, T. J. Park and X. Y. Lee, *Appl. Catal., A*, 1993, **95**, 151.
- 286 M. Miyamoto, T. Kamei, N. Nishiyama, Y. Egashira and K. Ueyama, *Adv. Mater.*, 2005, **17**, 1985–1988.
- 287 F. Porcher, Y. Dusausoy, M. Souhassou and C. Lecomte, *Mineral. Mag.*, 2000, **64**, 1.
- 288 J. M. Thomas and G. R. Millward, *J. Chem. Soc., Chem. Commun.*, 1982, 1380–1383.
- 289 A. M. Goossens, B. H. Wouters, V. Buschmann and J. A. Martens, *Adv. Mater.*, 1999, **11**, 561–564.

- 290 K. P. Lillerud and J. H. Raeder, *Zeolites*, 1986, **6**, 474–483.
- 291 Y. Bouizi, L. Rouleau and V. P. Valtchev, *Microporous Mesoporous Mater.*, 2006, **91**, 70–77.
- 292 A. Yonkeu, G. Mieke, H. Fuess, A. Goossens and J. Martens, *Microporous Mesoporous Mater.*, 2006, **96**, 396–404.
- 293 T. Wakihara, S. Yamakita, K. Iezumi and T. Okubo, *J. Am. Chem. Soc.*, 2003, **125**, 12388–12389.
- 294 Y. Bouizi, I. Diaz, L. Rouleau and V. P. Valtchev, *Adv. Funct. Mater.*, 2005, **15**, 1955–1960.
- 295 C. H. M. Tsang, P. S. E. Dai and R. H. Petty, *U.S. Pat.*, US5888921, 1999.
- 296 Y. Tao, H. Kanoh, L. Abrams and K. Kaneko, *Chem. Rev.*, 2006, **106**, 896–910.
- 297 S. van Donk, A. H. Janssen, J. H. Bitter and K. P. de Jong, *Catal. Rev.*, 2003, **45**, 297–319.
- 298 U. Lohse and M. Mildebrath, *Z. Anorg. Allg. Chem.*, 1981, **476**, 126–135.
- 299 J. S. Beck, J. C. Vartuli, G. J. Kennedy, C. T. Kresge, W. J. Roth and S. E. Schramm, *Chem. Mater.*, 1994, **6**, 1816–1821.
- 300 A. Karlsson, M. Stöcker and R. Schmidt, *Microporous Mesoporous Mater.*, 1999, **27**, 181–192.
- 301 N. Petkov, M. Hölzl, T. Metzger, S. Mintova and T. Bein, *J. Phys. Chem. B*, 2005, **109**, 4485–4491.
- 302 C. J. H. Jacobsen, C. Madsen, J. Houzvicka, I. Schmidt and A. Carlsson, *J. Am. Chem. Soc.*, 2000, **122**, 7116–7117.
- 303 Y. Tao, H. Kanoh and K. Kaneko, *J. Am. Chem. Soc.*, 2003, **125**, 6044–6045.
- 304 S. S. Kim, J. Shah and T. J. Pinnavaia, *Chem. Mater.*, 2003, **15**, 1664–1668.
- 305 I. Schmidt, A. Boisen, E. Gustavsson, K. Ståhl, S. Pehrson, S. Dahl, A. Carlsson and C. J. H. Jacobsen, *Chem. Mater.*, 2001, **13**, 4416–4418.
- 306 A. Sakthivel, S. J. Huang, W. H. Chen, Z. H. Lan, K. H. Chen, T. W. Kim, R. Ryoo, A. S. T. Chiang and S. B. Liu, *Chem. Mater.*, 2004, **16**, 3168–3175.
- 307 Y. Tao, M. Endo and K. Kaneko, *J. Am. Chem. Soc.*, 2009, **131**, 904–905.
- 308 B. T. Holland, L. Abrams and A. Stein, *J. Am. Chem. Soc.*, 1999, **121**, 4308–4309.
- 309 A. Dong, Y. Wang, Y. Tang, Y. Zhang, N. Ren and Z. Gao, *Adv. Mater.*, 2002, **14**, 1506–1510.
- 310 H. Zhu, Z. Liu, Y. Wang, D. Kong, X. Yuan and Z. Xie, *Chem. Mater.*, 2007, **20**, 1134–1139.
- 311 F. S. Xiao, L. Wang, C. Yin, K. Lin, Y. Di, J. Li, R. Xu, D. S. Su, R. Schlögl and T. Yokoi, *Angew. Chem.*, 2006, **118**, 3162–3165.
- 312 L. Wang, Z. Zhang, C. Yin, Z. Shan and F. S. Xiao, *Microporous Mesoporous Mater.*, 2010, **131**, 58–67.
- 313 S. Liu, X. Cao, L. Li, C. Li, Y. Ji and F. S. Xiao, *Colloids Surf., A*, 2008, **318**, 269–274.
- 314 H. Wang and T. J. Pinnavaia, *Angew. Chem., Int. Ed.*, 2006, **45**, 7603–7606.
- 315 M. Choi, H. S. Cho, R. Srivastava, C. Venkatesan, D. H. Choi and R. Ryoo, *Nat. Mater.*, 2006, **5**, 718–723.
- 316 K. Na, C. Jo, J. Kim, K. Cho, J. Jung, Y. Seo, R. J. Messinger, B. F. Chmelka and R. Ryoo, *Science*, 2011, **333**, 328.
- 317 V. Valtchev and S. Mintova, *Microporous Mesoporous Mater.*, 2001, **43**, 41–49.
- 318 W. Yang, X. Wang, Y. Tang, Y. Wang, C. Ke and S. Fu, *J. Macromol. Sci., Part A: Pure Appl. Chem.*, 2002, **39**, 509–526.
- 319 V. Valtchev, *Chem. Mater.*, 2002, **14**, 956–958.
- 320 V. Valtchev, *Chem. Mater.*, 2002, **14**, 4371–4377.
- 321 N. Van der Puil, F. Dautzenberg, H. Van Bekkum and J. Jansen, *Microporous Mesoporous Mater.*, 1999, **27**, 95–106.
- 322 S. Komarneni, H. Katsuki and S. Furuta, *J. Mater. Chem.*, 1998, **8**, 2327–2329.
- 323 W. Y. Dong, Y. J. Sun, H. Y. He and Y. C. Long, *Microporous Mesoporous Mater.*, 1999, **32**, 93–100.
- 324 T. Tang, C. Yin, L. Wang, Y. Ji and F. S. Xiao, *J. Catal.*, 2007, **249**, 111–115.
- 325 D. Bradshaw, S. El-Hankari and L. Lupica-Spagnolo, *Chem. Soc. Rev.*, 2014, **43**, 5431–5443.
- 326 M.-H. Pham, G.-T. Vuong, F.-G. Fontaine and T.-O. Do, *Cryst. Growth Des.*, 2012, **12**, 1008–1013.
- 327 T.-Y. Ma, H. Li, Q.-F. Deng, L. Liu, T.-Z. Ren and Z.-Y. Yuan, *Chem. Mater.*, 2012, **24**, 2253–2255.
- 328 S. Cao, G. Gody, W. Zhao, S. Perrier, X. Peng, C. Ducati, D. Zhao and A. K. Cheetham, *Chem. Sci.*, 2013, **4**, 3573–3577.
- 329 K. M. Choi, H. J. Jeon, J. K. Kang and O. M. Yaghi, *J. Am. Chem. Soc.*, 2011, **133**, 11920–11923.
- 330 M. Pang, A. J. Cairns, Y. Liu, Y. Belmabkhout, H. C. Zeng and M. Eddaoudi, *J. Am. Chem. Soc.*, 2013, **135**, 10234–10237.
- 331 L. H. Wee, C. Wiktor, S. Turner, W. Vanderlinden, N. Janssens, S. R. Bajpe, K. Houthoofd, G. Van Tendeloo, S. De Feyter and C. E. Kirschhock, *J. Am. Chem. Soc.*, 2012, **134**, 10911–10919.
- 332 Z. Xue, J. Zhang, L. Peng, B. Han, T. Mu, J. Li and G. Yang, *ChemPhysChem*, 2014, **15**, 85–89.
- 333 J. Reboul, S. Furukawa, N. Horike, M. Tsotsalas, K. Hirai, H. Uehara, M. Kondo, N. Louvain, O. Sakata and S. Kitagawa, *Nat. Mater.*, 2012, **11**, 717–723.
- 334 Y. Cui, S. J. Lee and W. Lin, *J. Am. Chem. Soc.*, 2003, **125**, 6014–6015.
- 335 L. Ma and W. Lin, *J. Am. Chem. Soc.*, 2008, **130**, 13834–13835.
- 336 F. Song, C. Wang, J. M. Falkowski, L. Ma and W. Lin, *J. Am. Chem. Soc.*, 2010, **132**, 15390–15398.
- 337 L. Ma, J. M. Falkowski, C. Abney and W. Lin, *Nat. Chem.*, 2010, **2**, 838–846.
- 338 C. Wang, M. Zheng and W. Lin, *J. Phys. Chem. Lett.*, 2011, **2**, 1701–1709.
- 339 Y. Yue, P. F. Fulvio and S. Dai, *Acc. Chem. Res.*, 2015, **48**, 3044–3052.
- 340 Y. Yue, Z.-A. Qiao, P. F. Fulvio, A. J. Binder, C. Tian, J. Chen, K. M. Nelson, X. Zhu and S. Dai, *J. Am. Chem. Soc.*, 2013, **135**, 9572–9575.
- 341 Y. Yue, A. J. Binder, R. Song, Y. Cui, J. Chen, D. K. Hensley and S. Dai, *Dalton Trans.*, 2014, **43**, 17893–17898.
- 342 J. L. Blin, A. Leonard, Z. Y. Yuan, L. Gigot, A. Vantomme, A. K. Cheetham and B. L. Su, *Angew. Chem., Int. Ed.*, 2003, **42**, 2872–2875.
- 343 B. E. Yoldas, *Asian J. Mater. Sci.*, 1986, **21**, 1087–1092.

- 344 D. Antonelli, *Microporous Mesoporous Mater.*, 1999, **33**, 209–214.
- 345 Y. Li, X. Y. Yang, G. Tian, A. Vantomme, J. Yu, G. Van Tendeloo and B. L. Su, *Chem. Mater.*, 2010, **22**, 3251–3258.
- 346 Z. Y. Yuan, T. Z. Ren and B. L. Su, *Adv. Mater.*, 2003, **15**, 1462–1465.
- 347 W. Deng, M. W. Toepke and B. H. Shanks, *Adv. Funct. Mater.*, 2003, **13**, 61–65.
- 348 Z. Y. Yuan, A. Vantomme, A. Léonard and B. L. Su, *Chem. Commun.*, 2003, 1558–1559.
- 349 A. Leonard, J.-L. Blin and B.-L. Su, *Chem. Commun.*, 2003, 2568–2569.
- 350 A. Collins, D. Carriazo, S. A. Davis and S. Mann, *Chem. Commun.*, 2004, 568–569.
- 351 A. Leonard and B.-L. Su, *Chem. Commun.*, 2004, 1674–1675.
- 352 T.-Z. Ren, Z.-Y. Yuan and B.-L. Su, *Chem. Commun.*, 2004, 2730–2731.
- 353 Z. Y. Yuan, T. Z. Ren, A. Vantomme and B. L. Su, *Chem. Mater.*, 2004, **16**, 5096–5106.
- 354 T. Z. Ren, Z. Y. Yuan and B. L. Su, *Langmuir*, 2004, **20**, 1531–1534.
- 355 A. Vantomme, Z. Y. Yuan and B. L. Su, *New J. Chem.*, 2004, **28**, 1083–1085.
- 356 T. Z. Ren, Z. Y. Yuan and B. L. Su, *Colloids Surf., A*, 2004, **241**, 67–73.
- 357 T.-Z. Ren, Z.-Y. Yuan and B.-L. Su, *Chem. Phys. Lett.*, 2004, **388**, 46–49.
- 358 W. Deng and B. H. Shanks, *Chem. Mater.*, 2005, **17**, 3092–3100.
- 359 B. L. Su, A. Leonard and Z. Y. Yuan, *C. R. Chim.*, 2005, **8**, 713–726.
- 360 A. Leonard and B. L. Su, *Chim. Nouv.*, 2005, **23**, 77–81.
- 361 Z. Y. Yuan, T. Z. Ren, A. Azioune, J. J. Pireaux and B. L. Su, *Catal. Today*, 2005, **105**, 647–654.
- 362 A. Léonard, A. Vantomme, C. Bouvy, N. Moniotte, P. Mariaulle and B. L. Su, *Nanopages*, 2006, **1**, 1–44.
- 363 Z. Y. Yuan and B. L. Su, *J. Mater. Chem.*, 2005, **16**, 663–677.
- 364 Z. Y. Yuan, T. Z. Ren, A. Azioune, J. J. Pireaux and B. L. Su, *Chem. Mater.*, 2006, **18**, 1753–1767.
- 365 T. Z. Ren, Z. Y. Yuan, A. Azioune, J. J. Pireaux and B. L. Su, *Langmuir*, 2006, **22**, 3886–3894.
- 366 B. L. Su, A. Vantomme, L. Surahy, R. Pirard and J. P. Pirard, *Chem. Mater.*, 2007, **19**, 3325–3333.
- 367 A. Vantomme and B. L. Su, in *Recent Progress in Mesoporous Structured Materials, Proceedings of the 5th International Mesoporous Structured Materials Symposium – Imms 2006*, ed. D. Zhao, S. Qiu, Y. Tang and C. Yu, Elsevier Science Bv, Amsterdam, 2007, vol. 165, pp. 235–238.
- 368 T. Z. Ren, Z. Y. Yuan and B. L. Su, in *Recent Progress in Mesoporous Structured Materials, Proceedings of the 5th International Mesoporous Structured Materials Symposium – Imms 2006*, ed. D. Zhao, S. Qiu, Y. Tang and C. Yu, Elsevier Science Bv, Amsterdam, 2007, vol. 165, pp. 287–290.
- 369 A. Vantomme, A. Léonard, Z.-Y. Yuan and B.-L. Su, *Colloids Surf., A*, 2007, **300**, 70–78.
- 370 A. Léonard and B.-L. Su, *Colloids Surf., A*, 2007, **300**, 129–135.
- 371 A. Vantomme, A. Leonard, Z. Y. Yuan and B. L. Su, *Key Eng. Mater.*, 2007, **336**, 1933–1938.
- 372 A. Lemaire and B. L. Su, *Langmuir*, 2010, **26**, 17603–17616.
- 373 A. Lemaire, J. C. Rooke, L. H. Chen and B. L. Su, *Langmuir*, 2011, **27**, 3030–3043.
- 374 A. Lemaire and B. L. Su, *Microporous Mesoporous Mater.*, 2011, **142**, 70–81.
- 375 P. Y. Dapsens, S. H. Hakim, B.-L. Su and B. H. Shanks, *Chem. Commun.*, 2010, **46**, 8980–8982.
- 376 X. Y. Yang, Y. Li, A. Lemaire, J. G. Yu and B. L. Su, *Pure Appl. Chem.*, 2009, **81**, 2265–2307.
- 377 S. H. Hakim and B. H. Shanks, *Chem. Mater.*, 2009, **21**, 2027–2038.
- 378 X.-Y. Yang, Y. Li, G. Van Tendeloo, F.-S. Xiao and B.-L. Su, *Adv. Mater.*, 2009, **21**, 1368–1372.
- 379 H. Chen, J. Gu, J. Shi, Z. Liu, J. Gao, M. Ruan and D. Yan, *Adv. Mater.*, 2005, **17**, 2010–2014.
- 380 S. Ota, S. Miyazaki, H. Matsuoka, K. Morisato, Y. Shintani and K. Nakanishi, *J. Biochem. Biophys. Methods*, 2007, **70**, 57–62.
- 381 T. Z. Ren, Z. Y. Yuan and B. L. Su, *Chem. Commun.*, 2004, 2730–2731.
- 382 J. Liu, S. Z. Qiao, S. Budi Hartono and G. Q. Lu, *Angew. Chem., Int. Ed.*, 2010, **49**, 4981–4985.
- 383 A. Vantomme and B. L. Su, *Stud. Surf. Sci. Catal.*, 2007, **165**, 235–238.
- 384 R. C. Schrodén, C. F. Blanford, B. J. Melde, B. J. S. Johnson and A. Stein, *Chem. Mater.*, 2001, **13**, 1074–1081.
- 385 A. Stein, F. Li and N. R. Denny, *Chem. Mater.*, 2007, **20**, 649–666.
- 386 R. Roy, *Science*, 1987, **238**, 1664.
- 387 M. Sadakane, T. Horiuchi, N. Kato, C. Takahashi and W. Ueda, *Chem. Mater.*, 2007, **19**, 5779–5785.
- 388 A. Esmanski and G. A. Ozin, *Adv. Funct. Mater.*, 2009, **19**, 1999–2010.
- 389 I. Alessandri, M. Zucca, M. Ferroni, E. Bontempi and L. E. Depero, *Small*, 2009, **5**, 336–340.
- 390 Y. J. Huang, C. H. Lai, P. W. Wu and L. Y. Chen, *J. Electrochem. Soc.*, 2010, **157**, P18.
- 391 X. Meng, R. Al-Salman, J. Zhao, N. Borissenko, Y. Li and F. Endres, *Angew. Chem., Int. Ed.*, 2009, **48**, 2703–2707.
- 392 M. Wu, Y. Li, Z. Deng and B. L. Su, *ChemSusChem*, 2011, **4**, 1481–1488.
- 393 J. Liu, J. Jin, Y. Li, H.-W. Huang, C. Wang, M. Wu, L.-H. Chen and B.-L. Su, *J. Mater. Chem. A*, 2014, **2**, 5051–5059.
- 394 P. M. Tessier, O. D. Velev, A. T. Kalambur, J. F. Rabolt, A. M. Lenhoff and E. W. Kaler, *J. Am. Chem. Soc.*, 2000, **122**, 9554–9555.
- 395 F. Li, Z. Wang and A. Stein, *Angew. Chem.*, 2007, **119**, 1917–1920.
- 396 Z. Wang and A. Stein, *Chem. Mater.*, 2008, **20**, 1029–1040.
- 397 Z. Wang, F. Li and A. Stein, *Nano Lett.*, 2007, **7**, 3223–3226.
- 398 F. Li, Y. Qian and A. Stein, *Chem. Mater.*, 2010, **22**, 3226–3235.
- 399 B. Fang, J. H. Kim, M. Kim and J. S. Yu, *Chem. Mater.*, 2009, **21**, 789–796.

- 400 S. W. Woo, K. Dokko, H. Nakano and K. Kanamura, *J. Mater. Chem.*, 2008, **18**, 1674–1680.
- 401 Z. Wang, M. A. Fierke and A. Stein, *J. Electrochem. Soc.*, 2008, **155**, A658.
- 402 Z. Wang, F. Li, N. S. Ergang and A. Stein, *Carbon*, 2008, **46**, 1702–1710.
- 403 M. Kamperman, A. Burns, R. Weissgraeber, N. van Vegten, S. C. Warren, S. M. Gruner, A. Baiker and U. Wiesner, *Nano Lett.*, 2009, **9**, 2756–2762.
- 404 S. Tao, J. Yin and G. Li, *J. Mater. Chem.*, 2008, **18**, 4872–4878.
- 405 Y. Yamada, T. Nakamura and K. Yano, *Langmuir*, 2008, **24**, 2779–2784.
- 406 Y. Yamada, H. Yamada, T. Nakamura and K. Yano, *Langmuir*, 2009, **25**, 13599–13605.
- 407 H. Yamada, T. Nakamura, Y. Yamada and K. Yano, *Adv. Mater.*, 2009, **21**, 4134–4138.
- 408 F. Zhang, Y. Deng, Y. Shi, R. Zhang and D. Zhao, *J. Mater. Chem.*, 2010, **20**, 3895–3900.
- 409 Y. Li, W. Cai, B. Cao, G. Duan, F. Sun, C. Li and L. Jia, *Nanotechnology*, 2006, **17**, 238.
- 410 Y. Li, C. Li, S. O. Cho, G. Duan and W. Cai, *Langmuir*, 2007, **23**, 9802–9807.
- 411 X. Xia, J. Tu, J. Zhang, X. Huang, X. Wang and X. Zhao, *Electrochim. Acta*, 2010, **55**, 989–994.
- 412 M. Etienne, S. Sallard, M. Schröder, Y. Guillemin, S. Mascotto, B. M. Smarsly and A. Walcarius, *Chem. Mater.*, 2010, **22**, 3426–3432.
- 413 P. Fratzl and R. Weinkamer, *Prog. Mater. Sci.*, 2007, **52**, 1263–1334.
- 414 S. A. Davis, S. L. Burkett, N. H. Mendelson and S. Mann, *Nature*, 1997, 420–423.
- 415 F. C. Meldrum and R. Seshadri, *Chem. Commun.*, 2000, 29–30.
- 416 L. Qi, J. Li and J. Ma, *Adv. Mater.*, 2002, **14**, 300.
- 417 G. Cook, P. L. Timms and C. Göltner-Spickermann, *Angew. Chem., Int. Ed.*, 2003, **42**, 557–559.
- 418 S. R. Hall, H. Bolger and S. Mann, *Chem. Commun.*, 2003, 2784–2785.
- 419 H. Zhou, X. Li, T. Fan, F. E. Osterloh, J. Ding, E. M. Sabio, D. Zhang and Q. Guo, *Adv. Mater.*, 2010, **22**, 951–956.
- 420 Y. Shin, L. Q. Wang, J. H. Chang, W. D. Samuels and G. J. Exarhos, *Stud. Surf. Sci. Catal.*, 2003, **146**, 447–451.
- 421 L. Q. Wang, Y. Shin, W. D. Samuels, G. J. Exarhos, I. L. Moudrakovski, V. Tersikh and J. Ripmeester, *J. Phys. Chem. B*, 2003, **107**, 13793–13802.
- 422 X. Y. Yang, Z. Q. Li, B. Liu, A. Klein-Hofmann, G. Tian, Y. F. Feng, Y. Ding, D. S. Su and F. S. Xiao, *Adv. Mater.*, 2006, **18**, 410–414.
- 423 L. Huang, H. Wang, C. Y. Hayashi, B. Tian, D. Zhao and Y. Yan, *J. Mater. Chem.*, 2003, **13**, 666–668.
- 424 C. Jeffries, J. Campbell, H. Li, J. Jiao and G. Rorrer, *Energy Environ. Sci.*, 2011, **4**, 3930–3941.
- 425 H. Zhou, P. Li, J. Guo, R. Yan, T. Fan, D. Zhang and J. Ye, *Nanoscale*, 2015, **7**, 113–120.
- 426 Z. Liu, T. Fan, D. Zhang, X. Gong and J. Xu, *Sens. Actuators, B*, 2009, **136**, 499–509.
- 427 Y. Jia, W. Han, G. Xiong and W. Yang, *J. Colloid Interface Sci.*, 2008, **323**, 326–331.
- 428 A. Zampieri, G. T. P. Mabande, T. Selvam, W. Schwieger, A. Rudolph, R. Hermann, H. Sieber and P. Greil, *Mater. Sci. Eng., C*, 2006, **26**, 130–135.
- 429 I. Gill and A. Ballesteros, *J. Am. Chem. Soc.*, 1998, **120**, 8587–8598.
- 430 S. M. Holmes, C. Markert, R. J. Plaisted, J. O. Forrest, J. R. Agger, M. W. Anderson, C. S. Cundy and J. Dwyer, *Chem. Mater.*, 1999, **11**, 3329–3332.
- 431 Y. Wang, Y. Tang, X. Wang, A. Dong, W. Shan and Z. Gao, *Chem. Lett.*, 2001, 1118–1119.
- 432 Y. Wang, Y. Tang, A. Dong, X. Wang, N. Ren and Z. Gao, *J. Mater. Chem.*, 2002, **12**, 1812–1818.
- 433 E. G. Vrieling, T. P. M. Beelen, R. A. van Santen and W. W. C. Gieskes, *Angew. Chem., Int. Ed.*, 2002, **41**, 1543–1546.
- 434 T. Y. Ma, X. J. Zhang and Z. Y. Yuan, *Microporous Mesoporous Mater.*, 2009, **123**, 234–242.
- 435 X. J. Zhang, T. Y. Ma and Z. Y. Yuan, *Eur. J. Inorg. Chem.*, 2008, 2721–2726.
- 436 J. H. Schattka, D. G. Shchukin, J. G. Jia, M. Antonietti and R. A. Caruso, *Chem. Mater.*, 2002, **14**, 5103–5108.
- 437 M. Breulmann, S. A. Davis, S. Mann, H. P. Hentze and M. Antonietti, *Adv. Mater.*, 2000, **12**, 502–507.
- 438 F. Z. Huang, M. F. Zhou, Y. B. Cheng and R. A. Caruso, *Chem. Mater.*, 2006, **18**, 5835–5839.
- 439 M. Zhou, F. Huang, X. Wang, J. du Plessis, A. B. Murphy and R. A. Caruso, *Aust. J. Chem.*, 2007, **60**, 533–540.
- 440 G. L. Drisko, V. Luca, E. Sizgek, N. Scales and R. A. Caruso, *Langmuir*, 2009, **25**, 5286–5293.
- 441 X. D. Wang, C. E. Egan, M. F. Zhou, K. Prince, D. R. G. Mitchell and R. A. Caruso, *Chem. Commun.*, 2007, 3060–3062, DOI: 10.1039/b704825d, ISSN 1359-7345.
- 442 D. G. Shchukin, A. A. Yaremchenko, M. G. S. Ferreira and V. V. Kharton, *Chem. Mater.*, 2005, **17**, 5124–5129.
- 443 W. J. Kim, T. J. Kim, W. S. Ahn, Y. J. Lee and K. B. Yoon, *Catal. Lett.*, 2003, **91**, 123–127.
- 444 L. Qian, A. Ahmed, A. Foster, S. P. Rannard, A. I. Cooper and H. F. Zhang, *J. Mater. Chem.*, 2009, **19**, 5212–5219.
- 445 J. Ren, Z. J. Du, C. Zhang and H. Q. Li, *Chin. J. Chem.*, 2006, **24**, 955–960.
- 446 H. Maekawa, J. Esquena, S. Bishop, C. Solans and B. F. Chmelka, *Adv. Mater.*, 2003, **15**, 591–596.
- 447 Y. J. Lee and K. B. Yoon, *Microporous Mesoporous Mater.*, 2006, **88**, 176–186.
- 448 M. Bognitzki, W. Czado, T. Frese, A. Schaper, M. Hellwig, M. Steinhart, A. Greiner and J. H. Wendorff, *Adv. Mater.*, 2001, **13**, 70–72.
- 449 M. Bognitzki, H. Q. Hou, M. Ishaque, T. Frese, M. Hellwig, C. Schwarte, A. Schaper, J. H. Wendorff and A. Greiner, *Adv. Mater.*, 2000, **12**, 637–640.
- 450 H. Q. Hou, Z. Jun, A. Reuning, A. Schaper, J. H. Wendorff and A. Greiner, *Macromolecules*, 2002, **35**, 2429–2431.
- 451 F. Ochanda and W. E. Jones, *Langmuir*, 2005, **21**, 10791–10796.
- 452 D. G. Shchukin and R. A. Caruso, *Chem. Mater.*, 2004, **16**, 2287–2292.

- 453 A. S. Deshpande, D. G. Shchukin, E. Ustinovich, M. Antonietti and R. A. Caruso, *Adv. Funct. Mater.*, 2005, **15**, 239–245.
- 454 D. G. Shchukin and R. A. Caruso, *Chem. Commun.*, 2003, 1478–1479, DOI: 10.1039/b304259f, ISSN 1359-7345.
- 455 C. A. Eckert, B. L. Knutson and P. G. Debenedetti, *Nature*, 1996, **383**, 313–318.
- 456 S. M. Howdle, M. S. Watson, M. J. Whitaker, V. K. Popov, M. C. Davies, F. S. Mandel, J. D. Wang and K. M. Shakesheff, *Chem. Commun.*, 2001, 109–110.
- 457 R. Butler, I. Hopkinson and A. Cooper, *J. Am. Chem. Soc.*, 2003, **125**, 14473–14481.
- 458 M. C. Gutiérrez, M. L. Ferrer and F. Del Monte, *Chem. Mater.*, 2008, **20**, 634–648.
- 459 S. Deville, *Adv. Eng. Mater.*, 2008, **10**, 155–169.
- 460 L. Qian and H. Zhang, *J. Chem. Technol. Biotechnol.*, 2011, **86**, 172–184.
- 461 J. M. DeSimone, Z. Guan and C. S. Elsbernd, *Science*, 1992, **257**, 945–947.
- 462 D. Ross, *Lancet*, 1962, **2**, 487.
- 463 G. Chen, T. Ushida and T. Tateishi, *Biomaterials*, 2001, **22**, 2563–2567.
- 464 M. H. Ho, P. Y. Kuo, H. J. Hsieh, T. Y. Hsien, L. T. Hou, J. Y. Lai and D.-M. Wang, *Biomaterials*, 2004, **25**, 129–138.
- 465 H.-W. Kang, Y. Tabata and Y. Ikada, *Biomaterials*, 1999, **20**, 1339–1344.
- 466 C. Y. Hsieh, S. P. Tsai, D. M. Wang, Y. N. Chang and H. J. Hsieh, *Biomaterials*, 2005, **26**, 5617–5623.
- 467 C. Y. Hsieh, S. P. Tsai, M. H. Ho, D. M. Wang, C. E. Liu, C. H. Hsieh, H. C. Tseng and H. J. Hsieh, *Carbohydr. Polym.*, 2007, **67**, 124–132.
- 468 W. F. Daamen, H. T. B. van Moerkerk, T. Hafmans, L. Buttafoco, A. A. Poot, J. H. Veerkamp and T. H. van Kuppevelt, *Biomaterials*, 2003, **24**, 4001–4009.
- 469 N. Dagalakis, J. Flink, P. Stasikelis, J. F. Burke and I. V. Yannas, *J. Biomed. Mater. Res.*, 1980, **14**, 511–528.
- 470 W. S. W. Shalaby, G. E. Peck and K. Park, *J. Controlled Release*, 1991, **16**, 355–363.
- 471 W. Mahler and M. F. Bechtold, *Nature*, 1980, **285**, 27–28.
- 472 D. W. Johnson and F. J. Schnettler, *J. Am. Ceram. Soc.*, 1970, **53**, 440–444.
- 473 P. K. Gallagher and F. Schrey, *Thermochim. Acta*, 1970, **1**, 465–476.
- 474 A. Landsberg and T. T. Campbell, *J. Met.*, 1965, **17**, 856–860.
- 475 T. Fukasawa, M. Ando, T. Ohji and S. Kanzaki, *J. Am. Ceram. Soc.*, 2001, **84**, 230–232.
- 476 S. W. Sofie and F. Dogan, *J. Am. Ceram. Soc.*, 2001, **84**, 1459–1464.
- 477 M. C. Gutiérrez, M. Jobbágy, N. Rapún, M. L. Ferrer and F. del Monte, *Adv. Mater.*, 2006, **18**, 1137–1140.
- 478 H. Zhang, I. Hussain, M. Brust, M. F. Butler, S. P. Rannard and A. I. Cooper, *Nat. Mater.*, 2005, **4**, 787–793.
- 479 H. Zhang and A. I. Cooper, *Adv. Mater.*, 2007, **19**, 1529–1533.
- 480 X. Tang and M. Pikal, *Pharm. Res.*, 2004, **21**, 191–200.
- 481 S. R. Mukai, H. Nishihara and H. Tamon, *Chem. Commun.*, 2004, 874–875.
- 482 H. Nishihara, S. R. Mukai, D. Yamashita and H. Tamon, *Chem. Mater.*, 2005, **17**, 683–689.
- 483 S. Deville, E. Saiz and A. P. Tomsia, *Biomaterials*, 2006, **27**, 5480–5489.
- 484 S. Deville, E. Saiz and A. P. Tomsia, *Acta Mater.*, 2007, **55**, 1965–1974.
- 485 M. A. C. Gutiérrez, M. A. L. Ferrer, C. R. Mateo and F. del Monte, *Langmuir*, 2009, **25**, 5509–5515.
- 486 A. W. Perriman, H. Cölfen, R. W. Hughes, C. L. Barrie and S. Mann, *Angew. Chem., Int. Ed.*, 2009, **48**, 6242–6246.
- 487 A. W. Perriman, A. P. S. Brogan, H. Cölfen, N. Tsoureas, G. R. Owen and S. Mann, *Nat. Chem.*, 2010, **2**, 622–626.
- 488 G. Widawski, M. Rawiso and B. Francois, *Nature*, 1994, **369**, 387–389.
- 489 O. Karthaus, N. Maruyama, X. Cieren, M. Shimomura, H. Hasegawa and T. Hashimoto, *Langmuir*, 2000, **16**, 6071–6076.
- 490 J. Peng, Y. Han, J. Fu, Y. Yang and B. Li, *Macromol. Chem. Phys.*, 2003, **204**, 125–130.
- 491 J. Peng, Y. Han, Y. Yang and B. Li, *Polymer*, 2004, **45**, 447–452.
- 492 T. Hayakawa and S. Horiuchi, *Angew. Chem.*, 2003, **115**, 2387–2391.
- 493 B. François, O. Pitois and J. François, *Adv. Mater.*, 1995, **7**, 1041–1044.
- 494 B. Francois, Y. Ederle and C. Mathis, *Synth. Met.*, 1999, **103**, 2362–2363.
- 495 M. H. Stenzel, *Aust. J. Chem.*, 2002, **55**, 239–243.
- 496 O. Pitois and B. Francois, *Eur. Phys. J. B*, 1999, **8**, 225–231.
- 497 T. Nishikawa, R. Ookura, J. Nishida, T. Sawadaishi and M. Shimomura, *RIKEN Rev.*, 2001, 43–47.
- 498 K. H. Wong, M. Hernández-Guerrero, A. M. Granville, T. P. Davis, C. Barner-Kowollik and M. H. Stenzel, *J. Porous Mater.*, 2006, **13**, 213–223.
- 499 M. Barrow, R. Jones, J. Park, M. Srinivasarao, P. Williams and C. Wright, *Spectrosc. Int. J.*, 2004, **18**, 577–586.
- 500 A. Böker, Y. Lin, K. Chiapperini, R. Horowitz, M. Thompson, V. Carreon, T. Xu, C. Abetz, H. Skaff and A. Dinsmore, *Nat. Mater.*, 2004, **3**, 302–306.
- 501 L. Song, R. K. Bly, J. N. Wilson, S. Bakbak, J. O. Park, M. Srinivasarao and U. H. F. Bunz, *Adv. Mater.*, 2004, **16**, 115–118.
- 502 M. Srinivasarao, D. Collings, A. Philips and S. Patel, *Science*, 2001, **292**, 79–83.
- 503 L. A. Connal, P. A. Gurr, G. G. Qiao and D. H. Solomon, *J. Mater. Chem.*, 2005, **15**, 1286–1292.
- 504 M. S. Park and J. K. Kim, *Langmuir*, 2004, **20**, 5347–5352.
- 505 M. S. Park and J. K. Kim, *Langmuir*, 2005, **21**, 11404–11408.
- 506 L. Rayleigh, *Nature*, 1911, **86**, 416–417.
- 507 J. Aitken, *Nature*, 1911, **86**, 516.
- 508 J. T. Baker, *Philos. Mag.*, 1922, **56**, 752.
- 509 A. Steyer, P. Guenoun, D. Beysens and C. Knobler, *Phys. Rev. B: Condens. Matter Mater. Phys.*, 1990, **42**, 1086.
- 510 M. H. Stenzel, C. Barner-Kowollik and T. P. Davis, *J. Polym. Sci., Part A: Polym. Chem.*, 2006, **44**, 2363–2375.
- 511 U. H. F. Bunz, *Adv. Mater.*, 2006, **18**, 973–989.

- 512 B. P. Khanal and E. R. Zubarev, *Angew. Chem., Int. Ed.*, 2007, **46**, 2195–2198.
- 513 L. Zhang, H.-Y. Si and H.-L. Zhang, *J. Mater. Chem.*, 2008, **18**, 2660–2665.
- 514 X. Xu, X. Wang, A. Nisar, X. Liang, J. Zhuang, S. Hu and Y. Zhuang, *Adv. Mater.*, 2008, **20**, 3702–3708.
- 515 H. Ma and J. Hao, *Chem. – Eur. J.*, 2010, **16**, 655–660.
- 516 L. A. Connal, R. Vestberg, C. J. Hawker and G. G. Qiao, *Adv. Funct. Mater.*, 2008, **18**, 3706–3714.
- 517 X. Xiong, W. Zou, Z. Yu, J. Duan, X. Liu, S. Fan and H. Zhou, *Macromolecules*, 2009, **42**, 9351–9356.
- 518 E. S. Toberer, A. Joshi and R. Seshadri, *Chem. Mater.*, 2005, **17**, 2142–2147.
- 519 G. Masing, *Z. Anorg. Allg. Chem.*, 1921, **118**, 293–308.
- 520 M. L. Bakker, D. J. Young and M. S. Wainwright, *Asian J. Mater. Sci.*, 1988, **23**, 3921–3926.
- 521 Y. Suzuki, N. Kondo and T. Ohji, *J. Am. Ceram. Soc.*, 2003, **86**, 1128–1131.
- 522 R. Suresh Singh, C. A. Grimes and E. C. Dickey, *Mater. Res. Innovations*, 2002, **5**, 178–184.
- 523 H. Kim, C. da Rosa, M. Boaro, J. M. Vohs and R. J. Gorte, *J. Am. Ceram. Soc.*, 2002, **85**, 1473–1476.
- 524 Y. Suzuki, T. Yamada, S. Sakakibara and T. Ohji, *24th Annual Conference on Composites, Advanced Ceramics, Materials, and Structures: B. Ceramic Engineering and Science Proceedings*, John Wiley & Sons, Inc., 2008, ch. 3, pp. 19–24, DOI: 10.1002/9780470294635.
- 525 P. Levitz, G. Ehret, S. Sinha and J. Drake, *J. Chem. Phys.*, 1991, **95**, 6151.
- 526 J. B. Wiley and R. B. Kaner, *Science*, 1992, **255**, 1093–1097.
- 527 C. H. Wallace, T. K. Reynolds and R. B. Kaner, *Chem. Mater.*, 1999, **11**, 2299–2301.
- 528 E. S. Toberer and R. Seshadri, *Chem. Commun.*, 2006, 3159–3165.
- 529 F. A. L. Dullien, *Porous media; fluid transport and pore structure*, Academic press, 1979.
- 530 A. M. Abdel-Mageed, S. Eckle and R. J. Behm, *J. Am. Chem. Soc.*, 2015, **137**, 8672–8675.
- 531 D. Alezi, A. M. Peedikakkal, L. J. Weselinski, V. Guillermin, Y. Belmabkhout, A. J. Cairns, Z. Chen, L. Wojtas and M. Eddaoudi, *J. Am. Chem. Soc.*, 2015, **137**, 5421–5430.
- 532 M. A. Alkhabbaz, P. Bollini, G. S. Foo, C. Sievers and C. W. Jones, *J. Am. Chem. Soc.*, 2014, **136**, 13170–13173.
- 533 S. Bach, V. R. Celinski, M. Dietzsch, M. Panthofer, R. Bienert, F. Emmerling, J. Schmedt auf der Gunne and W. Tremel, *J. Am. Chem. Soc.*, 2015, **137**, 2285–2294.
- 534 A. Boubnov, H. W. Carvalho, D. E. Doronkin, T. Gunter, E. Gallo, A. J. Atkins, C. R. Jacob and J. D. Grunwaldt, *J. Am. Chem. Soc.*, 2014, **136**, 13006–13015.
- 535 C. C. Chang, A. R. Teixeira, C. Li, P. J. Dauenhauer and W. Fan, *Langmuir*, 2013, **29**, 13943–13950.
- 536 Y. P. Chen, Y. Liu, D. Liu, M. Bosch and H. C. Zhou, *J. Am. Chem. Soc.*, 2015, **137**, 2919–2930.
- 537 H. J. Cho, P. Dornath and W. Fan, *ACS Catal.*, 2014, **4**, 2029–2037.
- 538 B. Coasne, A. Galarneau, C. Gerardin, F. Fajula and F. Villemot, *Langmuir*, 2013, **29**, 7864–7875.
- 539 B. Coasne, A. Galarneau, R. J. Pellenq and F. Di Renzo, *Chem. Soc. Rev.*, 2013, **42**, 4141–4171.
- 540 P. Deshlahra, R. T. Carr and E. Iglesia, *J. Am. Chem. Soc.*, 2014, **136**, 15229–15247.
- 541 K. Ding, A. Corma, J. A. Macia-Agullo, J. G. Hu, S. Kramer, P. C. Stair and G. D. Stucky, *J. Am. Chem. Soc.*, 2015, **137**, 11238–11241.
- 542 L. Emdadi, Y. Wu, G. Zhu, C.-C. Chang, W. Fan, T. Pham, R. F. Lobo and D. Liu, *Chem. Mater.*, 2014, **26**, 1345–1355.
- 543 A. Galarneau, F. Villemot, J. Rodriguez, F. Fajula and B. Coasne, *Langmuir*, 2014, **30**, 13266–13274.
- 544 F. Gao, C. Lian, L. Zhou, H. Liu and J. Hu, *Langmuir*, 2014, **30**, 11284–11291.
- 545 C. Gerardin, J. Reboul, M. Bonne and B. Lebeau, *Chem. Soc. Rev.*, 2013, **42**, 4217–4255.
- 546 S. Goel, S. I. Zones and E. Iglesia, *J. Am. Chem. Soc.*, 2014, **136**, 15280–15290.
- 547 K. Góra-Marek, K. Tarach and M. Choi, *J. Phys. Chem. C*, 2014, **118**, 12266–12274.
- 548 D. Gu and F. Schuth, *Chem. Soc. Rev.*, 2014, **43**, 313–344.
- 549 W. Gu, M. M. Stalzer, C. P. Nicholas, A. Bhattacharyya, A. Motta, J. R. Gallagher, G. Zhang, J. T. Miller, T. Kobayashi, M. Pruski, M. Delferro and T. J. Marks, *J. Am. Chem. Soc.*, 2015, **137**, 6770–6780.
- 550 F. Hayashi, Y. Tomota, M. Kitano, Y. Toda, T. Yokoyama and H. Hosono, *J. Am. Chem. Soc.*, 2014, **136**, 11698–11706.
- 551 C. M. Parlett, M. A. Isaacs, S. K. Beaumont, L. M. Bingham, N. S. Hondow, K. Wilson and A. F. Lee, *Nat. Mater.*, 2015, 178–182.
- 552 J. M. Holcroft, K. J. Hartlieb, P. Z. Moghadam, J. G. Bell, G. Barin, D. P. Ferris, E. D. Bloch, M. M. Algaradah, M. S. Nassar, Y. Y. Botros, K. M. Thomas, J. R. Long, R. Q. Snurr and J. F. Stoddart, *J. Am. Chem. Soc.*, 2015, **137**, 5706–5719.
- 553 C.-W. Hsu, Y.-W. Chen, B. S. Rana, R. Kumar, A. K. Sinha and D. W. Hwang, *J. Phys. Chem. C*, 2014, **118**, 20481–20487.
- 554 H. Y. Hsueh, C. T. Yao and R. M. Ho, *Chem. Soc. Rev.*, 2015, **44**, 1974–2018.
- 555 A. Huang, Q. Liu, N. Wang, Y. Zhu and J. Caro, *J. Am. Chem. Soc.*, 2014, **136**, 14686–14689.
- 556 G. S. Hutchings, Y. Zhang, J. Li, B. T. Yonemoto, X. Zhou, K. Zhu and F. Jiao, *J. Am. Chem. Soc.*, 2015, **137**, 4223–4229.
- 557 A. Inayat, B. Reinhardt, H. Uhlrig, W. D. Einicke and D. Enke, *Chem. Soc. Rev.*, 2013, **42**, 3753–3764.
- 558 I. Ivanova, II and E. E. Knyazeva, *Chem. Soc. Rev.*, 2013, **42**, 3671–3688.
- 559 J. W. Jeon, R. Sharma, P. Meduri, B. W. Arey, H. T. Schaef, J. L. Lutkenhaus, J. P. Lemmon, P. K. Thallapally, M. I. Nandasiri, B. P. McGrail and S. K. Nune, *ACS Appl. Mater. Interfaces*, 2014, **6**, 7214–7222.
- 560 A. M. Kaczmarek and R. Van Deun, *Chem. Soc. Rev.*, 2013, **42**, 8835–8848.
- 561 N. Kalutharage and C. S. Yi, *J. Am. Chem. Soc.*, 2015, **137**, 11105–11114.
- 562 K. C. Kao, C. H. Lin, T. Y. Chen, Y. H. Liu and C. Y. Mou, *J. Am. Chem. Soc.*, 2015, **137**, 3779–3782.

- 563 J. Karger and R. Valiullin, *Chem. Soc. Rev.*, 2013, **42**, 4172–4197.
- 564 T. C. Keller, J. Arras, S. Wershofen and J. Pérez-Ramírez, *ACS Catal.*, 2015, **5**, 734–743.
- 565 J. Kenvin, J. Jagiello, S. Mitchell and J. Perez-Ramirez, *Langmuir*, 2015, **31**, 1242–1247.
- 566 M. Kumar, H. Luo, Y. Roman-Leshkov and J. D. Rimer, *J. Am. Chem. Soc.*, 2015, 13007–13017, DOI: 10.1021/jacs.5b07477.
- 567 H. T. Kwon, H. K. Jeong, A. S. Lee, H. S. An and J. S. Lee, *J. Am. Chem. Soc.*, 2015, **137**, 12304–12311.
- 568 D.-W. Lee, M.-H. Jin, C.-B. Lee, S.-W. Lee, J.-W. Park, D. Oh, J. C. Park and J.-S. Park, *Chem. Mater.*, 2015, **27**, 5151–5160.
- 569 B. Li, K. Leng, Y. Zhang, J. J. Dynes, J. Wang, Y. Hu, D. Ma, Z. Shi, L. Zhu, D. Zhang, Y. Sun, M. Chrzanowski and S. Ma, *J. Am. Chem. Soc.*, 2015, **137**, 4243–4248.
- 570 D. Li, C. Lv, L. Liu, Y. Xia, X. She, S. Guo and D. Yang, *ACS Cent. Sci.*, 2015, **1**, 261–269.
- 571 Z. X. Li, F. B. Shi and C. H. Yan, *Langmuir*, 2015, **31**, 8672–8679.
- 572 Q. Lin, X. Bu, C. Mao, X. Zhao, K. Sasan and P. Feng, *J. Am. Chem. Soc.*, 2015, **137**, 6184–6187.
- 573 H. Liu, Y. Cao, F. Wang and Y. Huang, *ACS Appl. Mater. Interfaces*, 2014, **6**, 819–825.
- 574 J. E. Lofgreen and G. A. Ozin, *Chem. Soc. Rev.*, 2014, **43**, 911–933.
- 575 T. Y. Ma, L. Liu and Z. Y. Yuan, *Chem. Soc. Rev.*, 2013, **42**, 3977–4003.
- 576 J. A. Mason, T. M. McDonald, T. H. Bae, J. E. Bachman, K. Sumida, J. J. Dutton, S. S. Kaye and J. R. Long, *J. Am. Chem. Soc.*, 2015, **137**, 4787–4803.
- 577 W. A. Maza, R. Padilla and A. J. Morris, *J. Am. Chem. Soc.*, 2015, **137**, 8161–8168.
- 578 N. D. McNamara and J. C. Hicks, *ACS Appl. Mater. Interfaces*, 2015, **7**, 5338–5346.
- 579 D. D. Medina, J. M. Rotter, Y. Hu, M. Dogru, V. Werner, F. Auras, J. T. Markiewicz, P. Knochel and T. Bein, *J. Am. Chem. Soc.*, 2015, **137**, 1016–1019.
- 580 N.-L. Michels, S. Mitchell and J. Pérez-Ramírez, *ACS Catal.*, 2014, **4**, 2409–2417.
- 581 K. Moller and T. Bein, *Chem. Soc. Rev.*, 2013, **42**, 3689–3707.
- 582 M. Muruganandham, R. Amutha and M. Sillanpaa, *ACS Appl. Mater. Interfaces*, 2010, **2**, 1817–1823.
- 583 N. Musselwhite, K. Na, S. Alayoglu and G. A. Somorjai, *J. Am. Chem. Soc.*, 2014, **136**, 16661–16665.
- 584 N. Musselwhite, K. Na, K. Sabyrov, S. Alayoglu and G. A. Somorjai, *J. Am. Chem. Soc.*, 2015, **137**, 10231–10237.
- 585 K. Na, S. Alayoglu, R. Ye and G. A. Somorjai, *J. Am. Chem. Soc.*, 2014, **136**, 17207–17212.
- 586 K. Narsimhan, V. K. Michaelis, G. Mathies, W. R. Gunther, R. G. Griffin and Y. Roman-Leshkov, *J. Am. Chem. Soc.*, 2015, **137**, 1825–1832.
- 587 G. A. Olah, A. Goeppert, M. Czaun, T. Mathew, R. B. May and G. K. Prakash, *J. Am. Chem. Soc.*, 2015, **137**, 8720–8729.
- 588 M. Opanasenko, W. O. Parker, Jr, M. Shamzhy, E. Montanari, M. Bellettato, M. Mazur, R. Millini and J. Cejka, *J. Am. Chem. Soc.*, 2014, **136**, 2511–2519.
- 589 C. M. Parlett, K. Wilson and A. F. Lee, *Chem. Soc. Rev.*, 2013, **42**, 3876–3893.
- 590 C. Perego and R. Millini, *Chem. Soc. Rev.*, 2013, **42**, 3956–3976.
- 591 A. Primo and H. Garcia, *Chem. Soc. Rev.*, 2014, **43**, 7548–7561.
- 592 J. Qi, X. Lai, J. Wang, H. Tang, H. Ren, Y. Yang, Q. Jin, L. Zhang, R. Yu, G. Ma, Z. Su, H. Zhao and D. Wang, *Chem. Soc. Rev.*, 2015, **44**, 6749–6773.
- 593 Y. Q. Qiao, J. P. Tu, X. L. Wang, J. Zhang, Y. X. Yu and C. D. Gu, *J. Phys. Chem. C*, 2011, **115**, 25508–25518.
- 594 L. Ren, Q. Wu, C. Yang, L. Zhu, C. Li, P. Zhang, H. Zhang, X. Meng and F. S. Xiao, *J. Am. Chem. Soc.*, 2012, **134**, 15173–15176.
- 595 Z. Ristanovic, J. P. Hofmann, G. De Cremer, A. V. Kubarev, M. Rohnke, F. Meirer, J. Hofkens, M. B. Roeffaers and B. M. Weckhuysen, *J. Am. Chem. Soc.*, 2015, **137**, 6559–6568.
- 596 A. D. Roberts, X. Li and H. Zhang, *Chem. Soc. Rev.*, 2014, **43**, 4341–4356.
- 597 P. Rubio-Marqués, M. A. Rivero-Crespo, A. Leyva-Pérez and A. Corma, *J. Am. Chem. Soc.*, 2015, **137**, 11832–11837.
- 598 S. A. Saba, M. P. Mousavi, P. Buhlmann and M. A. Hillmyer, *J. Am. Chem. Soc.*, 2015, **137**, 8896–8899.
- 599 K. Sadowska, K. Góra-Marek and J. Datka, *J. Phys. Chem. C*, 2013, **117**, 9237–9244.
- 600 W. C. E. Schofield, C. D. Bain and J. P. S. Badyal, *Chem. Mater.*, 2012, **24**, 1645–1653.
- 601 Y. Seo, S. Lee, C. Jo and R. Ryoo, *J. Am. Chem. Soc.*, 2013, **135**, 8806–8809.
- 602 D. P. Serrano, J. M. Escola and P. Pizarro, *Chem. Soc. Rev.*, 2013, **42**, 4004–4035.
- 603 S. Smeets, L. B. McCusker, C. Baerlocher, D. Xie, C. Y. Chen and S. I. Zones, *J. Am. Chem. Soc.*, 2015, **137**, 2015–2020.
- 604 C. Sprung and B. M. Weckhuysen, *J. Am. Chem. Soc.*, 2015, **137**, 1916–1928.
- 605 A. R. Studart, J. Studer, L. Xu, K. Yoon, H. C. Shum and D. A. Weitz, *Langmuir*, 2011, **27**, 955–964.
- 606 Q. Sun, Z. Dai, X. Meng and F. S. Xiao, *Chem. Soc. Rev.*, 2015, **44**, 6018–6034.
- 607 J. Tang, R. R. Salunkhe, J. Liu, N. L. Torad, M. Imura, S. Furukawa and Y. Yamauchi, *J. Am. Chem. Soc.*, 2015, **137**, 1572–1580.
- 608 H. V. Thang, M. Rubes, O. Bludsky and P. Nachtigall, *J. Phys. Chem. A*, 2014, **118**, 7526–7534.
- 609 C. Triantafyllidis, M. S. Elsaesser and N. Husing, *Chem. Soc. Rev.*, 2013, **42**, 3833–3846.
- 610 M. Valla, A. J. Rossini, M. Caillot, C. Chizzallet, P. Raybaud, M. Digne, A. Chaumonnot, A. Lesage, L. Emsley, J. A. van Bokhoven and C. Coperet, *J. Am. Chem. Soc.*, 2015, 10710–10719.
- 611 J. Van Aelst, M. Haouas, E. Gobechiya, K. Houthoofd, A. Philippaerts, S. P. Sree, C. E. A. Kirschhock, P. Jacobs, J. A. Martens, B. F. Sels and F. Taulelle, *J. Phys. Chem. C*, 2014, **118**, 22573–22582.
- 612 H. E. van der Bij, D. Cicmil, J. Wang, F. Meirer, F. M. de Groot and B. M. Weckhuysen, *J. Am. Chem. Soc.*, 2014, **136**, 17774–17787.

- 613 P. Vanelderen, B. E. Snyder, M. L. Tsai, R. G. Hadt, J. Vancauwenbergh, O. Coussens, R. A. Schoonheydt, B. F. Sels and E. I. Solomon, *J. Am. Chem. Soc.*, 2015, **137**, 6383–6392.
- 614 L. E. Vargas and R. Q. Snurr, *Langmuir*, 2015, **31**, 10056–10065.
- 615 F. Villemot, A. Galarneau and B. Coasne, *J. Phys. Chem. C*, 2014, **118**, 7423–7433.
- 616 A. Vjunov, M. A. Derewinski, J. L. Fulton, D. M. Camaioni and J. A. Lercher, *J. Am. Chem. Soc.*, 2015, **137**, 10374–10382.
- 617 N. Vogel, M. Retsch, C. A. Fustin, A. Del Campo and U. Jonas, *Chem. Rev.*, 2015, **115**, 6265–6311.
- 618 A. Walcarius, *Chem. Soc. Rev.*, 2013, **42**, 4098–4140.
- 619 Y. Wang, M. Chen, Y. Xie, P. Wei, H. F. Schaefer, 3rd and G. H. Robinson, *J. Am. Chem. Soc.*, 2015, **137**, 8396–8399.
- 620 J. S. Wei, H. Ding, Y. G. Wang and H. M. Xiong, *ACS Appl. Mater. Interfaces*, 2015, **7**, 5811–5819.
- 621 R. J. White, A. Fischer, C. Goebel and A. Thomas, *J. Am. Chem. Soc.*, 2014, **136**, 2715–2718.
- 622 T. Willhammar, A. W. Burton, Y. Yun, J. Sun, M. Afeworki, K. G. Strohmaier, H. Vroman and X. Zou, *J. Am. Chem. Soc.*, 2014, **136**, 13570–13573.
- 623 Q. Wu, X. Liu, L. Zhu, L. Ding, P. Gao, X. Wang, S. Pan, C. Bian, X. Meng, J. Xu, F. Deng, S. Maurer, U. Muller and F. S. Xiao, *J. Am. Chem. Soc.*, 2015, **137**, 1052–1055.
- 624 S. H. Wu, C. Y. Mou and H. P. Lin, *Chem. Soc. Rev.*, 2013, **42**, 3862–3875.
- 625 Q. Xie, Y. Ma, D. Zeng, X. Zhang, L. Wang, G. Yue and D. L. Peng, *ACS Appl. Mater. Interfaces*, 2014, **6**, 19895–19904.
- 626 D. Yang, S. O. Odoh, T. C. Wang, O. K. Farha, J. T. Hupp, C. J. Cramer, L. Gagliardi and B. C. Gates, *J. Am. Chem. Soc.*, 2015, **137**, 7391–7396.
- 627 M. Yang, J. Liu, S. Lee, B. Zugic, J. Huang, L. F. Allard and M. Flytzani-Stephanopoulos, *J. Am. Chem. Soc.*, 2015, **137**, 3470–3473.
- 628 H. B. Yao, H. Y. Fang, X. H. Wang and S. H. Yu, *Chem. Soc. Rev.*, 2011, **40**, 3764–3785.
- 629 Y. Yue, Z. A. Qiao, P. F. Fulvio, A. J. Binder, C. Tian, J. Chen, K. M. Nelson, X. Zhu and S. Dai, *J. Am. Chem. Soc.*, 2013, **135**, 9572–9575.
- 630 T. Zeng, R. Hoffmann, R. Nesper, N. W. Ashcroft, T. A. Strobel and D. M. Proserpio, *J. Am. Chem. Soc.*, 2015, 12639–12652, DOI: 10.1021/jacs.5b07883.
- 631 A. Zhang, Q. Zhang, H. Bai, L. Li and J. Li, *Chem. Soc. Rev.*, 2014, **43**, 6938–6953.
- 632 H. Zhang, Z. Hu, L. Huang, H. Zhang, K. Song, L. Wang, Z. Shi, J. Ma, Y. Zhuang, W. Shen, Y. Zhang, H. Xu and Y. Tang, *ACS Catal.*, 2015, **5**, 2548–2558.
- 633 L. Zhang, K. Chen, B. Chen, J. L. White and D. E. Resasco, *J. Am. Chem. Soc.*, 2015, **137**, 11810–11819.
- 634 S. Y. Zhang, W. Shi, P. Cheng and M. J. Zaworotko, *J. Am. Chem. Soc.*, 2015, **137**, 12203–12206.
- 635 C. Zhu, D. Du, A. Eychmuller and Y. Lin, *Chem. Rev.*, 2015, **115**, 8896–8943.
- 636 L. D. Rollmann, *US Pat.*, US4088605, 1993.
- 637 J. J. Zheng, Q. H. Zeng, J. H. Ma, X. W. Zhang, W. F. Sun and R. F. Li, *Chem. Lett.*, 2010, 330–331.
- 638 Y. Bouizi, L. Rouleau and V. P. Valtchev, *Chem. Mater.*, 2006, **18**, 4959–4966.
- 639 X. Wei and P. G. Smirniotis, *Microporous Mesoporous Mater.*, 2006, **89**, 170–178.
- 640 M. Y. Kustova, P. Hasselriis and C. H. Christensen, *Catal. Lett.*, 2004, **96**, 205–211.
- 641 H. Xin, J. Zhao, S. Xu, J. Li, W. Zhang, X. Guo, E. J. M. Hensen, Q. Yang and C. Li, *J. Phys. Chem. C*, 2010, **114**, 6553–6559.
- 642 A. Boisen, I. Schmidt, A. Carlsson, S. Dahl, M. Brorson and C. J. H. Jacobsen, *Chem. Commun.*, 2003, 958–959.
- 643 A. Janssen, I. Schmidt, C. Jacobsen, A. Koster and K. De Jong, *Microporous Mesoporous Mater.*, 2003, **65**, 59–75.
- 644 W. Fan, M. A. Snyder, S. Kumar, P. S. Lee, W. C. Yoo, A. V. McCormick, R. L. Penn, A. Stein and M. Tsapatsis, *Nat. Mater.*, 2008, **7**, 984–991.
- 645 Y. Tao, H. Kanoh and K. Kaneko, *J. Phys. Chem. B*, 2003, **107**, 10974–10976.
- 646 Y. Hanzawa, H. Hatori, N. Yoshizawa and Y. Yamada, *Carbon*, 2002, **40**, 575–581.
- 647 Z. Xie, *Porous Catalytic Materials With New Structure And Improved Performance*, China Petrochem. Press, Beijing, 2010, p. 4.
- 648 F. S. Xiao, *Acta Petrolei Sinica*, 2006, 9–12.
- 649 J. C. Groen, T. Bach, U. Ziese, A. Donk, K. P. de Jong, J. A. Moulijn and J. Perez-Ramirez, *J. Am. Chem. Soc.*, 2005, **127**, 10792–10793.
- 650 J. C. Groen, J. A. Moulijn and J. Pérez-Ramírez, *J. Mater. Chem.*, 2006, **16**, 2121–2131.
- 651 M. Ogura, S. Shinomiya, J. Tateno, Y. Nara, M. Nomura, E. Kikuchi and M. Matsukata, *Appl. Catal., A*, 2001, **219**, 33–43.
- 652 L. Su, L. Liu, J. Zhuang, H. Wang, Y. Li, W. Shen, Y. Xu and X. Bao, *Catal. Lett.*, 2003, **91**, 155–167.
- 653 M. Ogura, *Catal. Surv. Asia*, 2008, **12**, 16–27.
- 654 F.-S. Xiao, L. Wang, C. Yin, K. Lin, Y. Di, J. Li, R. Xu, D. S. Su, R. Schlögl, T. Yokoi and T. Tatsumi, *Angew. Chem., Int. Ed.*, 2006, **45**, 3090–3093.
- 655 J. Zhao, Z. Hua, Z. Liu, Y. Li, L. Guo, W. Bu, X. Cui, M. Ruan, H. Chen and J. Shi, *Chem. Commun.*, 2009, 7578–7580.
- 656 M. B. Yue, L. B. Sun, T. T. Zhuang, X. Dong, Y. Chun and J. H. Zhu, *J. Mater. Chem.*, 2008, **18**, 2044–2050.
- 657 F. N. Gu, F. Wei, J. Y. Yang, N. Lin, W. G. Lin, Y. Wang and J. H. Zhu, *Chem. Mater.*, 2010, **22**, 2442–2450.
- 658 J. Song, L. Ren, C. Yin, Y. Ji, Z. Wu, J. Li and F.-S. Xiao, *J. Phys. Chem. C*, 2008, **112**, 8609–8613.
- 659 M. Choi, H. S. Cho, R. Srivastava, C. Venkatesan, D.-H. Choi and R. Ryoo, *Nat. Mater.*, 2006, **5**, 718–723.
- 660 M. Choi, K. Na, J. Kim, Y. Sakamoto, O. Terasaki and R. Ryoo, *Nature*, 2009, **461**, 246–249.
- 661 L. Ren, Q. Guo, P. Kumar, M. Orazov, D. Xu, S. M. Alhassan, K. A. Mkhoyan, M. E. Davis and M. Tsapatsis, *Angew. Chem., Int. Ed.*, 2015, **54**, 10848–10851.
- 662 A. Corma, V. Fornes, S. B. Pergher, T. L. M. Maesen and J. G. Buglass, *Nature*, 1998, **396**, 353–356.
- 663 A. Corma, V. Fornés, J. Martínez-Triguero and S. B. Pergher, *J. Catal.*, 1999, **186**, 57–63.

- 664 J. Sun, C. Bonneau, A. Cantin, A. Corma, M. J. Diaz-Cabanas, M. Moliner, D. Zhang, M. Li and X. Zou, *Nature*, 2009, **458**, 1154–1157.
- 665 G. Wang, C. Huang, W. Xing and S. Zhuo, *Electrochim. Acta*, 2011, **56**, 5459–5463.
- 666 W. Xuan, C. Zhu, Y. Liu and Y. Cui, *Chem. Soc. Rev.*, 2012, **41**, 1677–1695.
- 667 X. Wang, W. Yang, Y. Tang, Y. Wang, S. Fu and Z. Gao, *Chem. Commun.*, 2000, 2161–2162.
- 668 N. Chu, J. Wang, Y. Zhang, J. Yang, J. Lu and D. Yin, *Chem. Mater.*, 2010, **22**, 2757–2763.
- 669 A. Dong, Y. Wang, Y. Tang, N. Ren, Y. Zhang and Z. Gao, *Chem. Mater.*, 2002, **14**, 3217–3219.
- 670 A. Dong, Y. Wang, D. Wang, W. Yang, Y. Zhang, N. Ren, Z. Gao and Y. Tang, *Microporous Mesoporous Mater.*, 2003, **64**, 69–81.
- 671 A. Dong, Y. Wang, Y. Tang, D. Wang, N. Ren, Y. Zhang and Z. Gao, *Chem. Lett.*, 2003, 790–791.
- 672 J. Shi, N. Ren, Y. H. Zhang and Y. Tang, *Microporous Mesoporous Mater.*, 2010, **132**, 181–187.
- 673 A. Dong, N. Ren, W. Yang, Y. Wang, Y. Zhang, D. Wang, J. Hu, Z. Gao and Y. Tang, *Adv. Funct. Mater.*, 2003, **13**, 943–948.
- 674 N. Ren, Y. H. Yang, Y. H. Zhang, Q. R. Wang and Y. Tang, *J. Catal.*, 2007, **246**, 215–222.
- 675 W. De, Ju, T. Yi, D. An Gang and Y. J. W. Ya Hong Zhang, *Chin. Chem. Lett.*, 2003, **14**, 1299–1302.
- 676 D. Wang, Y. Zhang, A. Dong, Y. Tang, Y. Wang, J. Xia and N. Ren, *Adv. Funct. Mater.*, 2003, **13**, 563–567.
- 677 D. J. Wang, Y. Tang, A. G. Dong and Y. H. Zhang, *Acta Chim. Sin.*, 2003, **61**, 1425–1429.
- 678 C. Xiong, D. Coutinho and K. J. Balkus Jr, *Microporous Mesoporous Mater.*, 2005, **86**, 14–22.
- 679 G. Zhu, Y. Zhang, W. Yang, B. Wu, Y. Tang and Z. Xie, *New J. Chem.*, 2005, **29**, 272–274.
- 680 C. Mei, Z. Liu, P. Wen, Z. Xie, W. Hua and Z. Gao, *J. Mater. Chem.*, 2008, **18**, 3496–3500.
- 681 Y. Wang, M. Lin and A. Tuel, *Microporous Mesoporous Mater.*, 2007, **102**, 80–85.
- 682 Y. Wang and A. Tuel, *Microporous Mesoporous Mater.*, 2008, **113**, 286–295.
- 683 W. Song, R. Kanthasamy, V. Grassian and S. Larsen, *Chem. Commun.*, 2004, 1920–1921.
- 684 V. Valtchev, B. J. Schoeman, J. Hedlund, S. Mintova and J. Sterte, *Zeolites*, 1996, **17**, 408–415.
- 685 Y. Wang, Y. Tang, X. Wang, W. Yang and Z. Gao, *Chem. Lett.*, 2000, 1344–1345.
- 686 Y. J. Wang, J. H. Hu, Y. Tang, W. L. Yang, C. Ke and X. D. Wang, *Acta Chim. Sin. (Chin. Ed.)*, 2001, **59**, 1084–1088.
- 687 C. Ke, W. Yang, Z. Ni, Y. Wang, Y. Tang, Y. Gu and Z. Gao, *Chem. Commun.*, 2001, 783–784.
- 688 L. Huang, Z. Wang, J. Sun, L. Miao, Q. Li, Y. Yan and D. Zhao, *J. Am. Chem. Soc.*, 2000, **122**, 3530–3531.
- 689 Y. J. Wang, Y. Tang, Z. Ni, W. M. Hua, W. L. Yang, X. D. Wang, W. C. Tao and Z. Gao, *Chem. Lett.*, 2000, 510–511.
- 690 Y. Zhou and M. Antonietti, *Chem. Commun.*, 2003, 2564–2565.
- 691 A. Dong, N. Ren, W. Yang, Y. Wang, Y. Zhang, D. Wang, J. Hu, Z. Gao and Y. Tang, *Adv. Funct. Mater.*, 2003, **13**, 943–948.
- 692 Z. Wang, M. A. Al-Daous, E. R. Kiesel, F. Li and A. Stein, *Microporous Mesoporous Mater.*, 2009, **120**, 351–358.
- 693 B. Zhang, S. A. Davis, N. H. Mendelson and S. Mann, *Chem. Commun.*, 2000, 781–782.
- 694 B. Zhang, S. A. Davis and S. Mann, *Chem. Mater.*, 2002, **14**, 1369–1375.
- 695 Y. W. Kho, D. S. Kalika and B. L. Knutson, *Polymer*, 2001, **42**, 6119–6127.
- 696 W. Liu, C. Zeng, L. Zhang, H. Wang and N. Xu, *Mater. Chem. Phys.*, 2007, **103**, 508–514.
- 697 K. K. Unger, *Porous silica, its properties and use as support in column liquid chromatography*, Elsevier, 1979.
- 698 L. Han, J. Yao, D. Li, J. Ho, X. Zhang, C. H. C. Kong, Z. M. Zong, X. Y. Wei and H. Wang, *J. Mater. Chem.*, 2008, **18**, 3337–3341.
- 699 S. Naik, A. Chiang, R. Thompson and F. Huang, *Chem. Mater.*, 2003, **15**, 787–792.
- 700 H. Wang, L. Huang, Z. Wang, A. Mitra and Y. Yan, *Chem. Commun.*, 2001, 1364–1365.
- 701 Y. Huang, D. Dong, J. Yao, L. He, J. Ho, C. Kong, A. J. Hill and H. Wang, *Chem. Mater.*, 2010, **22**, 5271–5278.
- 702 V. Sebastián, I. Díaz, C. Tellez, J. Coronas and J. Santamaría, *Adv. Funct. Mater.*, 2008, **18**, 1314–1320.
- 703 V. Sebastián, C. Tellez, J. Coronas and J. Santamaría, *Eur. J. Inorg. Chem.*, 2008, 2448–2453.
- 704 J. Hua and Y. Han, *Chem. Mater.*, 2009, **21**, 2344–2348.
- 705 P. Vasiliev, F. Akhtar, J. Grins, J. Mouzon, C. Andersson, J. Hedlund and L. Bergström, *ACS Appl. Mater. Interfaces*, 2010, **2**, 732–737.
- 706 Y. J. Lee, J. S. Lee, Y. S. Park and K. B. Yoon, *Adv. Mater.*, 2001, **13**, 1259–1263.
- 707 Y. J. Lee, Y. W. Kim, K. W. Jun, N. Viswanadham, J. W. Bae and H. S. Park, *Catal. Lett.*, 2009, **129**, 408–415.
- 708 K. Xia, Q. Gao, J. Jiang and J. Hu, *Carbon*, 2008, **46**, 1718–1726.
- 709 W. Xing, C. Huang, S. Zhuo, X. Yuan, G. Wang, D. Hulicova-Jurcakova, Z. Yan and G. Lu, *Carbon*, 2009, **47**, 1715–1722.
- 710 D. Wu, Y. Liang, X. Yang, Z. Li, C. Zou, X. Zeng, G. Lv and R. Fu, *Microporous Mesoporous Mater.*, 2008, **116**, 91–94.
- 711 W. Xing, S. P. Zhuo and X. Gao, *Mater. Lett.*, 2009, **63**, 1177–1179.
- 712 B. Fang, M. Kim, J. H. Kim and J. S. Yu, *Langmuir*, 2008, **24**, 12068–12072.
- 713 D. W. Wang, F. Li, M. Liu, G. Q. Lu and H. M. Cheng, *Angew. Chem.*, 2008, **120**, 379–382.
- 714 Y. Xia, Z. Yang and R. Mokaya, *Nanoscale*, 2010, **2**, 639–659.
- 715 Z. Yang, Y. Xia and R. Mokaya, *Microporous Mesoporous Mater.*, 2005, **86**, 69–80.
- 716 L. Wang, J. Zhang, D. S. Su, Y. Ji, X. Cao and F. S. Xiao, *Chem. Mater.*, 2007, **19**, 2894–2897.
- 717 C. Zou, D. Wu, M. Li, Q. Zeng, F. Xu, Z. Huang and R. Fu, *J. Mater. Chem.*, 2010, **20**, 731–735.

- 718 R. Ostermann, J. Cravillon, C. Weidmann, M. Wiebcke and B. M. Smarsly, *Chem. Commun.*, 2011, **47**, 442–444.
- 719 X.-Y. Yang, G. Tian, L.-H. Chen, Y. Li, J. C. Rooke, Y.-X. Wei, Z.-M. Liu, Z. Deng, G. Van Tendeloo and B.-L. Su, *Chem. – Eur. J.*, 2011, **17**, 14987–14995.
- 720 L. H. Chen, X. Y. Li, G. Tian, Y. Li, H. Y. Tan, G. Van Tendeloo, G. S. Zhu, S. L. Qiu, X. Y. Yang and B. L. Su, *ChemSusChem*, 2011, **4**, 1452–1456.
- 721 L.-H. Chen, S.-T. Xu, X.-Y. Li, G. Tian, Y. Li, J. C. Rooke, G.-S. Zhu, S.-L. Qiu, Y.-X. Wei and X.-Y. Yang, *J. Colloid Interface Sci.*, 2012, **377**, 368–374.
- 722 L.-H. Chen, X.-Y. Li, G. Tian, Y. Li, J. C. Rooke, G.-S. Zhu, S.-L. Qiu, X.-Y. Yang and B.-L. Su, *Angew. Chem., Int. Ed.*, 2011, **50**, 11156–11161.
- 723 L.-H. Chen, X.-Y. Li, G. Tian, Y. Li, H.-Y. Tan, G. Van Tendeloo, G.-S. Zhu, S.-L. Qiu, X.-Y. Yang and B.-L. Su, *ChemSusChem*, 2011, **4**, 1452–1456.
- 724 H. Zhou, P. Li, J. Liu, Z. Chen, L. Liu, D. Dontsova, R. Yan, T. Fan, D. Zhang and J. Ye, *Nano Energy*, 2016, **25**, 128–135.
- 725 L. Hu, H. Zhou, H. Zhu, T. Fan and D. Zhang, *Energy Convers. Manage.*, 2015, **89**, 775–780.
- 726 D. Yang, T. Fan, D. Zhang, J. Zhu, Y. Wang, B. Du and Y. Yan, *Chem. – Eur. J.*, 2013, **19**, 4742–4747.
- 727 H. Zhou, T. Fan and D. Zhang, *ChemCatChem*, 2011, **3**, 513–528.
- 728 H. Zhou, T. Fan, X. Li, D. Zhang, Q. Guo and H. Ogawa, *J. Mater. Chem.*, 2009, **19**, 2695–2703.
- 729 X. Li, T. Fan, H. Zhou, S.-K. Chow, W. Zhang, D. Zhang, Q. Guo and H. Ogawa, *Adv. Funct. Mater.*, 2009, **19**, 45–56.
- 730 S. Chow, T. Fan, J. Ding and D. Zhang, *J. Am. Ceram. Soc.*, 2010, **93**, 40–43.
- 731 D. Yang, T. Fan, H. Zhou, J. Ding and D. Zhang, *PLoS One*, 2011, **6**, e24788.
- 732 H. Zhou, J. Pan, L. Ding, Y. Tang, J. Ding, Q. Guo, T. Fan and D. Zhang, *Int. J. Hydrogen Energy*, 2014, **39**, 16293–16301.
- 733 J. Jiang, H. Zhou, J. Ding, F. Zhang, T. Fan and D. Zhang, *Appl. Surf. Sci.*, 2015, **347**, 368–377.
- 734 D. Zhang, W. Zhang, J. Gu, T. Fan, Q. Liu, H. Su and S. Zhu, *Prog. Mater. Sci.*, 2015, **68**, 67–96.
- 735 X. Guo, T. Zhang, J. Li and T. Fan, *RSC Adv.*, 2014, **4**, 59508–59512.
- 736 W. Zhang, J. Gu, Q. Liu, H. Su, T. Fan and D. Zhang, *Phys. Chem. Chem. Phys.*, 2014, **16**, 19767–19780.
- 737 X. Guo, H. Zhou, D. Zhang and T. Fan, *RSC Adv.*, 2014, **4**, 3748–3752.
- 738 L. Ding, H. Zhou, S. Lou, J. Ding, D. Zhang, H. Zhu and T. Fan, *Int. J. Hydrogen Energy*, 2013, **38**, 8244–8253.
- 739 S. Lou, X. Guo, T. Fan and D. Zhang, *Energy Environ. Sci.*, 2012, **5**, 9195–9216.
- 740 H. Liu, Q. Zhao, H. Zhou, J. Ding, D. Zhang, H. Zhu and T. Fan, *Phys. Chem. Chem. Phys.*, 2011, **13**, 10872–10876.
- 741 M. Iwasaki, S. A. Davis and S. Mann, *J. Sol-Gel Sci. Technol.*, 2004, **32**, 99–105.
- 742 C. Wang, A. Geng, Y. Guo, S. Jiang, X. Qu and L. Li, *J. Colloid Interface Sci.*, 2006, **301**, 236–247.
- 743 J. Ortiz-Landeros, M. E. Contreras-Garcia and H. Pfeiffer, *J. Porous Mater.*, 2009, **16**, 473–479.
- 744 M. Lomoschitz, H. Peterlik, G. Friedbacher and U. Schubert, *J. Mater. Chem.*, 2009, **19**, 75–81.
- 745 M. Fujishima, Y. Okawa and K. Uchida, *J. Am. Ceram. Soc.*, 2008, **91**, 3749–3752.
- 746 R. Rios, M. Martinez-Escandell, M. Molina-Sabio and F. Rodriguez-Reinoso, *Carbon*, 2006, **44**, 1448–1454.
- 747 E. a. Iniesta, F. Sánchez, A. N. García and A. Marcilla, *J. Anal. Appl. Pyrolysis*, 2001, **58–59**, 967–981.
- 748 F. Kurosaki, K. Ishimaru, T. Hata, P. Bronsveld, E. Kobayashi and Y. Imamura, *Carbon*, 2003, **41**, 3057–3062.
- 749 F. Kurosaki, H. Koyanaka, M. Tsujimoto and Y. Imamura, *Carbon*, 2008, **46**, 850–857.
- 750 E. R. Buiel, A. E. George and J. R. Dahn, *Carbon*, 1999, **37**, 1399–1407.
- 751 S. A. Al-Muhtaseb and J. A. Ritter, *Adv. Mater.*, 2003, **15**, 101–114.
- 752 Z. Lei, Y. Zhang, H. Wang, Y. Ke, J. Li, F. Li and J. Xing, *J. Mater. Chem.*, 2001, **11**, 1975–1977.
- 753 K. T. Lee, J. C. Lytle, N. S. Ergang, S. M. Oh and A. Stein, *Adv. Funct. Mater.*, 2005, **15**, 547–556.
- 754 C.-Z. Lai, M. A. Fierke, A. Stein and P. Bühlmann, *Anal. Chem.*, 2007, **79**, 4621–4626.
- 755 M. A. Fierke, C.-Z. Lai, P. Bühlmann and A. Stein, *Anal. Chem.*, 2010, **82**, 680–688.
- 756 A. Stein, Z. Wang and M. A. Fierke, *Adv. Mater.*, 2009, **21**, 265–293.
- 757 S. Tabata, Y. Isshiki and M. Watanabe, *J. Electrochem. Soc.*, 2008, **155**, K42–K49.
- 758 K. Kanamori, K. Nakanishi and T. Hanada, *Adv. Mater.*, 2006, **18**, 2407–2411.
- 759 K. Kanamori, J. Hasegawa, K. Nakanishi and T. Hanada, *Macromolecules*, 2008, **41**, 7186–7193.
- 760 J. Hasegawa, K. Kanamori, K. Nakanishi, T. Hanada and S. Yamago, *Macromolecules*, 2009, **42**, 1270–1277.
- 761 J. Hasegawa, K. Kanamori, K. Nakanishi, T. Hanada and S. Yamago, *Macromol. Rapid Commun.*, 2009, **30**, 986–990.
- 762 K. I. K. Suzuki and H. Imai, *J. Am. Chem. Soc.*, 2004, **126**, 462.
- 763 S. P. B. Smarsly and M. Antonietti, *J. Phys. Chem. B*, 2001, **105**, 10453.
- 764 R. Weberskirch and O. Nuyken, *J. Macromol. Sci., Part A: Pure Appl. Chem.*, 1999, **36**, 843–857.
- 765 K. Stähler, J. Selb and F. Candau, *Langmuir*, 1999, **15**, 7565–7576.
- 766 P. Barthélémy, V. Tomao, J. Selb, Y. Chaudier and B. Pucci, *Langmuir*, 2002, **18**, 2557–2563.
- 767 M. Groenewolt, M. Antonietti and S. Polarz, *Langmuir*, 2004, **20**, 7811–7819.
- 768 S. Areva, C. Boissiere, D. Grosso, T. Asakawa, C. Sanchez and M. Linden, *Chem. Commun.*, 2004, 1630–1631.
- 769 J.-H. Sun, Z. Shan, T. Maschmeyer and M.-O. Coppens, *Langmuir*, 2003, **19**, 8395–8402.
- 770 S. A. Bagshaw, *J. Mater. Chem.*, 2001, **11**, 831–840.
- 771 Z. Y. Yuan, J. L. Blin and B. L. Su, *Chem. Commun.*, 2002, 504–505.

- 772 C. Tolksdorf and R. Zentel, *Adv. Mater.*, 2001, **13**, 1307–1310.
- 773 K. Morisato, S. Miyazaki, M. Ohira, M. Furuno, M. Nyudo, H. Terashima and K. Nakanishi, *J. Chromatogr. A*, 2009, **1216**, 7384–7387.
- 774 M. Kuang, D. Wang, H. Bao, M. Gao, H. Möhwald and M. Jiang, *Adv. Mater.*, 2005, **17**, 267–270.
- 775 B. Lebeau, C. E. Fowler, S. Mann, C. Farcet, B. Charleux and C. Sanchez, *J. Mater. Chem.*, 2000, **10**, 2105–2108.
- 776 T. Sen, G. J. T. Tiddy, J. L. Casci and M. W. Anderson, *Angew. Chem., Int. Ed.*, 2003, **42**, 4649–4653.
- 777 S. Vaudreuil, M. Bousmina, S. Kaliaguine and L. Bonneviot, *Adv. Mater.*, 2001, **13**, 1310–1312.
- 778 C. Danumah, S. Vaudreuil, L. Bonneviot, M. Bousmina, S. Giasson and S. Kaliaguine, *Microporous Mesoporous Mater.*, 2001, **44–45**, 241–247.
- 779 C.-G. Oh, Y. Baek and S.-K. Ihm, *Adv. Mater.*, 2005, **17**, 270–273.
- 780 J. S. Yun, M.-Y. Seong and S.-K. Ihm, *J. Phys. Chem. Solids*, 2007, **69**, 1129–1132.
- 781 A. Yachi, R. Takahashi, S. Sato, T. Sodesawa, K. Oguma, K. Matsutani and N. Mikami, *J. Non-Cryst. Solids*, 2005, **351**, 331–339.
- 782 K. Nakanishi, R. Takahashi, T. Nagakane, K. Kitayama, N. Koheiya, H. Shikata and N. Soga, *J. Sol-Gel Sci. Technol.*, 2000, **17**, 191–210.
- 783 A. Shimojima, Z. Liu, T. Ohsuna, O. Terasaki and K. Kuroda, *J. Am. Chem. Soc.*, 2005, **127**, 14108–14116.
- 784 M. Sakurai, A. Shimojima, M. Heishi and K. Kuroda, *Langmuir*, 2007, **23**, 10788–10792.
- 785 K. Nakanishi, Y. Sato, Y. Ruyat and K. Hirao, *J. Sol-Gel Sci. Technol.*, 2003, **26**, 567–570.
- 786 K. Nakanishi, T. Yamato and K. Hirao, *Mater. Res. Soc. Symp. Proc.*, 2002, **726**, Q9–7.
- 787 Y. Sato, K. Nakanishi, K. Hirao, H. Jinnai, M. Shibayama, Y. B. Melnichenko and G. D. Wignall, *Colloids Surf., A*, 2001, **187**, 117–122.
- 788 Y. Kobayashi, K. Nakanishi and K. Hirao, *MRS Online Proc. Libr.*, 2003, **788**, DOI: 10.1557/PROC-1788-LL1553.1510.
- 789 M. D'Arienzo, L. Armelao, A. Cacciamani, C. M. Mari, S. Polizzi, R. Ruffo, R. Scotti, A. Testino, L. Wahba and F. Morazzoni, *Chem. Mater.*, 2010, 4083–4089.
- 790 J. P. Bosco, K. Sasaki, M. Sadakane, W. Ueda and J. G. Chen, *Chem. Mater.*, 2009, **22**, 966–973.
- 791 X. H. Xia, J. P. Tu, J. Zhang, X. H. Huang, X. L. Wang and X. B. Zhao, *Electrochim. Acta*, 2010, **55**, 989–994.
- 792 S. Komarneni, *J. Mater. Chem.*, 1992, **2**, 1219–1230.
- 793 S. H. Hakim and B. H. Shanks, *Microporous Mesoporous Mater.*, 2010, **135**, 105–115.
- 794 O. D. Velev, P. M. Tessier, A. M. Lenhoff and E. W. Kaler, *Nature*, 1999, **401**, 548.
- 795 J. Wang, S. Ahl, Q. Li, M. Kreiter, T. Neumann, K. Burkert, W. Knoll and U. Jonas, *J. Mater. Chem.*, 2008, **18**, 981–988.
- 796 A. B. D. Nandiyanto, N. Hagura, F. Iskandar and K. Okuyama, *Acta Mater.*, 2010, **58**, 282–289.
- 797 A. Cabañas, E. Enciso, M. C. Carbajo, M. J. Torralvo, C. Pando and J. A. R. Renuncio, *Chem. Mater.*, 2005, **17**, 6137–6145.
- 798 A. Cabañas, E. Enciso, M. Carmen Carbajo, M. J. Torralvo, C. Pando and J. A. R. Renuncio, *Microporous Mesoporous Mater.*, 2007, **99**, 23–29.
- 799 B. T. Holland, C. F. Blanford, T. Do and A. Stein, *Chem. Mater.*, 1999, **11**, 795–805.
- 800 A. Léonard, J. L. Blin and B. L. Su, *Chem. Commun.*, 2003, 2568–2569.
- 801 A. Léonard and B. L. Su, *Chem. Commun.*, 2004, 1674–1675.
- 802 Q. Luo, L. Li, B. Yang and D. Zhao, *Chem. Lett.*, 2000, 378–379.
- 803 J. Yin and Z. L. Wang, *Appl. Phys. Lett.*, 1999, **74**, 2629.
- 804 L. A. Villaescusa, A. Mihi, I. Rodríguez, A. E. García-Bennett and H. Míguez, *J. Phys. Chem. B*, 2005, **109**, 19643–19649.
- 805 T. Sen, G. J. T. Tiddy, J. L. Casci and M. W. Anderson, *Chem. Mater.*, 2004, **16**, 2044–2054.
- 806 A. R. Loiola, L. R. D. da Silva, P. Cubillas and M. W. Anderson, *J. Mater. Chem.*, 2008, **18**, 4985–4993.
- 807 S. H. Kim, C. K. Shin, C. H. Ahn and G. J. Kim, *J. Porous Mater.*, 2006, **13**, 201–205.
- 808 M. Antonietti, *Silica nanocasting of lyotropic surfactant phases and organized organic matter: material science or an analytical tool?*, 2006.
- 809 G. Kaune, M. Memesa, R. Meier, M. A. Ruderer, A. Diethert, S. V. Roth, M. D'Acunzi, J. S. Gutmann and P. Müller-Buschbaum, *ACS Appl. Mater. Interfaces*, 2009, **1**, 2862–2869.
- 810 G. Guan, R. Zapf, G. Kolb, Y. Men, V. Hessel, H. Loewe, J. Ye and R. Zentel, *Chem. Commun.*, 2007, 260–262.
- 811 J. P. Dacquin, J. Dhainaut, D. Duprez, S. Royer, A. F. Lee and K. Wilson, *J. Am. Chem. Soc.*, 2009, **131**, 12896–12897.
- 812 N. Suzuki and Y. Yamauchi, *J. Sol-Gel Sci. Technol.*, 2010, **53**, 428–433.
- 813 Y. Kim, C. Kim and J. Yi, *Mater. Res. Bull.*, 2004, **39**, 2103–2112.
- 814 H. Li, L. Zhang, H. Dai and H. He, *Inorg. Chem.*, 2009, **48**, 4421–4434.
- 815 S. W. Bian, Y. L. Zhang, H. L. Li, Y. Yu, Y. L. Song and W. G. Song, *Microporous Mesoporous Mater.*, 2010, **131**, 289–293.
- 816 G. Hasegawa, K. Kanamori, K. Nakanishi and T. Hanada, *J. Sol-Gel Sci. Technol.*, 2010, **53**, 59–66.
- 817 T. Hirao, K. Fujita, S. Murai, K. Nakanishi and K. Hirao, *J. Non-Cryst. Solids*, 2006, **352**, 2553–2557.
- 818 Y. Yamauchi and K. Kuroda, *Electrochem. Commun.*, 2006, **8**, 1677–1682.
- 819 Z. Wang, E. R. Kiesel and A. Stein, *J. Mater. Chem.*, 2008, **18**, 2194–2200.
- 820 Y. Deng, C. Liu, T. Yu, F. Liu, F. Zhang, Y. Wan, L. Zhang, C. Wang, B. Tu, P. A. Webley, H. Wang and D. Zhao, *Chem. Mater.*, 2007, **19**, 3271–3277.
- 821 Z. Wang and A. Stein, *Chem. Mater.*, 2007, **20**, 1029–1040.
- 822 R. Liu, Y. Shi, Y. Wan, Y. Meng, F. Zhang, D. Gu, Z. Chen, B. Tu and D. Zhao, *J. Am. Chem. Soc.*, 2006, **128**, 11652–11662.
- 823 R. Liu, Y. Ren, Y. Shi, F. Zhang, L. Zhang, B. Tu and D. Zhao, *Chem. Mater.*, 2007, **20**, 1140–1146.
- 824 Y. Wan, H. Wang, Q. Zhao, M. Klingstedt, O. Terasaki and D. Zhao, *J. Am. Chem. Soc.*, 2009, **131**, 4541–4550.

- 825 Y. Shi, F. Zhang, Y.-S. Hu, X. Sun, Y. Zhang, H. I. Lee, L. Chen and G. D. Stucky, *J. Am. Chem. Soc.*, 2010, **132**, 5552–5553.
- 826 B. Alberts, A. Johnson, J. Lewis, M. Raff, K. Roberts and P. Walter, *Molecular biology of the cell*, Garland Science, New York, 2002.
- 827 X. Sun, C. Zheng, M. Qiao, J. Yan, X. Wang and N. Guan, *Chem. Commun.*, 2009, 4750–4752.
- 828 N. H. Mendelson, *Proc. Natl. Acad. Sci. U. S. A.*, 1978, **75**, 2478.
- 829 C. T. Kresge, M. E. Leonowicz, W. J. Roth, J. C. Vartuli and J. S. Beck, *Nature*, 1992, **359**, 710–712.
- 830 Y. Zhao, M. Wei, J. Lu, Z. L. Wang and X. Duan, *ACS Nano*, 2009, **3**, 4009–4016.
- 831 M. Hincke, J. Gautron, M. Panheleux, J. Garcia-Ruiz, M. McKee and Y. Nys, *Matrix Biol.*, 2000, **19**, 443–453.
- 832 Q. Dong, H. Su, C. Zhang, D. Zhang, Q. Guo and F. Kiessling, *Chem. Eng. J.*, 2008, **137**, 428–435.
- 833 Q. Dong, H. Su, W. Cao, D. Zhang, Q. Guo and Y. Lai, *J. Solid State Chem.*, 2007, **180**, 949–955.
- 834 H. A. Lowenstam and S. Weiner, *On biomineralization*, Oxford University Press, USA, 1989.
- 835 J. Aizenberg, J. C. Weaver, M. S. Thanawala, V. C. Sundar, D. E. Morse and P. Fratzl, *Science*, 2005, **309**, 275.
- 836 Q. Dong, H. Su, F. Song, D. Zhang and N. Wang, *J. Am. Ceram. Soc.*, 2007, **90**, 376–380.
- 837 Q. Dong, H. Su, D. Zhang, N. Zhu and X. Guo, *Scr. Mat.*, 2006, **55**, 799–802.
- 838 D. Yang, L. Qi and J. Ma, *Adv. Mater.*, 2002, **14**, 1543–1546.
- 839 T. Yui, K. Imada, K. Okuyama, Y. Obata, K. Suzuki and K. Ogawa, *Macromolecules*, 1994, **27**, 7601–7605.
- 840 V. Pedroni, P. Schulz, M. Gschaider de Ferreira and M. Morini, *Colloid Polym. Sci.*, 2000, **278**, 964–971.
- 841 M. Iwasaki, S. Davis and S. Mann, *J. Sol-Gel Sci. Technol.*, 2004, **32**(1), 99–105.
- 842 D. Fengel, G. Wegener and A. Greune, *Wood Sci. Technol.*, 1989, **23**, 123–130.
- 843 J. Fahlén and L. Salmén, *Biomacromolecules*, 2005, **6**, 433–438.
- 844 Y. Shin, J. Liu, J. H. Chang, Z. Nie and G. J. Exarhos, *Adv. Mater.*, 2001, **13**, 728–732.
- 845 A. S. Deshpande, I. Burgert and O. Paris, *Small*, 2006, **2**, 994–998.
- 846 A. S. Deshpande, N. Pinna, P. Beato, M. Antonietti and M. Niederberger, *Chem. Mater.*, 2004, **16**, 2599–2604.
- 847 U. Meyer, A. Larsson, H. P. Hentze and R. A. Caruso, *Adv. Mater.*, 2002, **14**, 1768–1772.
- 848 A. S. Deshpande, D. G. Shchukin, E. Ustinovich, M. Antonietti and R. A. Caruso, *Adv. Funct. Mater.*, 2005, **15**, 239–245.
- 849 M. L. Wang, C. H. Wang and W. Wang, *J. Mater. Chem.*, 2007, **17**, 2133–2138.
- 850 H. Zhang and A. I. Cooper, *Ind. Eng. Chem. Res.*, 2005, **44**, 8707–8714.
- 851 H. Zhang, I. Hussain, M. Brust and A. I. Cooper, *Chem. Commun.*, 2006, 2539–2541.
- 852 G. D. Sizgek, C. S. Griffith, E. Sizgek and V. Luca, *Langmuir*, 2009, **25**, 11874–11882.
- 853 A. Shigapov, G. Graham, R. McCabe and H. Plummer Jr, *Appl. Catal., A*, 2001, **210**, 287–300.
- 854 J. Huang and T. Kunitake, *J. Am. Chem. Soc.*, 2003, **125**, 11834–11835.
- 855 Y. Gu and J. Huang, *J. Mater. Chem.*, 2009, **19**, 3764–3770.
- 856 R. A. Caruso, J. H. Schattka and A. Greiner, *Adv. Mater.*, 2001, **13**, 1577–1579.
- 857 G. M. Kim, S. M. Lee, G. H. Michler, H. Roggendorf, U. Gosele and M. Knez, *Chem. Mater.*, 2008, **20**, 3085–3091.
- 858 R. A. Caruso and J. H. Schattka, *Adv. Mater.*, 2000, **12**, 1921–1923.
- 859 R. A. Caruso and M. Antonietti, *Adv. Funct. Mater.*, 2002, **12**, 307–312.
- 860 J. H. Schattka, E. H. M. Wong, M. Antonietti and R. A. Caruso, *J. Mater. Chem.*, 2006, **16**, 1414–1420.
- 861 G. L. Drisko, L. Cao, M. C. Kimling, S. Harrisson, V. Luca and R. A. Caruso, *ACS Appl. Mater. Interfaces*, 2009, **1**, 2893–2901.
- 862 D. G. Shchukin and R. A. Caruso, *Adv. Funct. Mater.*, 2003, **13**, 789–794.
- 863 C. P. Fonseca, M. C. A. Fantini and S. Neves, *Thin Solid Films*, 2005, **488**, 68–73.
- 864 C. P. Fonseca, R. M. Paula, E. M. J. A. Pallone and S. Neves, *Electrochim. Acta*, 2006, **51**, 6419–6425.
- 865 L. Huerta, C. Guillem, J. Latorre, A. Beltran, D. Beltran and P. Amoros, *Chem. Commun.*, 2003, 1448–1449.
- 866 L. Huerta, C. Guillem, J. Latorre, A. Beltran, D. Beltran and P. Amoros, *Solid State Sci.*, 2005, **7**, 405–414.
- 867 C. F. Xue, B. Tu and D. Y. Zhao, *Adv. Funct. Mater.*, 2008, **18**, 3914–3921.
- 868 C. F. Xue, J. X. Wang, B. Tu and D. Y. Zhao, *Chem. Mater.*, 2010, **22**, 494–503.
- 869 C. F. Xue, B. Tu and D. Y. Zhao, *Nano Res.*, 2009, **2**, 242–253.
- 870 L. Y. Xu, Z. G. Shi and Y. Q. Feng, *Microporous Mesoporous Mater.*, 2007, **98**, 303–308.
- 871 P. Blood, I. Brown and S. Sotiropoulos, *J. Appl. Electrochem.*, 2004, **34**, 1–7.
- 872 I. Brown, D. Clift and S. Sotiropoulos, *Mater. Res. Bull.*, 1999, **34**, 1055–1064.
- 873 S. Sotiropoulos, I. Brown, G. Akay and E. Lester, *Mater. Lett.*, 1998, **35**, 383–391.
- 874 M. S. Ahmed, Y. Lee, C. Park and N. Atalla, *Asia-Pac. J. Chem. Eng.*, 2009, **4**, 120–124.
- 875 M. C. Hermant, M. Verhulst, A. V. Kyrlyuk, B. Klumperman and C. E. Koning, *Compos. Sci. Technol.*, 2009, **69**, 656–662.
- 876 A. Menner, M. Salgueiro, M. S. P. Shaffer and A. Bismarck, *J. Polym. Sci., Part A: Polym. Chem.*, 2008, **46**, 5708–5714.
- 877 J. Normatov and M. S. Silverstein, *Polymer*, 2007, **48**, 6648–6655.
- 878 P. Pakeyangkoon, R. Magaraphan, P. Malakul and M. Nithitanakul, *Adv. Sci. Technol.*, 2009, **54**, 293–298.
- 879 Y. Zhang, H. Liang, C. Y. Zhao and Y. Liu, *Asian J. Mater. Sci.*, 2009, **44**, 931–938.
- 880 H. Tai, K. J. Shea and M. S. Silverstein, *PMSE Prepr.*, 2002, **86**, 235–237.

- 881 Y. Tokudome, K. Fujita, K. Nakanishi, K. Kanamori, K. Miura, K. Hirao and T. Hanada, *J. Ceram. Soc. Jpn.*, 2007, **115**, 925–928.
- 882 Y. Tokudome, K. Fujita, K. Nakanishi, K. Miura and K. Hirao, *Chem. Mater.*, 2007, **19**, 3393–3398.
- 883 K. Fujita, J. Konishi, K. Nakanishi and K. Hirao, *Appl. Phys. Lett.*, 2004, **85**, 5595.
- 884 P. Renaud and M. P. Sibi, *Radicals in Organic Synthesis*, Wiley, New York, 2001.
- 885 T. Z. Ren, Z. Y. Yuan and B. L. Su, *Chem. Phys. Lett.*, 2004, **388**, 46–49.
- 886 J. B. Miller and E. I. Ko, *Catal. Today*, 1997, **35**, 269–292.
- 887 J. Moore, *J. Polym. Sci., Part A: Gen. Pap.*, 1964, **2**, 835–843.
- 888 K. Nakanishi, *Hierarchically Struct. Porous Mater.*, 2012, 241–267.
- 889 G. Hasegawa, K. Kanamori, K. Nakanishi and T. Hanada, *Carbon*, 2010, **48**, 1757–1766.
- 890 F. Svec and J. M. J. Frechet, *Anal. Chem.*, 1992, **64**, 820–822.
- 891 M. Vallet-Regí and M. Manzano, *Hierarchically Structured Porous Materials*, Wiley-VCH Verlag & Co. KGaA, Germany, Weinheim, 2012, pp. 601–620.
- 892 K. Nakanishi, *Hierarchically Structured Porous Materials*, Wiley-VCH Verlag & Co. KGaA, Germany, Weinheim, 2012, pp. 517–529.
- 893 A. Menner, R. Verdejo, M. Shaffer and A. Bismarck, *Langmuir*, 2007, **23**, 2398–2403.
- 894 M. C. Hermant, B. Klumperman and C. E. Koning, *Chem. Commun.*, 2009, 2738–2740.
- 895 V. O. Ikem, A. Menner and A. Bismarck, *Langmuir*, 2010, **26**, 8836–8841.
- 896 V. O. Ikem, A. Menner and A. Bismarck, *Angew. Chem., Int. Ed.*, 2008, **47**, 8277–8279.
- 897 P. J. Colver and S. A. F. Bon, *Chem. Mater.*, 2007, **19**, 1537–1539.
- 898 Z. Li and T. Ngai, *Langmuir*, 2010, **26**, 16186.
- 899 M. Panda, M. Rajamathi and R. Seshadri, *Chem. Mater.*, 2002, **14**, 4762–4767.
- 900 E. S. Toberer, T. D. Schladt and R. Seshadri, *J. Am. Chem. Soc.*, 2006, **128**, 1462–1463.
- 901 E. S. Toberer, J. P. Löfvander and R. Seshadri, *Chem. Mater.*, 2006, **18**, 1047–1052.
- 902 G. Donnay and D. L. Pawson, *Science*, 1969, **166**, 1147–1150.
- 903 R. J. Park and F. C. Meldrum, *J. Mater. Chem.*, 2004, **14**, 2291–2296.
- 904 J. Aizenberg, D. A. Muller, J. L. Grazul and D. R. Hamann, *Science*, 2003, **299**, 1205–1208.
- 905 V. V. Doan and M. J. Sailor, *Science*, 1992, **256**, 1791–1792.
- 906 H. Kaji, K. Nakanishi and N. Soga, *J. Sol-Gel Sci. Technol.*, 1993, **1**, 35–46.
- 907 K. Kajihara, M. Hirano and H. Hosono, *Chem. Commun.*, 2009, 2580–2582.
- 908 R. Takahashi, S. Sato, T. Sodesawa and T. Azuma, *J. Sol-Gel Sci. Technol.*, 2004, **31**, 373–376.
- 909 J. Livage and M. Henry, ed. J. D. Mackenzie and D. R. Ulrich, *Ultrastructure processing of advanced ceramics*, John Wiley & Sons, New York, 1988, p. 183.
- 910 J. Konishi, K. Fujita, K. Nakanishi and K. Hirao, *Chem. Mater.*, 2006, **18**, 864–866.
- 911 M. Numata, R. Takahashi, I. Yamada, K. Nakanishi and S. Sato, *Appl. Catal., A*, 2010, **383**, 66–72.
- 912 S. Murai, K. Fujita, J. Konishi, K. Hirao and K. Tanaka, *Appl. Phys. Lett.*, 2010, **97**, 031118.
- 913 K. Fujita, S. Murai, K. Nakanishi and K. Hirao, *J. Non-Cryst. Solids*, 2006, **352**, 2496–2500.
- 914 Y. Tokudome, A. Miyasaka, K. Nakanishi and T. Hanada, *J. Sol-Gel Sci. Technol.*, 2011, **57**, 269–278.
- 915 S. A. Bagshaw, *Chem. Commun.*, 1999, 767–768.
- 916 F. Carn, A. Colin, M. F. Achard, H. Deleuze, Z. Saadi and R. Backov, *Adv. Mater.*, 2004, **16**, 140–144.
- 917 F. Carn, A. Colin, M. F. Achard, H. Deleuze, C. Sanchez and R. Backov, *Adv. Mater.*, 2005, **17**, 62–66.
- 918 K. Suzuki, K. Ikari and H. Imai, *J. Mater. Chem.*, 2003, **13**, 1812–1816.
- 919 S. R. Hall, D. Walsh, D. Green, R. Oreffo and S. Mann, *J. Mater. Chem.*, 2003, **13**, 186–190.
- 920 R. Del Real, J. Wolke and J. Jansen, *Biomaterials*, 2002, **23**, 3673–3680.
- 921 D. Zhao, P. Yang, B. F. Chmelka and G. D. Stucky, *Chem. Mater.*, 1999, **11**, 1174–1178.
- 922 J. S. Yu, S. B. Yoon, Y. J. Lee and K. B. Yoon, *J. Phys. Chem. B*, 2005, **109**, 7040–7045.
- 923 Y. Liu, W. Zhang and T. J. Pinnavaia, *J. Am. Chem. Soc.*, 2000, **122**, 8791–8792.
- 924 Y. Liu, W. Zhang and T. J. Pinnavaia, *Angew. Chem., Int. Ed.*, 2001, **40**, 1255–1258.
- 925 Y. Liu and T. J. Pinnavaia, *Chem. Mater.*, 2002, **14**, 3–5.
- 926 Z. T. Zhang, Y. Han, L. Zhu, R. W. Wang, Y. Yu, S. L. Qiu, D. Y. Zhao and F. S. Xiao, *Angew. Chem., Int. Ed.*, 2001, **40**, 1258–1262.
- 927 F. S. Xiao, Y. Han, Y. Yu, X. Meng, M. Yang and S. Wu, *J. Am. Chem. Soc.*, 2002, **124**, 888–889.
- 928 Y. Han, S. Wu, Y. Sun, D. Li, F. S. Xiao, J. Liu and X. Zhang, *Chem. Mater.*, 2002, **14**, 1144–1148.
- 929 D. T. On and S. Kaliaguine, *Angew. Chem., Int. Ed.*, 2001, **40**, 3248–3351.
- 930 D. Trong On, D. Lutic and S. Kaliaguine, *Microporous Mesoporous Mater.*, 2001, **44**, 435–444.
- 931 D. Trong On and S. Kaliaguine, *Angew. Chem., Int. Ed.*, 2002, **41**, 1036–1040.
- 932 D. Trong On and S. Kaliaguine, *J. Am. Chem. Soc.*, 2003, **125**, 618–619.
- 933 Y. Liu and M. Liu, *Adv. Eng. Mater.*, 2006, **8**, 89–93.
- 934 A. Lemaire, Q.-Y. Wang, Y. Wei, Z. Liu and B.-L. Su, *J. Colloid Interface Sci.*, 2011, **363**, 511–520.
- 935 J. Wang, Q. Li, W. Knoll and U. Jonas, *J. Am. Chem. Soc.*, 2006, **128**, 15606–15607.
- 936 Z. Zheng, K. Gao, Y. Luo, D. Li, Q. Meng, Y. Wang and D. Zhang, *J. Am. Chem. Soc.*, 2008, **130**, 9785–9789.
- 937 L. Wang, Y. Wan, Y. Li, Z. Cai, H.-L. Li, X. S. Zhao and Q. Li, *Langmuir*, 2009, **25**, 6753–6759.
- 938 Y. Wan, Z. Cai, L. Xia, L. Wang, Y. Li, Q. Li and X. S. Zhao, *Mater. Lett.*, 2009, **63**, 2078–2081.

- 939 J.-W. Kim, K. Tazumi, R. Okaji and M. Ohshima, *Chem. Mater.*, 2009, **21**, 3476–3478.
- 940 Z. Zhou and X. S. Zhao, *Langmuir*, 2005, **21**, 4717–4723.
- 941 B. Hatton, L. Mishchenko, S. Davis, K. H. Sandhage and J. Aizenberg, *Proc. Natl. Acad. Sci. U. S. A.*, 2010, **107**, 10354–10359.
- 942 L. Jia, W. Cai and H. Wang, *J. Mater. Chem.*, 2009, **19**, 7301–7307.
- 943 L. Jia, W. Cai, H. Wang, F. Sun and Y. Li, *ACS Nano*, 2009, **3**, 2697–2705.
- 944 G. Duan, W. Cai, Y. Luo, F. Lv, J. Yang and Y. Li, *Langmuir*, 2009, **25**, 2558–2562.
- 945 A. E. Saunders, J. L. Dickson, P. S. Shah, M. Y. Lee, K. T. Lim, K. P. Johnston and B. A. Korgel, *Phys. Rev. E: Stat., Nonlinear, Soft Matter Phys.*, 2006, **73**, 031608.
- 946 L. Billon, M. Manguian, V. Pellerin, M. Joubert, O. Etteradossi and H. L. N. Garay, *Macromolecules*, 2008, **42**, 345–356.
- 947 E. H. Min, K. H. Wong and M. H. Stenzel, *Adv. Mater.*, 2008, **20**, 3550–3556.
- 948 W. Sun, J. Ji and J. Shen, *Langmuir*, 2008, **24**, 11338–11341.
- 949 C. Yu, J. Zhai, Z. Li, M. Wan, M. Gao and L. Jiang, *Thin Solid Films*, 2008, **516**, 5107–5110.
- 950 S. H. Lee, J. S. Park, B. K. Lim, C. B. Mo, W. J. Lee, J. M. Lee, S. H. Hong and S. O. Kim, *Soft Matter*, 2009, **5**, 2343–2346.
- 951 B. Krause, H. J. P. Sijbesma, P. Munuklu, N. F. A. van der Vegt and M. Wessling, *Macromolecules*, 2001, **34**, 8792–8801.
- 952 B. Krause, K. Diekmann, N. F. A. van der Vegt and M. Wessling, *Macromolecules*, 2002, **35**, 1738–1745.
- 953 E. Reverchon and S. Cardea, *J. Membr. Sci.*, 2004, **240**, 187–195.
- 954 C. D. Wood and A. I. Cooper, *Macromolecules*, 2000, **34**, 5–8.
- 955 L. Qian, E. Willneff and H. Zhang, *Chem. Commun.*, 2009, 3946–3948.
- 956 J.-W. Moon, H.-J. Hwang, M. Awano and K. Maeda, *Mater. Lett.*, 2003, **57**, 1428–1434.
- 957 M. C. Gutiérrez, M. J. Hortigüela, J. M. Amarilla, R. Jiménez, M. L. Ferrer and F. del Monte, *J. Phys. Chem. C*, 2007, **111**, 5557–5560.
- 958 H. Ishiguro and B. Rubinsky, *Cryobiology*, 1994, **31**, 483–500.
- 959 M. B. Bryning, D. E. Milkie, M. F. Islam, L. A. Hough, J. M. Kikkawa and A. G. Yodh, *Adv. Mater.*, 2007, **19**, 661–664.
- 960 M. Panda, R. Seshadri and J. Gopalakrishnan, *Chem. Mater.*, 2003, **15**, 1554–1559.
- 961 T. L. Rogers, A. C. Nelsen, M. Sarkari, T. J. Young, K. P. Johnston and R. O. Williams, *Pharm. Res.*, 2003, **20**, 485–493.
- 962 M.-H. Sun, S.-Z. Huang, L.-H. Chen, Y. Li, X.-Y. Yang, Z.-Y. Yuan and B.-L. Su, *Chem. Soc. Rev.*, 2016, **45**, 3479–3563.